N° d'ordre : 4707

THÈSE

UNIVERSITÉ BORDEAUX 1

ÉCOLE DOCTORALE DES SCIENCES CHIMIQUES

Par Aikaterini BETHANI

POUR OBTENIR LE GRADE DE

DOCTEUR

SPÉCIALITÉ : Polymères

SYNTHESE DE COPOLYMERES DE TYPE POLYMERE SEMI-CONDUCTEUR-*bloc* -POLYMERE HYDROSOLUBLE: APPLICATION A LA DISPERSION DE NANOTUBES DE CARBONE

Directeurs de thèse: Prof. Georges Hadziioannou, Dr. Eric Cloutet

Soutenue le: 14 décembre 2012

Devant la commission d'examen formée de:

Mme DAGRON-LARTIGAU Christine, Maître de conférence/HDR, Université de Pau	Rapporteur
M. KALLITSIS Ioannis, Professeur, Université de Patras	Rapporteur
Mme MOINEAU-CHANE-CHING Kathleen, Directeur de recherche, Université de Toulouse	Examinateur
M. CRAMAIL Henri, Professeur, Université de Bordeaux	Examinateur
M. McCLENAGHAN Nathan D, Chargé de recherche/HDR, Université de Bordeaux	Examinateur
M. RONCALI Jean, Directeur de recherche, Université d'Angers	Examinateur
M. CLOUTET Eric, Directeur de recherche, Université de Bordeaux	Examinateur
M. HADZIIOANNOU Georges, Professeur, Université de Bordeaux	Examinateur

Université Bordeaux 1
Les Sciences et les Technologies au service de l'Homme et de l'environnement

List of abbreviations

ρ: Density

Ω: Ohm

λ: Wavelength

AFM: Atom Force Microscopy

Ag: Silver

AgNWs: Silver nanowires

Al: Aluminum

Ar: Argon

ATRP: Atom-transfer Radical Polymerization

Au: Gold

BF$_3$: Boron trifloride

C: Celsius

Cd: Cadmium

CDCl$_3$: Deuterated chloroform

CdO: Cadmium oxide

CMC: Critical Micelle Concentration

CNT: Carbon Nanotubes

Cr: Chromium

CVD: Chemical Vapor Deposition

DCE: 1,2 Dichloroethane

DCM: Dichloromethane

DMF: Dimethylformamide

DMSO: Dimethyl sulfoxide

EG: Ethylene Glycol

f: volume fraction

FeCl$_3$: Ferric Chloride

FTIR: Fourier transform infrared spectroscopy

Ga: Gallium

GNRs: Graphene Nanoribbons

GO: Graphene Oxide

GRIM: Grignard metathesis polymerization

H$_2$O: Water

HCl: Hydrochloric acid

ILs: Ionic Liquids

In: Indium

In$_2$O$_3$: Indium (III) Oxide

IR: Infrared

ITO: Indium Tin Oxide

K: Kelvin

MeOH: Methanol

MWCNTs: Multi Wall Carbon Nanotubes

NaOH: Sodium Hydroxide

Nb: Niobium

NBS: N-Bromosuccinimide

nButLi: n-butyllithium

Ni: Nickel

NIL: Nanoimprint lithography

NMP: N-Methylpyrrolidone

NMR: Nuclear Magnetic Resonance

NP: Nanoparticles

NWs: Nanowires

OLED: Organic light-emitting diode

OPV: Organic Photovoltaic

P3HT: Poly(3-hexylthiophene)

Pa: Pascal

Pd(PPh₃)₄: Tetrakis(triphenylphosphine)palladium(0)

PEDOT: Poly(3,4-ethylenedioxythiophene)

PET: Polyethylene terephthalate

PLD: Pulsed Laser Deposition

PMMA: Poly(methyl methacrylate)

PS: Polystyrene

PSS: Poly(styrenesulfonate)

PSSA: Poly (styrene sulfonic acid)

PSSNa: Polystyrene Sulfonate Sodium salt

Pt: Platinum

PVA: Poly(vinyl acetate)

PVAc: Poly(vinyl acetate)

R_{sq}: Conductivity

S: Siemens

SDBS: Sodium Dodecylbenzene Sulfonate

SDS: Sodium Dodecyl Sulfate

SEC: Size-exclusion Chromatography

SEM: Scanning Electron Microscopy

SiO₂: Silicon dioxide

SL: Sulfonation Level

Sn: Tin

SnO: Tin (II) Oxide

SnO₂: Tin Dioxide

sq: Square

SWCNTs: Single Wall Carbon Nanotubes

T (%): Transmittance

T: Temperature

TCE: Transparent Conductive Electrodes

TCO: Transparent Conductive Oxides

TEM: Transmission Electron Microscopy

T_g: Glass Transition Temperature

TGA: Thermogravimetric analysis

THF: Tetrahydrofuran

TiO₂: Titanium dioxide

UV-vis: Ultraviolet-visible

VAPE: Vacuum arc plasma evaporation

Zn: Zinc

TABLE OF CONTENTS

GENERAL INTRODUCTION

The last decade has seen the blossoming of numerous optoelectronic devices. Assure a human-machine interface, most of them require at least one layer of electrode which is transparent to visible light as well as being electrically conductive. The predominant material used to this day as transparent conductive electrode (TCE) is the Indium Oxide doped by tin metal (ITO). Indeed ITO shows excellent electrical properties as attested by its high conductivity (10^3-10^4 S.cm^{-1}) as well as a high optical transmittance of 80% across the UV-vis-NIR spectral range (350-1000 nm).[1] In addition ITO can be deposited in thin films by several deposition techniques, thus consolidating its top tier rank for TCE. However, ITO suffers from several limitations such as its ceramic nature leading to mechanically fragile films with high roughness; the vacuum process inherent to its deposition; its environmentally unfriendly nature. Moreover, technologies based on ITO are impeded by the difficulty of supply inherent to its strategic character (as witnessed by China's embargo on rare earths and its "sky-rocketing" price). **Consequently the development of alternative solutions for TCE in replacement of ITO constitutes a key issue for the organic opto-electronic field.**

Several materials, both carbon and metal based, have been investigated as replacements of ITO. Depending on the devices, there are several parameters (thickness and roughness of films, deposition technique etc) that should be considered. For instance, a promising alternative to ITO is foreseen through the silver nanowires, which exhibit excellent electrical properties (up to 25 Ω/sq) and can be formulated in inks. **Alternatively, and with the aim to design an "all carbon" optoelectronic device, several promising TCE can be targeted through the use of carbon based materials.** In order to be competitive, the "all carbon" TCE should exhibit several critical characteristics: *i.* the possibility to be deposited by roll-to-roll techniques; *ii.* a low roughness in the thin film configuration; *iii.* electrical and optical properties comparable to ITO (T> 70% and R< 10 Ω/sq). Following this concept, the Innovative Materials for Photovoltaic solar cell EleCtrodes (IMPEC) ANR project was started in January 2010, with the aim to design TCE by using two promising carbon based materials: the π-conjugated polymers and the Carbon Nanotubes (CNTs).

The polymeric organic materials with electronic, magnetic, electrical and optical properties of a semiconductor while in the same time retain their processibilty and mechanical properties are called semi-conducting polymers.[2] They were first discovered in 1977 by Shirakawa *and coll.* who also witnessed an increase of their electrical conductivity through doping with Br$_2$, I$_2$, or AsF$_5$.[3] Following these pioneering works, the scientists focused on the synthesis of new π-conjugated polymers with advanced properties. In 1992 a new promising

π-conjugated polymer was synthesized: the poly (3,4 ethylenedioxythiophene) (PEDOT).[4] Even though this polymer exhibits a high conductivity, was stable and could process in the thin film configuration, it deals with a serious drawback: the lack of solubility in all solvents. In order to overcome this limitation, the synthesis of aqueous dispersions of PEDOT in the presence of poly(4-styrenesulfonate) (PSS) was realized leading to stable dispersions of PEDOT/PSS. The presence of the PSS phase not only provides a dispersion solubility to the PEDOT but also acts as a counter anion to the positively charged PEDOT and as an oxidizing agent. These dispersions were examined as possible replacement of ITO but the conductivity values were not satisfying due to the low volume fraction of PEDOT in the dispersion.[5]

As an alternative to PEDOT the scientists examined other semi-conducting polymers for the design of TCEs. An example of these polymers is the poly (3-hexylthiophene) which is soluble in organic solvents and exhibits the electrical properties of a semiconductor in their undoped form.[6] Moreover the different synthetic routes leading to P3HT subsequently allow a versatile macromolecular design through the creation of various block copolymer architectures leading to materials with extra functionalities (such as aqueous solubility or ionic character).[7] While this type of materials can not solely be used as TCE due to their low intrinsic conductivity, their combination with conductive materials (*i.e* metal nanoparticles, PEDOT latexes) can be envisioned for applications in TCE due to their good solubility and the uniformity of the produced films.

At the other hand, carbon nanotubes have been discovered by Iijima in 1991 and they can be considered as sheets of graphene bent into a cylindrical shape with diameter in nanometers scale.[8] They can be divided in multi wall and single wall depending on the number graphene sheets that are wrapped. In addition, the wrapping chirality of the CNTs affects directly their electrical properties. For certain chiralities the nanotubes develop a metallic character while for others they behave like a semi-conductor. The main advantages of these materials are the high intrinsic conductivity (10^{-4} Ω.cm), the excellent mechanical properties and their possibility to be formulated as inks.

It appears obvious that CNTs have the necessary characteristics for application in TCEs. In addition their characteristic length of the nanoscale order allows them to be in the form of inks, and thus to be cast in films by roll-to-roll techniques. However, the as-produced CNTs are in the form of bundles, where a bundle is consisted of individual carbon nanotubes linked by Van der Waals forces. In that form, the nanotubes are not soluble and their electrical

properties are deteriorated. Consequently the dispersion of the CNTs bundles into individual tubes is a key parameter for the use of the CNTs as TCE. The dispersion by non-covalent interactions is preferred since the electrical properties of the nanotubes are not affected. The π-conjugated polymers have been used as dispersants of CNTs as they can develop strong π-π interactions with the surface of the nanotubes. In addition, block copolymers with a π-conjugated part result in stable dispersions both in organic and aqueous media.[9] The electrical properties of the CNTs/π-conjugated depend on several parameters like the percolation of the nanotubes and the inter tubes contacts. Consequently the size, the nature and the cooperative assembly of the dispersion aid with the CNTs should be tuned in order to find an optimum between the dispersibility, the conductivity and the film formation.

This thesis is, thus, dedicated to the synthesis of new π-conjugated based copolymers for the dispersion of CNTs in aqueous media with the aim to examine the potential of the films produced from these dispersions as TCEs.

In the first chapter of this manuscript a literature review is presented on the replacements on ITO. The replacement materials are divided in two categories: metal based and carbon based. This review is focused on the carbon based materials: *i.e.* graphene and CNTs. In addition a large part of this chapter is devoted to the comparison between the different dispersants of the CNTs with an emphasis on the dispersion in polymer matrix.

In the following chapters the results obtained during this thesis are presented. In the second chapter the strategy followed for the synthesis of the new copolymers is presented. The synthetic routes for the synthesis of copolymers, with PEDOT or P3HTas a π-conjugated part and the polyelectrolyte PSSA as hydrophilic block, are examined. Besides, a small comparative study was pursued on P3HT/PVA copolymers in order to underline the effect of the charges in the hydrophilic block. The chemical characterization of all the resulted products is also showed. Finally, well defined P3HT-*b*-(PS-*co*-PSSA), PVA-*g*-P3HT and P3HT-*b*-PVA copolymers were synthesized and were soluble in aqueous media.

The physical-chemical behavior of these amphiphilic copolymers was further studied. In particular, the self-assembly of the P3HT-*b*-(PS-*co*-PSSA) copolymer in water solutions was examined by AFM, TEM, Cryo-TEM techniques. The photophysical behavior of the copolymer, both in solution and solid state, was studied by UV-vis and photoluminescence methods. Similar studies were pursued on the PVA-*g*-P3HT copolymers.

All the synthesized polymers were then tested as dispersants for both single and multiwall carbon nanotubes. The stability of these dispersions over time was evaluated by zeta potential measurements. Microscopic techniques were used in order to visualize these dispersions in solution and in solid state. Further, the π-π interactions of the P3HT part with the surface of the CNTs were characterized by photophysical methods. The CNTs/copolymer dispersions were casted in thin films by several methods depending on the viscosity of the inks. The transmittance and the electrical conductivity of these films were measured targeting the values of the TCEs.

Finally, all the used materials, the experimental procedures and the supplementary characterizations are presented in the last chapter.

1.   Nath, P.; Bunshah, R. F., Preparation of In$_2$O$_3$ and tin-doped In$_2$O$_3$ films by a novel activated reactive evaporation technique. *Thin Solid Films* **1980,** *69* (1), 63-68.

2.   Chiang, C. K.; Fincher, C. R., Jr.; Park, Y. W.; Heeger, A. J.; Shirakawa, H.; Louis, E. J.; Gau, S. C.; MacDiarmid, A. G., Electrical Conductivity in Doped Polyacetylene. *Phys. Rev. Lett.* **1977,** *39* (17), 1098-1101.

3.   Shirakawa, H.; Louis, E. J.; MacDiarmid, A. G.; Chiang, C. K.; Heeger, A. J., Synthesis of electrically conducting organic polymers: halogen derivatives of polyacetylene, (CH). *J. Chem. Soc., Chem. Commun.* **1977,** (16), 578-580.

4.   Heywang, G.; Jonas, F., Poly(alkylenedioxythiophene)s—new, very stable conducting polymers. *Adv. Mater.* **1992,** *4* (2), 116-118.

5.   Nardes, A. M.; Kemerink, M.; de Kok, M. M.; Vinken, E.; Maturova, K.; Janssen, R. A. J., Conductivity, work function, and environmental stability of PEDOT:PSS thin films treated with sorbitol. *Organic Electronics* **2008,** *9* (5), 727-734.

6.   Kim, Y. H.; Spiegel, D.; Hotta, S.; Heeger, A. J., Photoexcitation and doping studies of poly(3-hexylthienylene). *Physical Review B* **1988,** *38* (8), 5490.

7.   Urien, M.; Erothu, H.; Cloutet, E.; Hiorns, R. C.; Vignau, L.; Cramail, H., Poly(3-hexylthiophene) Based Block Copolymers Prepared by "Click" Chemistry. *Macromolecules* **2008,** *41* (19), 7033-7040.

8.   Iijima, S., Helical microtubules of graphitic carbon. *Nature* **1991,** *354* (6348), 56-58.

9.   (a) Gonzalez-Dominguez, J. M.; Tesa-Serrate, M. A.; Anson-Casaos, A.; Diez-Pascual, A. M.; Gomez-Fatou, M. A.; Martinez, M. T., Wrapping of SWCNTs in Polyethylenoxide-Based Amphiphilic Diblock Copolymers: An Approach to Purification, Debundling, and Integration into the Epoxy Matrix. *The Journal of Physical Chemistry C* **2012**; (b) Spitalsky, Z.; Tasis, D.; Papagelis, K.; Galiotis, C., Carbon nanotube–polymer composites: Chemistry, processing, mechanical and electrical properties. *Prog. Polym. Sci.* **2010,** *35* (3), 357-401.

Chapter I

Literature Review

TABLE OF CONTENTS

Literature review

I   *Transparent conductive electrodes*

Transparent conductive electrodes are considered as one of the most strategic materials in the nanotechnology market for the coming years. Over the last decade there has been an increase demand for devices that require at least one transparent conducting layer. Devices like touch screens, electronic paper, OLED displays, organic electronics, organic photovoltaic, all use a material that is transparent in to visible light and at the same time electrically conductive. The organic electronics market is expected to be worth 8.2 billion dollars in 2012 and to grow up to 44.7 billion dollars in 2018.[1] Accordingly the total market of the transparent conductors is excepted to reach up to 10 billion dollars in 2018.[2] Consequently, there is a tremendous increase of scientific groups which are working on the development of new materials serving the field of organic electronics and transparent conductors. However, some crucial issues remain for the development of the organic electronics fabrication process and the cost of the materials will be of prime importance for its blossoming.

The main material used today as transparent electrode is the tin doped indium oxide (ITO), which has been studied and refined for over fifty years. ITO is formed by substitutional doping of In_2O_3 with tin (Sn) which replaces the In^{3+} atoms from the cubic bixbyite structure of the indium oxide. Consequently Sn reacts with the oxygen and forms SnO and SnO_2 oxides. The role of the Sn is directly related to the electrical properties of the ITO, since it is acting as donor n-type releasing electrons to the conduction band.[3] ITO exhibits excellent electrical properties with high conductivity (10^3-10^4 S.cm^{-1}) related to its higher carrier concentration (2 10^{20}- 12 10^{20} cm^{-3}). In addition ITO films have a direct optical bandgap greater than 3.75 eV resulting in high optical transmittance (> 80% for 370nm $< \lambda <$ 1000nm).[4] The combination of the optical transparence to visible light, the excellent electrical properties as well as the possibility of deposition in thin film by several methods (sputtering, thermal evaporation, screen printing) have made ITO a material of

choice. Consequently, several organic electronic devices currently use ITO as transparent conductive electrode. However, ITO has several drawbacks, like the difficulties of supply (which leads to dramatic price fluctuations); it requires vacuum processing; it is environmentally hazardous; and it has a ceramic nature. These material issues are being addressed by new transparent conductive materials which allow simple processing with more environmentally benign behavior. Thin films of such materials will greatly benefit the aforementioned key technologies, and will allow for instance innovative, low-cost solar power generation and energy efficient lighting products. Several new materials both of organic and inorganic nature were developed as replacements of the ITO. In the table 1 the typical characteristic values of new materials are presented and compared with the ITO film properties.

Table 1. Typical values and comparison of the ITO film and new transparent electrode materials.[5]

Type		Existing ITO film[*1]	New transparent electrode materials				
			Coated ITO[*2]	Ag wire ink[*3]	ZnO[*4]	Ag wire[*5]	Conductive polymer[*6]
Sheet resistance		350Ω/square	700Ω/square	250Ω/square	45Ω/square	0.2Ω/square	260Ω/square
Optical properties	Transmittance (no reflection prevention film)	88%	88%	91%	86.80%	80% min	About 85%
	Color	Slightly yellow or brown	Almost colorless	Almost colorless	Almost colorless	Almost colorless	Slightly blue
Durability	Bending	Inferior	Superior	Superior	Superior	Superior	Superior
	Environmental	Superior	Superior	Superior	Superior	Superior	Inferior, but acceptable
Freedom of base material selection (compared to ITO)		—	Superior	Superior	Equivalent or better	Superior	Equivalent or better
Manufacturing process		High-temperature vacuum (sputtering)	Coating and transfer	Coating, printing, etc	Room temperature vacuum (sputtering)	Coating, printing (roll-to-roll)	Coating, printing, etc
Commercialization date		In volume production	Commercial; in use by touch panel manufacturers	Commercial; to be used by touch panel manufacturers	ZnO film commercial; to be used by touch panel manufacturers	Sample-shipping; full-fledged sale to start in 2009	Sample-shipping

*1 For resistive membrane touch panel *2 TDK. 300Ω/square and 88% transparency in R&D *3 Cambrios Technologies
*4 Geomatec *5 Fujifilm *6 Bridgestone/electronic paper

II   *New materials for replacing ITO*

In the continuation of this chapter we will focus on the novel materials that could be used as replacements of ITO. We can divide these materials in two large categories: metal based materials and organic based materials. The metal based materials are chosen due to the good conductivity properties, though they suffer transmittance and film deposition problems. On the other hand, the carbon based materials field is open, since the synthesis of carbon materials with specific properties is still under development.

II.1 *Metal based materials for replacing ITO*

II.1.1   *Transparent conductive oxides (TCO)*

Transparent conductive oxides (TCOs) that contain a reduced amount or no indium were examined as replacements of ITO. TCOs are typically n-type doped metal oxides, though p-type metal oxides have also been reported.[6] Different kind of TCO thin films have been developed, with several combinations of host materials and dopants. First CdO doped by In or Sn was investigated with several deposition techniques.[7] However, the toxicity of the Cd and the high temperature treatment that CdO requires made it unsuitable for electronic applications. Titanium dioxide (TiO_2) and titanium-based oxides were also well studied as transparent conducting electrodes. In 2005, Furubayashi *et al.* reported the discovery of the Niobium (Nb)-doped anatase TiO_2 showing promising optical and electrical properties.[8] Anatase is the most common polymorph of TiO_2 and it is used as a photocatalyst for various environmental purifications. Films of $Ti_{1-x}Nb_xO_2$ with x~0.03, grown on single crystals by Pulsed Laser Deposition (PLD) technique, show low resistivity (8.8 x 10^{-5} Ω.cm at 5K) with high transmittance (95% for 400 nm < λ < 800 nm), values that are comparable to the electrical and optical properties measured for ITO films.

Following these promising results on the TiO_2 in the anatase phase doped by Nb, other dopants, like Tantalum (Ta), Tungsten (W), Fluorine (F), were incorporated. A comparison study of Nb-and Ta- doped TiO_2 films with almost the same amount of dopant, was carried out by Chen *et al.*[9] Even though both dopants of TiO_2 exhibit similar low resistivity when they are grown by PLD technique on glass substrates, Nb-doped TiO_2 had a better conductivity performance on glass substrate (annealed under vacuum at 650°C).

Similarly, W-doped TiO_2 were grown on single crystals and then compared with the $Ti_{0.94}Nb_{0.06}O_2$ films.[10] Resistivity of $2 \cdot 10^{-3}$ Ω.cm was measured for $Ti_{0.95}W_{0.05}O_2$ film, deposited under optimized conditions (T = 300 K, P_{O2} = $1 \cdot 10^{-5}$ Torr), which is ten times higher than the $Ti_{0.94}Nb_{0.06}O_2$. Comparable results were recently published, by using fluorine (F) as a dopant of anatase TiO_2.[11] F:TiO_2 epitaxial thin films were fabricated by PLD method. The $TiO_{1.95}F_{0.05}$ film showed low resistance of $1.6 \cdot 10^{-3}$ Ω.cm and optical transparency of 95% under optimal conditions (T = 400°C and P_{O2}= $1.0 \cdot 10^{-5}$ Torr). Although the promising results of the F-doped TiO_2, fluorine is a less attractive dopant due to the low doping efficiency of F^-(20%-30%).

In conclusion for the titanium oxide and titanium oxide based TCO thin films, promising results have been reported with low resistance and high optical transmittance. The drawback of these materials is related to the epitaxial growth on a single crystal substrate in order to obtain good electrical properties. For the same results on glass substrates, annealing treatment at high temperatures (above 300°C) is required. In both cases, there is a patterning problem which makes them difficult to be used for conventional transparent electrodes.

The alternative TCO containing reduced amount of indium or no indium, which have been studied as replacement of ITO in transparent electrode applications, are summarized in the figure 1. Multicomponent oxides composed of combinations of ZnO, SnO_2 and In_2O_3 are examples of reduced-indium TCO.

Figure 1. The scheme presents the In, Zn and Sn oxides and their combinations. In the table the obtainable properties of reduced-indium TCO thin films are presented.[12] Reproduced with permission from Elsevier, Copyright 2008.

TCO	In content (at.%)	Deposition temperature (°C)	Deposition method	Resistivity ρ (Ωcm)
ZnO-In$_2$O$_3$ (IZO)	60–90 (90)	180 (RT) (100)	MSD (VAPE)	3.5–2.9 × 10^{-4} (3.0 × 10^{-4})
In$_2$O$_3$-SnO$_2$ (In$_4$Sn$_3$O$_{12}$)	95–40 (50)	180 (RT) (350)	MSD	2.0–5.0 × 10^{-4} (2.0 × 10^{-4})
ITO-In$_4$Sn$_3$O$_{12}$	90–50	180 (RT)	MSD	3.5–4.8 × 10^{-4}
Zn$_2$In$_2$O$_5$ - In$_4$Sn$_3$O$_{12}$	80–40	180 (RT)	MSD	4.2–7.5 × 10^{-4}
ITO	90–95	RT–350	MSD	4.0–1.0 × 10^{-4}
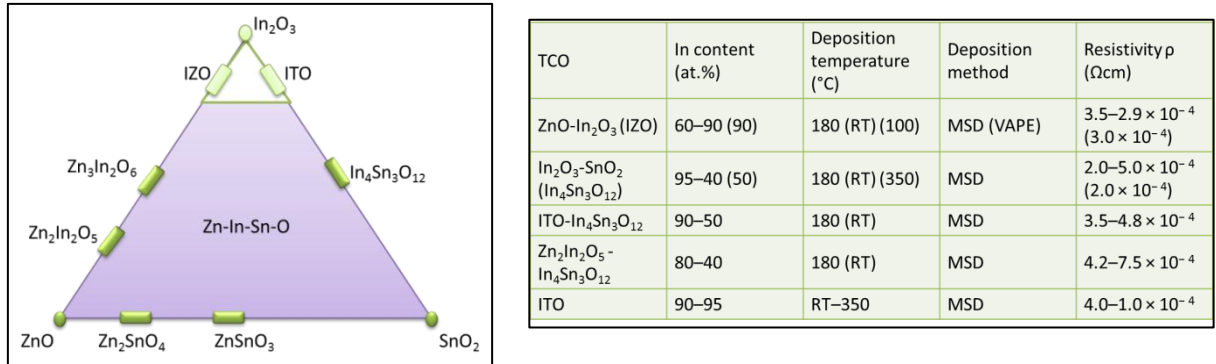
Several deposition techniques were used for the film formation of ZnO-In$_2$O$_3$ oxides. Moriga *et al.* deposited thin films of ZnO-In$_2$O$_3$ by sputtering method for different atomic ratios of cations (Zn/[Zn+In]) and compare them with ITO films made by the same method.[13] The minimum resistivity of 2.3 x 10^{-4} Ω.cm was obtained for a film deposited at 150°C with an atomic ratio of cations 0.22. Other developed techniques for preparation of thin films of multicomponent oxide are by vacuum arc plasma evaporation (VAPE)[14] and by dc magnetron sputtering deposition (dc-MSD).[15] The resistivities of these films were varied between 3.5 x 10^{-4} Ω.cm to 3 x 10^{-4} Ω.cm, depending on the temperature of deposition (Figure 1). The same deposition techniques (dc-MSD and VAPE) were used for the film formation of the multicomponent oxide In$_2$O$_3$-SnO$_2$. The amount of indium was varied from 40% to 95%. When the amount of In$_2$O$_3$ is around 90%-95% the resulting material is the ITO. The In$_2$O$_3$-SnO$_2$ oxides with 40%-60% indium are identified as In$_4$Sn$_3$O$_{12}$. Besides films with both ITO and In$_4$Sn$_3$O$_{12}$ oxides containing from 40% to 90% indium were prepared on substrates at 350°C.[16] In figure 1 a table containing the resistivity values of indium based metal oxide is presented. It is clear that the resistivity of the TCO films decreases when the amount of In$_2$O$_3$ increases with best performance when the TCO is the ITO.

In conclusion for the reduced-indium oxides, transparent conductive thin films were prepared by several techniques. The electrical properties of these films are close to the ones of ITO

but even if the amount of indium used in these materials is reduced, the availability and the cost problems remain. Among the indium-free TCO materials, Al and Ga doped ZnO (AZO, GZO), remained the most well studied and show the best optical and electrical properties. As for the rest of the oxides, AZO and GZO, deal with problems of film formation. Consequently, several deposition techniques were investigated for the fabrication of the TCO thin films with low resistivity on large area substrates with high deposition rate. Minami[12] and Yamamoto *et al.*[17] have demonstrated different versions of VAPE deposition method as well as rf and dc-MSD methods. The films made by these methods had an approximately uniform distribution and the resistivity was close to the expected values. Even though the first problem for the use of free-indium oxides is partially solved, the concerns about the electrical stability of the films upon exposure to humid environments remains especially for films with thickness below 100 nm.

In summary, the transparent conductive oxides that contain a small amount of In_2O_3 or free-indium metal oxides have been studied as replacements of ITO for transparent electrode material. Oxides based on Cd were examined first, but due to their high toxicity were not suitable for applications in electronics. Another important group of TCO, is the titanium based oxides, and more specifically the TiO_2 in the anatase phase. Several metals were used as dopants for the TiO_2. The optical and electrical properties of these materials were really close to the characteristic values of ITO, especially when tungsten (W) was used as a dopant. However, the titanium based oxides have a serious deposition problem, which involves either a deposition on single crystal, or deposition at high temperatures. The multi-component oxides that contain reduced amount of indium, like ZnO- In_2O_3 and In_2O_3-SnO_2, can not be considered as a replacement of ITO, since the use of reduced amount of indium (up to 50%) does not solve the problem of the indium accessibility. Finally, the Al and Ga doped ZnO were examined as alternative TCO materials. The scientists were able to overcome the first problem of these materials,i.e the film deposition, by developing new techniques such as VAPE. However, the electrical stability of the thin films of these materials has not been established.

II.1.2 Thin metal films

Metals are highly conductive materials due to their high free electron density. However, for the same reason, metals have high reflectivity in the visible range and are not very transparent. Three different techniques have been advanced to overcome the optical issues: ultrathin metal films, metal grid films and metal nanowires. Each of these methods, dealing with the optical issues, have their own advantages and drawbacks.

Metal thin films have quite low transparency. In order to obtain transmittance performance similar to the ITO, ultra thin films, usually less than 10nm, have to be cast. This low thickness does not influence significantly the conductivity properties of the films. Several metals have been deposited in ultra thin films, and full optical and electrical studies have been completed. Among the metals, Chromium (Cr) and Nickel (Ni) are metals that are cheap and highly competitive. Polycrystalline Ni films were reported with thickness from 2 nm up to 800 nm. The roughness of the films was quite satisfying (RMS at 0.5 nm and peak-to-valley roughness of 2.1 nm (figure 2(c)) and the transmittance and conductivity values close to the ones of ITO.[18] Similarly, ultrathin films of Cr have been successfully deposited. The optical properties of these films were similar to the ultra thin Ni films, with high transparence over a large wavelength range, but their electrical properties were minor to the Ni films.[19]

One of the crucial issues for the fabrication of ultrathin films is their fragility. Different paths of film deposition have been followed in order to overcome this difficulty.[20] Hatton *et al.* prepared glass substrates grafted with 3-mercaptopropyl (methyl)dimethoxysilane, creating a surface covered with free thiol moieties which can react with the gold atoms. By that technique, stable thin films of Au were made with good electrical and optical properties as well as with roughness values good enough for application in OLEDs.[21] An alternative to the Au thin films is the platinum (Pt) films, since Pt nanoparticles do not absorb at most of the UV-vis wavelengths.[22] Ultra thin Pt films (19 nm) have been successfully deposited and visualized (figure 2(b)). It is noteworthy that there is strong relation between the thickness of the metal films and the conductivity. In figure 2(a) a graph of the film thickness versus the resistivity for Ni thin films is presented, verifying the dependence between the two values.

In conclusion, the use of thin metal films as TCE deals with certain limitations. The main issue is the morphology of these films which have to be thin enough to be transparent, without becoming so thin that they are not homogenous, mechanically sound and with low electrical conductivity. In parallel the surface roughness of the films should be less than the thickness of the film, which is a big challenge for ultrathin films. These drawbacks make the thin metal films unfavorable for several electronic devices that require thin films with low roughness and high transparency. However, metal thin films have been commercialized by several companies, which sell silver and gold films on flexible PET surface serving different applications such as chemical and biological sensors or non-transparent electrodes.

Figure 2. (a) The dependence of electrical resistivity (µΩ cm) to the film thickness (Å) for ion-beam-deposited Ni thin films.[18] Reproduced with permission from Springer, Copyright 2007 (b) TEM cross-sectional view of Pt/glass interface for a Pt thin film of 19 nm.[22] Reproduced with permission from Wiley and Sons, Copyright 2006 (c) Typical AFM image of the surface morphology of thin metal films. Here AFM image of Ni thin film.[18] Reproduced with permission from Elsevier, Copyright 2000
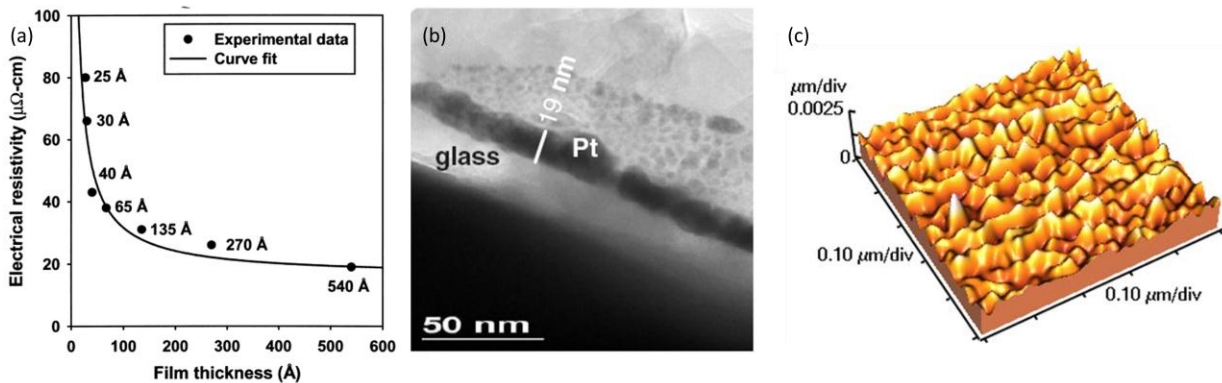
Another method of metal deposition is the use of patterned metal grids instead of casting a continuous metal film. Several approaches towards nanostructure fabrication have been exploited during the last years, however the nanoimprinting for metals is hard to achieve due to their high melting temperatures. In addition most of the fabrication methods are not easy to handle and they involve costly techniques. In contrast a new procedure for deposition of metal grids has been developed, the nanoimprint lithography (NIL).[23] It is a monovalent lithographic technique for high-throughput patterning, at low cost and it is well suited for the area of organic electronics. The methodology of NIL is presented in figure 3. A hard mold which contains a nanoscale pattern is pressed on a polymeric material casted on stable substrate. This polymeric pattern is then used for metal deposition by different methods.

Figure 3. (a) Schematic of a typical NIL process (b) SEM image of a fabricated mold with 10 nm pattern (c) SEM image of hole arrays imprinted by the previous mold on PMMA surface.[23] Reproduced with permission from Wiley and sons, Copyright 2007
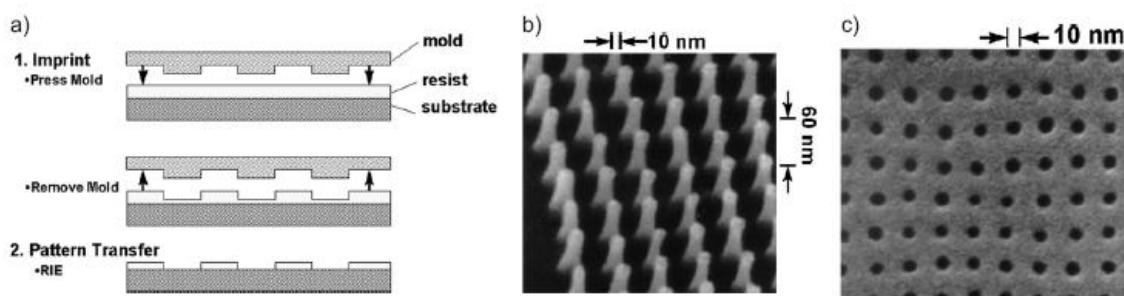
In 2007, Guo was the first to report the fabrication of a nanoimprinted semitransparent metal electrode. The grid pattern was created by applying NIL two times, using two grating molds. The first grating had a period of 700 nm and it is corresponding to the transparent part of the electrode while the second was imprinted orthogonally to the previous one with a period of 10 μm and provides the conductivity. By that method Au, Al and Cu metals were successfully deposited. Depending on the distance and the width of the grids, the transmittance and the conductivity can be tuned. Finally, metal electrodes with transmittance around 70% (400 nm < λ < 800 nm) and sheet resistance of 4.79 Ω/sq were fabricated. The advantages of this method are that it can be applied on a flexible substrate and that the transmittance and conductivity can be tuned depending on the application requirements.[24]

The same group later demonstrated that nanoimprinted transparent metal electrodes can find applications in organic photovoltaic devices. Metal (Cu) was deposited on a polydimethylsiloxane (PDMS) mold by a metal transfer process. Then the metal electrode was transferred onto a PEDOT:PSS surface coated on glass, using the flexible PDMS mask as a stamp. The use of a flexible mold is important for the roll-to-roll processing and in combination with the use of the inexpensive Cu as metal, makes this type of metal electrodes suitable for organic electronics devices.[25]

Consequently solar cells were fabricated using nanopatterned metals as electrodes and the characteristics of the devices were comparable to the ones with ITO as electrode.[26] As shown in the figure 4 the electrodes were printed on a PEDOT:PSS substrate by NIL. The main grating of 700 nm period resulted to highly transparent electrode (figure 4 (c)).

Figure 4. (a) Schematic of the fabrication of the nanopatterned metal electrodes on PEDOT:PSS-coated glass substrate using PDMS flexible mold (b) SEM image of the printed Cu electrode on the PEDOT:PSS substrate (scale 5 µm and 1 µm) (c) Optical transmittance of nanoimprinted Au, Cu, Ag electrodes compared to ITO electrodes in the visible range.[26] Reproduced with permission from Wiley and sons, Copyright 2008
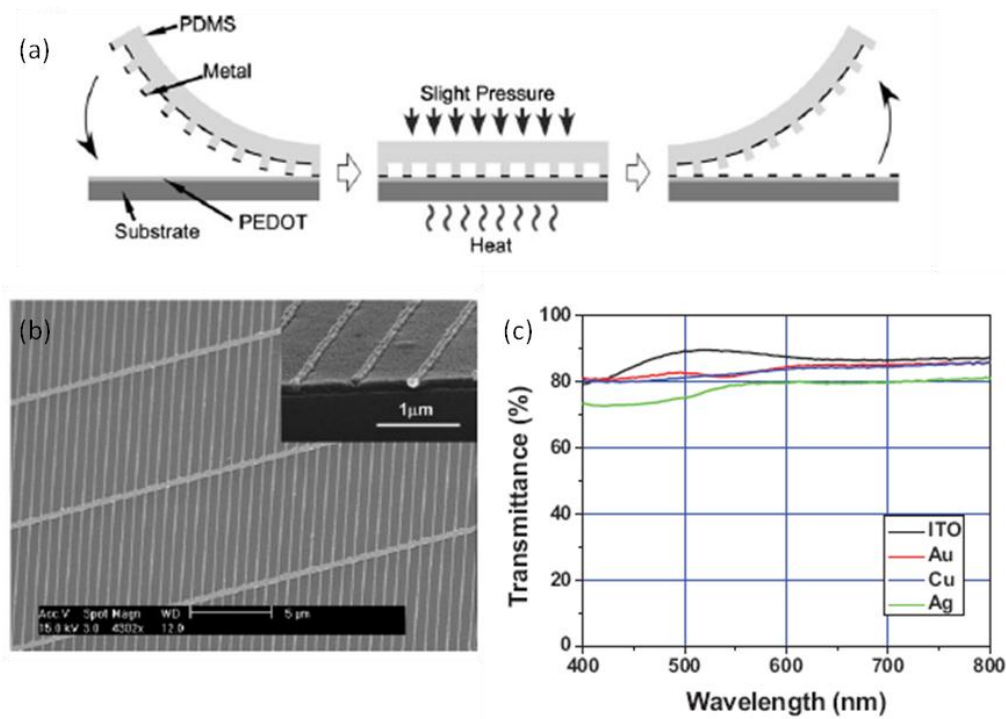
Different nanoimprinting processes have also been developed towards the decrease of the multiple steps that NIL comprises. A direct nanoimprinting process has been reported by the use of metal nanoparticles. The methodology of this procedure are presented in the figure 5 (b). The differences during the process are due to the direct deposition of a metal nanoparticle solution on a glass surface. Then the solution is patterned with a PDMS mold and during the final step, the particles are sintering by heating, exposing the metal.[27]

Recently, a new NIL deposition method was proposed resulting in more transparent metal electrodes with a simplified fabrication method. This method, as it is shown in figure 5 (a) combines three techniques: thermal nanoimprinting, thin deposition of the metal (Cu), and burnishing. Nanoimprinted PMMA substrates were prepared with the desired pattern. On these substrates thin films of Cu were deposited by electron-gun evaporation. Finally the residual layer of Cu was removed by burnishing leading to the fabrication of the Cu mesh electrode. By adjusting the thickness of the metal film, both transmittance and resistivity can be controlled.[28]

Figure 5. (a) Schematic of the deposition of Cu electrode in the PMMA surface and images of the cross-sectional view and top view of the electrode[28] Reproduced with permission from JSAP, Copyright 2012 (b) Schematic of a new NIL process combing nanoparticle nanoimpriting (A,B) dispersion of the particles in SiO$_2$/P + Si wafer (C,D) pressing of the PDMS mold on the solution (E,F) and remove of the mold by heating.[27] Reproduced with permission from American Chemical Society, Copyright 2007
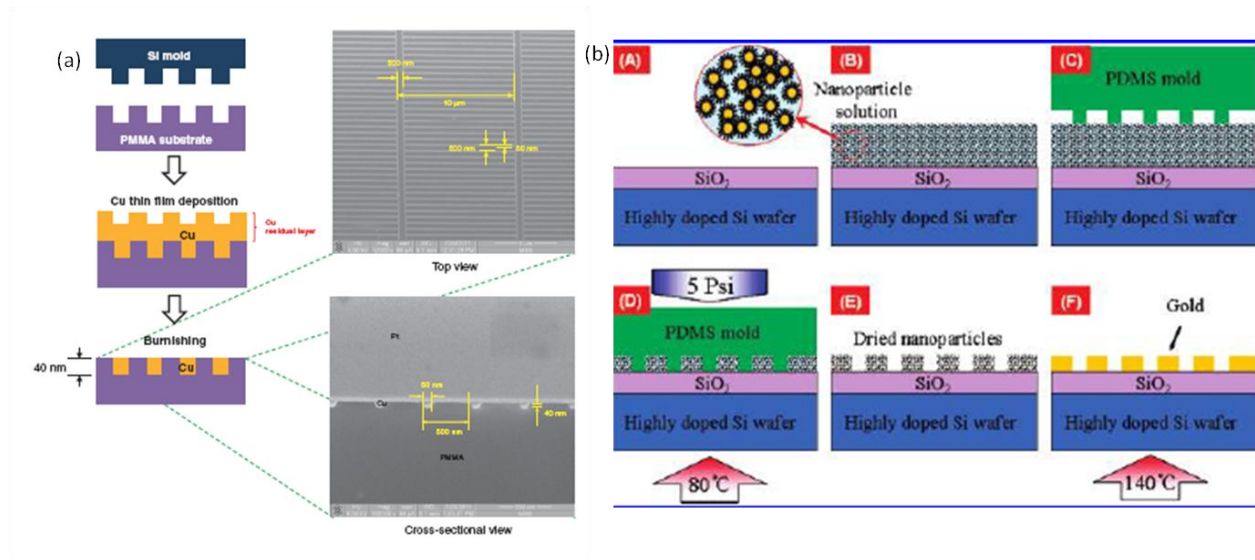
In conclusion transparent conductive electrodes were achieved by using NIL processes and their performance were close to ITO. However, there are concerns about the use of the patterned metal grids in the devices due to their high roughness, especially for devices with thin active layers. In addition for application in displays the patterned lines should be very small, so not to be visible, which will affect the electrical performance of the electrodes. On the other hand the new nanoimprinting methods that involve roll-to-roll procedures and Cu as metal are very promising for the future. Combination of the metal grids patterned on a conductive transparent surface is the next important challenge in this field.

II.1.3 Metal nanowires

Metal nanowires are a nanoscale material which has been also evaluated as replacement of ITO. By nanoscale materials we are referring to materials that have at least one dimension less than 100 nm. This class of materials has been widely developed during the last years, and processes about the controllable synthesis and purity of them have been invented. Nanomaterials are considered as favorable materials for TCE due to their optical, electrical, thermal and mechanical properties observed in bulk and in percolated films. Due to their small size these materials can form high conductive "wires", "tubes" or "sheets". Moreover ink formulations can be made with them and that they can be cast in films by several techniques

Transparent conductive electrodes consisting of a random network of metal nanowires have been realized. The predominant metal in this field is silver due to its high conductivity. The synthesis of silver nanowires (Ag NWs) is usually a low-cost solution process through the reduction of silver nitrate in the presence of poly(vinylpyrrolidone) (PVP) in ethylene glycol.[29] The nanowires have small diameters (40-200 nm) and lengths of 1-20 μm. After the film formation, an extra annealing step is required in order to remove the remaining PVP. The fact that the Ag NWs are directly synthesized in a solution allow them to be coated by roll-to-roll techniques. Ag NWs inks have been successfully deposited on both glass and flexible substrates. In figure 6 (b,c) an example of

26

Ag NWs coated on PET flexible substrate is presented. A common Ag NWs solution (length of nanowires ~ 10 µm) coated on plastic flexible surface leads to a 20 Ω/sq conductivity for 80% transmittance.[30]

Silver nanowire films exhibit high ratio of DC (direct current) to optical conductivity, comparing to carbon nanomaterials. DC conductivity is a method of calculating the conductivity of metals while the optical conductivity is a value representing the reflectivity and the transmittance over the photon energies of the films. The ratio of DC conductivity, σ_{DC}, over the optical conductivity, σ_{Op}, is a commonly used figure for evaluating TCEs performance. For instance the ratio σ_{Op}/σ_{DC} equals to 500 for ITO films. In the figure 6 (a) the σ_{Op}/σ_{DC} ratio for ITO, SWCNTs, silver and Ag NWs is presented. The transmittance and the σ_{Op}/σ_{DC} ratio for the thin metal films are related by the following equation:

$$T\,(\lambda) = \left(1 + \frac{Z_0}{2R_s}\frac{\sigma_{O\rho}(\lambda)}{\sigma_{DC}}\right)^{-2}$$

where R_s is the sheet resistance, Z_0 the impedance of free space and λ the wavelength that transmittance was measured. It is clear that the low sheet resistance and the high transmittance lead to increase of the σ_{op}/σ_{DC} value.

Figure 6. (a) Transmission (at 550 nm) plotted as a function of the film resistance (Ω/sq) and the σ_{DC}/σ_{Op} ratio for Ag NWs, ITO, SWCNTs and silver films[31] Reproduced with permission from American Chemical Society, Copyright 2009 (b) Ag NW film coated on PET substrate and (c) the SEM image of the film (scale 1 μm). The sheet resistance of the film is 50 Ω/sq. [29] Reproduced with permission from American Chemical Society, Copyright 2002
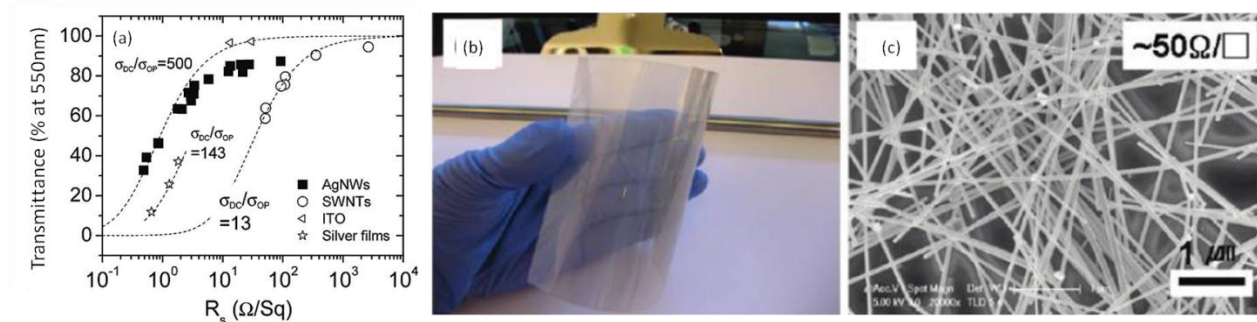
Sukanta *et al* studied the effect of the film thickness of the Ag NWs on the electrical conductivity and the transmittance.[31] For films with thickness below 160 nm the films act like 2D network resulting in high transparency while thicker films are more bulk like. The ratio σ_{Op}/σ_{DC} is higher for the thicker films, and the film with the best performance was measured with resistance at 13 Ω/sq for 85% transmittance at 550nm.

Despite the encouraging electrical and optical properties of the silver nanowire films, they suffer from serious drawbacks which limit their potentials. Ag NWs films have high mean roughness and non-conformal coverage of the substrate as well as high sensitivity to physical contact (can be removed by adhesion or friction). In order to change the morphology of the film and increase the mechanical stability, the use of nanoparticles (NP) and polymers has been reported. Small ZnO particles (~5 nm) have been spin-coated on the surface of Ag nanowire film, followed by annealing. After this preparation the ZnO particles have completely covered the nanowires and the film roughness has been decreased by 30 nm. The mechanical properties of the film have been improved after the addition of the ZnO, and the resistivity was slightly decreased from 4.8 Ω/sq to 4.2 Ω/sq but it remains stable during the annealing process, in contrast with the

Ag NW control films.[32] A recent publication on the same system, AgNWs/ ZnO NP claims that the most critical factor in improving the silver nanowire film properties is the filling of the voids between the wires with the nanoparticles.[33] The empty space within the nanowires network, not only increases the roughness and the instability of the film but they create a non-conductive area between each metal nanowire. Indeed, as shown in the figure 7, the Ag NWs films have lower roughness and they are more homogenous after the treatment with ZnO nanoparticles.

Figure 7. SEM images of Ag NW network with (a) standard ZnO and (b) the new developed ZnO filling the empty space between the nanowires.[33] Reproduced with permission from Elsevier, Copyright 2012
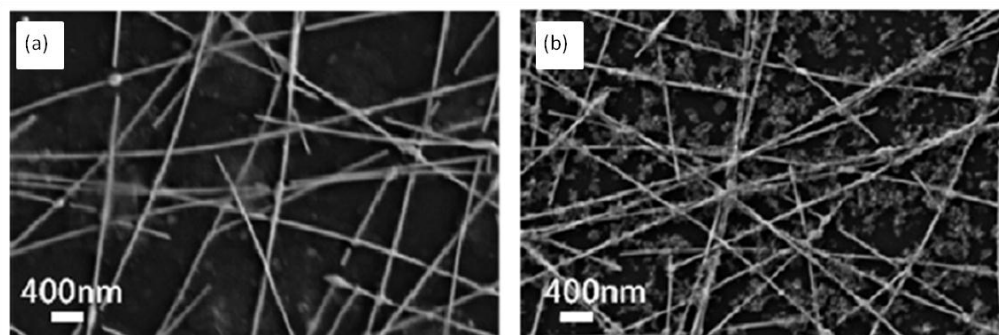
A polymer matrix was also used in order to reduce the Ag NWs films problems. In this methodology, Ag NWs are deposited on PET (flexible) or glass surface, and then a polymer solution is casted above it. The film Ag NW/polymer is then removed from the substrate and the electrical and optical characteristics were investigated. Poly(vinylalcohol) (PVA) had been chosen as a polymer matrix, due to its high transparency. The films were casted on PET substrate, and due to the presence of the PVA, the roughness of the film was significantly reduced. In addition the transmittance remained high but the resistivity was slightly reduced.[34] Good results have been reported with polyacrylate/Ag NW films.[35] The Ag nanowires were casted on glass substrate and

the acrylate monomers were polymerized by UV on the Ag NW's film surface. The final film was lifted-off from the glass, leading to an Ag NW film on a transparent polymeric flexible surface. The texture of this film was highly smooth since it was first formed on glass, and the nanowires and the polymer were closely packed.

It is obvious that the polymer should be chosen in order to give transparent films and to facilitate the casting by roll-to-roll techniques. Besides the flexible surfaces, on which the electrodes are deposited, should cover some characteristics depending on the application. Poly(dimethylsiloxane) (PDMS) was used as a substrate since it provides flexibility and can additionally contribute to the mechanical properties of the film. However, the PDMS surface is hydrophobic and the deposition of homogenous film of Ag NWs was not possible. This obstruction was overcome by the modification of the PDMS surface with dopamine, which makes the surface hydrophilic. Ag NWs were then successfully spray-coated on the dopamine modified PDMS resulting in a stretchable, transparent conductive electrode.[36]

A different direction to the improvement of the electrical properties of the metal nanowires is the modification of their size. It has been demonstrated that longer metal nanowires can improve the properties of their electrodes. [37] This problematic in combination with the development of new methods of fabrication for long nanofibers, was the reason why metal nanofibers were synthesized. Electrospinning is the most recent technique for fabrication of ultrathin nanofibers either oriented or laid in a random way on the surface. The setup of this method is presented in the figure 8 (a). By this method metal (Fe, Co, Ni) nanofibers have been fabricated.[38] Copper nanofibers were prepared by electrospining on flexible substrates in both random and aligned orientations. A small modification in the principal electrospining setup allows the oriented deposition of nanofibres (figure 8 (b-e). The best performance of these electrodes was at 25 Ω/sq for 90% transmittance (at 550 nm). The electrical properties of the Cu nanofiber films were comparable with the performances of Ag NWs films, even though Cu is less conductive that Ag.[39]

Figure 8. (a) Schematic of an electrospinning setup for the synthesis of Cu nanofibers (b) SEM image of Cu nanofibers synthesized by that method (c) modified electrospinning setup for oriented nanofibers (d),(e) SEM images of Cu nanofibers with controlled orientations.[39] Reproduced with permission from American Chemical Society, Copyright 2010
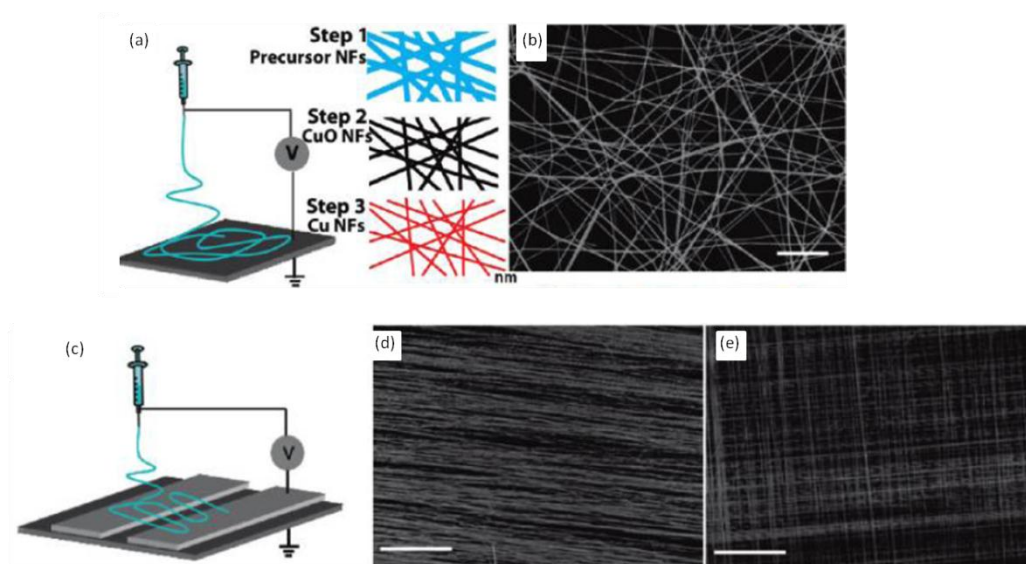
Metal nanoparticles, and more specifically silver nanowires, is a material which gathers all the requirements for flexible conductive transparent electrodes. The electrical properties are close to those of ITO, since Ag is a very conductive metal. Also the possible formulation of the nanowires in solution allows the film formation by roll-to-roll process. The σ_{op}/σ_{DC} ratio is high which implies good performance as transparent electrodes. However the roughness of the films is a critical issue for several applications of the electrodes. Blends of Ag NWs with polymer or nanoparticles could be the solution, but it has not been tested yet at the commercial scale. Additionally, light scattering due to the diameter of the nanowire, is an essential problem which has not yet been resolved. The long term electrical stability is an additional concern, as Ag could

be degradable after oxidation or sulfidation reactions. Despite these drawbacks, Ag NWs solutions have been commercialized from several companies (*e.g.* Blue Nano Inc) as well as their thin films (Zhejlang Kechuang Adv. Mat. Co., Carestream Adv.Mater.).

II.2 Carbon based materials for replacing ITO

Carbon is an important element for many technological applications, ranging from drugs to synthetic materials. One of the most interesting properties of carbon is that it is the only element that has stable allotropes in different dimensions. The structures of these allotropes are presented in the figure 9. There are two natural allotropes, the graphite and the diamond, each of them with different unique properties. Graphite is a 3rd dimension allotrope, with highly anisotropic thermal properties and with the ability to conduct electricity due to the electron delocalization within the carbon layers. In 1985, another 0 dimension carbon allotrope was observed for first time by Kroto *et al.*, the advent fullerenes.[40] The smallest stable and most important of the fullerenes is the C_{60}, which consists in a spherical network of sixty structural equivalent sp^2-hybridized carbon atoms in the shape of a soccer ball. Some years later, Iijima synthesized one dimension carbon allotrope in the form of tubes. Carbon nanotubes (CNT) with different number of walls and different diameters were observed at this first synthetic process.[41] The latest discovery in the field is the two dimension graphene. Even though graphene was an already known material, Geim *et al.* were the first who isolated a single graphene flake.[42] Graphene is a one-atom thick sheet of sp^2 bonded carbon atoms packed in a honeycomb crystal lattice.

Figure 9. Carbon allotropes in all dimensions, natural graphite (3D), graphene (2D), Carbon nanotubes (1D) and fullerenes (0D).
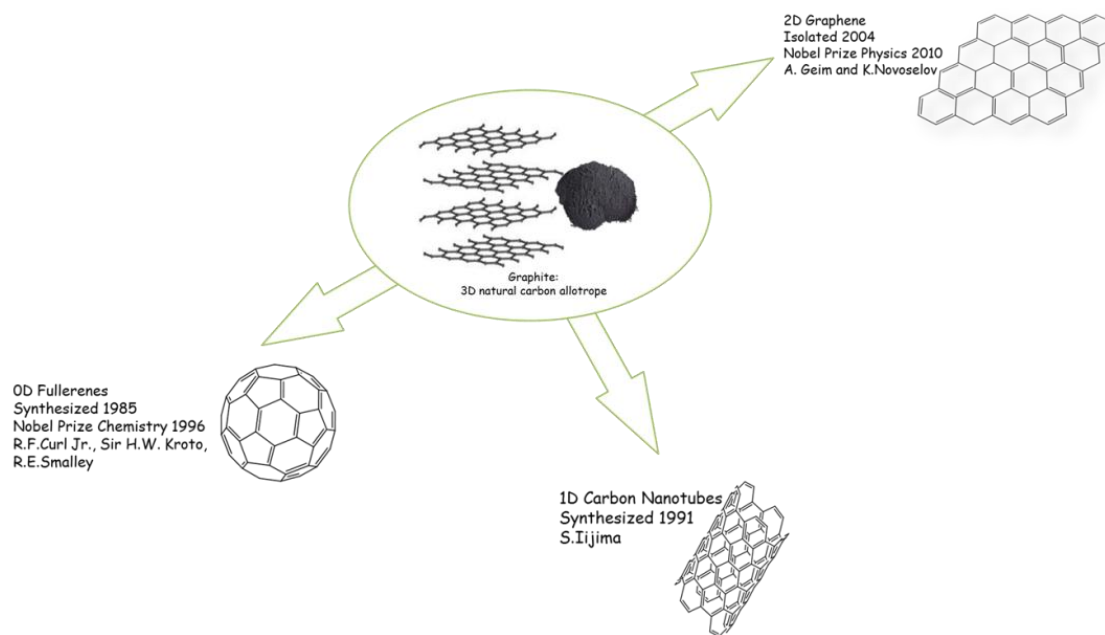
The graphene and the carbon nanotubes have been examined as replacements of ITO due to their electrical properties as well as their possibility to be formulated in solutions. Another carbon based material, with similar properties are the conjugated polymers. This type of polymers, under certain conditions, can exhibit excellent electrical and optical properties. In addition their polymeric nature allows them to form homogenous and strong films on flexible substrates. In the following paragraphs, the studies using the conjugated polymers, the graphene and the carbon nanotubes for transparent conductive electrode applications will be presented.

II.2.1   Conducting polymers

In 1977, conducting polymers and their ability to be doped were discovered.[43] Polymeric organic materials with electronic, magnetic, electrical and optical properties of a metal while at the

same time retain their processibilty and mechanical properties are called conducting polymers. Furthermore Shirakawa *et co* observed in 1977,[44] that films of the semi conductive polyacetylene can increase its conductivity by doping with either Br_2, I_2, or AsF_5. These discoveries made conducting polymers a promising material for several applications and they attract the research interest of the scientists, making them the most recent generation of polymers.[45] Numerous conjugated polymers, mostly aromatic, were studied in the following years, like poly(*para*-phenylene) (PPP), poly(thiophene) (PT), poly(pyrrole) (PPy), poly(aniline) (PANI), etc. The chemical structures of some of them are presented in the figure 10.

Figure 10. Chemical structures of some conjugated polymers.
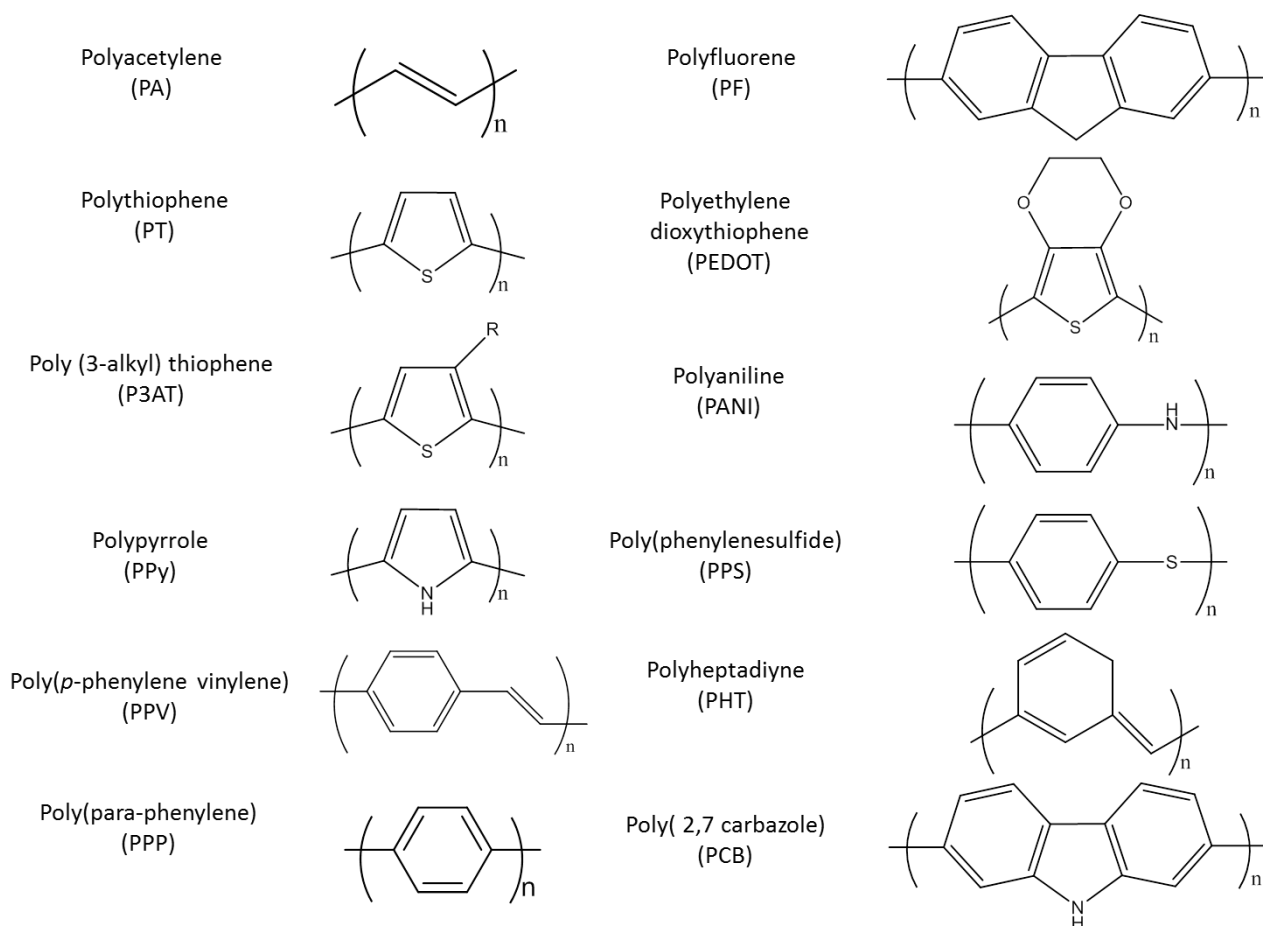
An important step in the development of the conducting polymers was related to the doping process. The doping is an oxidation-reduction reaction, in which the introduction of donors (doping of type n) or acceptors (doping of the type p) into the material can be accomplished in a number of ways. It is noteworthy that the doping of the semiconducting polymers is not always reversible and easy to control. In the figure 11 the possible ways for doping conjugated polymers are presented. Briefly, the chemical doping involves charge-transfer redox chemistry oxidation (p-type doping) or reduction (n-type doping). By this method the doping level is not easy to control. To deal with this difficulty, electrochemical doping was investigated where the electrode supplies the redox charge to the π-conjugate polymer and a polyelectrolyte is playing the role of the counter ion. The doping level is easily controlled by the voltage that is applied on the polymer.

Figure 11. Doping mechanisms of π-conjugated polymer, their advantages and applications.
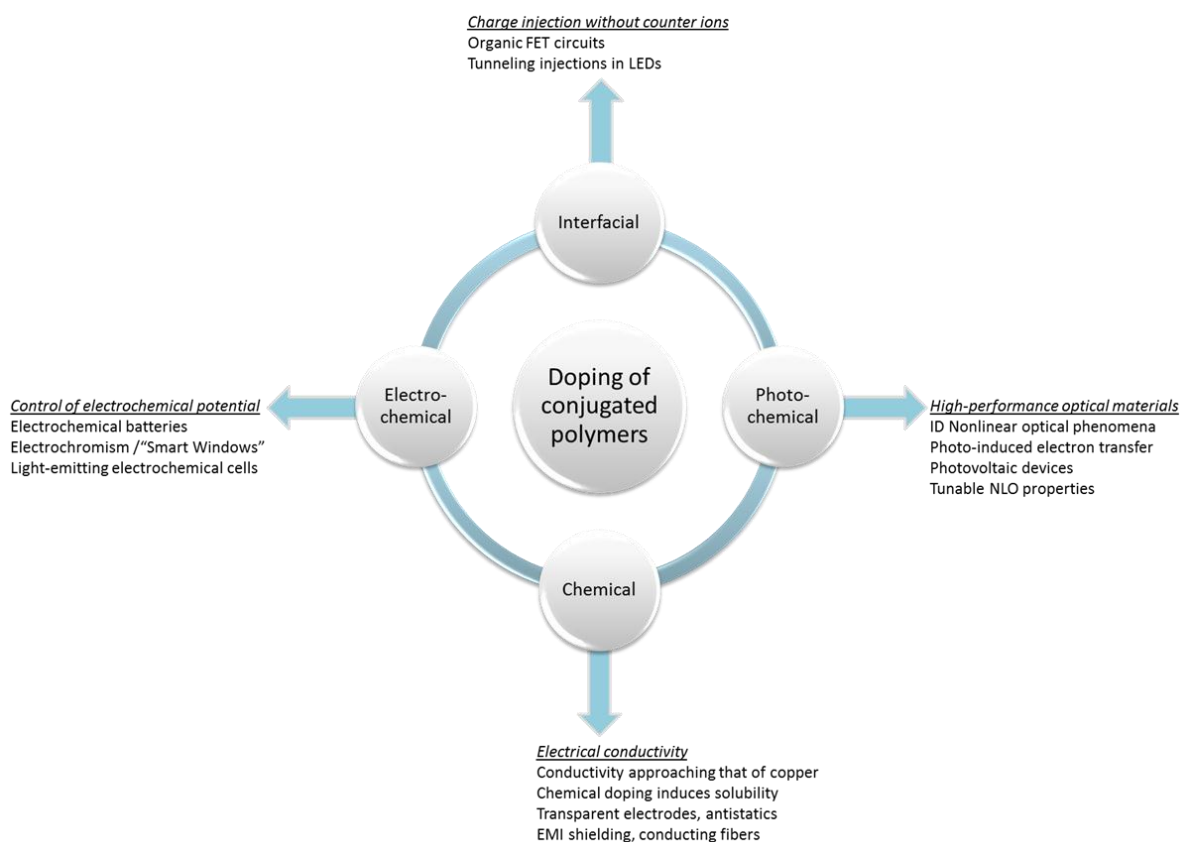
Similarly, conjugated polymers can be doped by photochemical oxidation and reduction or by the injection of electrons and holes. In general, the doping process is chosen based on the type of conjugated polymers, the required doping level and the application.

The synthesis of new conducting polymers with improved properties was a challenge for synthetic chemists in the 1980's. A promising conjugated polymer poly(3,4-ethylenedioxythiophene) (PEDOT) was synthesized by scientists at the Bayer AG research laboratories.[46] This new polymer shows high conductivity (300 S/cm), a quasi-transparency in the form of thin film and a very high stability in the oxidized state.[47] The only difficulty of this new polymer in order to be used as a possible replacement of ITO was the PEDOT insolubility in all solvents.

This difficulty was overcome by synthesizing PEDOT in the presence of poly(4-styrenesulfonate) (PSS) in an aqueous dispersion (figure 12). The PSS behaves as a counter anion to the positively doped PEDOT and as well as an oxidizing agent and charge compensator.[48] This new material, which is commercialized under the Clevios and Orgacon trade names, can make high quality films with high transparency, high mechanical flexibility and thermal stability through the conventional solution processing techniques.[49]

Figure 12. Chemical structure of PEDOT:PSS dispersion.
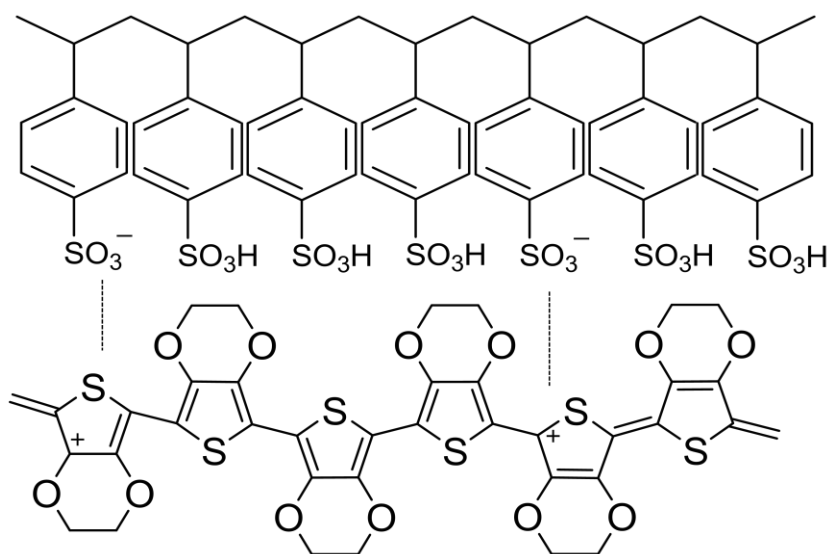
However, pristine PEDOT:PSS films made from aqueous polymer solution, usually have conductivity below 10 S.cm $^{-1}$, (which is much lower than ITO (1-5 10^3 S.cm^{-1})). Different approaches have been developed in order to increase the conductivity of the PEDOT:PSS, which is low due to the important amount of PSS that is required around PEDOT in order to be soluble. Moreover the addition of organic solvents was examined as a method to increase the conductivity of the PEDOT:PSS.

It is believed that the screening effect, due to the addition of a polar solvent between the PSS dopant and the PEDOT increases the charge transport properties of the system.[50] Solvents like DMSO, DMF, and THF were added in the PEDOT:PSS water solutions, and the conductivity of the mixture was higher than the pristine solution. From all the solvents the bigger effect was observed by the addition of DMSO and films with conductivity up to 590 S.cm^{-1} have been reported.[51]

In the PEDOT:PSS system, PEDOT is primary positively doped from the presence of the sulfonate anionic groups of PSS. In the literature there are plenty of reports about the addition of a second dopant in order to modify the morphology of the PEDOT:PSS and to increase the conductivity. These dopants can be small anions, acids, salts, ionic liquids and differ from the primary dopant since the enhanced properties may persist after its removal. The most studied secondary dopants for the PEDOT:PSS are the ethylene glycol (EG), the glycerol and the diethylene glycol (DEG). In that case the secondary dopant is an "inert" substance which influences the conductivity of the primary doped π-conjugated polymer.

The proposed mechanism for the role of these secondary dopants is related to the distribution of the PSS in the films. In the absence of the dopants the films are consisting of a thin non-conductive layer of PSS and the polymer blends behave like conducting grains in PSS matrix. By the addition of the secondary dopant the excess of the PSS is phase-segregated into PSS insulating domains while conductive PEDOT:PSS grains merge together (figure 13) forming a conductive 3D network. It is evident that the phase separation that was observed increases the conductivity but also increases the effective area rich in PEDOT, which is crucial for charge injection from a PEDOT:PSS electrode.[52]

Figure 13. AFM phase images of (a), (b) pure PEDOT:PSS films (scale 200nm and 50nm) and (c), (d) after the addition of PEG (scale 200nm and 50nm).[52] Reproduced with permission from American Chemical Society, Copyright 2006
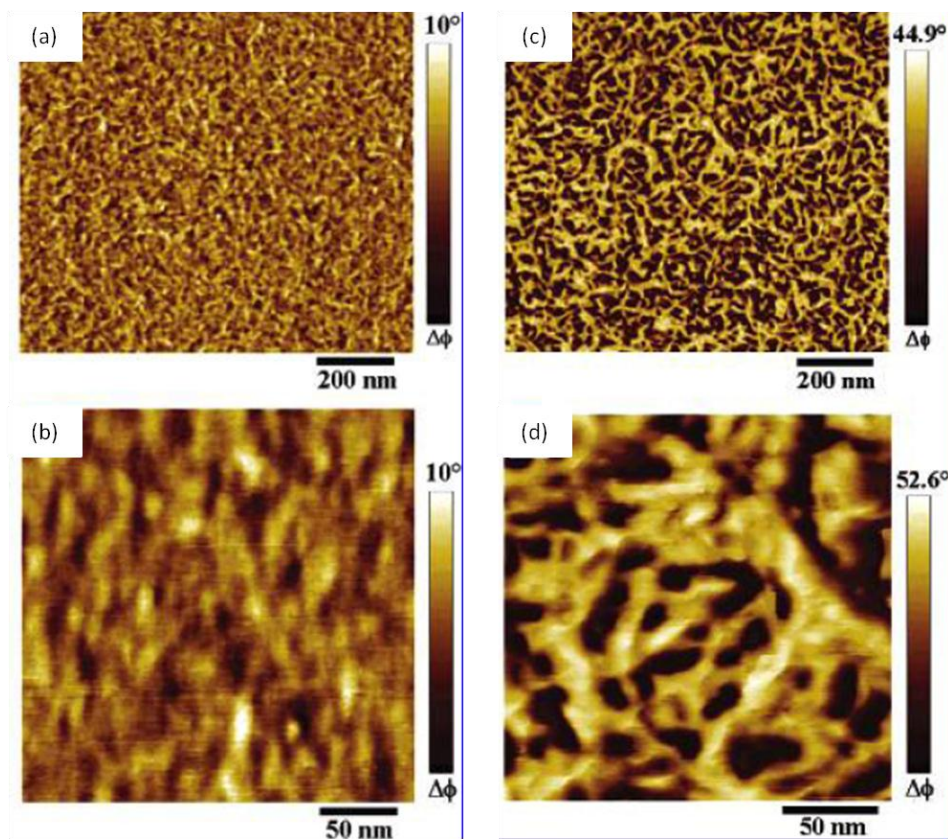
The secondary dopants ethylene glycol, glycerol and *meso*-erythritol were reported to increase the conductivity of the PEDOT:PSS by more than two orders of magnitude and thin films on glass and PET have been made with conductivity up to 160 S.cm^{-1}.[53] Recently Muller-Mekamp

et al report a solvent post-treatment method for PEDOT:PSS films after the addition of the EG, which increase the conductivity up to 1418 S cm^{-1}.[54] Another method to increase the conductivity of PEDOT:PSS, is the use of certain salts or acids. Different salts ($MgCl_2$, $CuCl_2$, $NaCl_2$, $AgNO_3$, $CuSO_4$, $Cu(CH_3COO)_2$, $InBr_3$, $InCl_3$) were added in the PEDOT:PSS solution and the conductivity was increased even by 700 times, for certain salts and certain salt concentrations.[55] The anion effect on the conductivity of the PEDOT:PSS solution is related to the competition of two reactions. The first phenomenon is the dissociation of the salts and the other is the association with the positively charged one, leading to the PEDOT doping (figure 14(a)). So, in order to observe a significant effect on the conductivity, a salt with a high dissociation constant is required.[56]

Though the salt treatment is a simple method for increasing the conductivity of the PEDOT:PSS the electrical properties, so far, are not satisfying and also there are concerns that the anion can diffuse out of the film. Recently Ouyang *et al.* tried to overcome these concerns by using zwitterions, which have both negative and positive charges. Films with conductivity of 100 S.cm^{-1} were reported with low ion diffusion, which make zwitterions a promising material to treat the PEDOT:PSS.[57] The mechanism involving the zwitterions treatment is presented in figure 14 (b). Treatment of the PEDOT:PSS films with several acids at temperatures from 120°C to 160°C can significantly increase the conductivity.[58] Films treated with acetic acid, propionic acid or hydrochloric acid showed an increase of conductivity up to 200 S cm^{-1}, though films treated with 1M sulfuric acid solution at 160°C had conductivity up to 2200 S cm^{-1}.

Figure 14. (a) Schematic structure of the affect of salt (CuCl₂) addition in the PEDOT:PSS[55] Reproduced with permission from American Chemical Society, Copyright 2009 (b) schematic structure of the PEDOT:PSS before and after the zwitterions treatment.[57] Reproduced with permission from Royal Society of Chemistry, Copyright 2010
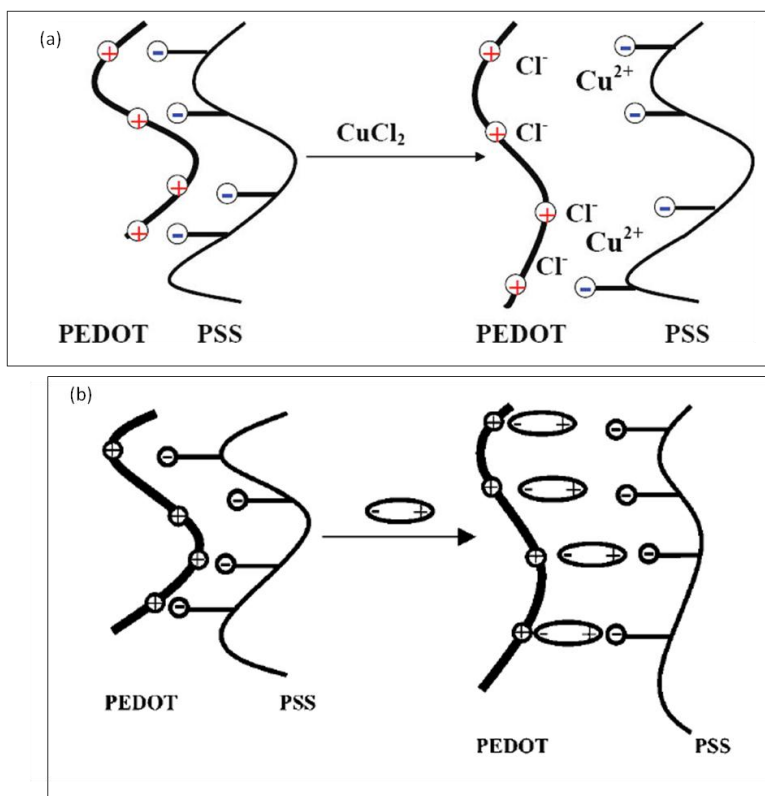
In summary, PEDOT:PSS is an important material with good electrical and mechanical properties. Besides it can be deposited in films with solution techniques leading to transparent thin films. For these reasons PEDOT:PSS is already widely used in the organic photovoltaics as a conductive layer. The conductivities, however, of the commercial PEDOT:PSS solutions are not high enough in order to replace the ITO electrode. The scientists are trying to increase the conductivity by various methods described above. None of these methods though gave films with resistance comparable to the ITO. In addition the use of acids or salts raises concerns about the

pollution of the final devices due to their presence. The zwitterions approach is a promising method, and maybe with the synthesis of more suitable molecules, the conductivity increase will be higher. Additional mechanical and stability issues are impeding the used of PEDOT:PSS dispersions are transparent conductive electrodes.

II.2.2 Carbon based nanomaterials

Carbon based nanomaterials have been also investigated as replacements of the ITO. In this category belong the most popular and promising materials for the next generation of transparent conductive electrodes: the graphene and the carbon nanotubes. The main advantage of the nanoscale carbon materials over the conducting polymers is their superior electrical properties even in thin films. As nanomaterials can be formulated in inks, therefore to be casted as films from solutions, covering all the requirments for the thin film electronics. Casting films from solutions allow the industries to use the roll-to-roll coating equipment, which already exists in the ink and paint coating industries, making the film formation cheaper comparing to the high temperature and high vacuum depositions that TCOs require. The combination of electrical and optical properties of the nanomaterials with the high volume and inexpensive roll-to-roll coating technique is pushing the scientists and the industries to intensify the research into these materials.

Some of these new nanomaterials are suitable for application as transparent electrode. In this category we find two carbon based nanomaterials: carbon nanotubes (CNTs) and graphene. These materials possess impressive electrical and optical properties. Moreover they have chemical and thermal stability and do not absorb in almost all the visible range. Combination of these properties with the low cost film deposition techniques, led the scientists to consider them as promising transparent conductors for the organic electronics field.

II.2.2.1 *Graphene*

Graphene is a two dimensional atomically thick sheet of sp^2-bonded carbon atoms packed in a honeycomb crystal lattice. Long-range π-conjugation in graphene yields to extraordinary thermal, mechanical and electrical properties. Examples of the characteristics of graphenes are the high current density, the ballistic transport, the chemical inertness, the high thermal conductivity, the optical transmittance and the high hydrophobicity in nanometer scale. Graphene is characterized as a semi-metal or zero-gap semiconductor and its opto-electrical characterization has shown low absorption in white light and remarkably high electronic mobility at room temperature.[59] The corresponding resistivity of a graphene sheet is 10^{-6} $\Omega.cm^{-1}$, and it is considered as the lowest resistivity substance at room temperature.[60]

In order to benefit from its properties, the synthesis of a single layer graphene on a suitable substrate is required. Therefore, the synthesis in a controlled way of pure, isolated and high yields of graphene sheets, which can be applied in the industry, is a key issue. The methods of graphene fabrication can be divided in two categories: the solution processes (mechanical and liquid exfoliation, reduced graphene oxide) and the direct growth (epitaxial growth by chemical vapor deposition, unzipping of CNTs). Each of these approaches has equally advantages and limitations.

II.2.2.1.1 Bulk deposition processes for graphene synthesis

The chemical vapor deposition (CVD) technique for the uniform deposition of graphene has been widely studied. This method is based on the decomposition of hydrocarbon gas to carbon over a transition metal surface, at high temperatures. A fraction of the carbon atoms/metal in a solid solution at elevated temperatures is known to precipitate as a graphene film upon cooling (figure 17). It is obvious that the thickness of the graphene film can be controlled by varying the solubility of carbon atoms dissolved in the metal at high temperatures and by varying the thickness of the metal. In addition the metallic surfaces are chosen in order to be able to transfer the graphene film onto another substrate.

This methodology has been achieved for graphenes grown on Ni[61] and Cu[62] surfaces presented in figure 15 (a). The main difference between the two metals is the carbon solubility. When the carbon atoms are formed and come in contact with the metal surface, they can either get mixed with the metal, (soluble) or remain at the surface (poor solubility). Since the carbon atoms are less soluble in Cu than in Ni, they remain longer at the metal surface resulting in larger and single layers of graphene. In comparison graphene synthesized on Ni surfaces mainly consists of several layer, since the carbon atoms are soluble and they are present in more layers of the metal. The graphene films grown by CVD can be transferred on glass and flexible substrates by several techniques. A characteristic method to transfer graphene films made by CVD on flexible substrates was proposed by Kim *et al*.[63] Indeed Ni substrate layers can be etched by the use of acids or $FeCl_3$. Graphene sheets were deposited by CVD on Ni substrates, further etched by acids or $FeCl_3$, and transferred on PDMS stamp surface. The procedure is shown in figure 15 (b).

Figure 15. (a) Schematic of the CVD technique for the synthesis of graphene layers (b) Proposed method for the transport of graphene film made by CVD on PDMS surface.[63] Reproduced with permission from Nature Publishing Group, Copyright 2009
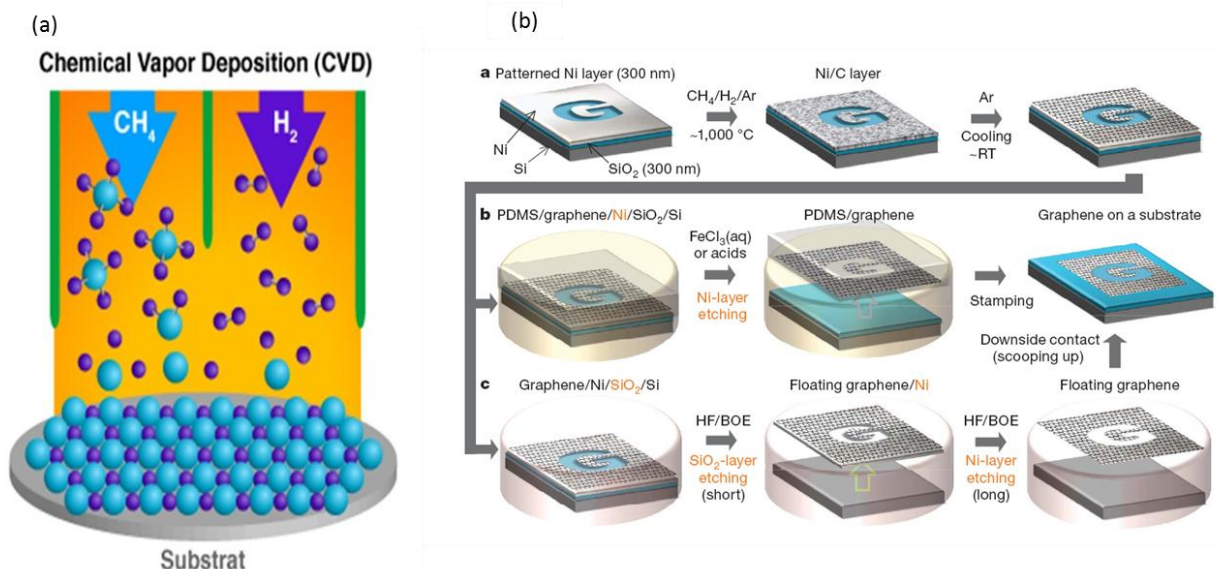
The graphene layers made by CVD are of high quality and large area layers can be formed under certain conditions. In addition, CVD method is already used in the industry, reducing the cost of the commercially synthesized graphene. However this process deals with some limitations. The duration of this method can be long, especially if the transport of the graphene films to other substrates is necessary. In addition, there are limitations on the size of the transfer layer and issues of homogeneity of the films have been raised.

Another technique for the growth of graphene layers on a surface is by cutting carbon nanotubes (figure 16 (a)). During the synthesis process the resulting graphene layers or nanoribbons can be functionalized and thus be soluble in organic and aqueous solutions. In 2009 Jiao *et al* used multi-wall carbon nanotubes (MWCNTs) as the starting material for the synthesis of graphene. The MWCNTs were deposited on a Si substrate and coated with PMMA. After treatment with Ar plasma, graphene nanoribbons (GNRs) of 1, 2 or 3 layers were created.[64] Following this strategy several chemical methods were developed for the unzipping of the carbon nanotubes.

A chemical multi-step approach to produce graphene form CNTs contains treatment with sulfuric acid, $KMnO_4$ and H_2O_2 and finally reduction in NH_4OH and hydrazine solution.[65] TEM image of the resulting graphene sheets is presented in the figure 16 (b). The graphene sheets are functionalized with oxide groups, leading to water soluble material. A simpler method of only two steps has been reported by Elias *et al*.[66] Calcined MWCNTs were dispersed in a 1,2 dichloroethane (DCE) organic solution of poly(m-phenylenevinylene-*co*-2,5-dioctoxy-p-phenylenevinylene) (PmPV) by sonication. It has been shown that the calcined MWCNTs under these conditions are unzipped with an efficiency of more than 60%. An ultracentrifugation step is required for the purification of the product, resulting in a solution with ~2% completely open nanotubes. The process of this method is presented in figure 16 (d). Even though it is much faster, compared to other procedures, the yield of the unzipped nanotubes has to be improved. The catalytic cutting of MWCNTs was firstly reported from Elias *et al*. Co or Ni nanoparticles were used to unzip the tubes and graphene sheets and nanoribbons were produced. This method does not include any aggressive treatment and is easy to apply.[67]

Figure 16. (a) Representation of the gradual unzipping of a single wall carbon nanotube to form graphene nanoribbon. (b) TEM images of the synthesis of graphene nanoribbons by chemical treatment of MWCNTs[65] Reproduced with permission from Nature Publishing Group, Copyright 2009 (c) Schematic of the unzipping of CNTs to produce nanoribbons by an Ar plasma etching method[64] Reproduced with permission from Nature Publishing Group, Copyright 2009 (d) Unzipping nanotubes in two steps in gas and liquid phases. Schematic of the procedure and the AFM images of each step.[66] Reproduced with permission from Nature Publishing Group, Copyright 2010
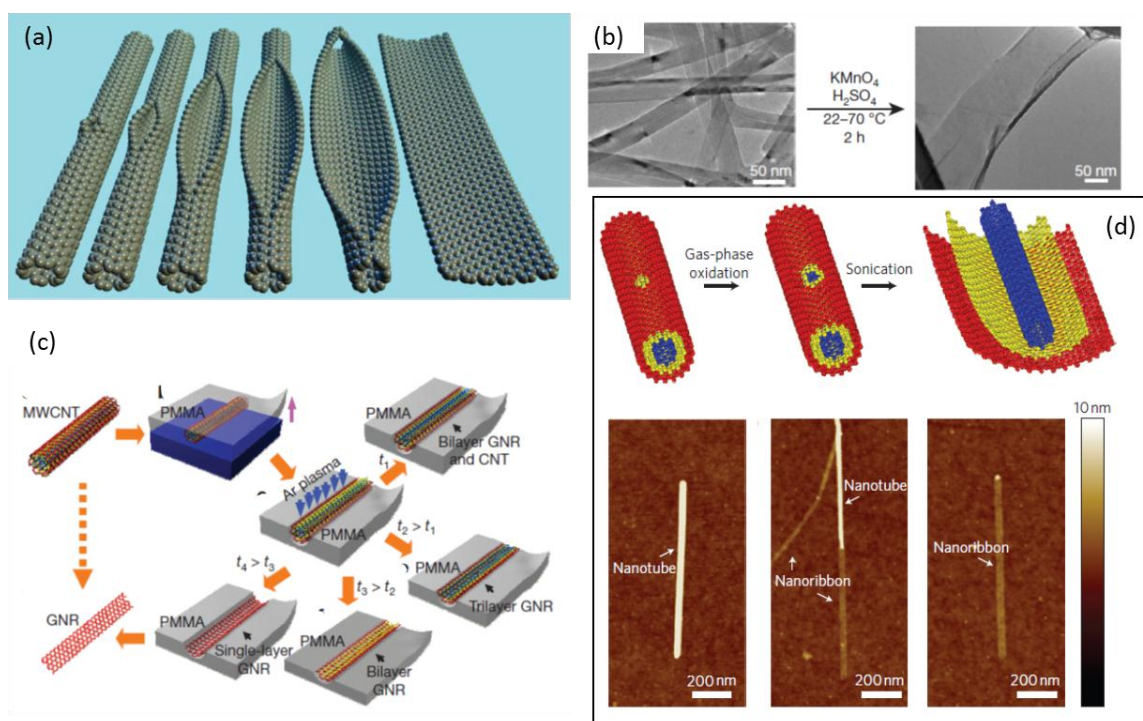
The idea of unzipping CNTs for the synthesis of graphene nanoribbons appears to be extremely powerful in terms of mass production, since the synthesis of CNTs is already well developed in the industry. However, low cost and more efficient methods, with higher yield of graphene nanoribbons still need to be developed.

II.2.2.1.2 Solution processes for graphene synthesis

The first method that was applied to the synthesis of graphene monolayers was **mechanical exfoliation**. In this procedure highly-oriented pyrolitic graphite was used as starting material and was deposited in the form of small cubes (mesas) on a glass substrate. Then, scotch tape was used to repeatedly peel off flakes of graphite from the mesas. The thin flakes after washing processes in water and ultrasound bath in propanol, remained on the surfaces of the solution. Optical, electron-beam and atomic force microscopy were used to determine the substrates containing single layer graphene (figure 17).[42]

Figure 17. (a) Photograph (in simple white light) of multilayer graphene flake deposited on glass substrate (b) AFM image of a single layer graphene (red color in center) 0.8nm height. Reproduced with permission.[42] Reproduced with permission from American Association for the Advancement of Science, Copyright 2004
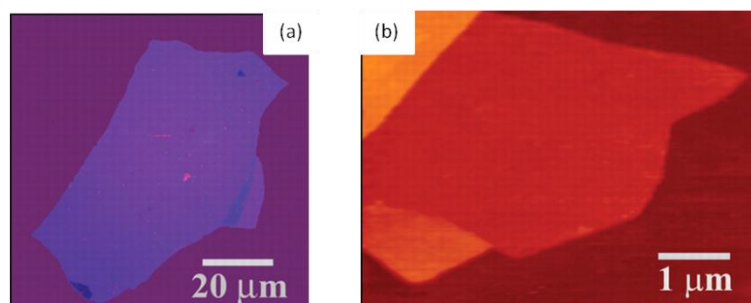
By this method high quality, large and flat graphene flakes have been produced. However, this approach is inapplicable for large-scale production and the size of the flakes can not be controlled.

A similar approach is the **exfoliation** of natural or highly oriented pyrolytic graphite **in the liquid phase**. Several polar and non-polar organic solvents have been tested as dispersant media. The exfoliation process occurs because of the strong interaction between the solvent and the composing layers of graphite. In 2008 Hernandez *et al.* prepared graphene colloids by liquid phase exfoliation of graphite in *N*-methylpyrrolidone (NMP). The dispersion consists of graphenes with a maximum of 5 sheets thickness; the amount of monolayer graphene was around 1% wt. and the concentration was 0.01 mg/ml.[68] A new report on graphene flakes dispersed in NMP manage to increase the concentration at 1.2 mg/ml and the mass of single sheets at 4% by increasing the time of sonication and reducing the power.[69] Low polar solvents were also tested, like *ortho*-dichlorobenzene (ODB), and graphene dispersions of concentration at 0.03 mg/ml were prepared. The thickness of the layers was around 7-10 nm but the advantage of this solvent methodology is the possibility of further covalent functionalization of graphene by alkyl and aryl groups.[70] The main drawback of the exfoliation is the high boiling temperature during the sonication process, which makes the use of organic solvents difficult.

As an alternative, dispersions of graphene in aqueous media has been proposed, with the help of polymers, aromatic compounds or surfactants as dispersion aids. The dispersion mechanism includes either π-π or carbon–hydrogen interactions between the graphene sheets and the dispersion aids. The aromatic molecule, tetrasodium-1,3,6,8-pyrenetetrasulfonic acid (TPA), has been used to exfoliate graphite in graphene sheets in aqueous solutions(figure 18 (a, b)).[71] Almost 90% of the graphenes were monolayer, and non-covalent interaction of the graphene surface with the aromatic ring was observed (figure 18 (d)). The charge transfer through π-π interactions of the aromatic compound and the graphene flakes was verified by Raman spectroscopy. Following the same strategy, poly(vinylpyrrolidone) (PVP) was used for the production of high quality graphene flakes and the amount of single one's was 10-20%.[72]

Figure 18. (a) Simulation image of the π-π interactions between the graphene and TPA molecule (b) chemical structure of TPA molecule[71] Reproduced with permission from APS Physics, Copyright 2009 (c) Simulation image of the interactions between graphene and PVP dispersant (d) TEM image of single graphene flakes dispersed by PVP polymer and the corresponding SAED pattern.[72] Reproduced with permission from Elsevier, Copyright 2009
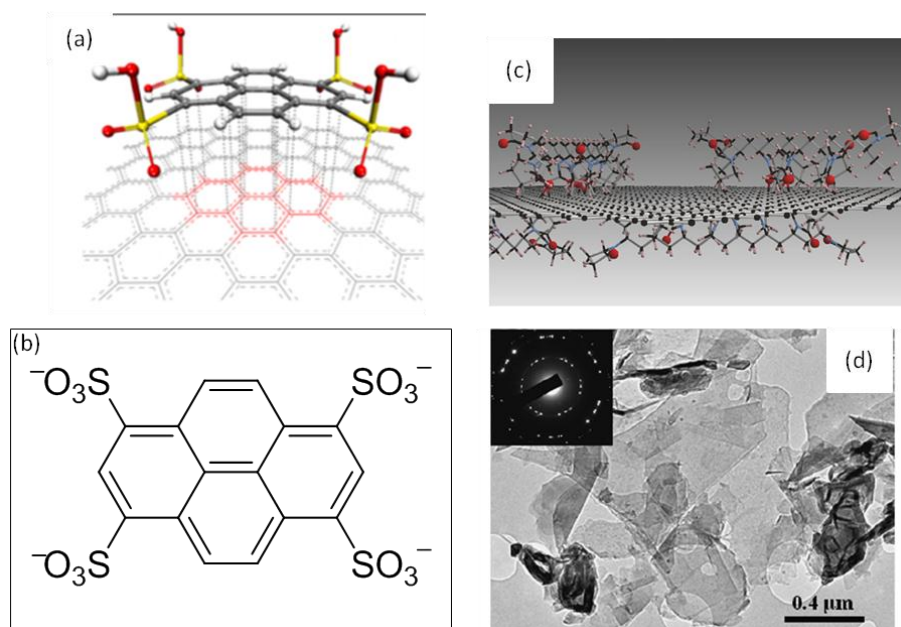
Inspired by the carbon nanotubes dispersions scientists turned to surfactants as dispersant aids in water solutions. Coleman's group has examined different surfactants for dispersion and exfoliation of graphite to graphene. Sodium dodecylbenzene sulfonate (SDBS) in excess was added to a water solution of graphite and the mixture was sonicated.[73] More than 40% of the created graphenes had less than 5 layers and a 3% of them had a single layer. Over time, big flakes precipitated while the small ones stayed dispersed in the solution. Films were able to be made by spray coating vacuum deposition but the electrical properties were not appropriate, probably due to the presence of the surfactant. By the use of sodium cholate as surfactant the concentration in

graphene was increased as well as the percentage of monolayer graphenes.[74] Dispersions with 0.3mg/ml concentration of small-layers graphene were made and up to 20% of them were single.

Another medium that was proposed for liquid phase exfoliation is the ionic liquids (ILs). ILs are organic or partial inorganic salts, liquid at temperature below 100°C, that have the possibility to be polymerized. In 2008, Liu *et al.* reported the preparation of graphite electrochemically functionalized by several ILs, which yielded to functionalized graphene sheets after exfoliation.[75] Electrochemical exfoliation of graphite using ionic liquids has also been reported but the resulting product is a mixture of carbon nanoribbons, nanoparticles and graphene.[76] By sonication of graphite in 1-hexyl-3-methylimidazolium hexafluorophosphate (HMIH) dispersed graphene sheets can be easily obtained, in concentrations up to 5.33 mg/ml.[77] The amount of dispersed graphene sheets depends on the sonication time. Being the IL used for the dispersions can be purified and recycled.

Liquid exfoliation is a promising method for the production of graphenes. The formulation of dispersed graphenes in organic or aqueous solutions allows the film deposition by roll-to-roll techniques, which is an important step for the transparent conductive electrodes. However the graphene solutions made by liquid exfoliation are not homogeneously dispersed (mono-bi-multi layers of graphenes) and the size of the single-layer flakes is small due to the long sonication time. These limitations lead to non-homogenous films, with poor optical properties and high resistivity.

II.2.2.1.3 Reduction of graphene oxide for graphene synthesis

The most popular way of producing graphene in solution, in large scale and with low cost, is by reducing graphene oxide (GO) to graphene. The process commonly followed, with small changes, for the production of GO is the one proposed by W.S. Hummers and R.E. Offeman.[78] The oxidation of graphite to graphitic oxide is made by the use of concentrated water solutions of sulfuric acid, sodium nitrate and potassium permanganate followed by intercalation and exfoliation. GO made by this procedure is a hydrophilic water soluble molecule, while the exact structure has not yet been determined. A proposed structure is presented in figure 19. The

reduction of the GO in graphene is taking place in the presence of hydrazine. During the reduction of the GOs into graphene the flakes lose their hydrophilic character and precipitate. The reduced graphene can not be re-dispersed even by ultrasonication or by surfactants.

Figure 19. A proposed schematic of graphene oxide structure. The hydroxyl groups are mainly located at the ends of the flake.[79] Reproduced with permission from Elsevier, Copyright 1998
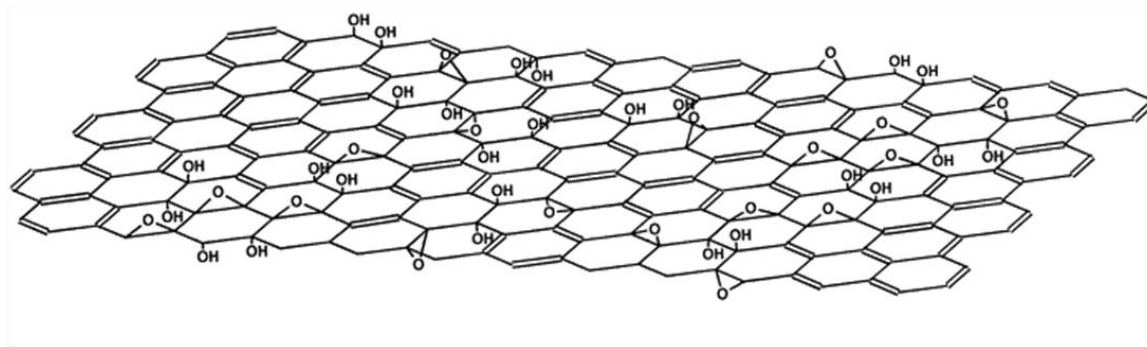
In order to overcome the solubility problems of the reduced graphene, the use of polymers, surfactants, biomolecules or large aromatic compounds has been explored.[80] Here we will report some examples of stabilizers for graphene after the reduction process. The first report of stable aqueous dispersion of graphene produced from hydrazine reduction of GO was from Stankovich *et al*. in 2006. In the presence of the anionic polymer poly(styrene sulfonate sodium salt) PSSNa, the graphene sheets remain dispersed in the solution creating a stable colloid system. In this case, the graphene flakes are covered from both sides with the polymer and the interactions between them are due to hydrophobic attraction. Following the same strategy, nafion polymer was used for stabilizing graphene in water solution.[81] Nafion has a beneficial effect on the conductivity properties of the films prepared from the colloidal dispersions: sheet resistance as low as 30 kΩ/sq for a transmittance of 80% at 550 nm was measured, which is much lower than for other graphene films obtained by chemical reduction.

Several groups have been investigating the dispersion of graphene stabilized by aromatic molecules and polymers through π-π interactions. These aromatic compounds could help, not only

the stability of the dispersion, but also, they could influence the electronic properties of graphene due to the charge transfer between the components. Pyrene moieties are known to have strong affinity with the surface of the graphene through π-π stacking. Stable aqueous dispersion of graphene with a pyrene derivative, 1-pyrenebutyrate (PB⁻), as stabilizer has been reported.[82] On the basis of this dispersion, a large flexible film was made by filtration, with conductivity of 2.10^2 S/m. Other pyrene based aromatic molecule used as stabilizer for graphene dispersions made from RGO, is the 1,3,6,8,-pyrenetetrasulfonic acid (TPA).[83] H.Liu *et al.* managed to disperse graphene flakes, made from chemical reduction of GO, with a water soluble aromatic electroactive dye, the methylene green (MG).[84] The non-covalent interaction between the graphene and the MG did not only provide the solubility of the nanocomposite in the solution but also endows the graphene sheet with good electrochemical properties and electrocatalytic activity toward oxidation reaction.

A new approach was presented from X. Feng and K. Müllen by the use of large aromatic donor and acceptor molecules as dispersants of graphene.[85] This combination gives rise to a new category of graphene composites with high electronic properties. Pyrene-1-sulfonic acid sodium salt (PyS) was chosen as an electron donor and the diasodium salt of 3,4,9,10-perylenetracarboxylic diimide bis-benzenesulfonic acid (PDI) as an acceptor. Both of them have large aromatic structure so the π-π interactions with the graphene sheets are suspected to be strong. In addition the negative charges of these molecules will help in the stabilization of the dispersed graphenes.

The reduction of the graphene oxide to graphene is a low cost approach for graphene production on a large scale and consequently the most favored. However, the drawback of this method is that, during the reduction, sp^2 carbon bonds are destroyed leading to sp^3 carbon. These lattice vacancies can not be repaired, affecting the electrical properties of the graphenes by reducing the conductivity and the carrier mobility.[86]

II.2.2.1.4 Transparent conductive thin films based on graphene

As already mentioned graphene sheets are an excellent candidate for next generation transparent electrodes, due to the high electrical conductivity, the low absorption and the thermal stability. For the first time, K.Müllen and *coll.* studied transparent conductive graphene film as transparent electrode.[87] In order to obtain ultra thin graphene films, first GO sheets were deposited by dip coating on hydrophilic substrate followed by thermal reduction. The thickness of the films was about 10 nm and exhibit high conductivity of 550 S/cm for a transparency above 70% (1000 nm $< \lambda <$ 3000 nm). The films show good electrical and optical features along with low roughness and good thermal stability. Following the same procedure for the formation of graphene films, studies about the reduction conditions were published. The temperature of the reduction as well as the different chemical treatments can change the transmittance and the conductivity values of the resulting films.[88,89]

In order to control the number of graphene flakes, casting by vacuum filtration was proposed (figure 20 (a)). By controlling the volume of the filtered dispersion, the thickness, the transparency and the number of the graphene layers can be regulated.[90] Graphene films in large scale were coated by roll-to-roll procedure, and the performance as transparent electrode was investigated.[91] The production process involves a CVD deposition of the graphene film on a copper foil, and by the use of roll-to-roll technology the film was transferred on PET film, as shown in figure 20(b). Film up to 30-inch were fabricated by that method, and various transmittance and conductivities were achieved depending on the number of the graphene layers and the doping state, with, as best result, a four-layer p-doped graphene with 90% transparency and sheet resistance at 30 Ω/sq (figure 20(c)).

Films made out of solutions of reduced graphenes in the presence of molecules or polymers have been also reported. Graphene sheets stabilized by pyrene based donor-acceptor molecules PyS/PDI were deposited on substrates and the effect of the thermal annealing was examined.[85] The conductivity of the films is increasing with the annealing temperature, with best performance of 1314 S/cm for the graphene/PyS system. This electrode was further tested as anode in bulk-heterojunction solar cell, yielding to a power efficiency of 1.12% in comparison to 0.78% for the

graphene electrode. In another study, graphene flakes stabilized with PEDOT:PSS in aqueous solution were filtered under vacuum in order to form films, which were further transferred on PET or quartz surfaces. The sheet resistance of these formulations on quartz substrate is 27.3 kΩ/sq at a transparency of 81% (at 550 nm) and after doping with $SOCl_2$ dropped to 2.3 kΩ/sq without serious change at the optical properties.

Figure 20. (a) Graphene solution made by reduced GO, cast by filtration (left) and then transferred on glass (middle) and PET (right) substrate[90] (b) Schematic of the roll-to-roll production of graphene films grown on Cu substrate and then transferred-printed to the targeted substrate (c) Photos of the roll-to-roll production of graphene films. Left column from the top to the bottom: Synthesis of graphene by CVD on Cu foil, roll-to-roll transfer of graphene on PET surface and the resulting film. Right column: screen printing process, the flexible touch screen and a graphene-based touch screen connected to a computer with control software.[91] Reproduced with permission from Nature Publishing Group, Copyright 2010
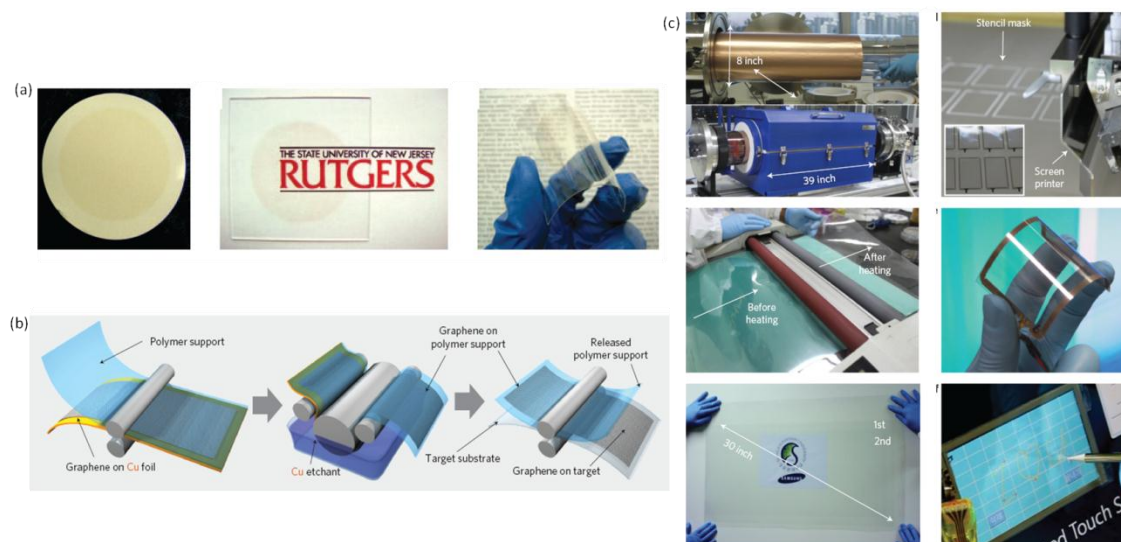
It is obvious that graphene will play an important role in the field of organic electronics. The mechanical and thermal stability as well as the electrical and optical properties make it a popular and promising candidate for the new generation of transparent electrodes. Though, there are several issues which should be solved before graphene electrodes become a commercial transparent electrode. A synthesis process resulting in high yield monolayer graphenes and in parallel remaining low cost and easily applicable must be discovered. In addition more efforts in the formulation of graphene solution will lead to better graphene film formations.

II.2.2.2 Carbon nanotubes

Carbon nanotubes (CNTs) can be considered as sheets of graphene bent into a cylindrical shape and their diameter is at the nanometer scale. They are one dimension materials with high aspect ratio (more than 1000). Depending on the synthesis process, CNTs exist as single-walled CNTs (SWCNTs) and multi-walled CNTs (MWCNTs). In the electron micrograph images (figure 21) the different number of the nanotubes walls can be clearly seen. SWCNTs consist of one graphene layer rolled in a cylindrical form and the MWCNTs consist of two or more graphene layers arranged around a central hollow with Van der Walls forces between the layers.

In order to specify the atomic structure of the nanotubes, the term of tube chirality (or helicity) has been usedand it is defined by the chiral vector, $\vec{C}_h$, and the chiral angle, θ (figure 23). The chiral vector is defined by the following equation:

$$\overrightarrow{C_h} = n\vec{a}_1 + m\vec{a}_2$$

The integers (n,m) are the number of steps along the carbon bonds of the hexagonal lattice and the $\vec{a}_1$ and $\vec{a}_2$ are the unit vectors of the graphene in real space.[92] Depending on the chiral angle θ related to the twisting of the graphene sheet, three chiralities of the tubes can be defined: armchair, zigzag and chiral. The structures of the nanotubes with the different chiralities are presented in the figure 21.When the chiral angle is 0° then the m integer is equal to 0 and the nanotubes are called "zigzag". In the case that the integers have the same value, n=m, the chiral angle is 30° and the nanotubes called "armchair". For all the other combinations of integers and chiral angles, the nanotubes are called "chiral".

The chirality of the nanotubes has a serious influence on their electrical properties. For a certain n,m chirality of the nanotube, if (2n+m) is a multiple of 3 then the tube is called metallic due to the electrical properties that it develops. Alternatively the nanotubes are called semiconducting, and their electrical properties are similar to a semiconductor. If no chiral angle is preferred during the synthesis of CNTs, there should be twice as many semiconducting tubes as metallic. From the chiral vector, one can also calculate the diameter of the nanotubes since the inter-atomic spacing of the carbon atoms is known. In the figure 21 a chirality map is presented displaying also the diameter of each of the SWCNT structure.

Figure 21. (a) Electron micrographs MWCNTs with different number of layers as observed form Ijima[41] Reproduced with permission from Nature Publishing Group, Copyright 1991 (b) Schematic graph showing the chiral vector, and the different roll up chiralities[93] Reproduced with permission from Elsevier, Copyright 2010 (c) Chirality map displaying the average standard potentials associated to each of the SWNT structures[94] Reproduced with permission from ACS Publications, Copyright 2008 (d) Lattice structures for ideal zigzag (12,0), chiral (8,6) and armchair (8,8) tubes from the left to the right respectively.
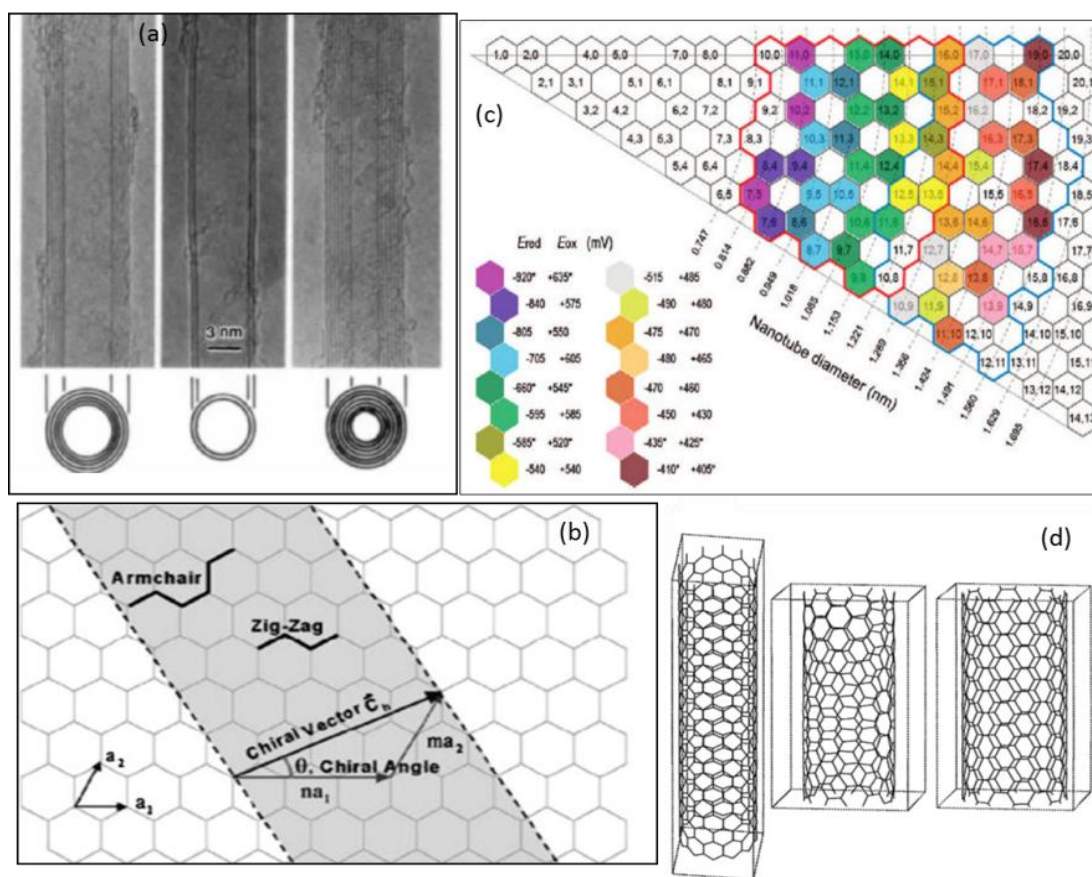
II.2.2.2.1 Synthesis of Carbon nanotubes

Since carbon nanotubes started to attract the interest of the scientists and the industries, several methods of production of carbon nanotubes have been developed. These procedures can be divided in two categories: physical and chemical. The physical processes are based on the physical principles of carbon conversion into nanotubes. In this group are included the arc discharge, which was one of the oldest methods, and the laser ablation which was first discovered in 1995 at Rice University.[95] The chemical processes are based on gas-phase techniques where the tubes are formed by decomposition of a carbon-containing gas and the main representative is the CVD method.

The synthesis of CNTs has been exclusively described [96] and we will refer to the most important synthetic routes. The arc discharge technique was utilized by Iijima to produce new type of carbon structures in a way similar to the ones used for the production of fullerenes.[41] The principal of the arc discharge method is based on the deposition of charged carbon vapor on a cathode electrode in the presence of a catalyst. The analytical process has been described in several publications and books.[97,98] By this method high quality nanotubes can be synthesized in high yield. The main drawbacks are that it is an expensive and complicated procedure.

The laser ablation process is also based on the formation of carbon vapor. For that reason laser power is used to strike at graphite in high temperature conditions. The nanotubes made by this method form bundles of 10-20 nm while their length is up to 100 μm. The diameter and the length of the nanotubes can be controlled by varying several parameters of the process.[98] The carbon nanotubes that are produced by this method are characterized as high quality, due to their perfect carbon structure and their excellent electrical and optical properties. However, the cost of this procedure is very high.

In general the physical processes suffer from three main drawbacks: the large amount of energy that is needed (which increases also the cost), the difficulty of supplying large amounts of solid carbon/graphite for the large production of nanotubes and the purification process that is required for the removal of side products.

The chemical methods for the synthesis of CNTs are based on the chemical vapor deposition (CVD) technique. Two variations of this method were developed: the HiPco by Nikolaev *et al*[99], where high pressure was used, and the CoMoCAT by Resasco *et al*[100] with the use of two catalysts (Co and Mo) in CO gases. The diameter of the nanotubes depends on the size of the catalyst particles on which the nanotubes are built on, while the deposition technique can affect the electrical properties of the tubes. Plasma assisted CVD has been developed for production of vertically grown carbon nanotubes. The CVD method is easy to apply, since the reaction reactor is common and the raw materials are readily available in the form of gases. In addition good yields of high quality CNTs are produced with relatively low cost. Of course there are lot of improvements that needed to made, especially in the purity and the price of the tubes, but the CVD is currently the most promising solution.

The advantages and the drawbacks of both the physical and chemical procedures are summarized in table 2. As a conclusion we remark that the CVD method is the most promising for large production of CNTs, but the price of the pure CNTs remains high. The main issue of the nanotubes production concerns their impurities (amorphous carbon, catalysts) that remain in the product after the synthetic procedure. In addition, during the synthesis of CNTs in large scale, the diameter and chirality of the nanotubes can not be controlled. New synthetic and purification methods are required as CNTs are becoming a necessary material for the organic electronics.

Table2. Comparison of the main characteristics for the different processes of CNTs synthesis.

Characteristics	Synthetic processes		
	Arc-discharge	**Laser ablation**	**Chemical vapor deposition**
Raw materials availability	Difficult	Difficult	Easy
Energy requirement	High	High	Moderate
Process	Difficult	Difficult	Easy and it can be automated
Reactor design	Difficult	Difficult	Easy and it can be design for large production
Purity of the product / purification	High/ require refining	High/ require refining	Good/ No extensive refining required
Process nature/ Yield	Batch type/ 70%	Batch type/ 85%	Continuous: 95%
Cost per unit	High	High	Low

II.2.2.2.2 Electrical and mechanical properties of Carbon nanotubes

The electrical and mechanical properties of individually grown SWCNTs have been widely studied. As we already mentioned the chirality of the tubes plays an important role on their electrical properties since it is responsible for the metal or semi-conducting character of the carbon nanotubes.[101] The metallic nanotubes have the same electronic band as the metals, making them highly conductive (up to 400000 S.cm^{-1}) while the semiconducting carbon nanotubes show the

electronic character of a semi-conductor. It has been also reported that each single wall nanotube with different geometry exhibits unique electrical properties.[102] Regarding the optical properties of the two types of CNTs, the metallic ones have low transmittance, like the metals, but the semi-conductive nanotubes can result in transparent films. Regarding the field of transparent conductive electrodes, the semiconducting carbon nanotubes are favorable since they can form conductive and transparent thin films.

During the synthesis of CNTs a mixture of metallic and semi-conducting nanotubes are produced. For the separation of the two types several methods have been proposed, including physical and chemical methods. Electrophoresis and density gradient have been employed for the separation of the nanotubes.[103] The chemical methods include covalent and non-covalent functionalization such as adsorption of metals,[104] anion, aromatic molecules[105] and polymers.[105] These approaches are always limited in the yield of the separated nanotubes and they can only be applied on small scale samples.

The CNTs that are commonly used in the research are a mixture semi-conductive and metallic tubes, in the form of a random network. Thin films made out of these networks show a semiconductor-metal transition which depends on the thickness of the films.[106] When the density of the thin CNT films is close to the percolation threshold they present semiconductor behavior, which is favorable for applications in transistors and sensors.[107] For film thickness between 10-100 nm the CNTs films are highly transparent and the electrical conductivity values are satisfying enough for use as electrodes in organic electronic devices.[108]

In addition to the impressive electrical properties of the CNTs, individually or in a mixture, they also have specific mechanical properties. With diameter size of few nanometers and length up to several μm, CNTs are considered as materials with high aspect ratio. The strength of the nanotubes is a result from the covalent sp^2 bonds formed between the carbon atoms. Both theoretical and experimental calculations result in a Young's modulus E_p= 1040 GPa for the SWCNTs,[109,110] and for the MWCNTs from E_p= 1080 GPa up to 1800GPa in some theoretical approaches.[111,112] For comparison, steel has a Young's modulus of ≈200 GPa with a three times higher density.

Carbon nanomaterials are difficult to handle since the as-produced CNTs are not soluble in any organic solvent or aqueous solution. In order to be used as transparent conductive electrodes

their formulation in inks is necessary. Therefore the dispersion of the CNTs in organic and aqueous media is one of the primary areas of research. Several solutions have been proposed involving either the chemical treatment of the nanotubes or the use of dispersion aids like surfactant, polymers etc.

II.2.2.3   Dispersion of Carbon nanotubes

The dispersion of the CNTs is an extremely difficult procedure due to the strong Van der Waals interactions that keep the tubes stacked together in the form of large bundles.[113] In addition there are several factors that should be considered when these dispersions are used for the formation of conductive transparent thin films: (1) the dispersion procedure should not influence the CNTs quality and properties, (2) the nanotubes ink should be stable over time and with high dispersion degree (3) the possibility to remove the dispersion aids if they affect the optical and electrical properties of the films.

There has been an enormous effort in the development of the best dispersion aid for the CNTs. Here we will focus in three general categories of dispersion aids which have been mostly investigated, focusing on the electrical and optical properties of the formed inks. The first way of ink formulation is the direct dispersion in several organic solvents, either with the help of small molecules or through the functionalization of the CNTs. An alternative method, which allows the dispersion in organic and aqueous media, is by chemical functionalization of the CNTs. Last, CNTs can be dispersed in both organic and water solution by non-covalent interactions with several type of molecules and polymers/copolymers.

II.2.2.3.1   Direct dispersion of Carbon nanotubes in organic solvents

CNT dispersions in organic solvents were proposed as an ink formation method, since after the film formation and the solvent evaporation there is not any undesired material left. This technique

was tested for both as-fabricated CNTs and for post functionalized nanotubes. The dispersion is taking place under sonication and there are at least two competitive forces involved, the van der Wals forces that keep the tubes in bundles and the interactions between the CNTs and the solvent. For that reason the scientists used different parameters to characterize the solubility properties of CNTs in the organic solvents. The individual Hansen parameters were used at the beginning, since they provide information regarding the origin of the interaction between the solvent and the solute.[114] This way of calculation was rejected later because it does not include other parameters that influence the dispersion like the time of sonication, and replaced by the Hildebrand solubility parameter, which provides a numerical estimation of the intermolecular attractive force which must be overcome in the dispersion process.[115]

Cheng *et al.* who also report the comparison of the two parameters, studied dispersion properties of several organic solvents. The maximum concentration of dispersed SWCNTs was ~ 0.02 mg/ml in the following organic solvents: dimethylformamide (DMF), 1,2 dichlorobenzene (o-DCB) and N-methyl-2-pyrrolidone (NMP).[116] DMF and NMP are solvents that have been widely used to make solutions with CNTs (figure 22). An explanation for the good dispersion properties of these two solvents is that they are Lewis bases but not hydrogen donors.[117] In low CNTs concentration (0.01mg/mL) the dispersion in NMP is so good that up to 70% of the nanotubes are individually dispersed.[118] The diameter of the nanotubes is a parameter that influences the concentration of the dispersed nanotubes in the organic solvents. For small carbon nanotubes (diameter ~0.7 nm) dispersions in o-DCB (95 mg/L), chloroform (31 mg/L), 1-methylnaphthalene (25 mg/L), NMP (10 mg/L) were made by sonication and the concentration of the dispersed tubes was higher than for SWCNTs with bigger diameters.[119]

In order to increase the purity of the dispersed carbon nanotubes in amide solvents, Furtado *et al* study the effects of the chemical treatment of the nanotubes. For the removal of the catalyst particles and the amorphous carbon, which are left from the synthesis of the nanotubes, an initial dry oxidation step is followed by the metal removal by acid treatment with acids like HCl, HNO_3 or HCl/H_2SO_4. The post treated CNTs are then sonicated in NMP and DMF, and high yield dispersions were observed.[120,121] However, the tubes tried by acid, are functionalized by covalent agents, so the electrical properties of the SWCNTs are deteriorated.

Even though the dispersion of CNTs in organic solvent seems an easy and efficient method, it has several drawbacks. The CNTs concentrations that can be dispersed is very low and not suitable for applications in organic electronics. In addition the stability of the inks is very low for all the organic solvents that have been tested. All efforts that have been made in order to increase the amount of the nanotubes in the dispersion compromise the covalent modification of the surface of the CNTs, tainting their electrical structure.

II.2.2.3.2   *Dispersion of chemically functionalized Carbon nanotubes*

A different technique for the dispersion of CNTs in both organic and aqueous media is through chemical functionalization of the side walls of the tubes. This method includes chemical covalent bonding of the CNTs with the dispersant, which can be simple molecules, (co)polymers, or biomolecules. However, the functionalization of the sidewalls by covalent bonds is not straightforward due to the low reactivity of the nanotubes, their low solubility in common solvents and their bundle super-structure. For these reasons highly reactive agents should be used in order to successfully obtain functionalized CNTs.

One of the first reactions tested on the CNTs was the fluorination in continuation to the chemical modification of graphite. The reaction takes place on well dried CNTs in the presence of fluorine gas at different temperatures (300K-523K).[122] Better functionalization of the nanotubes has been observed at higher temperatures since the graphitic network can be relatively decomposed. The fluorinated CNTs were used as initial material for further functionalization reactions. Substitution of the fluorinated groups can be achieved leading to various functional groups were introduced. The fluorinated groups were replaced by alkyl reagents and the resulted alkylated CNTs were dispersed in common organic solvents.[123]

Alkylidene diamines were also used as functional groups of CNTs, after a nucleophilic substitution reaction of fluorinated CNTs. The presence of amino groups on the surface of the nanotubes provides their solubility in dilute acids and water, and with further modifications could be used to bind various biomolecules to the sidewalls of the CNTs.[124] Even though fluorination of CNTs is an easy method for functionalization of the tubes and the fluorinated groups can react with several other molecules, it has been reported that the CNTs lose their conductivity properties after modification and this behavior remains even after the removal of the functional groups.[125] These results indicate that this approach cannot be used for CNT dispersions targeting applications in organic electronics.

Prato *and coll* developed a new functionalization methodology, which can be applied for both multi and single wall carbon nanotubes.[126] The CNTs are suspended in DMF and the functionalization is achieved through a cycloaddition reaction. The functionalized CNTs are soluble at high concentrations (~50 mg/mL) in almost all of organic solvent and in water, without sonication. The good solubility results are related to the big amount of functional groups per nanotube. Different functional groups have been added by this method, creating modified CNTs for several applications.[127]

As we had mentioned before, the purification procedure of the CNTs involves oxidation reactions with acids. This treatment induces the opening of the nanotube cups but also the creation of holes on the surface of the tubes. In place of these defects, carboxylic groups are present these functions were consequently exploited by the scientists for further functionalization reactions. The first attempt was made with long alkylamine chains via acylation reaction. The resulted CNTs were soluble in organic solvents and for first time well characterized.[128] It was shown that, the solubility properties of the tubes depend on the length of the functional chains.[129] Numerous reactions have been investigated using the carboxylic groups of the CNTs, like esterification, amidation, acylation etc; and functionalized nanotubes with different solubility properties and targeting several applications were synthesized.[130]

Here we just mentioned some examples of the covalent functionalization of the nanotubes with dispersing agents. An comprehensive review on this topic was published in 2006 by Prato *et co*.[130]

II.2.2.3.3   *Dispersion of Carbon nanotubes by covalent functionalization with polymers*

The covalent reaction of the carbon nanotubes with polymers has been investigated, as the long chains of the polymers can help in the dispersion of the CNTs even at a low degree of functionalization. There are two main methodologies for the covalent modification of the CNTs by polymers. The "grafting to" approach involves the synthesis of a polymer with a certain molecular weight terminated with a reactive group or radical precursor. The polymer then is attached on the surface of the CNTs by a chemical reaction. In comparison, the "grafting from" approach involves the direct growing of the polymer chain from the surface of the nanotubes via *in situ* polymerization of monomers initiated by chemical species immobilized on the CNT sidewalls.

II.2.2.3.3.1   *Functionalization of CNTs by "grafting to" method*

Several copolymers have been used for the functionalization of both single and multi wall carbon nanotubes. The common functional groups of the CNTs for the "grafting to" method are the carboxylic and amino groups, and the copolymers are grafted by ester and amide linkages. The oxidized CNTs contain carboxylic and hydroxyl groups that can be easily reacted with polymers with similar functions by esterification reaction. For example poly(vinylalcohol) (PVA) was grafted by carbodiimide activated esterification reaction to multi and single wall CNTs functionalized with carboxylic groups (see figure 23 (a)).[131] The modified CNTs were soluble in the same solvents as PVA (DMSO, H_2O) as well as in the PVA polymer matrix. Homogenous thin films were casted from these dispersions.

Water soluble single wall CNTs were made by grafting poly(aminobenzene sulfonic acid) (PABS) and poly(ethylene glycol) (PEG) on the acyl chloride functional groups of the tubes.[132] The ratio CNTs/PABS is 30% and CNTs/PEG is 70%, while the water solubility is about 5 mg/mL. Grafting reactions of acyl chloride MWCNTs with hydroxyl terminated poly(methyl methacrylate) (PMMA) and copolymer PMMA with 2-hydroxyethyl methacrylate (HEMA) were carried out in different solvents and temperatures.[133]

Since it is not possible to functionalize all the polymers with carboxylic groups the solution of copolymers was proposed. The copolymers are consisting of one polymer which contains the proper functionality in order to react with nanotubes and the other block is chosen for the solubility properties. Following this strategy hydroxyl-MWCNTs were modified with styrene-maleic anhydride (SMA) copolymer, with the maleic part being grafted on the tubes.[134]

Besides, in order to increase the reactivity of the surface of the modified CNTs, the carboxylic ends can be further functionalized in thionyl chloride and acyl chloride; allowing larger variety of polymers to be grafted. Hydroxyl terminated poly(styrene) (PS) and poly(ethylene oxide) (PEO) were covalently grafted on thionyl chloride functionalized MWCNTs, and the resulting nanotubes were soluble in common organic solvents.[135] Copolymers of the 4-(4'-vinylphenyl)-3-oxabutanol) with PS and poly(*N*-vinyl carbazole) (PVK), have been reported as grafting agents of acyl chloride SWCNTs. The reaction methodology is presented in the figure 22 (b). In both cases the nanotubes were dispersed in organic solvents and they were fully characterized.[136] [137]

Figure 22. (a) "Grafting to" reaction of carboxyl functionalized SWCNTs with PVA polymer and the HRTEM image (scale 10nm) of the SWCNT-g-PVA system. The surface of the nanotube is covered with an amorphous material possibly PVA[131] Reproduced with permission from American Chemical Society, Copyright 2003 (b) "Grafting to" reaction for the synthesis of CNT-*g*-(PVK-*co*-PVO) and the SEM image (scale 200nm) of the dispersed nanotubes in THF.[137] Reproduced with permission from Elsevier, Copyright 2005.
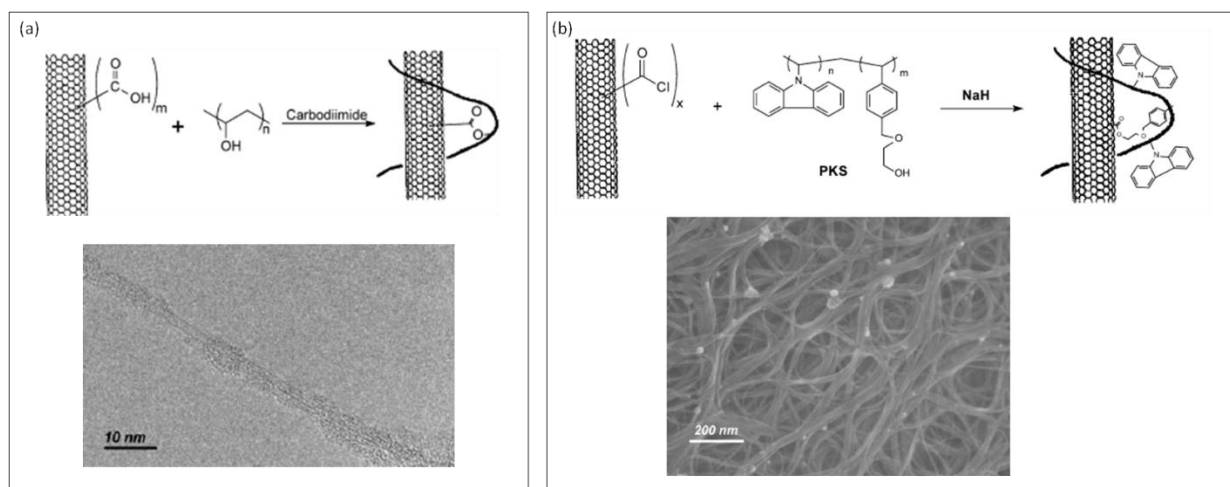
Copolymers can also react with the oxidized CNTs by creating amide linkages. Poly(propionylethylenimine-*co*-etherimide) (PPEI-EI) was grafted to acyl-activated CNTs by heating or by the presence of carbodiimides. The amount of polymer on the surface of the tubes was ~30% for the acylation-amidation method and ~40% for the heating method, and the grafted tubes were soluble in organic media. Amino terminated polymers, like PEO and PEG have been successfully grafted on oxidized CNTs while keeping good solubility.[138] Other ways for grafting polymers on the CNTs are by radical mechanism, nucleophilic addition/coupling and by cycloaddition.

II.2.2.3.3.2   Functionalization of CNTs by "grafting from" method

The "grafting from" approach is involving the polymerization of monomers from surface-derived initiators on both MW and SW carbon nanotubes. The initiators are covalently attached on the surface of the nanotubes by chemical methods that have been developed for the functionalization of small molecules. All the known polymerization mechanisms can be applied in the grafting from method. Here we will give some examples of each one, without covering all existing references. The molecular weight of the grafted polymers cannot be characterized by the usual methods, so only the amount of the polymer on the tubes can be determined by TGA analysis.

Yao *et al* functionalized SWCNTs with phenol groups by cycloaddition reaction followed by the addition of 2-bromoisobutyryl bromide.[139] The attached groups on the walls of the nanotubes are initiators for atom transfer radical polymerization (ATRP). The functionalization reaction of the nanotubes for the synthesis of ATRP initiators is presented in the figure 23 (a).The monomers methyl methacrylate and *tert*-butyl acrylate were polymerized on the surface of the functionalized tubes. The resulting polymers, PMMA and P(*t*BuA), had high molecular weights and large dispersities as a result of the non-controlled polymerization. The SWCNTs-*g*-PMMA were not soluble while the SWCNTs-*g*-P(*t*BuA) were soluble in organic solvent and after acidic hydrolysis the nanotubes were functionalized with poly(acrylic acid) (PAA) providing solubility in aqueous solutions. Following the same procedure MWCNTs were grafted with anionic polyelectrolytes, i.e PAA and PSS, resulting in the formation of core-shell nanostructures (figure 23 (b)). The polyelectrolytes were the brush like or hairy shell and the MWCNT the hard backbone, making the system soluble in water.[140]

Figure 23. (a) Functionalization reaction of the surface of CNTs with ATRP initiator[141] Reproduced with permission from Elsevier, Copyright 2010 (b) ATRP "grafting from" polymerization of *t* BA on the surface of SWCNTs and formation of water soluble MWCNT-*g*-PAA.[140] Reproduced with permission from Elsevier, Copyright 2005
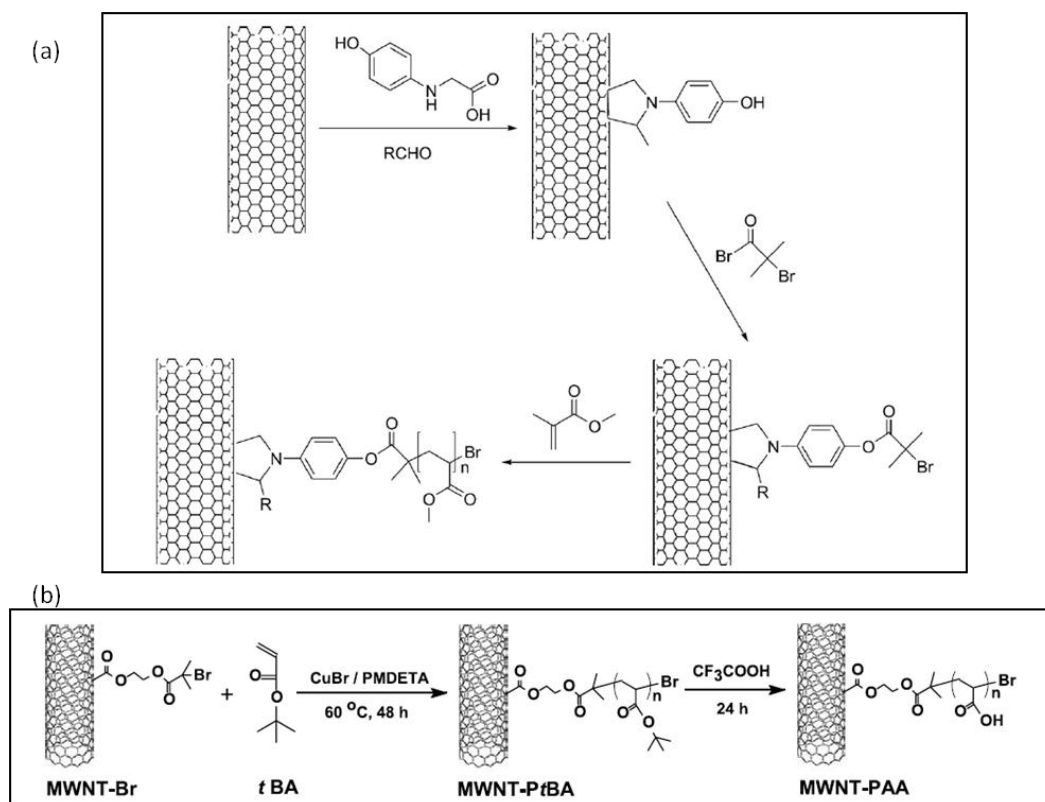
Copolymers were also successfully covalently attached on CNTs by *in situ* "grafting from" method via ATRP polymerization.[142] The typical procedure involves the functionalization of oxidized CNTs with an ATRP initiator, the addition of the first monomer under certain conditions of temperature and time, followed by the addition of second monomer which will be polymerized on the surface of the tubes were there is already the first polymer. In all the published examples of "grafting from" CNTs by ATRP the size of the polymers was tried to be controlled by the amount

of the monomer, the ratio between monomer/initiator and catalyst, the duration of the polymerization and the temperature. It has been noted that the presence of the nanotubes influences the conditions of the ATRP polymerization, leading to a quenching of the polymerization and an increase of the polymer dispersity. In addition, an increase of the glass transition temperature, T_g, of the polymers was observed when they are grafted on the nanotubes.

Styrene and acrylate monomers can be easily polymerized from the MWCNTs sidewalls via reversed addition-fragmentation chain transfer (RAFT) polymerization. Oxidized MWCNTs are functionalized first with an alkyl-bromide end and further reacted with PhC(S)SMgBr moiety, creating a RAFT agent on the surface of the wall of the CNTs. A typically RAFT polymerization involves the MWCNTs-SC(S)Ph dispersed in an organic solvent , the addition of AIBN and the monomer, and the reaction starts when the mixture is heated at certain temperature.[143] Following this route MWCNTs grafted with PS, PAM, PNIPAAM have been synthesized and the created nanostructures were soluble in organic or aqueous solvents.[144] A typical RAFT polymerization on the surface of the nanotubes is presented in the figure 24. Moreover block copolymers have been reported to be grafted on MWCNTs via RAFT polymerization, and the reaction methodology is similar to the ATRP grafted blocks.[145]

The RAFT method was used for grafting water soluble anionic, cationic and zwitterionic polymers on the CNTs. Poly[2-(dimethylamino)ethyl methacrylate] (PDMEMA), PAA and poly[3-(N-(3-methacrylamidopropyl)-N,N-dimethyl) ammoniopropane sulfonate] (PMDMAS) were grafted on MWCNTs providing them with water solubility.[146] In most of the examples above, the size of the synthesized polymer exhibited a linear increase with increasing the polymerization time, indicating the "living" character of the RAFT polymerization. The polymers grafted via RAFT polymerization had a controlled size and better dispersity in comparison to the polymers made by ATRP method.

Figure 24. Schematic of the functionalization of carbon nanotubes with RAFT agent (5) and the "grafting from" RAFT polymerization of NIPAM on the surface of MWCNTs (6). Reproduced with permission. Reproduced with permission from America, Chemical Society, Copyright 2005
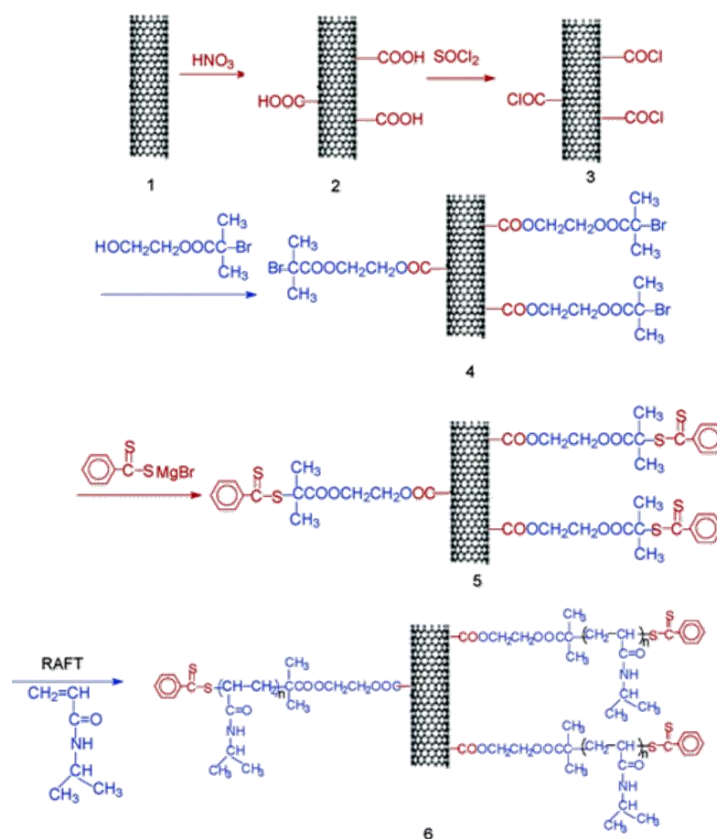
Free radical polymerization is another method for grafting polymers on the surface of carbon nanotubes. During the polymerization, the CNTs are consuming initiator-derived radicals which are added to π-bonds of the carbon network. PMMA, PS, and water soluble PAA and PSSNa have been synthesized by that method and the size of the polymers depends on the reactivity and the amount of the radical initiator.[147]

Viswanathan *et al.* developed the *in situ* anionic polymerization of styrene on modified SWCNTs.[148] Carbanions were introduced on the surface of the tubes that served to exfoliate the

bundles and to provide initiating sites for the polymerization of styrene. A similar method was used for the polymerization of PMMA.[149]

The practical differences in the two techniques for grafting polymers on the CNTs are obvious. In more detail, the "grafting to" method involves well defined polymers, with known molecular weights and dispersities. The size of polymer chain can be also tuned in order to achieve highly soluble systems. However, the initial binding of the polymer chains sterically hinders diffusion of additional macromolecules to the CNTs surface leading to a low grafting density. There is also a limitation with the polymers that can be used, since their functionalization with the suitable groups is not always possible. On the other hand, "grafting from" approach has no steric hindrance limit, allowing high molecular weight polymers to be efficiently grafted. Also, the nanotube-polymer composites deal with a quite high grafting density. However, controlled polymerization by this method is not easy and it requires the strict control of the polymerization conditions and the amount of initiator. In addition, polymer chain growth is slow and high molecular weights cannot be easily achieved, decreasing the solubility of the system. For both techniques, "grafting from" and "grafting to", here we reported only the most interesting strategies, emphasizing on the studies that were focusing on the dispersion properties of the CNTs and not to the general modification of them for precise applications. Finally, literature is abundant regarding all the possible covalent functionalization of the CNTs.[141,150,151]

The covalent modification of the walls of CNTs by molecules or polymers in order to be dispersed in organic and aqueous media has been widely studied. These dispersions were stable over time due to the strong chemical bonds of the CNTs with the dispersants. For the dispersions directly in solvents and when small molecules are used as functional groups of the CNTs the concentration of the dispersed tubes is low. The CNT grafted with polymer compounds gave dispersions with high concentrations. The covalent dispersion though deals with a serious disadvantage: it influences the electrical properties of the nanotubes. During the chemical modification of the CNTs, the long range π conjugated character is disrupted, since the carbon are changing from sp^2 to sp^3. As a result, the conductivity of these nanotubes is decreased and the mechanical strength is also influenced. In conclusion the covalent dispersion of CNTs is an

efficient way, but it is not a wise choice if these dispersions will be used in application where high conductivity is required.

II.2.2.4   Dispersion of Carbon nanotubes by non-covalent functionalization

Another approach for dispersing CNTs that does not include chemical modification of their surface is by the establishment of non-covalent interactions between CNTs and molecules or polymers. The dispersion aids should bring two functionalities to the system. Firstly they should be able to interact with the CNTs by Van der Waals forces or by π-π stacking. Besides, they should provide the solubility to the system.

Such double functionamlities can be achieved by the adsorption of amphiphilic molecules, such as surfactants and amphiphilic copolymers or polyaromatic molecules with hydrophilic or hydrophobic groups. The hydrophilic segments of surfactants interact with polar solvent molecules, and the hydrophobic regions can adsorb onto nanotubes, as shown in the figure 25(a). The adsorption of π-conjugated polymers onto the surface of the CNTs with strong π-π interactions leads to the wrapping of the polymer around the nanotube (figure 25(b)).

Figure 25. (a) Schematic representation of the adsorption of surfactants on the surface of CNTs [152] Reproduced with permission from American chemical society, Copyright 2003 (b) schematic representation of the wrapping of a π-conjugated polymer around the CNTs in helical structure.[153] Reproduced with permission from American Institute of Physics, Copyright 2009
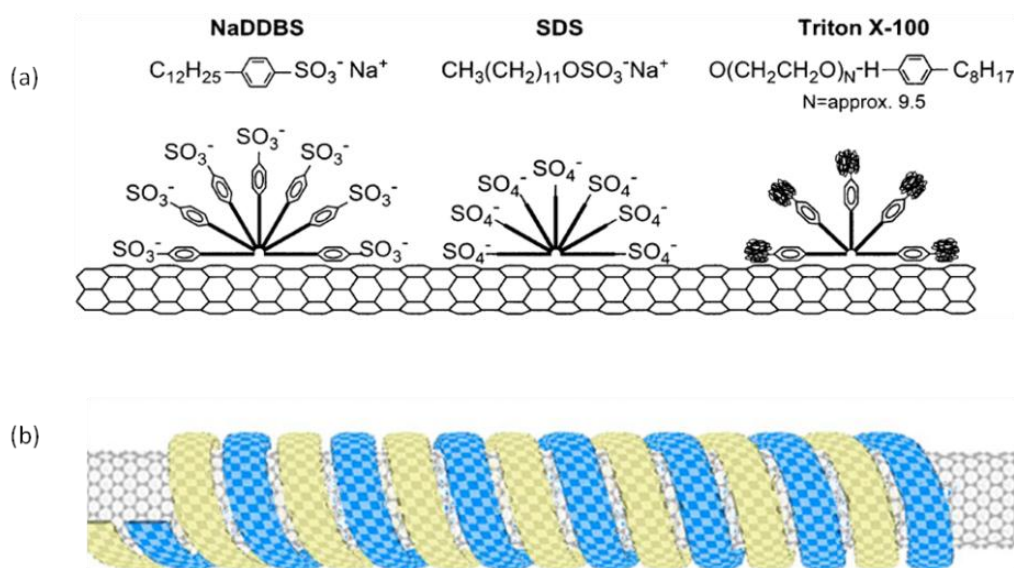
II.2.2.4.1 *Dispersion of Carbon nanotubes by non-covalent functionalization with surfactants*

There are three kinds of surfactants that have been used for the dispersions of the CNTs: anionic caring negative charges in water solutions; cationic which are positively charged in water and neutral which contain no charge in aqueous media. The surfactant aids help in the dispersion of the CNTs by interaction of the hydrophobic end of the surfactant with the surface of the

nanotubes while the hydrophilic part enhances the dispersion of the CNTs in a polar media. The hydrophobic ends create the strongest interactions with tubes when they contain aromatic groups, due to the π-π stacking with the benzyl rings of the CNTs. The hydrophobic group, the length of the hydrophilic part and the surfactant molecular weight influence the dispersion properties. Other parameters which are related with the dispersion of the CNTs by the surfactants are the supramolecular organization of these amphiphilic agents, the pH of the solutions and the dispersion conditions (temperature, sonication time).

Several comparative studies investigated the different parameters that influence the dispersion properties. As already mentioned, the surfactants in solutions may self-assemble and form micelles that occur only above the critical micelle concentration (CMC). It is believed that efficient dispersions of CNTs are taking place at surfactant concentrations above the CMC.[154] Among surfactants, sodium dodecyl sulfate (SDS) and sodium dodecyl-benzene sulfate (SDBS or NaDDBS) are the most widely studied and are often used as references for comparing the properties of new surfactants. A recent study on these surfactants concludes that the dispersions of MWCNTs by SDBS are the most efficient.[155] This result was explained by the difference of the structure of the two surfactants, since SDBS has a benzyl ring which is attached on the nanotubes by π-π interactions. The surfactant structure has also an influence in the diameter distribution of the dispersed tubes, since SDBS has an increased affinity for the narrower nanotubes.

Islam *et al.* had previously compared several surfactants of which only the SDS, SDBS and octyl phenol ethoxylate (Triton X-100 or TX100) achieve SWCNTs dispersion.[152] The concentrations of the surfactants were above the CMC, and dispersing capabilities were for SDS ≤ 0.1 mg/ml, TX100 ≤ 0.5 mg/mL while SDBS was again superior with dispersed nanotube concentrations up to 20 mg/ml. The better dispersing capability of SDBS against the TX100 can also be explained by the electrostatic repulsion of the sulfuric acid group which leads to the charged stabilization of the

tubes. The stability of the dispersions over time was tested for the SDBS surfactant, and no aggregations nor sedimentation were observed after three months. The effect of the dispersion conditions were also examined, by comparing two techniques for the three surfactants. The same SWCNTs were dispersed by high power tip-sonicator and by bath sonication, and the diameter and the length of the nanotubes were measured before and after dispersion. As it is known the long nanotubes can break when high energy from the sonication is applied. This phenomenon was observed for the dispersions under tip-sonication but not for the bath sonicated tubes.

The same group reports a model of hemi-micelles that sheath the surface of the nanotubes to explain the dispersion of CNTs by the surfactants. Following this model, the alkyl chain of the surfactants lies flat on the surface of the tubes. If this model is correct, the size of the alkyl chain plays an important role in the dispersion. Even though there are plenty of studies on the characterization of the CNTs dispersions with surfactants aids there is no clear answer about how the surfactants are assembled on the surface of the tubes. For example the aggregate morphology of dispersions with SDS result in different shapes for different SDS concentrations and SDS/CNT ratios.

The get some insight in the mechanism explaining the dispersion of CNTs by surfactant, an interesting simulation study has been made by Wang *and coll* concerning the demanding energy and the minimum amount of SDS for the dispersion of two nanotubes, taking in account also the assembly of the surfactant around the tube.[156]

Besides, based on the good dispersion capability of the NaDDBS, plenty of studies have been made investigating all the parameters that influence the CNTs dispersion. The nature of the interactions between the NaDDBS and SWCNTs was determined to be hydrophobic, as analyzed by adsorption isotherms.

The pH also influenced the dispersion only for pH values far from the points of zero charge (5.5 < pH < 7). The adsorption studies also showed that the surfactant creates a monolayer around the tube and based on this conclusion the minimum amount of NaDDBS needed for dispersion can be calculated. Notably, this amount can be below the CMC therefore the formation of micelles is not necessary for a stable dispersion.[157,158].

The ζ-potential is a good measure of the colloidal stability and the scientists have used it to evaluate the ability of the surfactants to stabilize the CNTs. This electrokinetic potential is the difference between the dispersion medium and the stationary layer or fluid. The dispersions of SWCNTs with several anionic, cationic and neutral surfactants have been examined with ζ-potential measurements.[159] From the theory of colloid systems it is known that particles with zeta potential less than -25 mV and more than 25 mV are expected to be stable from electrostatic considerations. Typical examples of the zeta-potential values for the surfactants that we have been already mentioned are: TX100 = -23 mV, NaDDBS = -68 mV and SDS = -70 mV. The zeta potential distribution for several surfactants is presented in the figure 26 (a). The most interesting conclusion of these studies is that the ζ-potential distribution can be tuned by changing the surfactant concentration and the length of the alkyl chain of the anionic alkyl sulfate surfactants.[160] SDS molecules with different lengths of alkyl chains were used as models for the dispersion of SWCNTs. The results from the zeta-potential analysis showed that the SDS with 10 carbons length had higher negative value than the surfactants with 12 and 14 carbons resulted in more stable dispersions. In addition the increase of the concentration of SDS in the dispersion leads to the absolute decrease of the zeta-potential (more stable dispersion) and to the increase of the conductivity (figure 26 (b)).

Figure 26. (a) The zeta potential distribution curves for individual SWCNT dispersed by several surfactants (b) The influence of the SDS concentration to the conductivity and the stability of the dispersion.[160] Reproduced with permission from American Chemical Society, Copyright 2007.
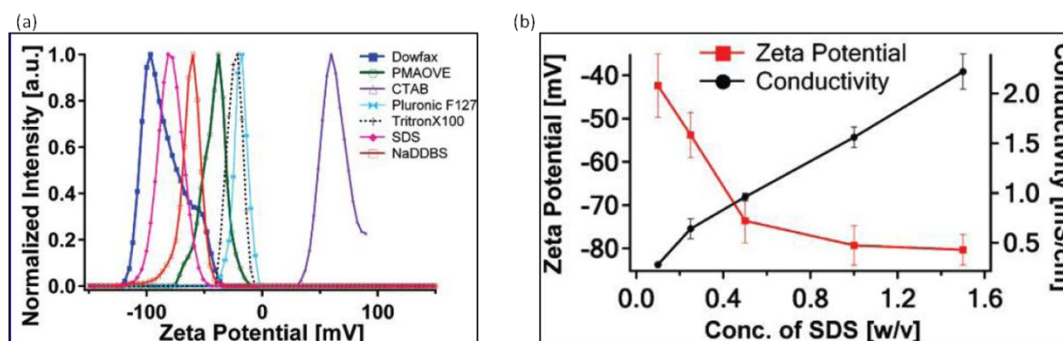
Biomolecules and ionic liquids (ILs) have also been examined as non-covalent dispersants of CNTs. Peptides and enzymes are attractive molecules since they consist of aromatic groups that can interact with the nanotubes and hydrophilic parts that can help to the dispersion.[161,162] These dispersions are very important for applications were the interface between biological systems and carbon nanomaterials is requested. In the same concept, ionic liquids have been investigated as dispersant of CNTs. The length of the alkyl chain of the ILs can be easily controlled and an aromatic hydrophobic part is present. Carbazole-tailed amphiphilic imidazolium ILs and Gemini type ILs have successfully disperse both single and multi wall carbon nanotubes.[163,164]

In conclusion the use of surfactants as dispersants for CNTs resulted in stable dispersions over time with high concentrations of nanotubes and well separated individual CNTs. One of the great advantages of the surfactants is obtained when these dispersions are used for film fabrications. Indeed the surfactant can be removed from the films by simply dipping in water solutions, leaving mostly percolated nanotubes on the films. The rinsing of the dispersant from the

films is responsible for the increase of the conductivity without affecting the transmittance, an important property for applications in organic electronics. The non covalent interactions of the surfactants with the nanotubes are an additional advantage over the dispersion methods described above, making them the ideal dispersant. A way to ameliorate the dispersion capability of the surfactants is by synthesizing longer hydrophilic tails. It has been reported that polymers or surfactants with long hydrophilic groups have better capability on dispersing CNTs and to isolate individual nanotubes.

II.2.2.5 *Dispersion of Carbon nanotubes by non-covalent functionalization with polymers*

Polymers are an excellent dispersant of CNTs in both organic and aqueous media. The long polymer chains provide better and more stable dispersion of CNTs in comparison to the molecular surfactants. The type of polymers that can disperse CNTs are divided in three categories: the polyelectrolytes which interact with the surface of the nanotubes via cation-π interactions, the linear polymers which create CH-π interplays and the π-conjugated polymers which absorb on the surface of the tubes by π-π interactions. Several examples have been reported for numerous polymers as well as copolymers. The assemblies of polymers around the dispersed CNTs are either linear or helical. When the polymer has a helical structure on the surface of the CNTs, it is called "wrapping" of the tubes. Depending on the use of the CNT dispersion the suitable polymer should be chosen. Apart the dispersion media, polymers can provide additional mechanical, optical and electrical properties to the nanotube dispersion for several targeted applications.

II.2.2.5.1 Linear polymers as dispersants of CNTs

Non-covalent functionalization of single wall and multi wall CNTs have been achieved with several linear homopolymers. The adsorption of these polymers on the surface of the nanotubes is occurring from molecular interactions between the carbon-hydrogen (CH) groups of the polymers and the π benzyl rings of the nanotubes backbone. Although these interactions are weak (only one-tenth of the hydrogen bond) they are enough for the dispersion of the CNTs due to their large number.

Baskaran *et al.* studied the dispersion capability of five different linear polymers with MWCNTs, in organic solvents.[165] Poly(butadiene), poly(isoprene), PMMA, PS, and poly(ethylene oxide) (PEO) resulted in stable MWCNTs dispersions for dilute $CHCl_3$ solutions. The amount of nanotubes that could be dispersed was increased by raising the temperature of the solutions. The CNTs dispersions with poly(butadiene) and PMMA were studied by Infrared (IR) and Raman spectroscopies in order to confirm the presence of CH-π interactions. Indeed, in IR spectra, small shifts of the CH stretching vibration were observed, due to the interactions of the polymer with the CNTs. In addition, in the Raman spectra of the MWCNTs, the G-band peak is shifted for the dispersed nanotubes, and the shift is related to the amount of the polymer in the solution. These two results indicate the existence of the weak interactions between the linear polymers and the CNTs.

Dispersions based on PEO polymers were not stable over time. Amphiphilic macromolecules of siloxane polyether copolymer (PSPEO) were examined as dispersant for MWCNTs in aqueous solutions.[166] The dispersions were stable for more than three months, due to the additional hydrophobic interactions between the polymer and the CNTs. Dispersion of MWCNTs in water solution was achieved by non covalent interactions with the polyvinyl pyrrolidone (PVP) polymer.[167] These dispersions were compared with water dispersions of chemically functionalized MWCNTs with carboxylic groups. Hydrophobicity, size distribution and zeta potential were the methods used for characterizing the quality and the stability of both dispersions. The dispersions made by non-covalent interactions of MWCNTs and the PVP polymer were found to contain more individual nanotubes and no aggregates were formed over time. In addition, these dispersions were influenced by the addition of certain electrolytes (the dispersions were stable for shorter time) in comparison to the covalently functionalized nanotubes. PVP had been also studied earlier by Smalley *and coll.*, and they demonstrated that the possible assembly of the polymer around

SWCNTs with chirality of (8,8) is wrapping either in double or triple helix.[168] In addition the presence of the polymer is uniform and strong along the sides of the tubes and for that reason, an excess of the polymer it is not needed for good dispersions.

Even though the linear polymers were successfully used for the dispersion of the CNTs there are several drawbacks in these dispersions. The carbon-hydrogen interactions between the polymers and the nanotubes are not strong enough and leads to stability problems. In addition the linear polymers are not conductive, so they create an insulating environment around the nanotubes. This will decrease the conductivity of the system since it is blocking the percolation of the CNTs.

II.2.2.5.2   *Polyelectrolytes as dispersants of CNTs*

Polyelectrolytes, such as PSS and quaternized poly(allylamine), have been used as dispersant aids for CNTs. The charges that surround the nanotubes, when polyelectrolytes are wrapping them, provide good water solubility. Besides the tubes can not re-aggregate since the charges keep them apart due to electrostatic impulsions. In addition the charge functionalities can be used for the creation of organized films, the fabrication of layer by layer nanostructures, and to carry bio-based molecules or metals. The ionic conductivity that is created from the presence of the polyelectrolyte is also an important aspect for the electrical properties of the CNTs dispersions.

SWCNTs were dispersed in acidic water solution in the presence of poly(allylamine) (PAL).[169] The polyelectrolyte self-assembled around the tubes by ionic-π interactions and the concentration of dispersed nanotubes was high (figure 29). Similarly PSS in the acid form was used for the dispersion of MWCNTs. Hong *et al.* used these dispersions for transistor electrodes.[170] Non covalent functionalized MWCNTs by poly(diallyldimethylammonium chloride) (PPDA) were dispersed in water solutions. The positive charges on the surfaces of the nanotubes were used for the *in situ* deposition and formation of platinum nanoparticles.[171]

Zhu *et al*. used the layer by layer deposition of dispersed SWCNTs for the formation of new transparent electrodes.[172] The CNTs were dispersed in the presence of the sulfonated poly(etheretherketone) (SPEEK), which not only stabilize the nanotubes in the solution but also "dopes" the SWCNTs. The doping is based on the electron transfer from valence bands of nanotubes to unoccupied level of SPEEK through the π-π interactions. For the layer by layer depositions, the hydroxyethyl cellulose was used as an intermediate material. The architecture of these films is presented in the figure 27. The surface resistivity of this system is 920 Ω/sq and transmittance of 86.7% at 550nm. Apart the good electrical and optical properties of this system, the most interesting observation concern the π-doping of the CNTs by the dispersing polymers. Until now doping of CNTs has been reported with the use of several acids but the stability over time of these films was not satisfying. Polymers could be better dopants since there is a continued electron exchange between them and the CNTs.

Figure 27. (a) Schematic of the dispersion SWCNT by poly(allylamine) (PAL) polyelectrolyte[169] Reproduced with permission from Wiley and Sons, Copyright 2007 (b) Ideal architecture of the LBL films and the chemical structure of the hydroethyl cellulose (HOCS), poly(etheretherketone) (PEEK), SPPEK/CNTs.[172] Reproduced with permission from American Chemical Society, Copyright 2011
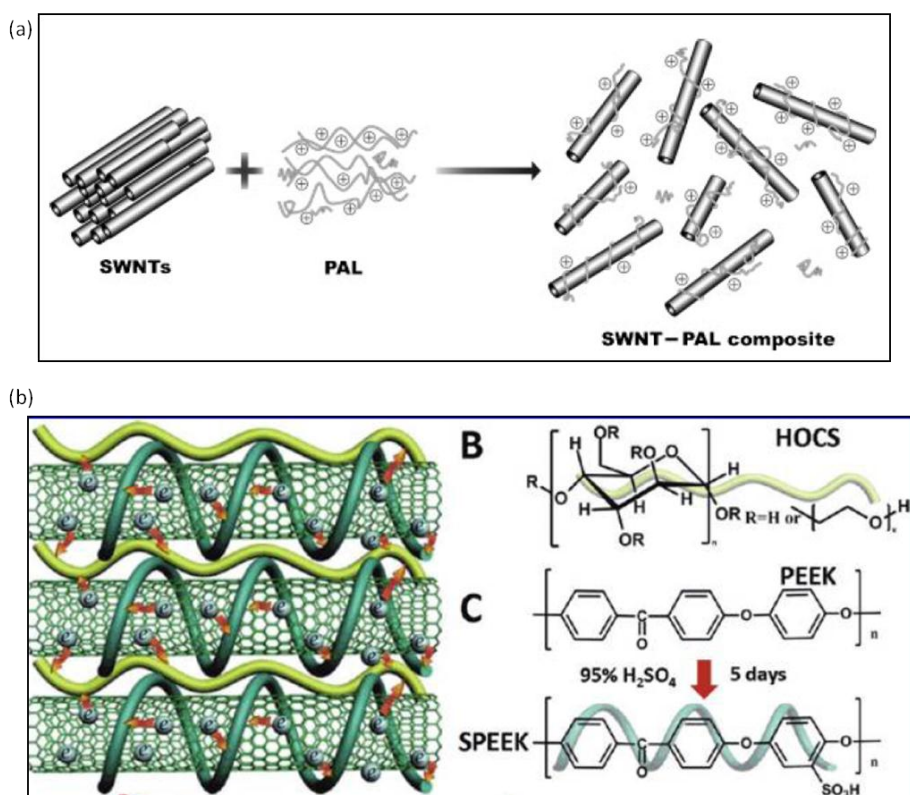
In conclusion by the use of polyelectrolytes as dispersion aids, carbon nanotube dispersion in aqueous media can be achieved. In addition the charges around the CNTs help in the stability of the dispersion as well as the film formation. Some drawbacks of the polyelectrolytes as dispersants for the CNTs are their por electrical properties and the weak interactions developed with the tubes. The combination of the polyelectrolytes with a segment which will be strongly attached on the nanotubes could improve the CNT dispersions as well as add an electronic functionality.

II.2.2.5.3   *π-conjugated polymers as dispersants of CNTs*

Among all the types of polymers for the dispersion of CNTs, the most widely studied are the π-conjugated polymers. These polymers are adsorbed on the surface of the CNTs by π-π interactions, which are stronger than all the other types of interactions between the polymers and nanotubes. Due to those interactions the inter-tube Van der Wall bonds are becoming weaker and that the nanotubes are highly dispersed. Since the fact that the π-conjugated polymers are semi-conductors and they have the possibility to be doped, CNTs covered by conjugated polymers are expected to show enhanced electrical properties, and to find applications in organic electronics.

One of the first π-conjugated polymers that was tested as dispersant of CNTs was poly (metaphenylenevinylene) (PmPV).[173] The SWCNTs were dispersed in organic solvents, and they were characterized by UV-vis and ^{1}H NMR spectroscopy. The characteristic peaks in the UV-vis spectra of the PmPV were broaded for the solution of PmPV/SWCNTs, as a result of the π-π interactions between them. Similar conclusions were obtained from ^{1}H NMR analysis. Polyimides were also screened for dispersion of CNTs, targeting stable dispersions over time. An interesting example is the 2,6-bis(3-aminophenoxy) benzonitrile/ dianhydride, 4,4-oxydiphthalic anhydride ((β-CN)APB/ODPA) polyimide polymer due to the presence of nitrile functionalized aromatic moieties, which are known as good electron acceptors.[174] Based on IR spectra and RAMAN spectra, it has been proved that the SWCNTs are stabilized by way of a donor/acceptor interaction between the tubes and the polymer.

In another study, dispersion of SWCNTs into various alcohols was achieved by using poly(4-vinylpyridine) (P4VP) as a dispersing agent.[175] The ratio P4VP/SWCNTs was fixed at 2/1 and several solution concentrations were tested. The high dispersion was visualized by Scanning Electron Micrograph (SEM) and the interaction between polymer and CNTs was verified by Raman and UV-vis spectra. Kymakis *et al.* studied the effect of the CNTs concentration on the CNT/conjugated polymer dispersion regarding the conductivity values of the polymer.[176] Poly(3-octylthiophene) (P3OT) has a very low conductivity (10^{-8} S/m) and it is therefore compared to an insulator. Dispersions of SWCNTs stabilized by P3OT were made in chloroform and the weight fraction of CNTs was varied from 1 to 35 %. These dispersions were then casted in films and the

conductivity was measured. As it was expected the conductivity of the film is increasing (up to 0.05 S/m for 30% CNTs) with the amount of CNTs.

In addition two types of CNTs were compared, purified and non-purified, the purified ones showing better electrical properties. This observation can be explained by the absence of catalyst and amorphous carbon in the films of the purified nanotubes. In addition the increase of the temperature on the films seems to affect positively the conductivity. These studies are a good example of the potential abilities that the π-conjugated polymer/ CNTs systems have, and how different parameters can influence the electrical properties and obtain highly conductive films. It is a big challenge to understand and to visualize how the conjugated polymers are adsorbed onto the surface of the nanotubes.

Inspired by the dispersions with the PmPV, Kang *et al.* focused on the assembly of the polymer on the surface of the nanotubes.[177] Water soluble poly[*p*-{2,5-bis(3-propoxysulfonicacid sodium salt)} phenylene] ethynylene (PPES) was used for dispersion of SWCNTs in aqueous media. The conjugated part of this amphiphilic polymer reacts by π-π interactions with the SWCNTs and the alkoxy sulfonate side chains provide water solubility to the system. Even though the polymer has linear orientation, it was proved that it forms a helical superstructure upon associating with the CNTs. In addition, the dispersions were rich in individual dispersed nanotubes, with a percentage around 80%.

It has been observed that certain conjugated polymers create π-interactions only with nanotubes of certain diameters and chiralities, mostly with semi-conducting nanotubes. This leads establishment of methodologies for the separation of the semi-conducting tubes from the metallic ones, resulting in dispersions with higher electrical and optical properties. Gao *et al.* discovered that the poly[9,9-dioctylfluorenyl-2,7-diyl] (PFO) adsorbed on certain SWCNTs in toluene dispersions.[178] The polymer nanotubes interactions are based on the octyl-octyl zipping mechanism and the polymer interacts with nanotubes of certain diameters and chiralities. The diameter affects the coiling of the chains and the carbon-carbon motif of backbones need a certain direction in order to obtain a strong contact. The nanotubes that fulfill these criteria are the semi-conducting ones for dispersions in toluene.

Fluorene-and carbazole-based polymers, were also found to selectively disperse semi-conducting SWCNTs.[179] The dispersions in toluene with these polymers resulted in aromatic π-backbones interacting via their 1,5-positions in order to create a spiral arrangement favorable for certain nanotube diameters. In particular, the fluorene-based polymers dispersed semi-conducting SWCNTs in high concentrations.

One of the most studied family of the π-conjugated polymers, in the field of the organic electronics, is the poly (alkylthiophenes) (PAT), and more specifically the poly(3-hexylthiophene) (P3HT) due to its outstanding electronic and optical properties and the quite good solubility in organic solvents. It has been reported that the thiophene rings of the P3HT interact by π-π stacking with the surface of the CNTs. Upon adsorption, the alkyl chains are orthogonally oriented to the backbone, assisting in the polymer organization. Both experiments and theoretical calculations conclude that the P3HT is helically wrapped onto the CNTs. The angle of the helix of the P3HT polymer depends on the chirality of the tubes that are wrapped.[153]

Based on this preferable wrapping of the CNTs by the P3HT, Bao *and coll.* examine PAT with different length of side alkyl chains. The poly(3-dodecylthiophene) polymer is selectively dispersing semi-conducting SWCNTs in toluene at 50°C.[180] By the use of this type of dispersant, the separation of metallic and semi-conducting nanotubes can be achieved. MWCNTs dispersed by P3HT functionalized with a pyrene unit were compared with chemically functionalized MWCNT/P3HT dispersions in THF. [181] From the films made out of these dispersions, it was observed by microscopy techniques the formation of P3HT fibrils arranged vertically to the nanotubes. These images were similar for the covalent and non-covalent modified CNTs, proving once again that the π-π interactions of the conjugated polymers and the nanotube are very strong and that the covalent bonding of the P3HT on the MWCNTs are not necessary to disperse CNTs.

Dispersions of SWCNTs with P3HT were made in chloroform solution and in different ratios.[182] These solutions were casted in thin films by spin coating techniques and tested as transparent electrodes. In order to increase the conductivity values, a post treatment of the films with $SOCl_2$ was realized. The presence of the $SOCl_2$ affects the nanotubes by doping them, as it has been reported before,[183] and the P3HT by degrading the P3HT of the composite. The films with the best electrical results were made out of dispersion with ratio P3HT/SWCNTs 1/15 and sheet resistance

of about 80 Ω/sq and 72% transmittance at 550 nm. These results are very promising for the conjugated polymer/CNTs systems as replacements of ITO.

In conclusion, stable dispersions were achieved with use of π-conjugated polymers. Even though their use is very promising due to the strong π-π interactions that they develop with the surface of the nanotubes, they have certain limitations. First of all, the π-conjugated polymers are soluble only in organic solvents, so aqueous dispersions are not possible. In addition they also deal with aggregation problems, since they can develop intermolecular π-π interactions, resulting in CNTs dispersions that are not stable over time. The formulation of the π-conjugated polymers with another moiety that will prevent the aggregation will be the one of the most promising system for the CNT dispersion.

II.2.2.5.4   Block copolymers as dispersants of CNTs

Even though the dispersion of CNTs with the use of homopolymers was successful, the use of copolymers seems to be a better option. Indeed, the homopolymers suffer from solubility problems. The polymers that interact with the CNTs by CH-π interactions need to have either high molecular weight or long alkyl chains in order to achieve good solubility and stable dispersibility. Since those polymers are not conductive, their large size could affect the electrical properties of the final dispersions when cast as films due to the presence of insulating polymers between the nanotubes. The π-conjugated homo-polymers suffer both from solubility and miscibility issues, since they have the tendency to aggregate due to the strong inter chain π-π interactions. Thus using a copolymer which could bring multiple functionalities appears to be promising (*i.e* electronic conductivity and water solubility).

Kang and Taton synthesized an amphiphilic block copolymer PS-*b*-PAA for the dispersion of SWCNTs.[184] The dispersion method that they propose is by encapsulation of the SWCNTs in the copolymer micelles. The CNTs and the copolymer were solubilized in DMF where the copolymer does not make micelles. By the slow addition of water they force the self-assembly of

the copolymer, pushing the nanotubes into the hydrophobic core. The chains of the hydrophilic PAA were cross-linked by the addition of a difunctional linker stabilizing therefore the system.

Two different amphiphilic block copolymers based on polyethylene oxide (PEO) were studied as dispersants of SWCNTs and they were compared with dispersions of oxidized SWCNTs.[185] Both PEO-*b*-PPO (PPO= polypropyleneoxide) and PEO-*b*-PE (PE= polyethylene) disperse SWCNTs in water resulting in stable dispersions. The electrical conductivity of the dispersions of the SWCNTs by the polymer were higher by 10 orders of magnitude compared to the oxidized CNTs dispersions, proving once more that the non-covalent dispersion retains the electrical properties of the nanotubes.[186]

One of the advantages in the use of block copolymers for the dispersion of CNTs, is that they can be designed accordingly to the needs of the applications. An example of this possibility is the synthesis of amphiphilic copolymers reported by Park *et al.*[187] Thus different functional groups were grafted onto a poly(acrylic acid) (PAA) backbone: a hydrophobic moiety (alkyl chain or benzyl group) for anchoring onto the CNTs surface, a hydrophilic poly(ethylene glycol) (PEG) for blocking protein adsorption. Meuer *et al.* synthesized block copolymers with one PMMA block and pyrene oligomer block. Oligomers with different number of pyrene units were tested and compared with the PMMA-*b*-P4VP copolymer.[188] With the use of thermogravimetric analysis (TGA), the amount of copolymer on the MWCNTs was quantified. It was found that there is an optimum of pyrene units attached on the CNTs since big anchor block can lead to reduction of the grafting density.

Micelle formations of amphiphilic block copolymers have been used as dispersants of CNTs. The amphiphilic block copolymer PS-*b*-P4VP is soluble in both polar and non-polar solvents, and it self-assemblies in micelles (figure 30). SWCNTs have been successfully dispersed in THF, where the PS corona is selectively adsorbed on the surface of the tubes, and in ethanol by the interactions of the P4VP corona block with the nanotubes.[189] Metal nanoparticles, like silver, can be selectively formed on the P4VP therefore decorating the surface of the SWCNTs (figure 28). The electrical properties of SWCNTs dispersions in toluene were also examined. The PS core is interacting with the tubes, but it was observed that some micelles were "broken" on the surface of the tubes and P4VP was creating π-π stacking. Gold(III) chloride trihydrate (HAuCl$_4$ 3H$_2$O) was used as a doping agent of the P4VP.[190] The sheet resistance of the copolymer alone is at 10^{14} Ω/sq

and it is decreasing at 10^6 Ω/sq by loading 5% of SWCNTs. For the same amount of nanotubes the sheet resistance is at $7 \cdot 10^4$ Ω/sq by adding HAuCl$_4$ 3H$_2$O. Even though conductivity increases with the amount of doping agent the transmittance decreases to lower values.

Figure 28. (a) Schematic of the micelles formed in polar and non-polar solvent of the amphiphilic copolymer PS-*b*-P4VP (b) Left: TEM image of the SWCNTs dispersed by the PS-*b*-P4VP copolymer in toluene. Right: TEM image of the same dispersions after the addition of Ag nano-particles shown as black small spots (diameter 20 nm).[189] Reproduced with permission from American Chemical Society, Copyright 2005
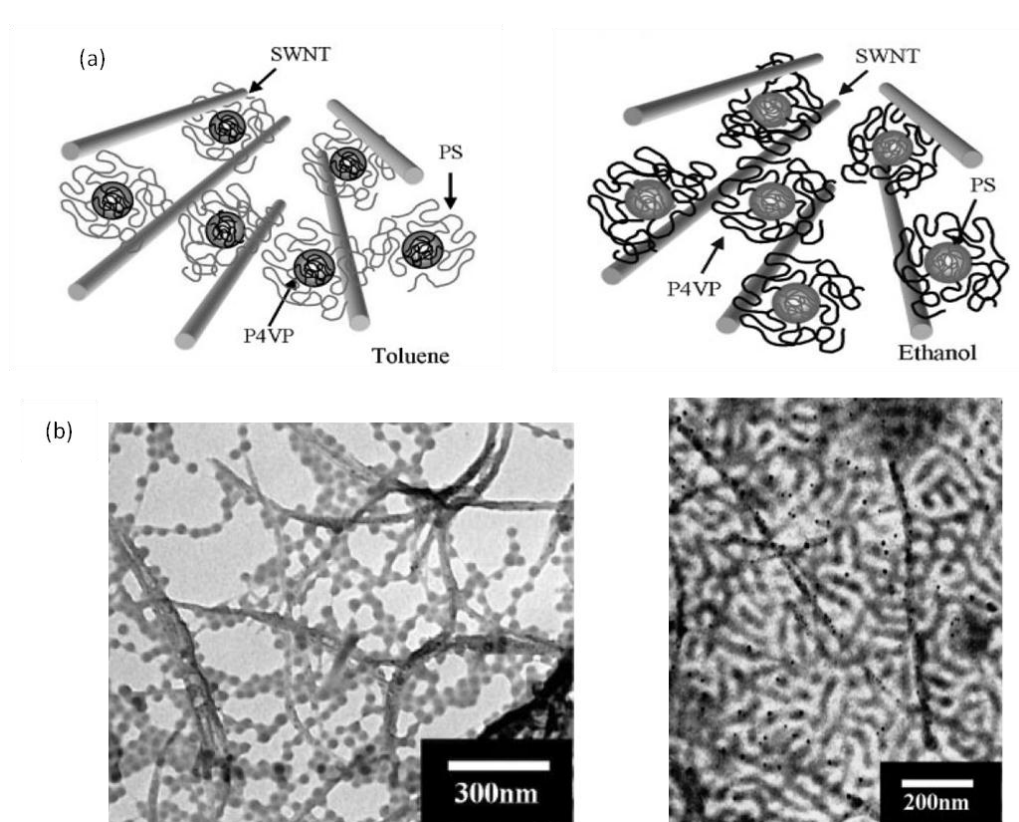
Block copolymers containing a π-conjugated segment have also been used as dispersants of CNTs. The dispersion of the CNTs by this type of copolymers is based on the π-π interactions that the π-conjugated block will develop with the surface of the nanotubes. In this way the dispersions will be more stable and with higher efficiency. In addition, the solubility problems that we report

for the π-conjugated homopolymers are overcome due to their macromolecular design in the form of block copolymers.

Copolymers of poly(*N*-phenyl maleimide) (PPhMI) and PMMA were used as dispersants of SWCNTs in chloroform. Different molecular weights of PPhMI were tested, showing that the long conductive chains lead to less individual tubes and poor dispersions. The long chains of the conjugated polymer, were not completely adsorbed on the surface of the nanotubes, and they were creating intermolecular π-interactions.[191]

Block copolymers with P3HT as the π-conjugated polymer have been synthesized and used as dispersants of CNTs.[192] SWCNTs were dispersed in the presence of the P3HT-*b*-PMMA block copolymers in THF solutions. The stability of these dispersions was compared with dispersions of SWCNTs only with PMMA. The block copolymer/CNTs systems showed better thermal and mechanical stability. P3HT-*b*-PPEG (PPEG= poly(poly(ethylene glycol) methyl ether acrylate) was used for dispersion of MWCNTs in various organic solvents. A shift of the P3HT peak in the UV-vis absorption spectra was observed for the dispersions in chloroform and in methanol. The red shift is due to the aggregation of the P3HT block of the copolymer when it is assembled in poor solvents.

Both single and multi wall carbon nanotubes were dispersed in chloroform by P3HT-*b*-PS copolymer.[193] For the dispersions small amount of copolymer was needed, proving that the high efficiency of the dispersant. The π-π interactions between the P3HT and the nanotubes were followed by UV-vis and Raman spectroscopy. The film properties of these dispersions were also tested and the films were cast by roll-to-roll techniques.[194] The films were highly hydrophobic (water contact angle= 154°-160°, sliding angle < 5°), strong and with good conductivity (30–100 S cm^{-1}).

Several block copolymers have been used for the dispersion of the CNTs in aqueous and organic media. The advantages of using block copolymers for non-covalent dispersions are their solubility and physicochemical properties. In addition, each block can contribute with its own properties and to design a system covering several properties. Besides all these advantages most of the block copolymers are not conductive influencing the conductivity of the dispersion. This is one

of the reasons that π-conjugated block copolymers were investigated for CNTs dispersions. In the family of π-conjugated block copolymers, the P3HT based block copolymers are the most widely studied as dispersants of CNTs. The big advantage of the P3HT is that it is soluble in organic solvents, allowing the controlled synthesis of its block copolymers. In addition it is a semi-conducting polymer and can create strong interactions with the CNTs. The P3HT part is helping to the break up the nanotubes bundles leading to their separation into individual tubes while the second block is keeping the system well dispersed and prevents the re-aggregation.

II.2.2.6   *Challenges in achieving more conductive dispersions*

After exploring the different paths followed for the dispersions of CNTs we can conclude that the use of non-covalent dispersants is mandatory in order to preserve the electrical properties of the nanotubes. Yet, the electrical properties of the CNTs/dispersant composites are influenced from another factor the electrical percolation of the tubes.

Percolation is a statistical concept and it is controlled by thermodynamics. It occurs above a concentration is which a composite of insulating matrix loaded with conductive particles becomes conductive. Numerous studies have been made concerning the electrical percolation of CNTs in polymer composites.[195] In figure 29 different CNTs networks formed in polymeric matrix are presented. It is important to mention that a good dispersion does not always lead to a conductive composite. A low percolation threshold is an important parameter for the dispersions in order to reduce the cost and to facilitate the processing of the composite.

Figure 29. Illustration of the electrically conductive networks of CNTs in polymeric matrix. (a) The CNTs and the polymer are contacting by overlapping configuration (b) CNTs and polymer with an in-plane contact configuration.[196] Reproduced with permission from Elsevier, Copyright 2011.
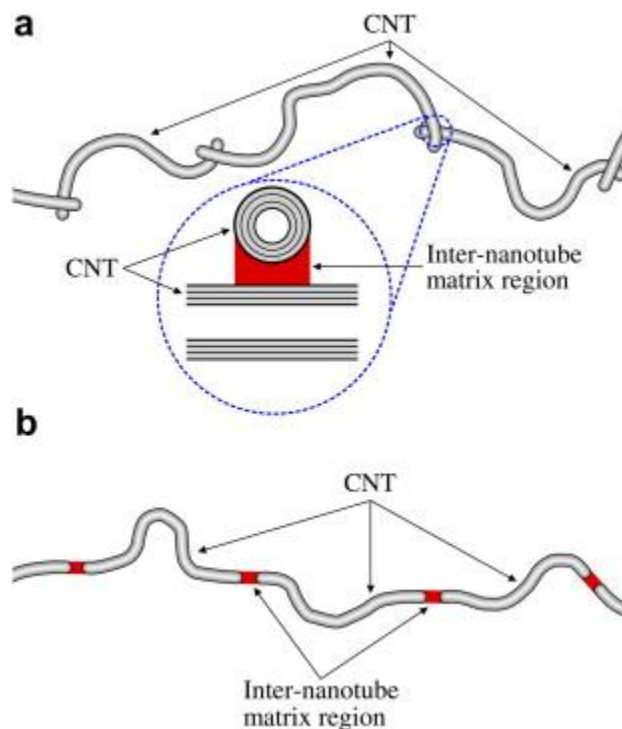
The decrease of the percolation threshold concerns the type of the dispersant. Rod-like particles with big volume, like the polymers, have lower percolation threshold in comparison to surfactant micelles.[197] The polymeric coil chains exhibit a larger excluded volume than the spheres for the same weight. In addition, the length of the nanotube can help to increase the conductivity and to decrease the percolation threshold. The presence of long nanotubes results in the creation of a continuous conductive pathway. For that reason the dispersion process should not affect the length of the nanotubes.

The electrical conductivity of the nanotube network in a polymeric matrix is influenced also by the CNTs/polymer contacts. The creation of a consecutive conductive network can be

achieved by the use of conductive dispersants. By that way, the insulating matrix is reduced and the electrical conductivity of the composite can be increased.[196] Following the theoretical and experimental studies concerning the electrical percolation of the nanotubes/dispersion composites we can conclude that the rod π-conjugated polymers are an ideal dispersant. These polymers can disperse CNTs by non-covalent interaction and, at the same time decrease the percolation threshold of the composite. Even though they suffer from some solubility problems, their design in form of block copolymers allow them to be soluble in organic and aqueous media.

III   Conclusion

In this literature review the main materials that have been tested as replacements of ITO were presented. These materials can be divided in two categories: metal based and carbon based. The metal based materials, like TCO have deposition problems, since no roll-to-roll process can be applied. In addition toxicity and stability issues have been mentioned for this type of material. The deposition of metal by NIL is a promising technique, but it remains a multi-step process increasing its cost. Metal nanoparticles and more specifically metal nanowires are materials which fulfill all the requirements for the TCEs. The high conductivity along with the formulation in solutions make them the most promising candidate as a replacement of ITO. Though, the roughness intence to their deposition as films is a key issue which should be overcome in order to be widely used in the field of organic electronics.

From the carbon based materials, carbon nanotubes and grapheme satisfy all the prerequisites of conductive transparent materials. Graphene is a new and promising material but the problems of synthesis in few layers graphenes in a large scale deters their potentials. Carbon nanotubes can be produced in a large scale, and the synthesis procedures are evolved resulting in more pure and less expensive material. The solubility problem of carbon nanotubes is their only drawback which can be overcome by the use of dispersion aids. The interaction of these aids with the CNTs should be non-covalent in order to preserve their electrical properties.

Consequently π-conjugated polymers, especially in the form of block copolymers, are an ideal dispersant for the CNTS. The mechanism of the dispersion is simple, involving the π-π interaction between the surface of the nanotubes and the π-conjugated part while the other block will provide solubility to the system. The role of the second block is important for the stability of the dispersion and for the type of the media (organic or aqueous) that the system will be dispersed. This kind of formulations can be used for the deposition of flexible transparent conductive films, making them promising candidates for the replacement of ITO.

1.   Internet site/Market watch. 1)   http://www.marketwatch.com/story/organic-electronics-market-will-reach-usd-448-billion-globally-in-2018-transparency-market-research-2012-04-10 (accessed May 2012).

2.   Nanosite Internet site. http://www.nanomarkets.net/index.php/news/article/nanomarkets_issues_new_report_addressing_the_business_case_for_transparent_conductors_ito_and_alternatives (accessed May 2012).

3.   Chopra, K. L.; Major, S.; Pandya, D. K., Transparent conductors—A status review. *Thin Solid Films* **1983,** *102* (1), 1-46.

4.   Nath, P.; Bunshah, R. F., Preparation of In2O3 and tin-doped In2O3 films by a novel activated reactive evaporation technique. *Thin Solid Films* **1980,** *69* (1), 63-68.

5.   On, T. Ineternet site. http://techon.nikkeibp.co.jp/article/HONSHI/20090929/175753/?P=2 (accessed Mat 2012).

6.   Sheng, S.; Fang, G.; Li, C.; Xu, S.; Zhao, X., p-type transparent conducting oxides. *physica status solidi (a)* **2006,** *203* (8), 1891-1900.

7.   Haacke, G., Transparent electrode properties of cadmium stannate. *Appl. Phys. Lett.* **1976,** *28* (10), 622-623.

8.   Furubayashi, Y.; Hitosugi, T.; Yamamoto, Y.; Inaba, K.; Kinoda, G.; Hirose, Y.; Shimada, T.; Hasegawa, T., A transparent metal: Nb-doped anatase TiO[sub 2]. *Appl. Phys. Lett.* **2005,** *86* (25), 252101-3.

9.   Chen, D.-m.; Xu, G.; Miao, L.; Nakao, S.; Jin, P., Sputter deposition and computational study of M-TiO2 (M = Nb, Ta) transparent conducting oxide films. *Surf. Coat. Technol.* **2011,** *206* (5), 1020-1023.

10.   Takeuchi, U.; Chikamatsu, A.; Hitosugi, T.; Kumigashira, H.; Oshima, M.; Hirose, Y.; Shimada, T.; Hasegawa, T., Transport properties and electronic states of anatase Ti[sub 1 - x]W[sub x]O[sub 2] epitaxial thin films. *J. Appl. Phys.* **2010,** *107* (2), 023705-4.

11.   Mohri, S.; Hirose, Y.; Nakao, S.; Yamada, N.; Shimada, T.; Hasegawa, T., Transparent conductivity of fluorine-doped anatase TiO[sub 2] epitaxial thin films. *J. Appl. Phys.* **2012,** *111* (9), 093528-5.

12.   Minami, T., Substitution of transparent conducting oxide thin films for indium tin oxide transparent electrode applications. *Thin Solid Films* **2008,** *516* (7), 1314-1321.

13.   Moriga, T.; Okamoto, T.; Hiruta, K.; Fujiwara, A.; Nakabayashi, I.; Tominaga, K., Structures and Physical Properties of Films Deposited by Simultaneous DC Sputtering of ZnO and In2O3 or ITO Targets. *J. Solid State Chem.* **2000,** *155* (2), 312-319.

14.   Minami, T.; Ida, S.; Miyata, T.; Minamino, Y., Transparent conducting ZnO thin films deposited by vacuum arc plasma evaporation. *Thin Solid Films* **2003,** *445* (2), 268-273.

15.   Minami, T.; Kakumu, T.; Takeda, Y.; Takata, S., Highly transparent and conductive ZnO・In2O3 thin films prepared by d.c. magnetron sputtering. *Thin Solid Films* **1996,** *290–291* (0), 1-5.

16.   Minami, T.; Takeda, Y.; Takata, S.; Kakumu, T., Preparation of transparent conducting In4Sn3O12 thin films by DC magnetron sputtering. *Thin Solid Films* **1997,** *308–309* (0), 13-18.

17.   Shirakata, S.; Sakemi, T.; Awai, K.; Yamamoto, T., Electrical and optical properties of large area Ga-doped ZnO thin films prepared by reactive plasma deposition. *Superlattices Microstruct.* **2006,** *39* (1–4), 218-228.

18.   Giurgola, S.; Rodriguez, A.; Martinez, L.; Vergani, P.; Lucchi, F.; Benchabane, S.; Pruneri, V., Ultra thin nickel transparent electrodes. *J. Mater. Sci.: Mater. Electron.* **2009,** *20* (0), 181-184.

19.   Ghosh, D. S.; Martinez, L.; Giurgola, S.; Vergani, P.; Pruneri, V., Widely transparent electrodes based on ultrathin metals. *Opt. Lett.* **2009,** *34* (3), 325-327.

20.   Stec, H. M.; Williams, R. J.; Jones, T. S.; Hatton, R. A., Ultrathin Transparent Au Electrodes for Organic Photovoltaics Fabricated Using a Mixed Mono-Molecular Nucleation Layer. *Adv. Funct. Mater.* **2011,** *21* (9), 1709-1716.

95

21.   Hatton, R. A.; Willis, M. R.; Chesters, M. A.; Briggs, D., A robust ultrathin, transparent gold electrode tailored for hole injection into organic light-emitting diodes. *J. Mater. Chem.* **2003,** *13* (4), 722-726.

22.   Conoci, S.; Petralia, S.; Samorì, P.; Raymo, F. M.; Di Bella, S.; Sortino, S., Optically Transparent, Ultrathin Pt Films as Versatile Metal Substrates for Molecular Optoelectronics. *Adv. Funct. Mater.* **2006,** *16* (11), 1425-1432.

23.   Guo, L. J., Nanoimprint Lithography: Methods and Material Requirements. *Adv. Mater. (Weinheim, Ger.)* **2007,** *19* (4), 495-513.

24.   Kang, M. G.; Guo, L. J., Nanoimprinted Semitransparent Metal Electrodes and Their Application in Organic Light-Emitting Diodes. *Adv. Mater. (Weinheim, Ger.)* **2007,** *19* (10), 1391-1396.

25.   Kang, M.-G.; Joon Park, H.; Hyun Ahn, S.; Jay Guo, L., Transparent Cu nanowire mesh electrode on flexible substrates fabricated by transfer printing and its application in organic solar cells. *Sol. Energy Mater. Sol. Cells* **2010,** *94* (6), 1179-1184.

26.   Kang, M.-G.; Kim, M.-S.; Kim, J.; Guo, L. J., Organic Solar Cells Using Nanoimprinted Transparent Metal Electrodes. *Adv. Mater. (Weinheim, Ger.)* **2008,** *20* (23), 4408-4413.

27.   Ko, S. H.; Park, I.; Pan, H.; Grigoropoulos, C. P.; Pisano, A. P.; Luscombe, C. K.; Fréchet, J. M. J., Direct Nanoimprinting of Metal Nanoparticles for Nanoscale Electronics Fabrication. *Nano Lett.* **2007,** *7* (7), 1869-1877.

28.   Chia-Meng Chen, C.-W. H., Cheng-Fang Ho, Cheng-Kuo Sung Insertion Structures for Transparent Metal Electrodes Prepared by NIL. http://apex.jsap.jp/link?APEX/5/044202/.

29.   Sun, Y.; Gates, B.; Mayers, B.; Xia, Y., Crystalline Silver Nanowires by Soft Solution Processing. *Nano Lett.* **2002,** *2* (2), 165-168.

30.   Hu, L.; Kim, H. S.; Lee, J.-Y.; Peumans, P.; Cui, Y., Scalable Coating and Properties of Transparent, Flexible, Silver Nanowire Electrodes. *ACS Nano* **2010,** *4* (5), 2955-2963.

31.   De, S.; Higgins, T. M.; Lyons, P. E.; Doherty, E. M.; Nirmalraj, P. N.; Blau, W. J.; Boland, J. J.; Coleman, J. N., Silver Nanowire Networks as Flexible, Transparent, Conducting Films: Extremely High DC to Optical Conductivity Ratios. *ACS Nano* **2009,** *3* (7), 1767-1774.

32.   Morgenstern, F. S. F.; Kabra, D.; Massip, S.; Brenner, T. J. K.; Lyons, P. E.; Coleman, J. N.; Friend, R. H., Ag-nanowire films coated with ZnO nanoparticles as a transparent electrode for solar cells. *Appl. Phys. Lett.* **2011,** *99* (18), 183307-3.

33.   Ajuria, J.; Ugarte, I.; Cambarau, W.; Etxebarria, I.; Tena-Zaera, R.; Pacios, R., Insights on the working principles of flexible and efficient ITO-free organic solar cells based on solution processed Ag nanowire electrodes. *Sol. Energy Mater. Sol. Cells* **2012,** *102* (0), 148-152.

34.   Zeng, X.-Y.; Zhang, Q.-K.; Yu, R.-M.; Lu, C.-Z., A New Transparent Conductor: Silver Nanowire Film Buried at the Surface of a Transparent Polymer. *Adv. Mater. (Weinheim, Ger.)* **2010,** *22* (40), 4484-4488.

35.   Yu, Z.; Zhang, Q.; Li, L.; Chen, Q.; Niu, X.; Liu, J.; Pei, Q., Highly Flexible Silver Nanowire Electrodes for Shape-Memory Polymer Light-Emitting Diodes. *Adv. Mater. (Weinheim, Ger.)* **2011,** *23* (5), 664-668.

36.   Akter, T.; Kim, W. S., Reversibly Stretchable Transparent Conductive Coatings of Spray-Deposited Silver Nanowires. *ACS Appl. Mater. Interfaces* **2012,** *4* (4), 1855-1859.

37.   Bergin, S. M.; Chen, Y.-H.; Rathmell, A. R.; Charbonneau, P.; Li, Z.-Y.; Wiley, B. J., The effect of nanowire length and diameter on the properties of transparent, conducting nanowire films. *Nanoscale* **2012,** *4* (6), 1996-2004.

38.   Wu, H.; Zhang, R.; Liu, X.; Lin, D.; Pan, W., Electrospinning of Fe, Co, and Ni Nanofibers: Synthesis, Assembly, and Magnetic Properties. *Chem. Mater.* **2007,** *19* (14), 3506-3511.

39.   Wu, H.; Hu, L.; Rowell, M. W.; Kong, D.; Cha, J. J.; McDonough, J. R.; Zhu, J.; Yang, Y.; McGehee, M. D.; Cui, Y., Electrospun Metal Nanofiber Webs as High-Performance Transparent Electrode. *Nano Lett.* **2010,** *10* (10), 4242-4248.

40.   Kroto, H. W.; Heath, J. R.; O'Brien, S. C.; Curl, R. F.; Smalley, R. E., C60: Buckminsterfullerene. *Nature* **1985,** *318* (6042), 162-163.

41.   Iijima, S., Helical microtubules of graphitic carbon. *Nature* **1991,** *354* (6348), 56-58.

42.   Novoselov, K. S.; Geim, A. K.; Morozov, S. V.; Jiang, D.; Zhang, Y.; Dubonos, S. V.; Grigorieva, I. V.; Firsov, A. A., Electric Field Effect in Atomically Thin Carbon Films. *Science* **2004,** *306* (5696), 666-669.

43.   Shirakawa, H.; Louis, E. J.; MacDiarmid, A. G.; Chiang, C. K.; Heeger, A. J., Synthesis of electrically conducting organic polymers: halogen derivatives of polyacetylene, (CH). *J. Chem. Soc., Chem. Commun.* **1977,** (16), 578-580.

44.   Chiang, C. K.; Fincher, C. R., Jr.; Park, Y. W.; Heeger, A. J.; Shirakawa, H.; Louis, E. J.; Gau, S. C.; MacDiarmid, A. G., Electrical Conductivity in Doped Polyacetylene. *Phys. Rev. Lett.* **1977,** *39* (17), 1098-1101.

45.   Heeger, A. J., Semiconducting and Metallic Polymers: The Fourth Generation of Polymeric Materials (Nobel Lecture). *Angewandte Chemie International Edition* **2001,** *40* (14), 2591-2611.

46.   Heywang, G.; Jonas, F., Poly(alkylenedioxythiophene)s—new, very stable conducting polymers. *Adv. Mater. (Weinheim, Ger.)* **1992,** *4* (2), 116-118.

47.   (a) Winter, I.; Reese, C.; Hormes, J.; Heywang, G.; Jonas, F., The thermal ageing of poly(3,4-ethylenedioxythiophene). An investigation by X-ray absorption and X-ray photoelectron spectroscopy. *Chem. Phys.* **1995,** *194* (1), 207-213; (b) Nardes, A. M.; Kemerink, M.; de Kok, M. M.; Vinken, E.; Maturova, K.; Janssen, R. A. J., Conductivity, work function, and environmental stability of PEDOT:PSS thin films treated with sorbitol. *Organic Electronics* **2008,** *9* (5), 727-734.

48.   Groenendaal, L.; Jonas, F.; Freitag, D.; Pielartzik, H.; Reynolds, J. R., Poly(3,4-ethylenedioxythiophene) and Its Derivatives: Past, Present, and Future. *Adv. Mater. (Weinheim, Ger.)* **2000,** *12* (7), 481-494.

49.   Cho, C.-K.; Hwang, W.-J.; Eun, K.; Choa, S.-H.; Na, S.-I.; Kim, H.-K., Mechanical flexibility of transparent PEDOT:PSS electrodes prepared by gravure printing for flexible organic solar cells. *Sol. Energy Mater. Sol. Cells* **2011,** *95* (12), 3269-3275.

50.   Kim, J. Y.; Jung, J. H.; Lee, D. E.; Joo, J., Enhancement of electrical conductivity of poly(3,4-ethylenedioxythiophene)/poly(4-styrenesulfonate) by a change of solvents. *Synth. Met.* **2002,** *126* (2–3), 311-316.

51.   Do, H.; Reinhard, M.; Vogeler, H.; Puetz, A.; Klein, M. F. G.; Schabel, W.; Colsmann, A.; Lemmer, U., Polymeric anodes from poly(3,4-ethylenedioxythiophene):poly(styrenesulfonate) for 3.5% efficient organic solar cells. *Thin Solid Films* **2009,** *517* (20), 5900-5902.

52.   Crispin, X.; Jakobsson, F. L. E.; Crispin, A.; Grim, P. C. M.; Andersson, P.; Volodin, A.; van Haesendonck, C.; Van der Auweraer, M.; Salaneck, W. R.; Berggren, M., The Origin of the High Conductivity of Poly(3,4-ethylenedioxythiophene)–Poly(styrenesulfonate) (PEDOT–PSS) Plastic Electrodes. *Chem. Mater.* **2006,** *18* (18), 4354-4360.

53.   Ouyang, J.; Chu, C. W.; Chen, F. C.; Xu, Q.; Yang, Y., High-Conductivity Poly(3,4-ethylenedioxythiophene):Poly(styrene sulfonate) Film and Its Application in Polymer Optoelectronic Devices. *Adv. Funct. Mater.* **2005,** *15* (2), 203-208.

54.   Kim, Y. H.; Sachse, C.; Machala, M. L.; May, C.; Müller-Meskamp, L.; Leo, K., Highly Conductive PEDOT:PSS Electrode with Optimized Solvent and Thermal Post-Treatment for ITO-Free Organic Solar Cells. *Adv. Funct. Mater.* **2011,** *21* (6), 1076-1081.

55.   Xia, Y.; Ouyang, J., Salt-Induced Charge Screening and Significant Conductivity Enhancement of Conducting Poly(3,4-ethylenedioxythiophene):Poly(styrenesulfonate). *Macromolecules* **2009,** *42* (12), 4141-4147.

56.   Xia, Y.; Ouyang, J., Anion effect on salt-induced conductivity enhancement of poly(3,4-ethylenedioxythiophene):poly(styrenesulfonate) films. *Organic Electronics* **2010,** *11* (6), 1129-1135.

57.   Xia, Y.; Zhang, H.; Ouyang, J., Highly conductive PEDOT:PSS films prepared through a treatment with zwitterions and their application in polymer photovoltaic cells. *J. Mater. Chem.* **2010,** *20* (43), 9740-9747.

58.   Xia, Y.; Ouyang, J., Significant Conductivity Enhancement of Conductive Poly(3,4-ethylenedioxythiophene): Poly(styrenesulfonate) Films through a Treatment with Organic Carboxylic Acids and Inorganic Acids. *ACS Appl. Mater. Interfaces* **2010,** *2* (2), 474-483.

59.   Kuzmenko, A. B.; van Heumen, E.; Carbone, F.; van der Marel, D., Universal Optical Conductance of Graphite. *Phys. Rev. Lett.* **2008,** *100* (11), 117401.

60.   Geim, A. K.; Novoselov, K. S., The rise of graphene. *Nat. Mater.* **2007,** *6* (3), 183-191.

61.   Kumar, S.; McEvoy, N.; Lutz, T.; Keeley, G. P.; Nicolosi, V.; Murray, C. P.; Blau, W. J.; Duesberg, G. S., Gas phase controlled deposition of high quality large-area graphene films. *Chem. Commun. (Cambridge, U. K.)* **2010,** *46* (9), 1422-1424.

62.   Cai, W.; Zhu, Y.; Li, X.; Piner, R. D.; Ruoff, R. S., Large area few-layer graphene/graphite films as transparent thin conducting electrodes. *Appl. Phys. Lett.* **2009,** *95* (12), 123115.

63.   Kim, K. S.; Zhao, Y.; Jang, H.; Lee, S. Y.; Kim, J. M.; Kim, K. S.; Ahn, J.-H.; Kim, P.; Choi, J.-Y.; Hong, B. H., Large-scale pattern growth of graphene films for stretchable transparent electrodes. *Nature* **2009,** *457* (7230), 706-710.

64.   Jiao, L.; Zhang, L.; Wang, X.; Diankov, G.; Dai, H., Narrow graphene nanoribbons from carbon nanotubes. *Nature* **2009,** *458* (7240), 877-880.

65.   Kosynkin, D. V.; Higginbotham, A. L.; Sinitskii, A.; Lomeda, J. R.; Dimiev, A.; Price, B. K.; Tour, J. M., Longitudinal unzipping of carbon nanotubes to form graphene nanoribbons. *Nature* **2009,** *458* (7240), 872-876.

66.   Jiao, L.; Wang, X.; Diankov, G.; Wang, H.; Dai, H., Facile synthesis of high-quality graphene nanoribbons. *Nat Nano* **2010,** *5* (5), 321-325.

67.   Elías, A. L.; Botello-Méndez, A. s. R.; Meneses-Rodríguez, D.; Jehová González, V.; Ramírez-González, D.; Ci, L.; Muñoz-Sandoval, E.; Ajayan, P. M.; Terrones, H.; Terrones, M., Longitudinal Cutting of Pure and Doped Carbon Nanotubes to Form Graphitic Nanoribbons Using Metal Clusters as Nanoscalpels. *Nano Lett.* **2009,** *10* (2), 366-372.

68.   Hernandez, Y.; Nicolosi, V.; Lotya, M.; Blighe, F. M.; Sun, Z.; De, S.; McGovern, I. T.; Holland, B.; Byrne, M.; Gun'Ko, Y. K.; Boland, J. J.; Niraj, P.; Duesberg, G.; Krishnamurthy, S.; Goodhue, R.; Hutchison, J.; Scardaci, V.; Ferrari, A. C.; Coleman, J. N., High-yield production of graphene by liquid-phase exfoliation of graphite. *Nat Nano* **2008,** *3* (9), 563-568.

69.   Khan, U.; O'Neill, A.; Lotya, M.; De, S.; Coleman, J. N., High-Concentration Solvent Exfoliation of Graphene. *Small* **2010,** *6* (7), 864-871.

70.   Hamilton, C. E.; Lomeda, J. R.; Sun, Z.; Tour, J. M.; Barron, A. R., High-Yield Organic Dispersions of Unfunctionalized Graphene. *Nano Lett.* **2009,** *9* (10), 3460-3462.

71.   Dong, X.; Shi, Y.; Zhao, Y.; Chen, D.; Ye, J.; Yao, Y.; Gao, F.; Ni, Z.; Yu, T.; Shen, Z.; Huang, Y.; Chen, P.; Li, L.-J., Symmetry Breaking of Graphene Monolayers by Molecular Decoration. *Phys. Rev. Lett.* **2009,** *102* (13), 135501.

72.   Bourlinos, A. B.; Georgakilas, V.; Zboril, R.; Steriotis, T. A.; Stubos, A. K.; Trapalis, C., Aqueous-phase exfoliation of graphite in the presence of polyvinylpyrrolidone for the production of water-soluble graphenes. *Solid State Commun.* **2009,** *149* (47–48), 2172-2176.

73.   Lotya, M.; Hernandez, Y.; King, P. J.; Smith, R. J.; Nicolosi, V.; Karlsson, L. S.; Blighe, F. M.; De, S.; Wang, Z.; McGovern, I. T.; Duesberg, G. S.; Coleman, J. N., Liquid Phase Production of Graphene by Exfoliation of Graphite in Surfactant/Water Solutions. *J. Am. Chem. Soc.* **2009,** *131* (10), 3611-3620.

74.   Lotya, M.; King, P. J.; Khan, U.; De, S.; Coleman, J. N., High-Concentration, Surfactant-Stabilized Graphene Dispersions. *ACS Nano* **2010,** *4* (6), 3155-3162.

75.   Liu, N.; Luo, F.; Wu, H.; Liu, Y.; Zhang, C.; Chen, J., One-Step Ionic-Liquid-Assisted Electrochemical Synthesis of Ionic-Liquid-Functionalized Graphene Sheets Directly from Graphite. *Adv. Funct. Mater.* **2008,** *18* (10), 1518-1525.

76.   Lu, J.; Yang, J.-x.; Wang, J.; Lim, A.; Wang, S.; Loh, K. P., One-Pot Synthesis of Fluorescent Carbon Nanoribbons, Nanoparticles, and Graphene by the Exfoliation of Graphite in Ionic Liquids. *ACS Nano* **2009,** *3* (8), 2367-2375.

77.   Nuvoli, D.; Valentini, L.; Alzari, V.; Scognamillo, S.; Bon, S. B.; Piccinini, M.; Illescas, J.; Mariani, A., High concentration few-layer graphene sheets obtained by liquid phase exfoliation of graphite in ionic liquid. *J. Mater. Chem.* **2011,** *21* (10), 3428-3431.

78.   Hummers, W. S.; Offeman, R. E., Preparation of Graphitic Oxide. *J. Am. Chem. Soc.* **1958,** *80* (6), 1339-1339.

79.   He, H.; Klinowski, J.; Forster, M.; Lerf, A., A new structural model for graphite oxide. *Chem. Phys. Lett.* **1998,** *287* (1–2), 53-56.

80.   Grayfer, E. D.; Makotchenko, V. G.; Nazarov, A. S.; Kim, S. J.; Fedorov, V. E., Graphene: chemical approaches to the synthesis and modification. *Russ. Chem. Rev.* **2011,** *80* (8), 751.

81.   Liu, Y.; Gao, L.; Sun, J.; Wang, Y.; Zhang, J., Stable Nafion-functionalized graphene dispersions for transparent conducting films. *Nanotechnology* **2009,** *20* (46), 465605.

82.   Xu, Y.; Bai, H.; Lu, G.; Li, C.; Shi, G., Flexible Graphene Films via the Filtration of Water-Soluble Noncovalent Functionalized Graphene Sheets. *J. Am. Chem. Soc.* **2008,** *130* (18), 5856-5857.

83.   Dong, X.; Su, C.-Y.; Zhang, W.; Zhao, J.; Ling, Q.; Huang, W.; Chen, P.; Li, L.-J., Ultra-large single-layer graphene obtained from solution chemical reduction and its electrical properties. *Phys. Chem. Chem. Phys.* **2010,** *12* (9), 2164-2169.

84.   Liu, H.; Gao, J.; Xue, M.; Zhu, N.; Zhang, M.; Cao, T., Processing of Graphene for Electrochemical Application: Noncovalently Functionalize Graphene Sheets with Water-Soluble Electroactive Methylene Green. *Langmuir* **2009,** *25* (20), 12006-12010.

85.   Su, Q.; Pang, S.; Alijani, V.; Li, C.; Feng, X.; Müllen, K., Composites of Graphene with Large Aromatic Molecules. *Adv. Mater. (Weinheim, Ger.)* **2009,** *21* (31), 3191-3195.

86.   Gómez-Navarro, C.; Weitz, R. T.; Bittner, A. M.; Scolari, M.; Mews, A.; Burghard, M.; Kern, K., Electronic Transport Properties of Individual Chemically Reduced Graphene Oxide Sheets. *Nano Lett.* **2007,** *7* (11), 3499-3503.

87.   Wang, X.; Zhi, L.; Mullen, K., Transparent, Conductive Graphene Electrodes for Dye-Sensitized Solar Cells. *Nano Lett.* **2007,** *8* (1), 323-327.

88.   Becerril, H. A.; Mao, J.; Liu, Z.; Stoltenberg, R. M.; Bao, Z.; Chen, Y., Evaluation of Solution-Processed Reduced Graphene Oxide Films as Transparent Conductors. *ACS Nano* **2008,** *2* (3), 463-470.

89.   Su, C.-Y.; Xu, Y.; Zhang, W.; Zhao, J.; Tang, X.; Tsai, C.-H.; Li, L.-J., Electrical and Spectroscopic Characterizations of Ultra-Large Reduced Graphene Oxide Monolayers. *Chem. Mater.* **2009,** *21* (23), 5674-5680.

90.   Eda, G.; Fanchini, G.; Chhowalla, M., Large-area ultrathin films of reduced graphene oxide as a transparent and flexible electronic material. *Nat Nano* **2008,** *3* (5), 270-274.

91.   Bae, S.; Kim, H.; Lee, Y.; Xu, X.; Park, J.-S.; Zheng, Y.; Balakrishnan, J.; Lei, T.; Ri Kim, H.; Song, Y. I.; Kim, Y.-J.; Kim, K. S.; Ozyilmaz, B.; Ahn, J.-H.; Hong, B. H.; Iijima, S., Roll-to-roll production of 30-inch graphene films for transparent electrodes. *Nat Nano* **2010,** *5* (8), 574-578.

92.   Dresselhaus, M. S.; Dresselhaus, G.; Saito, R., Physics of carbon nanotubes. *Carbon* **1995,** *33* (7), 883-891.

93.   Ma, P.-C.; Siddiqui, N. A.; Marom, G.; Kim, J.-K., Dispersion and functionalization of carbon nanotubes for polymer-based nanocomposites: A review. *Composites Part A: Applied Science and Manufacturing* **2010,** *41* (10), 1345-1367.

94.   Paolucci, D.; Franco, M. M.; Iurlo, M.; Marcaccio, M.; Prato, M.; Zerbetto, F.; Pénicaud, A.; Paolucci, F., Singling out the Electrochemistry of Individual Single-Walled Carbon Nanotubes in Solution. *J. Am. Chem. Soc.* **2008,** *130* (23), 7393-7399.

95.   Guo, T.; Nikolaev, P.; Thess, A.; Colbert, D. T.; Smalley, R. E., Catalytic growth of single-walled manotubes by laser vaporization. *Chem. Phys. Lett.* **1995,** *243* (1–2), 49-54.

96.   Kumar, M.; Ando, Y., Chemical Vapor Deposition of Carbon Nanotubes: A Review on Growth Mechanism and Mass Production. *J. Nanosci. Nanotechnol.* **2010,** *10* (6), 3739-3758.

97.   Kim, H. H.; Kim, H. J., Preparation of carbon nanotubes by DC arc discharge process under reduced pressure in an air atmosphere. *Materials Science and Engineering: B* **2006,** *133* (1–3), 241-244.

98.   P.Lambin, V. N. P. a., *Carbon Nanotubes: From Basic Research to Nanotechnology*. Springer: 2006; Vol. 222, p 253.

99.   Nikolaev, P.; Bronikowski, M. J.; Bradley, R. K.; Rohmund, F.; Colbert, D. T.; Smith, K. A.; Smalley, R. E., Gas-phase catalytic growth of single-walled carbon nanotubes from carbon monoxide. *Chem. Phys. Lett.* **1999,** *313* (1–2), 91-97.

100.   Resasco, D. E.; Alvarez, W. E.; Pompeo, F.; Balzano, L.; Herrera, J. E.; Kitiyanan, B.; Borgna, A., A Scalable Process for Production of Single-walled Carbon Nanotubes (SWNTs) by Catalytic Disproportionation of CO on a Solid Catalyst. *Journal of Nanoparticle Research* **2002,** *4* (1), 131-136.

101.   Wilder, J. W. G.; Venema, L. C.; Rinzler, A. G.; Smalley, R. E.; Dekker, C., Electronic structure of atomically resolved carbon nanotubes. *Nature* **1998,** *391* (6662), 59-62.

102.   Ebbesen, T. W.; Lezec, H. J.; Hiura, H.; Bennett, J. W.; Ghaemi, H. F.; Thio, T., Electrical conductivity of individual carbon nanotubes. *Nature* **1996,** *382* (6586), 54-56.

103.   Arnold, M. S.; Green, A. A.; Hulvat, J. F.; Stupp, S. I.; Hersam, M. C., Sorting carbon nanotubes by electronic structure using density differentiation. *Nat Nano* **2006,** *1* (1), 60-65.

104.   Chen, Z.; Du, X.; Du, M.-H.; Rancken, C. D.; Cheng, H.-P.; Rinzler, A. G., Bulk Separative Enrichment in Metallic or Semiconducting Single-Walled Carbon Nanotubes. *Nano Lett.* **2003,** *3* (9), 1245-1249.

105.   Voggu, R.; Rao, K. V.; George, S. J.; Rao, C. N. R., A Simple Method of Separating Metallic and Semiconducting Single-Walled Carbon Nanotubes Based on Molecular Charge Transfer. *J. Am. Chem. Soc.* **2010,** *132* (16), 5560-5561.

106.   Bekyarova, E.; Itkis, M. E.; Cabrera, N.; Zhao, B.; Yu, A.; Gao, J.; Haddon, R. C., Electronic Properties of Single-Walled Carbon Nanotube Networks. *J. Am. Chem. Soc.* **2005,** *127* (16), 5990-5995.

107.   Unalan, H. E.; Fanchini, G.; Kanwal, A.; Du Pasquier, A.; Chhowalla, M., Design Criteria for Transparent Single-Wall Carbon Nanotube Thin-Film Transistors. *Nano Lett.* **2006,** *6* (4), 677-682.

108.   Zhang, D.; Ryu, K.; Liu, X.; Polikarpov, E.; Ly, J.; Tompson, M. E.; Zhou, C., Transparent, Conductive, and Flexible Carbon Nanotube Films and Their Application in Organic Light-Emitting Diodes. *Nano Lett.* **2006,** *6* (9), 1880-1886.

109.   Yu, M.-F.; Files, B. S.; Arepalli, S.; Ruoff, R. S., Tensile Loading of Ropes of Single Wall Carbon Nanotubes and their Mechanical Properties. *Phys. Rev. Lett.* **2000,** *84* (24), 5552-5555.

110.   WenXing, B.; ChangChun, Z.; WanZhao, C., Simulation of Young's modulus of single-walled carbon nanotubes by molecular dynamics. *Physica B: Condensed Matter* **2004,** *352* (1–4), 156-163.

111.   Yu, M.-F.; Lourie, O.; Dyer, M. J.; Moloni, K.; Kelly, T. F.; Ruoff, R. S., Strength and Breaking Mechanism of Multiwalled Carbon Nanotubes Under Tensile Load. *Science* **2000,** *287* (5453), 637-640.

112.   Li, C.; Chou, T.-W., Elastic moduli of multi-walled carbon nanotubes and the effect of van der Waals forces. *Composites Science and Technology* **2003,** *63* (11), 1517-1524.

113.   Ruoff, R. S.; Tersoff, J.; Lorents, D. C.; Subramoney, S.; Chan, B., Radial deformation of carbon nanotubes by van der Waals forces. *Nature* **1993,** *364* (6437), 514-516.

114.   Hansen, C. M., *Hansen solubility parameters: A user's Handbook*. Boca Raton, Fla: CRC Press: 2007; Vol. Second edition.

115.   Greenhalgh, D. J.; Williams, A. C.; Timmins, P.; York, P., Solubility parameters as predictors of miscibility in solid dispersions. *J. Pharm. Sci.* **1999,** *88* (11), 1182-1190.

116.   Cheng, Q.; Debnath, S.; O'Neill, L.; Hedderman, T. G.; Gregan, E.; Byrne, H. J., Systematic Study of the Dispersion of SWNTs in Organic Solvents. *The Journal of Physical Chemistry C* **2010,** *114* (11), 4857-4863.

117.   Ausman, K. D.; Piner, R.; Lourie, O.; Ruoff, R. S.; Korobov, M., Organic Solvent Dispersions of Single-Walled Carbon Nanotubes: Toward Solutions of Pristine Nanotubes. *J. Phys. Chem. B* **2000,** *104* (38), 8911-8915.

118.   Giordani, S.; Bergin, S.; Nicolosi, V.; Lebedkin, S.; Blau, W. J.; Coleman, J. N., Fabrication of stable dispersions containing up to 70% individual carbon nanotubes in a common organic solvent. *physica status solidi (b)* **2006,** *243* (13), 3058-3062.

119.   Bahr, J. L.; Mickelson, E. T.; Bronikowski, M. J.; Smalley, R. E.; Tour, J. M., Dissolution of small diameter single-wall carbon nanotubes in organic solvents? *Chem. Commun. (Cambridge, U. K.)* **2001,** (2), 193-194.

120.   Furtado, C. A.; Kim, U. J.; Gutierrez, H. R.; Pan, L.; Dickey, E. C.; Eklund, P. C., Debundling and Dissolution of Single-Walled Carbon Nanotubes in Amide Solvents. *J. Am. Chem. Soc.* **2004,** *126* (19), 6095-6105.

121.   Maeda, Y.; Kimura, S.-i.; Hirashima, Y.; Kanda, M.; Lian, Y.; Wakahara, T.; Akasaka, T.; Hasegawa, T.; Tokumoto, H.; Shimizu, T.; Kataura, H.; Miyauchi, Y.; Maruyama, S.; Kobayashi, K.; Nagase, S., Dispersion of Single-Walled Carbon Nanotube Bundles in Nonaqueous Solution. *J. Phys. Chem. B* **2004,** *108* (48), 18395-18397.

122.   Kawasaki, S.; Komatsu, K.; Okino, F.; Touhara, H.; Kataura, H., Fluorination of open- and closed-end single-walled carbon nanotubes. *Phys. Chem. Chem. Phys.* **2004,** *6* (8), 1769-1772.

123.   (a) Boul, P. J.; Liu, J.; Mickelson, E. T.; Huffman, C. B.; Ericson, L. M.; Chiang, I. W.; Smith, K. A.; Colbert, D. T.; Hauge, R. H.; Margrave, J. L.; Smalley, R. E., Reversible sidewall functionalization of buckytubes. *Chem. Phys. Lett.* **1999,** *310* (3–4), 367-372; (b) Saini, R. K.; Chiang, I. W.; Peng, H.; Smalley, R. E.; Billups, W. E.; Hauge, R. H.; Margrave, J. L., Covalent Sidewall Functionalization of Single Wall Carbon Nanotubes. *J. Am. Chem. Soc.* **2003,** *125* (12), 3617-3621.

124.   Stevens, J. L.; Huang, A. Y.; Peng, H.; Chiang, I. W.; Khabashesku, V. N.; Margrave, J. L., Sidewall Amino-Functionalization of Single-Walled Carbon Nanotubes through Fluorination and Subsequent Reactions with Terminal Diamines. *Nano Lett.* **2003,** *3* (3), 331-336.

125.   Pehrsson, P. E.; Zhao, W.; Baldwin, J. W.; Song, C.; Liu, J.; Kooi, S.; Zheng, B., Thermal Fluorination and Annealing of Single-Wall Carbon Nanotubes. *J. Phys. Chem. B* **2003,** *107* (24), 5690-5695.

126.   Georgakilas, V.; Kordatos, K.; Prato, M.; Guldi, D. M.; Holzinger, M.; Hirsch, A., Organic Functionalization of Carbon Nanotubes. *J. Am. Chem. Soc.* **2002,** *124* (5), 760-761.

127.   Tagmatarchis, N.; Prato, M., Functionalization of carbon nanotubes via 1,3-dipolar cycloadditions. *J. Mater. Chem.* **2004,** *14* (4), 437-439.

128.   Chen, J.; Hamon, M. A.; Hu, H.; Chen, Y.; Rao, A. M.; Eklund, P. C.; Haddon, R. C., Solution Properties of Single-Walled Carbon Nanotubes. *Science* **1998,** *282* (5386), 95-98.

129.   Hamon, M. A.; Chen, J.; Hu, H.; Chen, Y.; Itkis, M. E.; Rao, A. M.; Eklund, P. C.; Haddon, R. C., Dissolution of Single-Walled Carbon Nanotubes. *Adv. Mater. (Weinheim, Ger.)* **1999,** *11* (10), 834-840.

130.   Tasis, D.; Tagmatarchis, N.; Bianco, A.; Prato, M., Chemistry of Carbon Nanotubes. *Chem. Rev. (Washington, DC, U. S.)* **2006,** *106* (3), 1105-1136.

131.   Lin, Y.; Zhou, B.; Shiral Fernando, K. A.; Liu, P.; Allard, L. F.; Sun, Y.-P., Polymeric Carbon Nanocomposites from Carbon Nanotubes Functionalized with Matrix Polymer. *Macromolecules* **2003,** *36* (19), 7199-7204.

132.   Zhao, B.; Hu, H.; Yu, A.; Perea, D.; Haddon, R. C., Synthesis and Characterization of Water Soluble Single-Walled Carbon Nanotube Graft Copolymers. *J. Am. Chem. Soc.* **2005,** *127* (22), 8197-8203.

133.   Baskaran, D.; Dunlap, J. R.; Mays, J. W.; Bratcher, M. S., Grafting Efficiency of Hydroxy-Terminated Poly(methyl methacrylate) with Multiwalled Carbon Nanotubes. *Macromol. Rapid Commun.* **2005,** *26* (6), 481-486.

134.   Wang, G.; Qu, Z.; Liu, L.; Shi, Q.; Guo, J., Study of SMA graft modified MWNT/PVC composite materials. *Materials Science and Engineering: A* **2008,** *472* (1–2), 136-139.

135.   Baskaran, D.; Mays, J. W.; Bratcher, M. S., Polymer adsorption in the grafting reactions of hydroxyl terminal polymers with multi-walled carbon nanotubes. *Polymer* **2005,** *46* (14), 5050-5057.

136.   Hill, D. E.; Lin, Y.; Rao, A. M.; Allard, L. F.; Sun, Y.-P., Functionalization of Carbon Nanotubes with Polystyrene. *Macromolecules* **2002,** *35* (25), 9466-9471.

137.   Wang, W.; Lin, Y.; Sun, Y.-P., Poly(N-vinyl carbazole)-functionalized single-walled carbon nanotubes: Synthesis, characterization, and nanocomposite thin films. *Polymer* **2005,** *46* (20), 8634-8640.

138.   Sano, M.; Kamino, A.; Okamura, J.; Shinkai, S., Self-Organization of PEO-graft-Single-Walled Carbon Nanotubes in Solutions and Langmuir–Blodgett Films. *Langmuir* **2001,** *17* (17), 5125-5128.

139.   Yao, Z.; Braidy, N.; Botton, G. A.; Adronov, A., Polymerization from the Surface of Single-Walled Carbon Nanotubes – Preparation and Characterization of Nanocomposites. *J. Am. Chem. Soc.* **2003,** *125* (51), 16015-16024.

140.   Kong, H.; Luo, P.; Gao, C.; Yan, D., Polyelectrolyte-functionalized multiwalled carbon nanotubes: preparation, characterization and layer-by-layer self-assembly. *Polymer* **2005,** *46* (8), 2472-2485.

141.   Spitalsky, Z.; Tasis, D.; Papagelis, K.; Galiotis, C., Carbon nanotube–polymer composites: Chemistry, processing, mechanical and electrical properties. *Prog. Polym. Sci.* **2010,** *35* (3), 357-401.

142.   (a) Baskaran, D.; Mays, J. W.; Bratcher, M. S., Polymer-Grafted Multiwalled Carbon Nanotubes through Surface-Initiated Polymerization. *Angewandte Chemie International Edition* **2004,** *43* (16), 2138-2142; (b) Shanmugharaj, A. M.; Bae, J. H.; Nayak, R. R.; Ryu, S. H., Preparation of poly(styrene-co-acrylonitrile)-grafted multiwalled carbon nanotubes via surface-initiated atom transfer radical polymerization. *Journal of Polymer Science Part A: Polymer Chemistry* **2007,** *45* (3), 460-470.

143.   Cui, J.; Wang, W.; You, Y.; Liu, C.; Wang, P., Functionalization of multiwalled carbon nanotubes by reversible addition fragmentation chain-transfer polymerization. *Polymer* **2004,** *45* (26), 8717-8721.

144.   (a) Hong, C.-Y.; You, Y.-Z.; Pan, C.-Y., Synthesis of Water-Soluble Multiwalled Carbon Nanotubes with Grafted Temperature-Responsive Shells by Surface RAFT Polymerization. *Chem. Mater.* **2005,** *17* (9), 2247-2254; (b) Wang, G.-J.; Huang, S.-Z.; Wang, Y.; Liu, L.; Qiu, J.; Li, Y., Synthesis of water-soluble single-walled carbon nanotubes by RAFT polymerization. *Polymer* **2007,** *48* (3), 728-733.

145.   (a) Hong, C.-Y.; You, Y.-Z.; Pan, C.-Y., A new approach to functionalize multi-walled carbon nanotubes by the use of functional polymers. *Polymer* **2006,** *47* (12), 4300-4309; (b) Xu, G.; Wu, W.-T.; Wang, Y.; Pang, W.; Zhu, Q.; Wang, P.; You, Y., Constructing polymer brushes on multiwalled carbon nanotubes by in situ reversible addition fragmentation chain transfer polymerization. *Polymer* **2006,** *47* (16), 5909-5918.

146.   You, Y.-Z.; Hong, C.-Y.; Pan, C.-Y., Directly growing ionic polymers on multi-walled carbon nanotubes via surface RAFT polymerization. *Nanotechnology* **2006,** *17* (9), 2350.

147.   (a) Jia, Z.; Wang, Z.; Xu, C.; Liang, J.; Wei, B.; Wu, D.; Zhu, S., Study on poly(methyl methacrylate)/carbon nanotube composites. *Materials Science and Engineering: A* **1999,** *271* (1–2), 395-400; (b) Shaffer, M. S. P.; Koziol, K., Polystyrene grafted multi-walled carbon nanotubes. *Chem. Commun. (Cambridge, U. K.)* **2002,** (18), 2074-2075; (c) Du, F.; Wu, K.; Yang, Y.; Liu, L.; Gan, T.; Xie, X., Synthesis and electrochemical probing of water-soluble poly(sodium 4-styrenesulfonate-co-acrylic acid)-grafted multiwalled carbon nanotubes. *Nanotechnology* **2008,** *19* (8), 085716.

148.   Viswanathan, G.; Chakrapani, N.; Yang, H.; Wei, B.; Chung, H.; Cho, K.; Ryu, C. Y.; Ajayan, P. M., Single-Step in Situ Synthesis of Polymer-Grafted Single-Wall Nanotube Composites. *J. Am. Chem. Soc.* **2003,** *125* (31), 9258-9259.

149.   Liang, F.; Beach, J. M.; Kobashi, K.; Sadana, A. K.; Vega-Cantu, Y. I.; Tour, J. M.; Billups, W. E., In Situ Polymerization Initiated by Single-Walled Carbon Nanotube Salts. *Chem. Mater.* **2006,** *18* (20), 4764-4767.

150.   Kim, S. W.; Kim, T.; Kim, Y. S.; Choi, H. S.; Lim, H. J.; Yang, S. J.; Park, C. R., Surface modifications for the effective dispersion of carbon nanotubes in solvents and polymers. *Carbon* **2012,** *50* (1), 3-33.

151.   Rahmat, M.; Hubert, P., Carbon nanotube–polymer interactions in nanocomposites: A review. *Composites Science and Technology* **2011,** *72* (1), 72-84.

152.   Islam, M. F.; Rojas, E.; Bergey, D. M.; Johnson, A. T.; Yodh, A. G., High Weight Fraction Surfactant Solubilization of Single-Wall Carbon Nanotubes in Water. *Nano Lett.* **2003,** *3* (2), 269-273.

153.   Giulianini, M.; Waclawik, E. R.; Bell, J. M.; Crescenzi, M. D.; Castrucci, P.; Scarselli, M.; Motta, N., Regioregular poly(3-hexyl-thiophene) helical self-organization on carbon nanotubes. *Appl. Phys. Lett.* **2009,** *95* (1), 013304.

154.   Richard, C.; Balavoine, F.; Schultz, P.; Ebbesen, T. W.; Mioskowski, C., Supramolecular Self-Assembly of Lipid Derivatives on Carbon Nanotubes. *Science* **2003,** *300* (5620), 775-778.

155.   Bystrzejewski, M.; Huczko, A.; Lange, H.; Gemming, T.; Büchner, B.; Rümmeli, M. H., Dispersion and diameter separation of multi-wall carbon nanotubes in aqueous solutions. *J. Colloid Interface Sci.* **2010,** *345* (2), 138-142.

156.   Duan, W. H.; Wang, Q.; Collins, F., Dispersion of carbon nanotubes with SDS surfactants: a study from a binding energy perspective. *Chemical Science* **2011,** *2* (7), 1407-1413.

157.   Tan, X.; Fang, M.; Chen, C.; Yu, S.; Wang, X., Counterion effects of nickel and sodium dodecylbenzene sulfonate adsorption to multiwalled carbon nanotubes in aqueous solution. *Carbon* **2008,** *46* (13), 1741-1750.

158.   Matarredona, O.; Rhoads, H.; Li, Z.; Harwell, J. H.; Balzano, L.; Resasco, D. E., Dispersion of Single-Walled Carbon Nanotubes in Aqueous Solutions of the Anionic Surfactant NaDDBS. *J. Phys. Chem. B* **2003,** *107* (48), 13357-13367.

159.   Sun, Z.; Nicolosi, V.; Rickard, D.; Bergin, S. D.; Aherne, D.; Coleman, J. N., Quantitative Evaluation of Surfactant-stabilized Single-walled Carbon Nanotubes: Dispersion Quality and Its Correlation with Zeta Potential. *The Journal of Physical Chemistry C* **2008,** *112* (29), 10692-10699.

160.   White, B.; Banerjee, S.; O'Brien, S.; Turro, N. J.; Herman, I. P., Zeta-Potential Measurements of Surfactant-Wrapped Individual Single-Walled Carbon Nanotubes. *The Journal of Physical Chemistry C* **2007,** *111* (37), 13684-13690.

161.   Cousins, B. G.; Das, A. K.; Sharma, R.; Li, Y.; McNamara, J. P.; Hillier, I. H.; Kinloch, I. A.; Ulijn, R. V., Enzyme-Activated Surfactants for Dispersion of Carbon Nanotubes. *Small* **2009,** *5* (5), 587-590.

162.   Alpatova, A. L.; Shan, W.; Babica, P.; Upham, B. L.; Rogensues, A. R.; Masten, S. J.; Drown, E.; Mohanty, A. K.; Alocilja, E. C.; Tarabara, V. V., Single-walled carbon nanotubes dispersed in aqueous media via non-covalent functionalization: Effect of dispersant on the stability, cytotoxicity, and epigenetic toxicity of nanotube suspensions. *Water Res.* **2010,** *44* (2), 505-520.

163.   Dong, B.; Su, Y.; Liu, Y.; Yuan, J.; Xu, J.; Zheng, L., Dispersion of carbon nanotubes by carbazole-tailed amphiphilic imidazolium ionic liquids in aqueous solutions. *J. Colloid Interface Sci.* **2011,** *356* (1), 190-195.

164.   Liu, Y.; Yu, L.; Zhang, S.; Yuan, J.; Shi, L.; Zheng, L., Dispersion of multiwalled carbon nanotubes by ionic liquid-type Gemini imidazolium surfactants in aqueous solution. *Colloids and Surfaces A: Physicochemical and Engineering Aspects* **2010,** *359* (1–3), 66-70.

165.   Baskaran, D.; Mays, J. W.; Bratcher, M. S., Noncovalent and Nonspecific Molecular Interactions of Polymers with Multiwalled Carbon Nanotubes. *Chem. Mater.* **2005,** *17* (13), 3389-3397.

166.   Hu, C.; Liao, H.; Li, F.; Xiang, J.; Li, W.; Duo, S.; Li, M., Noncovalent functionalization of multi-walled carbon nanotubes with siloxane polyether copolymer. *Mater. Lett.* **2008,** *62* (17–18), 2585-2588.

167.   Ntim, S. A.; Sae-Khow, O.; Witzmann, F. A.; Mitra, S., Effects of polymer wrapping and covalent functionalization on the stability of MWCNT in aqueous dispersions. *J. Colloid Interface Sci.* **2011,** *355* (2), 383-388.

168.   O'Connell, M. J.; Boul, P.; Ericson, L. M.; Huffman, C.; Wang, Y.; Haroz, E.; Kuper, C.; Tour, J.; Ausman, K. D.; Smalley, R. E., Reversible water-solubilization of single-walled carbon nanotubes by polymer wrapping. *Chem. Phys. Lett.* **2001,** *342* (3-4), 265-271.

169.   Kim, J.-B.; Premkumar, T.; Lee, K.; Geckeler, K. E., A Facile Approach to Single-Wall Carbon Nanotube/Poly(allylamine) Nanocomposites. *Macromol. Rapid Commun.* **2007,** *28* (3), 276-280.

170.   Hong, K.; Kim, S. H.; Yang, C.; Yun, W. M.; Nam, S.; Jang, J.; Park, C.; Park, C. E., Photopatternable Poly(4-styrene sulfonic acid)-Wrapped MWNT Thin-Film Source/Drain Electrodes for Use in Organic Field-Effect Transistors. *ACS Appl. Mater. Interfaces* **2010,** *3* (1), 74-79.

171.   Wang, S.; Jiang, S. P.; Wang, X., Polyelectrolyte functionalized carbon nanotubes as a support for noble metal electrocatalysts and their activity for methanol oxidation. *Nanotechnology* **2008,** *19* (26), 265601.

172.   Zhu, J.; Shim, B. S.; Di Prima, M.; Kotov, N. A., Transparent Conductors from Carbon Nanotubes LBL-Assembled with Polymer Dopant with π–π Electron Transfer. *J. Am. Chem. Soc.* **2011,** *133* (19), 7450-7460.

173.   Star, A.; Stoddart, J. F.; Steuerman, D.; Diehl, M.; Boukai, A.; Wong, E. W.; Yang, X.; Chung, S.-W.; Choi, H.; Heath, J. R., Preparation and Properties of Polymer-Wrapped Single-Walled Carbon Nanotubes. *Angewandte Chemie International Edition* **2001,** *40* (9), 1721-1725.

174.   Wise, K. E.; Park, C.; Siochi, E. J.; Harrison, J. S., Stable dispersion of single wall carbon nanotubes in polyimide: the role of noncovalent interactions. *Chem. Phys. Lett.* **2004,** *391* (4–6), 207-211.

175.   Rouse, J. H., Polymer-Assisted Dispersion of Single-Walled Carbon Nanotubes in Alcohols and Applicability toward Carbon Nanotube/Sol–Gel Composite Formation. *Langmuir* **2004,** *21* (3), 1055-1061.

176.   Kymakis, E.; Amaratunga, G. A. J., Electrical properties of single-wall carbon nanotube-polymer composite films. *J. Appl. Phys.* **2006,** *99* (8), 084302.

177.   Kang, Y. K.; Lee, O.-S.; Deria, P.; Kim, S. H.; Park, T.-H.; Bonnell, D. A.; Saven, J. G.; Therien, M. J., Helical Wrapping of Single-Walled Carbon Nanotubes by Water Soluble Poly(p-phenyleneethynylene). *Nano Lett.* **2009,** *9* (4), 1414-1418.

178.   Gao, J.; Loi, M. A.; de Carvalho, E. J. F.; dos Santos, M. C., Selective Wrapping and Supramolecular Structures of Polyfluorene–Carbon Nanotube Hybrids. *ACS Nano* **2011,** *5* (5), 3993-3999.

179.   Berton, N.; Lemasson, F.; Tittmann, J.; Stürzl, N.; Hennrich, F.; Kappes, M. M.; Mayor, M., Copolymer-Controlled Diameter-Selective Dispersion of Semiconducting Single-Walled Carbon Nanotubes. *Chem. Mater.* **2011,** *23* (8), 2237-2249.

180.   Lee, H. W.; Yoon, Y.; Park, S.; Oh, J. H.; Hong, S.; Liyanage, L. S.; Wang, H.; Morishita, S.; Patil, N.; Park, Y. J.; Park, J. J.; Spakowitz, A.; Galli, G.; Gygi, F.; Wong, P. H. S.; Tok, J. B. H.; Kim, J. M.; Bao, Z., Selective dispersion of high purity semiconducting single-walled carbon nanotubes with regioregular poly(3-alkylthiophene)s. *Nat Commun* **2011,** *2*, 541.

181.   Boon, F.; Desbief, S.; Cutaia, L.; Douhéret, O.; Minoia, A.; Ruelle, B.; Clément, S.; Coulembier, O.; Cornil, J.; Dubois, P.; Lazzaroni, R., Synthesis and Characterization of Nanocomposites Based on Functional Regioregular Poly(3-hexylthiophene) and Multiwall Carbon Nanotubes. *Macromol. Rapid Commun.* **2010,** *31* (16), 1427-1434.

182.   Hellstrom, S. L.; Lee, H. W.; Bao, Z., Polymer-Assisted Direct Deposition of Uniform Carbon Nanotube Bundle Networks for High Performance Transparent Electrodes. *ACS Nano* **2009,** *3* (6), 1423-1430.

183.   Dettlaff-Weglikowska, U.; Skákalová, V.; Graupner, R.; Jhang, S. H.; Kim, B. H.; Lee, H. J.; Ley, L.; Park, Y. W.; Berber, S.; Tománek, D.; Roth, S., Effect of SOCl2 Treatment on Electrical and Mechanical Properties of Single-Wall Carbon Nanotube Networks. *J. Am. Chem. Soc.* **2005,** *127* (14), 5125-5131.

184.   Kang, Y.; Taton, T. A., Micelle-Encapsulated Carbon Nanotubes: A Route to Nanotube Composites. *J. Am. Chem. Soc.* **2003,** *125* (19), 5650-5651.

185.   González-Domínguez, J. M.; Ansón-Casaos, A.; Díez-Pascual, A. M.; Ashrafi, B.; Naffakh, M.; Backman, D.; Stadler, H.; Johnston, A.; Gómez, M.; Martínez, M. T., Solvent-Free Preparation of High-Toughness Epoxy–SWNT Composite Materials. *ACS Appl. Mater. Interfaces* **2011,** *3* (5), 1441-1450.

186.   Gonzalez-Dominguez, J. M.; Tesa-Serrate, M. A.; Anson-Casaos, A.; Diez-Pascual, A. M.; Gomez-Fatou, M. A.; Martinez, M. T., Wrapping of SWCNTs in Polyethylenoxide-Based Amphiphilic Diblock Copolymers: An Approach to Purification, Debundling, and Integration into the Epoxy Matrix. *The Journal of Physical Chemistry C* **2012**.

187.   Park, S.; Yang, H.-S.; Kim, D.; Jo, K.; Jon, S., Rational design of amphiphilic polymers to make carbon nanotubes water-dispersible, anti-biofouling, and functionalizable. *Chem. Commun. (Cambridge, U. K.)* **2008,** (25), 2876-2878.

188.   Meuer, S.; Braun, L.; Zentel, R., Pyrene Containing Polymers for the Non-Covalent Functionalization of Carbon Nanotubes. *Macromol. Chem. Phys.* **2009,** *210* (18), 1528-1535.

189.   Shin, H.-i.; Min, B. G.; Jeong, W.; Park, C., Amphiphilic Block Copolymer Micelles: New Dispersant for Single Wall Carbon Nanotubes. *Macromol. Rapid Commun.* **2005,** *26* (18), 1451-1457.

190.   Sung, J.; Jo, P. S.; Shin, H.; Huh, J.; Min, B. G.; Kim, D. H.; Park, C., Transparent, Low-Electric-Resistance Nanocomposites of Self-Assembled Block Copolymers and SWNTs. *Adv. Mater. (Weinheim, Ger.)* **2008,** *20* (8), 1505-1510.

191.   Morishita, T.; Matsushita, M.; Katagiri, Y.; Fukumori, K., Effects of the composition and molecular weight of maleimide polymers on the dispersibility of carbon nanotubes in chloroform. *Carbon* **2011,** *49* (15), 5185-5195.

192.   Zou, J.; Khondaker, S. I.; Huo, Q.; Zhai, L., A General Strategy to Disperse and Functionalize Carbon Nanotubes Using Conjugated Block Copolymers. *Adv. Funct. Mater.* **2009,** *19* (3), 479-483.

193.   Zou, J.; Liu, L.; Chen, H.; Khondaker, S. I.; McCullough, R. D.; Huo, Q.; Zhai, L., Dispersion of Pristine Carbon Nanotubes Using Conjugated Block Copolymers. *Adv. Mater. (Weinheim, Ger.)* **2008,** *20* (11), 2055-2060.

194.   Zou, J.; Chen, H.; Chunder, A.; Yu, Y.; Huo, Q.; Zhai, L., Preparation of a Superhydrophobic and Conductive Nanocomposite Coating from a Carbon-Nanotube-Conjugated Block Copolymer Dispersion. *Adv. Mater. (Weinheim, Ger.)* **2008,** *20* (17), 3337-3341.

195.   Bauhofer, W.; Kovacs, J. Z., A review and analysis of electrical percolation in carbon nanotube polymer composites. *Composites Science and Technology* **2009,** *69* (10), 1486-1498.

196.   Takeda, T.; Shindo, Y.; Kuronuma, Y.; Narita, F., Modeling and characterization of the electrical conductivity of carbon nanotube-based polymer composites. *Polymer* **2011,** *52* (17), 3852-3856.

197.   Vigolo, B.; Coulon, C.; Maugey, M.; Zakri, C.; Poulin, P., An Experimental Approach to the Percolation of Sticky Nanotubes. *Science* **2005,** *309* (5736), 920-923.

Chapter II

Synthesis and characterization of π-conjugated based block copolymers

TABLE OF CONTENTS

Synthesis and characterization of π-conjugated based block copolymers

I   Introduction

The objective of our work is the design of new organic materials formulated in conductive inks which can be caste by printing techniques in transparent and conductive films. The combination of CNTs and copolymers was chosen for the composition of these inks. Indeed, as regard to the literature review, carbon nanotubes possess excellent electrical and optical properties even when they are caste in thin films. The limitations for the use of this material as transparent conductive electrodes are the lack of solubility and dispersibility (as described in chapter 1) and the high roughness of their films. In order to overcome these problems, the use of copolymers is proposed. The π-conjugated copolymer dispersants will also assist in lowering the percolation threshold of the dispersion since a conductive polymer will be in direct contact with the nanotubes.

Consequently, the synthesis of new conductive copolymers designed for the dispersion of the CNTs and for the homogeneity of the films was targeted. The block copolymer architecture w preferred in order to combine two different functionalities (*i.e* electrical and water solubility) in the same macromolecule. As was reported in the chapter I, semi-conducting block copolymers are able to be adsorbed on the surface of the nanotubes and to improve the electrical features of the dispersions. Also the charged segments (polyelectrolytes, surfactants) are known to well disperse CNTs due to the charges that surround the dispersed nanotubes.

I.1   Strategy followed

Based on the literature, we chose to synthesize a new type of dispersant for the CNTs, which will combine a semi-conductive part and a polyelectrolyte moiety in the form of block copolymer (figure 1). The semi-conductive part is participating at the dispersion of CNTs since it breaks the nanotube bundles by developing strong π-π interactions with the π-carbons of the nanotubes. This type of polymer-nanotubes interactions have been characterized as strong, resulting in stable dispersions over time. In addition, the presence of a conductive block around the CNTs will help in the creation of a CNTs/copolymer conductive network and decrease the percolation threshold.

The role of the polyelectrolyte block influences the electrical properties of the copolymer as well as the stability of the CNTs dispersion. The polyelectrolyte can influence the electrical properties of the composite by two ways: (1) by either acting as a dopant of the semi-conductive block or as a counter anion of the already doped semi conducting block (2) by increasing the ion conductivity of the copolymers resulting in the increase of the charge mobility of the system. In addition, the presence of a polyelectrolyte will allowed dispersions in aqueous media. The dispersions will exhibit enhanced colloidal stability due to the polyelectrolyte shell surrounding the CNTs.

The combination of these two polymers (π-conjugated and polyelectrolyte) in the form of a block copolymer has several advantages. Firstly, the size and the macromolecular characteristics of the block copolymers can be controlled and tuned during the synthesis. In addition the insulating polyelectrolyte part could be removed after the film formation, thus improving the electrical properties of the films.

Figure 1. Schematic of the strategy for the synthesis of new copolymers for dispersion of CNTs.
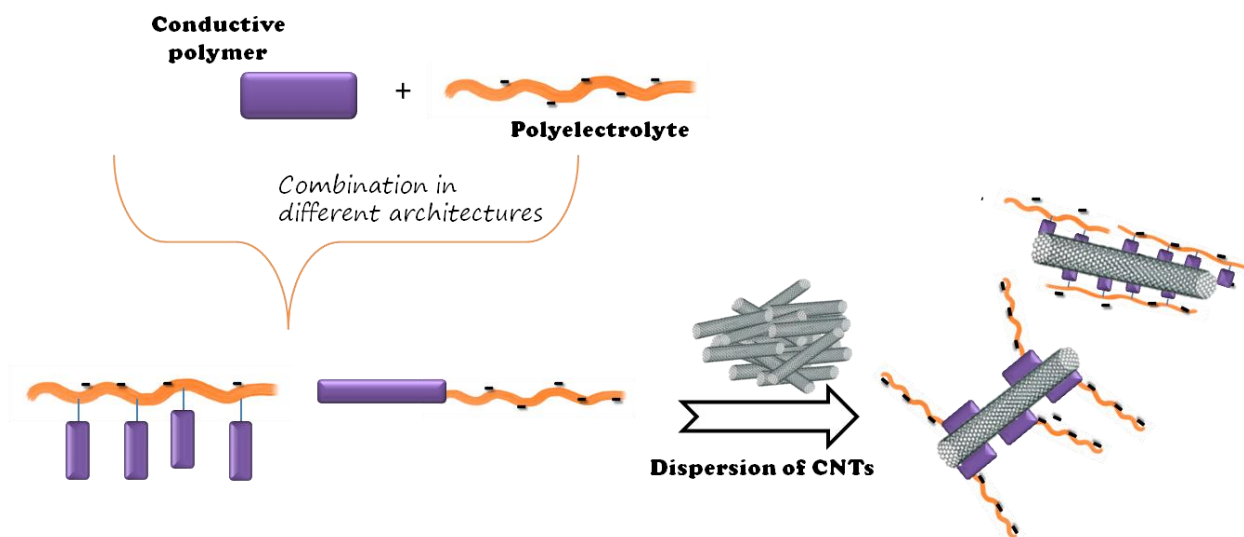
I.2 Characteristics of poly (3,4-ethylenedioxythiophene) and poly (3-hexylthiophene) polymers

Among the π-conjugated polymers, we focused on the poly(3,4-ethylenedioxythiophene) (PEDOT) and the poly(3-hexylthiophene). Both these polymers have good electrical and optical properties and they are interesting materials for use in the field of organic electronics. Their characteristics, the synthetic routes for their polymerization and their possibility to be formulated in block copolymers will be further analyzed.

I.2.1 *Characteristics of poly (3,4-ethylenedioxythiophene)polymers*

PEDOT is a well-known polymer with high conductivity, a quasi-transparency in the form of thin film and a very high stability in its oxidized state. However, it faces solubility problems, since PEDOT is insoluble in most solvents. This difficulty was first overcome by synthesizing PEDOT in the presence of poly(4-styrenesulfonate) (PSS) in aqueous dispersion (figure 2).[1] In these dispersions the PSS behaves as a counter anion to the positively doped PEDOT and also it serves as an oxidizing agent and charge compensator. The polymerization methods followed for the synthesis of PEDOT are the oxidative and the coupling polymerizations. Both of them are non-controlled polymerization methods and they are based on the use of oxidants or Lewis acids.

Another way for the synthesis of soluble PEDOT was proposed first by Roncali *and coll* followed by Reynolds *and coll.* starting from the functionalization of the EDOT monomers with long alkyl chains.[2,3] These new monomers were then polymerized by controlled polymerization resulting in soluble polymers for certain lengths of the alkyl chains. In figure 2 the chemical structures of some soluble EDOT based polymers are presented.

Recently the synthesis of soluble PEDOT based copolymers was reported.[4] The polymerization method that was followed was based on the Pd catalyzed arylation polycondensation reaction of EDOT and 2,7-dibromo-9,9-dioctylfluorene (figure 2). The presence on an acid was necessary for achieving high molecular weights and the final copolymers were soluble in organic solvents (chloroform). In addition, by this methodology end-capped copolymers were synthesized by chemical treatment of the Br end group.

Figure 2 Different methods for synthesis of soluble π-conjugated based polymers (a) PEDOT/PSS aqueous dispersions (b) GRIM polymerization of functionalized EDOT monomers[5] (c) Pd catalyzed arylation of EDOT and 2,7-dibromo-9,9-dioctylfluorene.[4]

(a)

(b)

R= Hexyl, ethylhexyl,
CH$_2$O-ethylhexyl,
CH$_2$O-C$_{18}$H$_{38}$

(c)

X= H, EDOT
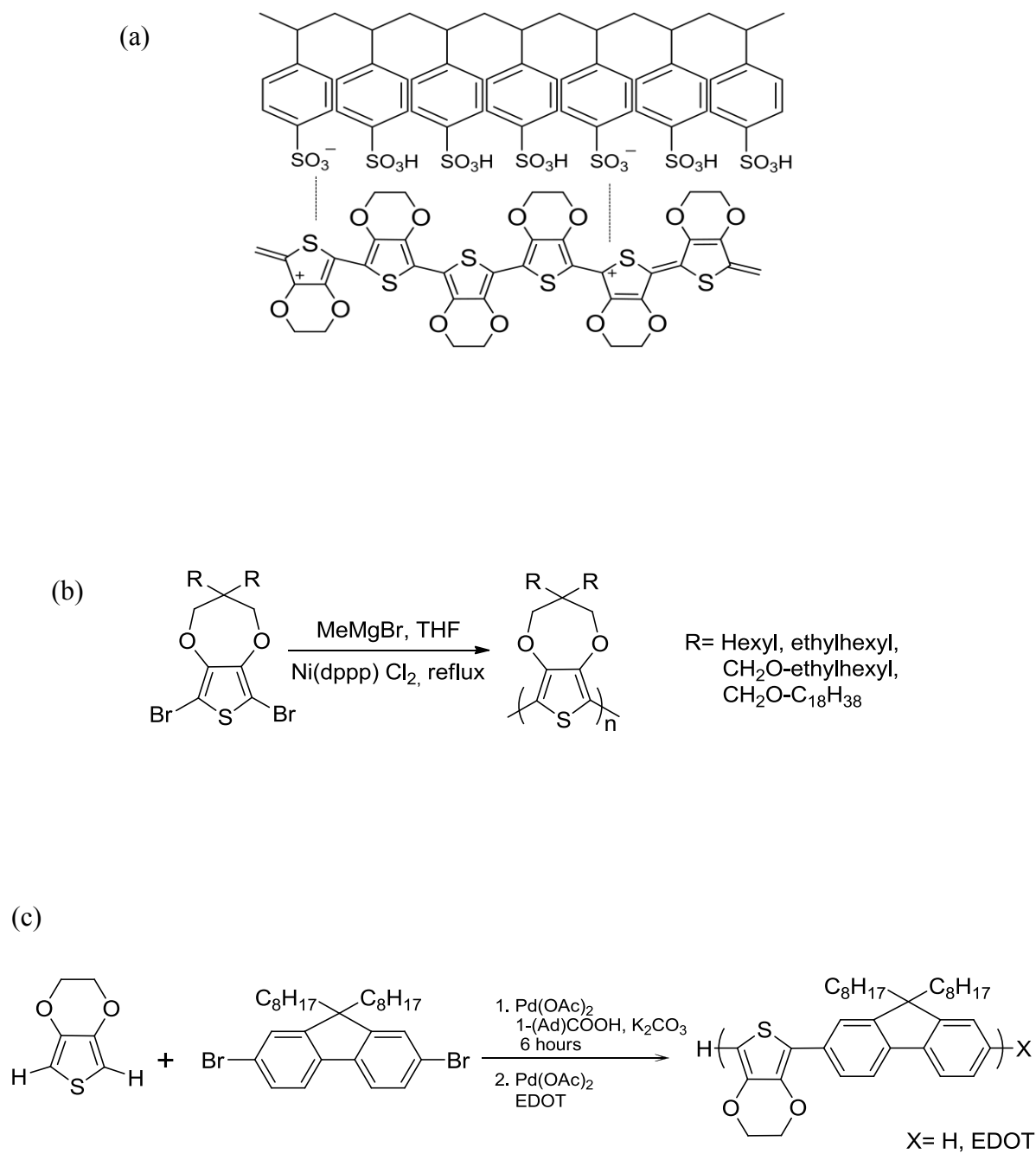
Nevertheless the synthesis of PEDOT based block copolymers has not been reported confirming the difficulties on the synthesis of controlled PEDOT polymers. Even though the choice of PEDOT for the synthesis of block copolymers seems challenging the great electrical properties and the lack of alternatives in the new PEDOT based composite, gave us the impetus to try new chemical routes for the synthesis of soluble PEDOT copolymers.

I.2.2   *Characteristics of poly (3-hexylthiophene)polymers*

Parallel to PEDOT, P3HT is a π-conjugated polymer with good solubility properties but with lower conductivity values than the PEDOT. The synthesis of P3HT polymer can be achieved by all the common polymerization methods used for the polythiophenes. These methods though do not have regiochemical control over head-to-tail couplings between the thiophene rings. Since the 3-hexylthiophene is a non symmetrical molecule, polymerization may occur in a nonregiospecific way forming three types of dyad structures (head-to-head, head-to-tail, and tail-to-tail) and four types of spectroscopically distinct triad structures. Among them, the regioregular (rr) head-to-tail coupled P3HT are more favorable, because they can easily self-assembly both in solution and in the solid state. In addition the rr-P3HT has superior electrical and photonic properties when compared to the other structures of P3HT.[6]

For the synthesis of rr-P3HT polymers McCullough proposed the Grignard metathesis polymerization (GRIM)[7,8] while Yokozawa developed the nickel catalyzed chain-growth polymerization.[9] Even though the two methods are similar, the GRIM polymerization is simpler and allows the end-functionalization of the P3HT. The synthetic procedure is presented in the figure 3 and it begins with the treatment of a 2,5-dibromo-3-hexylthiophene monomer with an alkyl or vinyl Grignard reagent through a reaction referred as Grignard metathesis. This reaction proceeds with a moderate degree of regioselectivity and the polymerization continues with the addition of the dichloro(1,3-bis(diphenylphosphino)propane)nickel ($Ni(II)(dppp)Cl_2$) catalyst. An associated pair of two 2-bromo-3-hexyl-5-chloromagnesium-thiophene is created by tail-to-tail coupling. The catalytic cycle of Ni(II) continues in three steps: oxidative addition, transmetalation and reductive elimination. The dimer is then released and the catalyst is the zero-

valent form (Ni(0)). The polymerization continues with the oxidative addition of a new monomer followed by the reductive elimination of the oligomer.
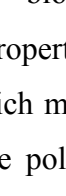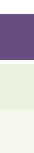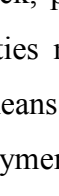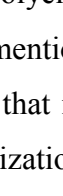
Figure 3. Proposed mechanism for End-Capped GRIM polymerization of P3HT and a table with different Grignard reagents and the resulting polymer.[10]
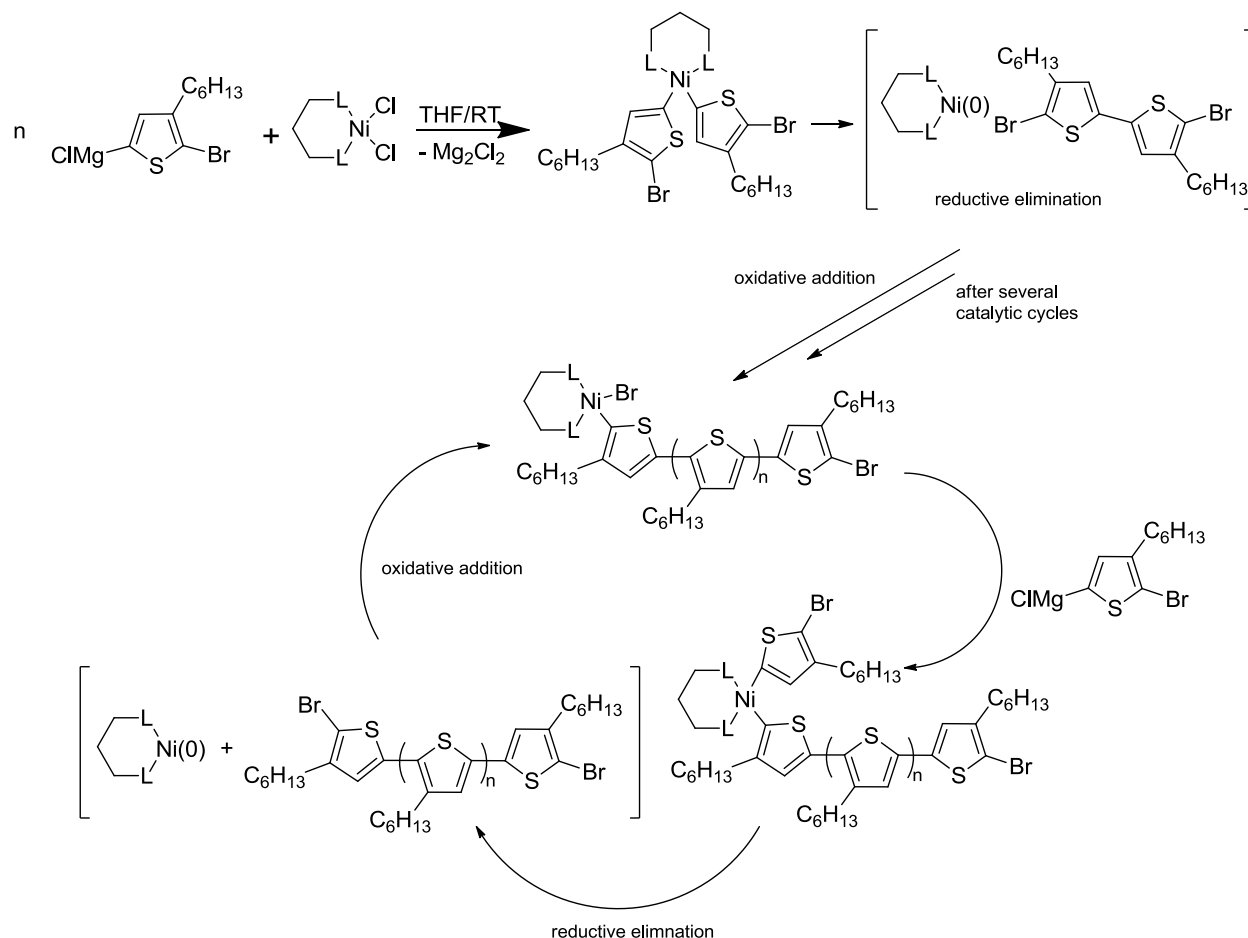
The reaction is terminated either by the addition of a Grignard reagent which contains the desired end-group. Depending on the nature of the functional Grignard reagent the P3HT polymers can be di- or mono- capped.[10] As it is shown in the table 1, polymers terminated with vinyl, allyl, or ethynyl end groups result mostly mono-capped polymers, while end groups like phenyl or *p*-tolyl groups di-capped polymers. This synthetic route, which leads to the synthesis of

rr-P3HT chains carrying a functional end group, is the initiative for the synthesis of P3HT-based block copolymers. Well defined di- and tri- block copolymers have been synthesized starting from an end-capped P3HT by several polymerization methods, like ATRP, "click" chemistry or RAFT polymerization.[11,12] The facile and controlled synthesis of mono- or di- functionalized P3HT copolymers allow us to try to synthesize new rod-coil block copolymers designed according the needs of our project.

Table 1. Several Grignard reagents used for end-capping P3HT chains and the type of resulted polymers.

Mono-capped polymers		Di-capped polymers	
Grignard reagent	**End group**	**Grignard reagent**	**End group**
VinylMgBr		PhenylMgBr	
AllylMgBr		TolylMgBr	
EthynylMgBr		BenzylMgCl	

I.3   *Water soluble coil blocks*

For the coil-block, or "flexible" block, polyelectrolyte polymer was selected for water solubility reasons and the electrical properties mentioned before. Poly(4-styrenesulfonic acid) (PSSA) is a strong polyelectrolyte, which means that it is fully charged in solution. A synthetic route for this polymer begins with the polymerization of the monomer's salt, the sodium 4-styrrenesulfonate (NaSS), resulting in the poly(sodium styrene sulfonate) (PSS) which after hydrolysis turns in the acid form of the PSSA. An alternative methodology has been proposed, by the controlled addition of sulfonate groups on the styrene units of a PS chain.[13] By this technique

the sulfonation degree can be easily controlled and calculated by ^{1}H-NMR by following the characteristic peak at 7.5 ppm corresponding to the sulfonic acid styrene units.

Another water soluble coil polymer that we used was the poly(vinyl alcohol) (PVA), which is not charged and it has excellent physical properties and film formation.[14] It has been widely used in dispersions of CNTs either as stabilizer or in order to assist in the mechanical properties of the system.[15,16] The PVA polymer cannot be polymerized from the corresponding monomer, instead it is produced from the hydrolysis of poly(vinyl acetate) (PVAc).

In this chapter the synthesis of well-defined rod-coil block copolymers will be presented with the rod block being a π-conjugated polymer (P3HT or PEDOT) and the coil block a polyelectrolyte (PPSA). In addition the beginning of a comparison work will be presented, where the coil block water is soluble but not charged (PVA). The chemical structures of the targeted copolymers are presented in the figure 4.

Figure 4. The chemical structures of the targeted copolymers.
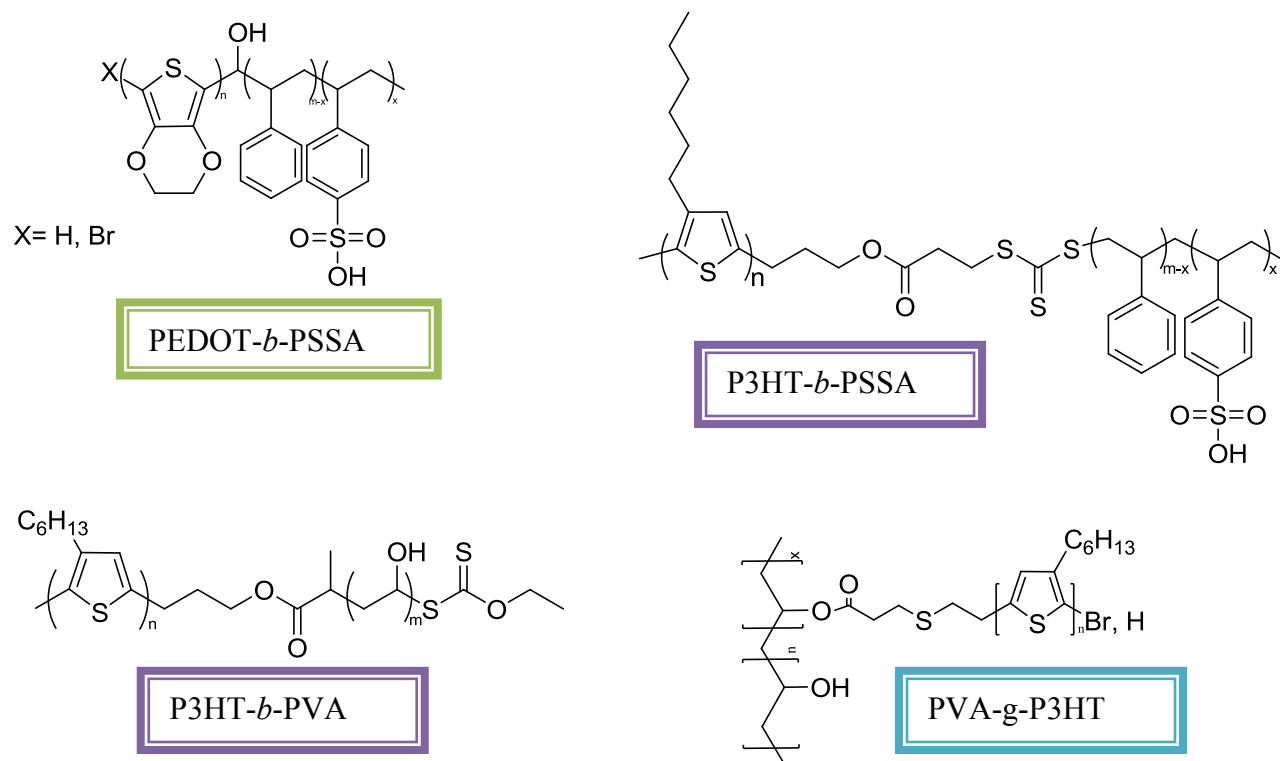
II   Results and discussion

II.1   Synthesis and characterization of PEDOT based block copolymers

The strategy, followed for the synthesis of PEDOT based block copolymers is illustrated in the figure 5 and it was based on the Suzuki coupling polymerization of the EDOT monomers. This type of polymerization is a palladium catalyzed cross-coupling between organoboron compounds and organic halides leading to the formation of carbon-carbon bonds. In order to avoid the precipitation of the PEDOT, since it is insoluble in most solvents, we proposed to end cap a classical polymer chain with an EDOT moiety that can further participate in the formation of PEDOT polymers by Suzuki coupling. By that way, well defined PEDOT polymers could be synthesized and by coupling with a flexible chain would remain also soluble in the solution. The synthesis of the required compounds as well as the methodology of the polymerization will be presented in the two following parts. The resulting copolymers could be a mixture of di-blocks and tri-blocks PEDOT-*b*-PS and of course PEDOT homopolymer which will be easily eliminated due to the solubility differences with the block copolymers. In addition, the same strategy was followed for non-controlled polymerization methods like oxidation polymerization and coupling polymerization. These polymerizations are usually used for the polymerization of EDOT and we chose them because they are common and efficient methods for the synthesis of PEDOT.

Figure 5. Schematic of the followed strategy for the synthesis of PEDOT-based copolymers.
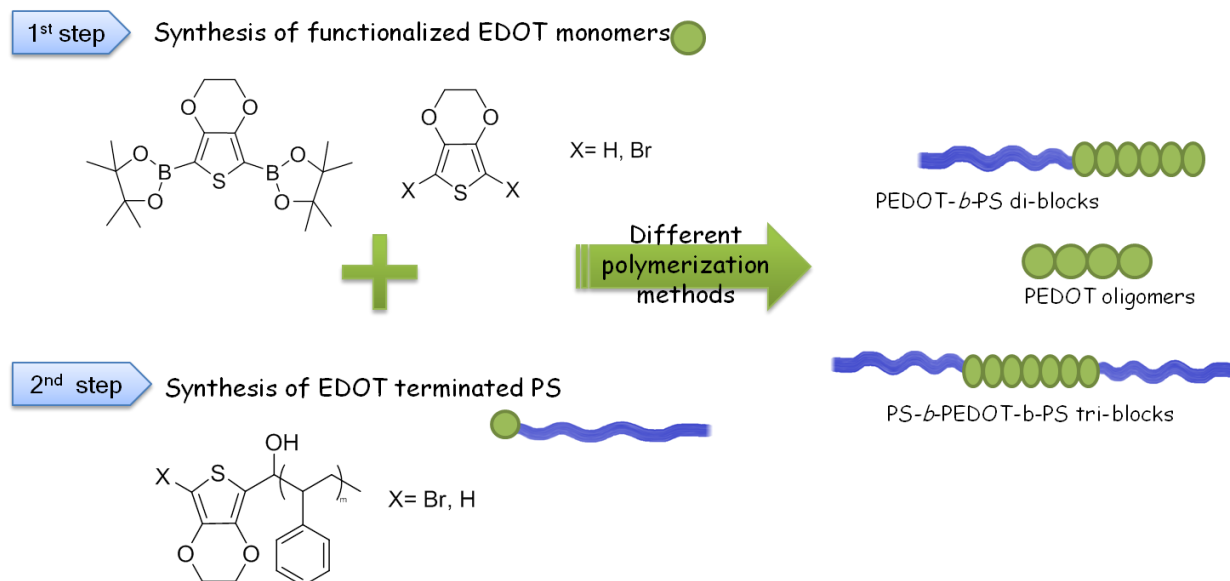
II.1.1 Synthesis of functionalized EDOT monomers

II.1.1.1 Synthesis of 2,5–dibromo-3,4-ethylenedioxythiophene monomers

Functionalized EDOT monomers with several functional groups were successfully synthesized. The synthesis of 2,5–dibromo-3,4-ethylenedioxythiophene (Br₂EDOT) is a simple one step reaction with the addition of N-bromosuccinimide (NBS) on the EDOT monomer, in a mixture of CHCl₃/CH₃COOH as solvents. Even though the procedure is simple, there are certain conditions that should be respected during the synthesis, since the Br₂EDOT is a sensitive monomer and it can be easily auto-polymerized. The flask containing the EDOT solution was placed in an ice/water bath, with temperature around 4 °C, before the addition of the 2.5 eq of NBS. The cold bath was remained during the first hour of the reaction. After eight hours the

reaction is complete and the solution has a yellow color. The purification of the Br$_2$EDOT was made by phase separation, using basic water and dichloromethane. The product was then recrystallized from MeOH solution at -20°C resulting in white crystals.

^{1}H-NMR spectrum in CDCl$_3$, is presented in the figure 6, verifying the functionalization of the EDOT and the purity of the product. The disappearance of the characteristic peaks of the thiophene group of the EDOT at around 6.3 ppm and the shift of the peak at 4.27 ppm prove the functionalization of the monomer with the two bromide atoms. The absence of the NBS peak at 2.5 ppm is a proof of the purity of the product.

Figure 6. (a) Synthesis of 2,5–dibromo-3,4-ethylenedioxythiophene and the ^{1}H-NMR spectra of the (b) 3,4-ethylenedioxythiophene and (c) 2,5–dibromo-3,4-ethylenedioxythiophene in CDCl$_3$ (400 MHz).
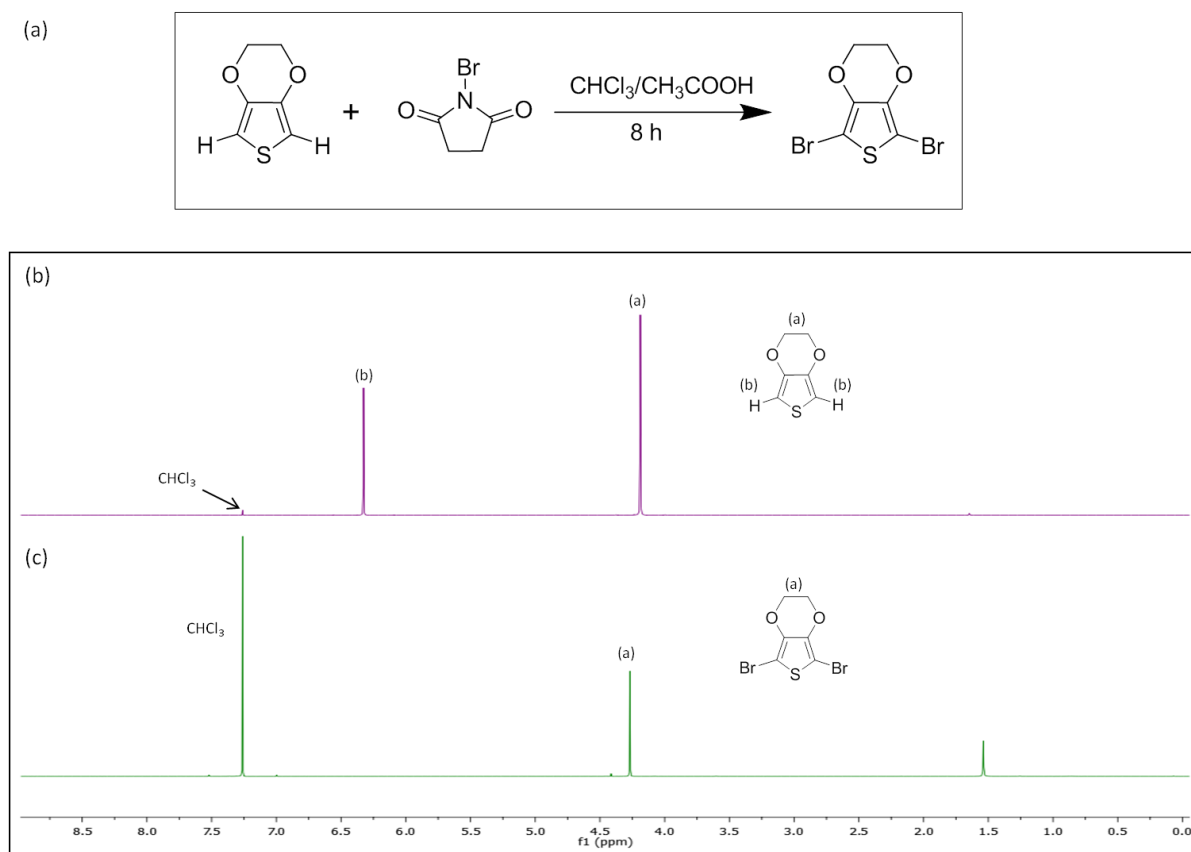
II.1.1.2 Synthesis of 2,5 di-(1,3,2-dioxaboralane)-EDOT monomers

We first targeted EDOT monomers bearing boronic acid moieties with the aim to be polymerized through Suzuki coupling. However, the resulting monomer was not soluble in organic solvents, consequently EDOT monomers with 1,3,2-dioxaboralane functional groups were synthesized instead. Two different synthetic routes were followed for the synthesis of the 2,5-di(-1,3,2-dioxaborolane)-3,4-ethylenedioxythiphene (DBoEDOT) and they are presented in scheme 1.

Scheme 1. Two different routes toward the synthesis of 2,5-di(1,3,2-dioxaborolane)-3,4-ethylenedioxythiophene.
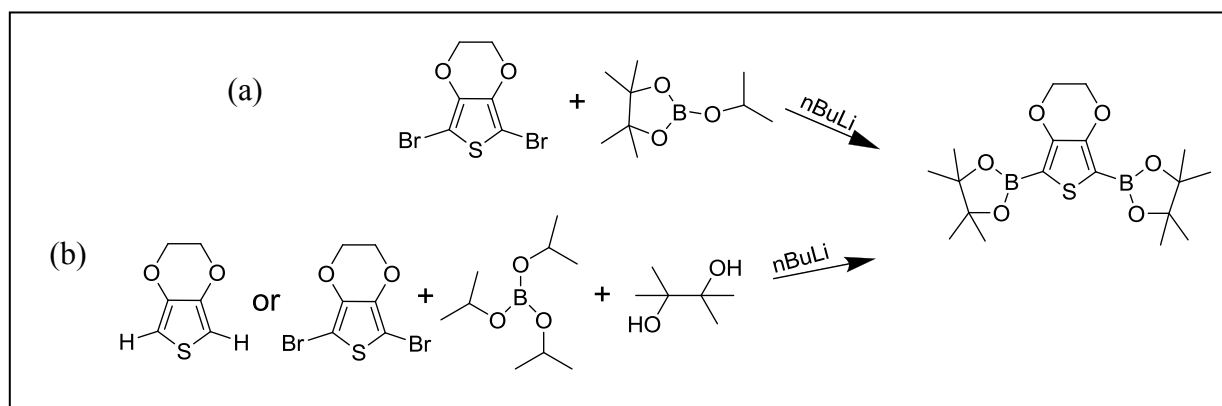
The first route (scheme 1 (a)) is a one step reaction starting from the Br_2EDOT moiety. First, Br_2EDOT was dissolved under dry conditions in THF, and the solution was cooled at -80°C, followed by the dropwise addition of 2eq of the nBu-Li 1.6 M. The system was then allowed to heat up to room temperature for one hour. The addition of the 2-isopropoxy-4,4,5,5-tetramethyl-1,3,2-dioxaborolane was made at -80 °C and the reaction was left for 48 hours at room temperature. A mixture of ice and water was added at the solution and the product was collected

by phase separation with water and diethyl ether as solvents. For further purification the product (yellow oil) was passed through a column chromatography with a mixture of heptane: ethyl acetate 3:1 as solvents. The ^{13}C-NMR is presented in figure 7, and the presence of some unknown peaks at 51 ppm and 32 ppm led us to conclude that the product was not sufficiently pure enough.

Figure 7. ^{13}C-NMR spectrum of the 2,5-di(1,3,2-dioxaborolane)-3,4-ethylenedioxythiophene synthesized by the first route in CDCl₃ (100 MHz).
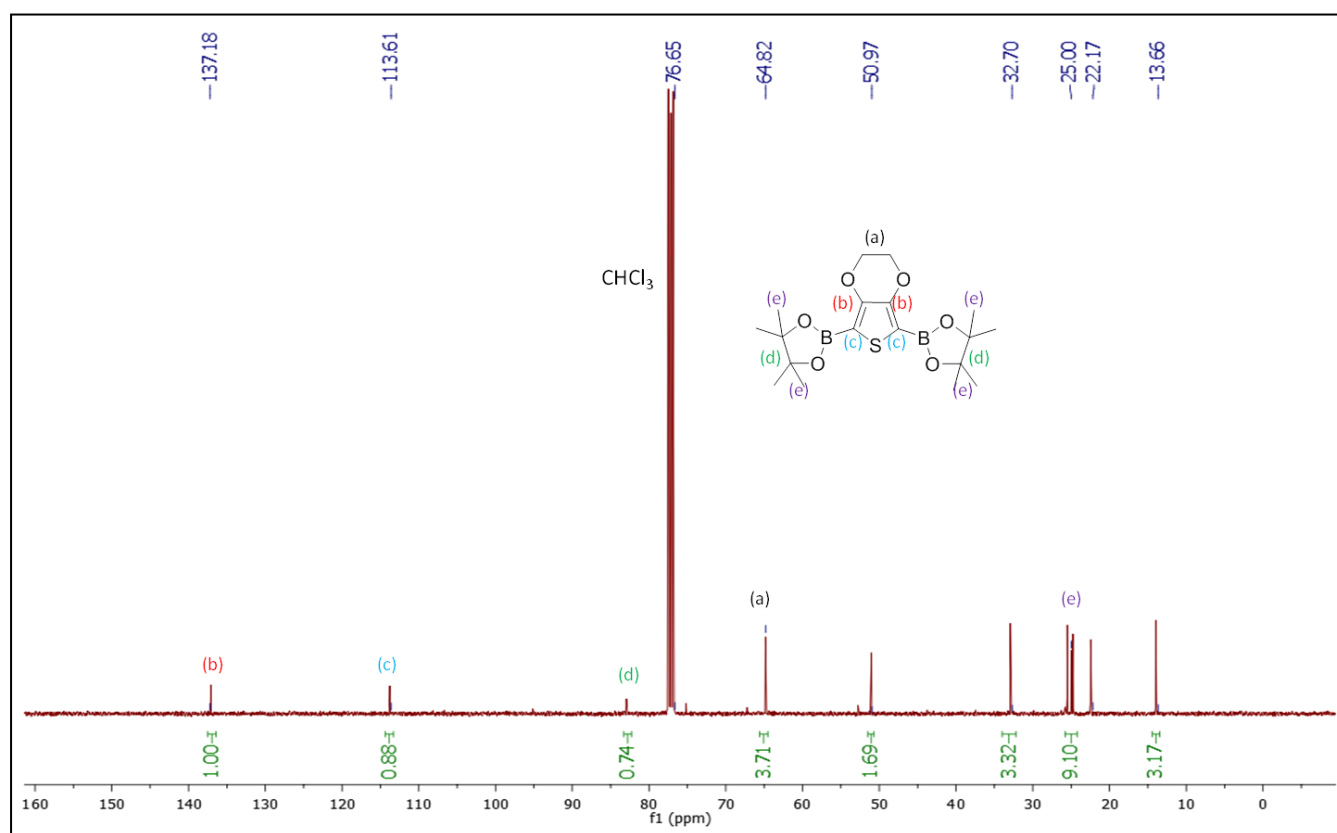
One of the difficulties of this reaction is the use of the Br₂EDOT, which is a very sensitive compound and it is not commercially available. In order to avoid the use of this compound new synthetic route (scheme 1(b) was proposed which can be initiated by either the commercially available EDOT or the Br₂EDOT.

123

A solution of EDOT in THF was prepared and cooled at -40°C. Keeping a low temperature (-20°C), 2.5 equivalent of n-butyllithium were added followed from the addition of 2.5 eq of triisopropyl borate after 30 minutes. The reaction continued for two hours at -40°C and for one hour at room temperature. A THF solution of 2 eq pinacol was added in acid conditions and the solution was left under stirring for two more hours. The product was purified by column chromatography with heptane: ethyl acetate 3:2 as eluents. In the ^{1}H-NMR analysis presented in figure 8, we observed some small amounts of reactants remaining that could be eliminated by passing through the column several times, reducing though the final yield.

Figure 8. ^{1}H-NMR spectra of the (a) 3,4-ethylenedioxythiophene and the (b) 2,5-di(1,3,2-dioxaborolane)-3,4-ethylenedioxythiophene synthesized by the second way in CDCl$_3$ after purification with benzene (400 MHz).
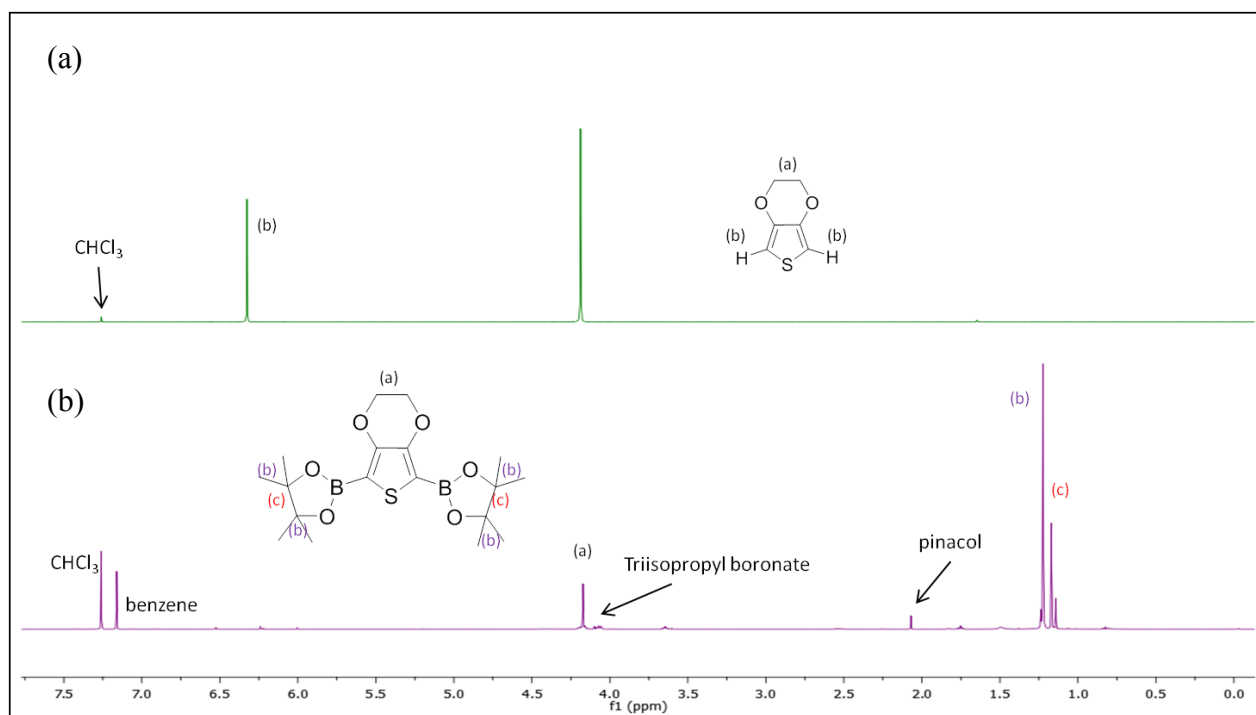
In summary, the synthesis of 2,5-di(-1,3,2-dioxaborolane)-3,4-ethylenedioxythiphene was tried by two different methods. The synthetic route which involves EDOT and the addition of pinacol and triisopropyl borate is easier and can afford larger amount of product. Even if the production of monomers with a high purity requires some supplementary purification steps, the monomers used for the Suzuki coupling reaction (paragraph II.1.3.1) were prepared following this second method.

II.1.1.3   Synthesis of formaldehyde-EDOT monomers as terminating group

As described in the figure 5, the synthesis of a flexible chain terminated by an EDOT monomer is required for the synthesis of PEDOT-based block copolymers. These monomers should contain a functional group that will be attached on the flexible chain and a moiety that will participate in the EDOT polymerization. The formaldehyde group was selected because it can act as a terminating group in anionic polymerizations (scheme 2). EDOT and Br$_2$EDOT monomers mono-functionalized with a formaldehyde end group were successfully synthesized. The preparation of the 2-bromo-5-formaldehyde-3,4-ethylenedioxythiophene is an one step reaction. BrEDOT was dissolved in distilled diethyl ether and the solution was cooled at -80°C. 1.2 eq of n-butyllithium 2.5M were added and the reaction was kept at the same temperature for three hours. After the addition of DMF at 0°C, the reaction continued for 24 hours. The product was collected by phase separation and purified by column chromatography using heptane: DCM 1:1 as eluents.

Similar method was followed for the synthesis of the 2-formaldehyde-3,4-ethylenedioxythiophene. The formylation of EDOT was carried out with N,N-dimethylformamide in the presence of n-BuLi in diethyl ether as solvent and the product was purified by column chromatography using heptane: DCM 1:1 as eluents. Both monomers were characterized by ^{1}H-NMR spectroscopy and the spectra are presented in figure 9.

After the successful synthesis of the functionalized EDOT monomers, they were tested as terminating groups for PS chains. The reaction procedure is presented in the scheme 2.

Figure 9. ^{1}H-NMR spectra of (a) 2-bromo-5-formaldehyde-3,4-ethylenedioxythiophene and (b) 2-formaldehyde-3,4- ethylenedioxythiophene in CDCl$_3$ (400 MHz).
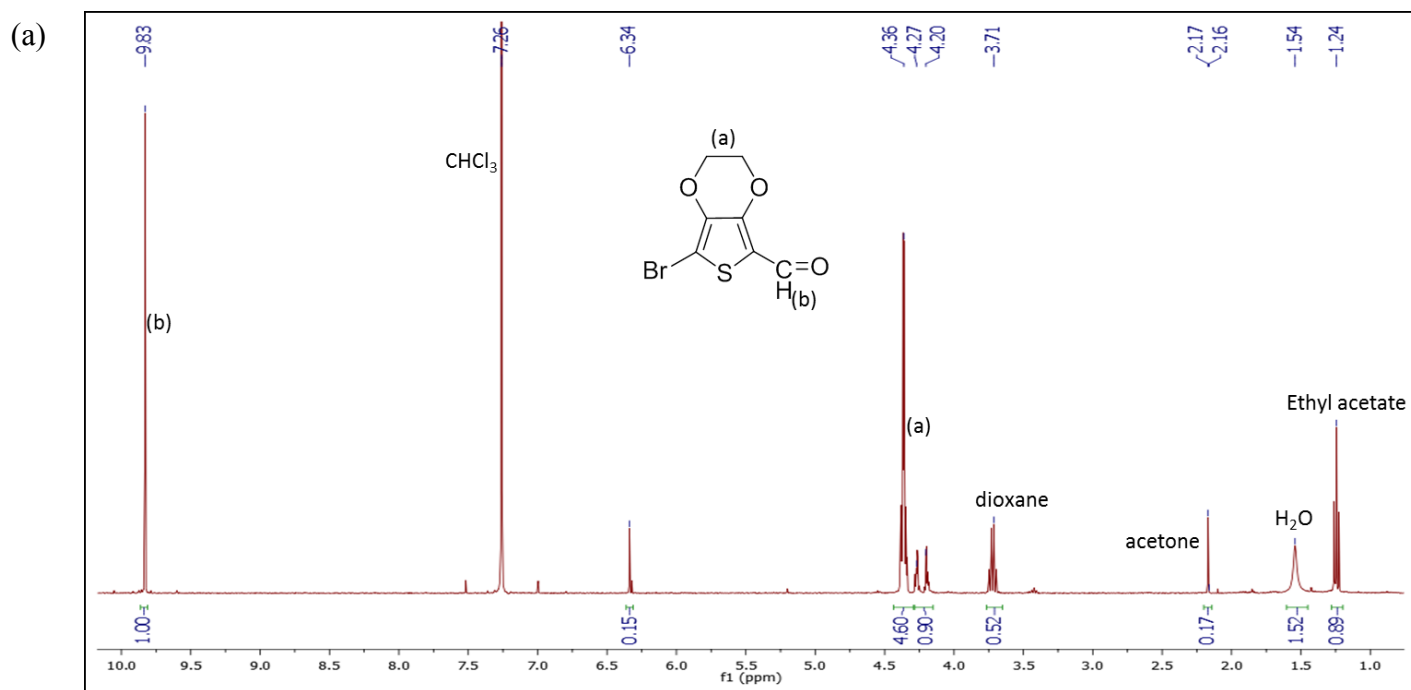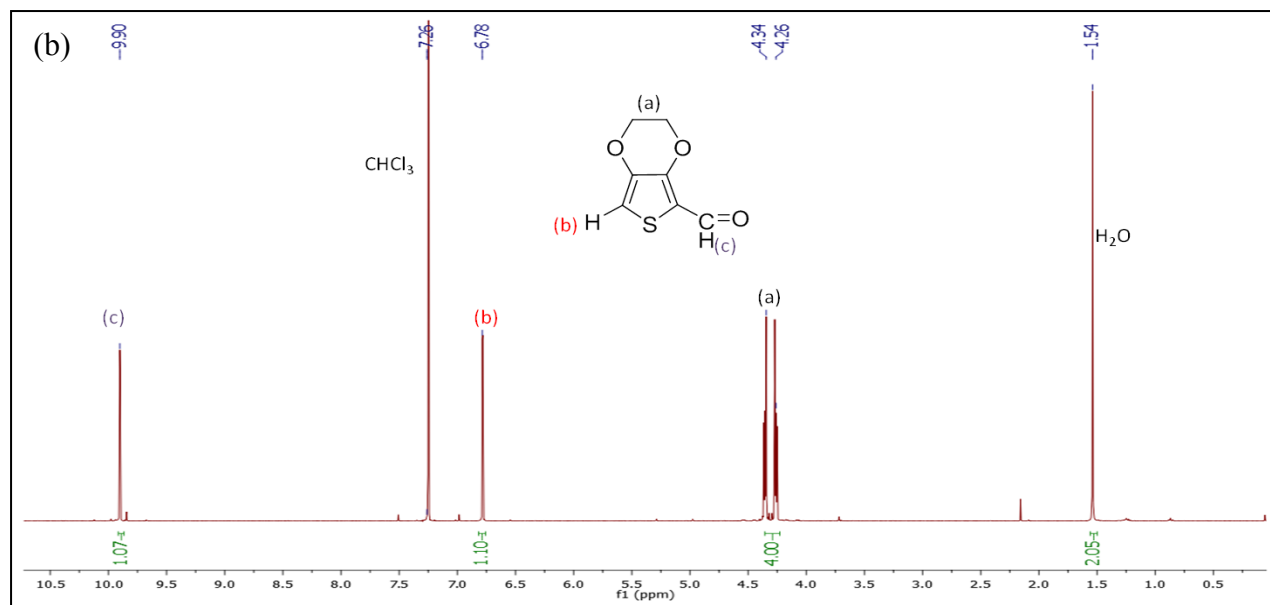
II.1.2 Synthesis of functionalized PS macro-monomers

In the introduction of this chapter we have exposed our strategy which includes the synthesis of PEDOT based block copolymers. As coil block was chosen the poly(sodium styrene sulfonate) (PSSA) polyelectrolyte. We chose to synthesize the PSSA by the addition of sulfuric groups on the styrene units of a polystyrene chain, in order to have the ability to control the sulfonation degree. This procedure will be further analyzed in the paragraph II.2.2. For that reason the synthesis of PEDOT-*b*-PS copolymers was first targeted.

Polystyrene was synthesized by anionic polymerization, a method that allows us to control the end group functionality. Under neat conditions, the styrene monomer was dissolved in distilled toluene and under stirring sec-butyllithium 1.6 M was added. The molecular weight of the PS was controlled by the ratio monomer/ initiator (M/I). The target molecular weights of the PS were from 10000 to 20000 g/mol for the first tried and then were changed in smaller weight (e.g 2000-5000 g/mol). The compounds used as terminal groups were degassed before the addition in the solution containing the leaving PS chains and then followed by the addition of degassed MeOH. Three different EDOT units were tried as end groups of PS, the 2-bromo-5-formaldehyde-3,4-

ethylenedioxythiophene, the 2-formaldehyde-3,4-ethylenedioxythiophene and the Br₂EDOT (scheme 2).

Scheme 2. (a) The different functionalized EDOT units used as terminating end groups (b) and the mechanism of the anionic polymerization of PS.

(a)

(b)

Formation of polymer

X= H, Br
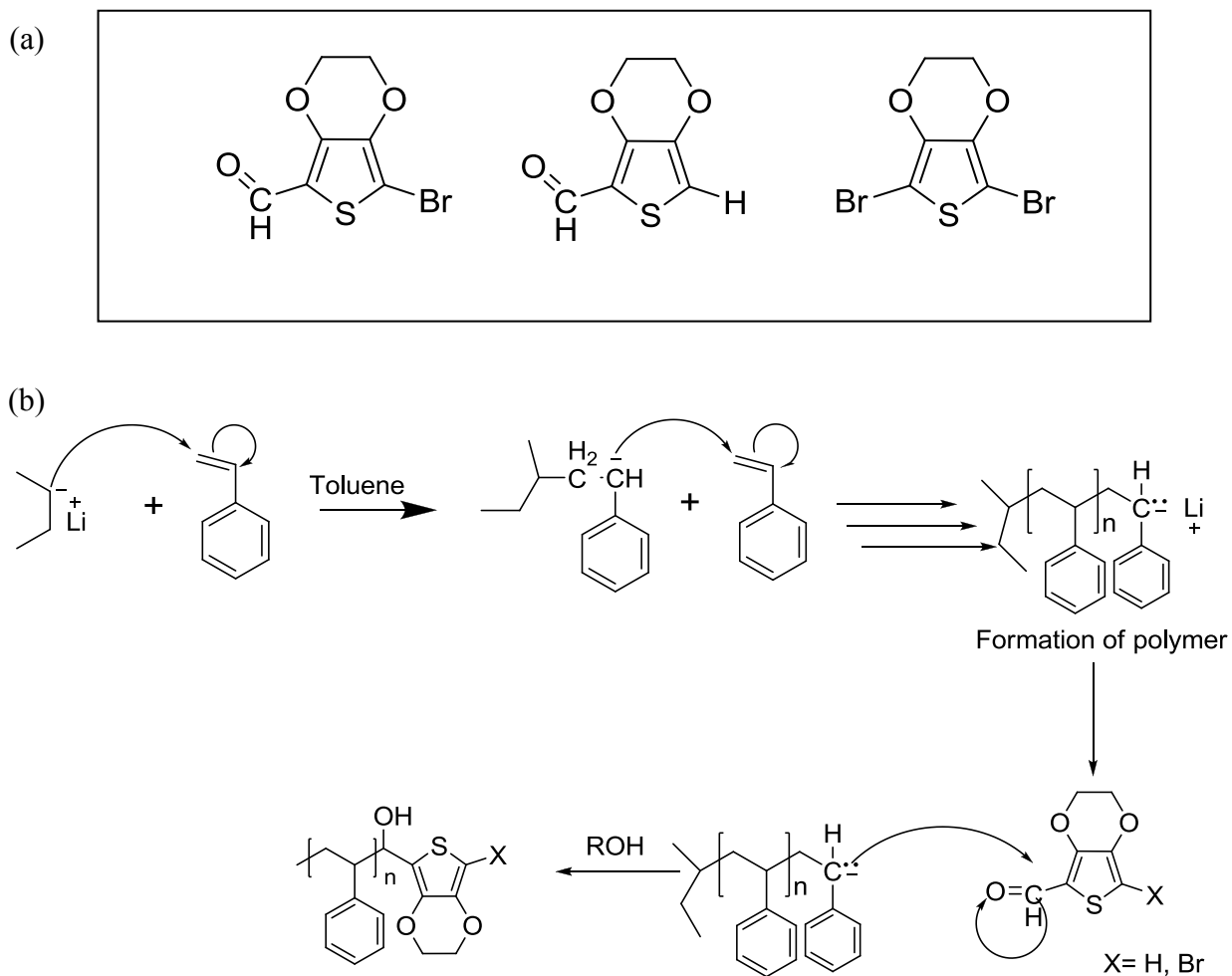
The Size-exclusion chromatography (SEC) of the PS terminated by the 2-bromo-5-formaldehyde-3,4-ethylenedioxythiophene showed a bimodal distribution with one main peak that corresponds to PS and a peak at high molecular weight that could correspond to the coupling product (PS-PS). This type of trace is typical for coupled polymers, meaning that one EDOT unit is linked to two

polymer chains. Similar results were obtained with the use of the 2-formaldehyde-3,4-ethylenedioxythiophene monomer.

We assume that this behavior is due to the competition between the formaldehyde group and the Br or H group, since they can both react with the leaving PS even though formaldehyde should be more reactive. The coupling effect was reduced by the increase of the ratio terminal group/PS$^-$Li$^+$ but it was not eliminated. In the figure 10 SEC chromatographs of PS terminated by 2-formaldehyde-3,4-ethylenedioxythiophene monomer with different terminal group/PS$^-$Li$^+$ ratios are presented. It is clear that when we use the 2-bromo-5-formaldehyde-3,4-ethylenedioxythiophene monomer as terminated agent of the PS we obtain more coupled chains (bigger peak of the high Mn) than when we use the 2-formaldehyde-3,4-ethylenedioxythiophene monomer. This behavior can be explained since both Br and CHO can react with the PS chains.

Figure 10. SEC (RI) in THF of PS terminated by 2-bromo-5-formaldehyde-3,4-ethylenedioxythiophene (green) and by 2-formaldehyde-3,4-ethylenedioxythiophene in two different concentrations (red and black).
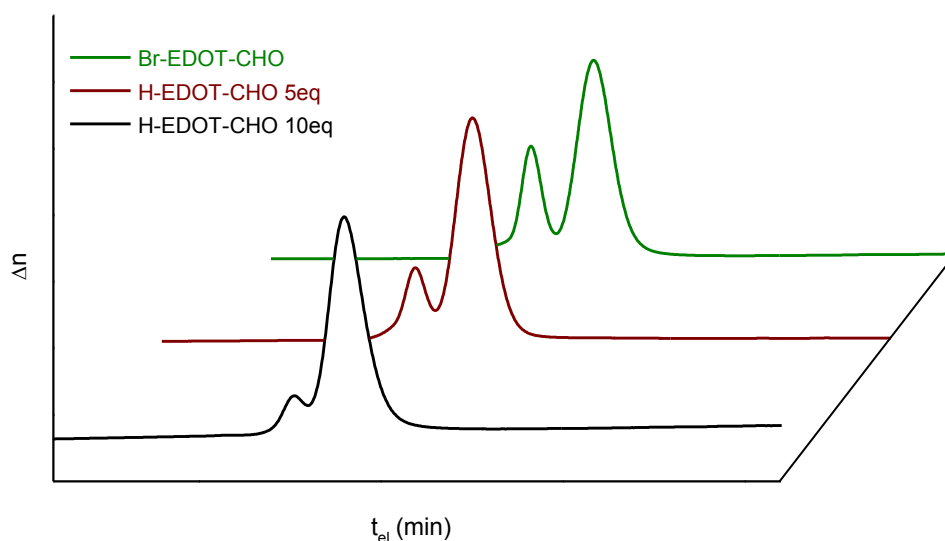
In order to eliminate this coupling side reaction, Br$_2$EDOT was used as terminating agent of the PS. The living PS chains are sensitive to oxygen or to any impurity that the terminal groups may contain, making the synthesis of mono-dispersed EDOT functionalized PS difficult. Different methods of purification of the terminating agents as well as different addition techniques (changing the solutions concentration, the speed of the addition of the terminating agents) were tried without achieving monodispersed functionalized PS.

Figure 11. SEC (RI detector) in THF of PS terminated by Br$_2$EDOT monomer (calibration with PS standards).
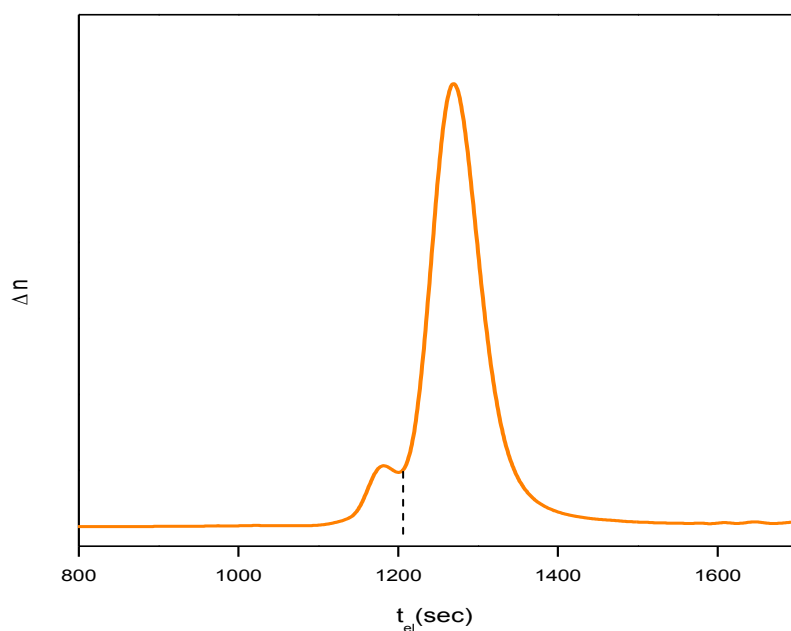
	Mn(g/mol)	Area %
Main PS chain	3700	95
Coupled PS chains	9500	5

II.1.3 Synthesis of PEDOT-based block copolymers

II.1.3.1 Suzuki coupling

In scheme 3 the Suzuki coupling of EDOT monomers in the presence of a quenching PS polymer as ω-EDOT-PS is presented. The PEDOT polymer chains will start growing in the first step of the reaction by the coupling of the EDOT monomers, while the PS-EDOT-Br will act in a second step of the process as a chain stopper. The amount of each component was calculated based on the molecular weight of the PS and an example of this calculation is also presented in the scheme 3. All the products were lyophilized under dioxane before the polymerization. THF and water solution 1M NaHCO$_3$ were degassed and refluxed at 90°C for three hours before their use. The Pd(PPh$_3$)$_4$ catalyst (1% in mol) was added TO THE SOLUTION and the reaction was maintained under reflux for four days.

Scheme 3. Suzuki coupling reaction for the polymerization of EDOT.
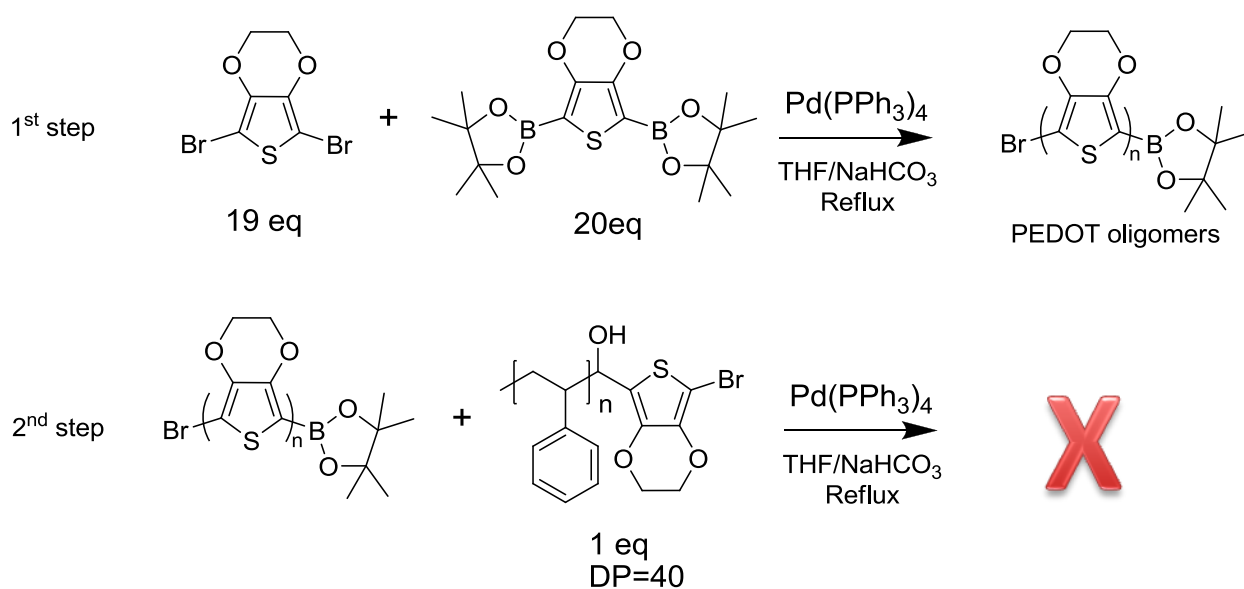
The resulting product was recovered by precipitation in MeOH and had a brown color. By ^{1}H-NMR we can clearly see the characteristic peaks of PS at 7 ppm and 6.5 ppm and a sharp peak at 4.2 ppm which corresponds to the EDOT units and probably not to PEDOT polymer. The fact that there was no polymerization of EDOT was also verified by SEC analysis, since there is only a small shift in the PS peak (figure 12). Even though the reaction was repeated several times, modifying the time and the equivalent of the components, no polymerization of EDOT was observed.

Figure 12 (a) ^{1}H-NMR spectra (1) of the PS-EDOT before the coupling reaction and (2) of the products after Suzuki reaction (CDCl₃, 400 MHz) (b) SEC (UV detector at 260nm) of PS-EDOT and of the final product after Suzuki polymerization in THF (PS calibration).
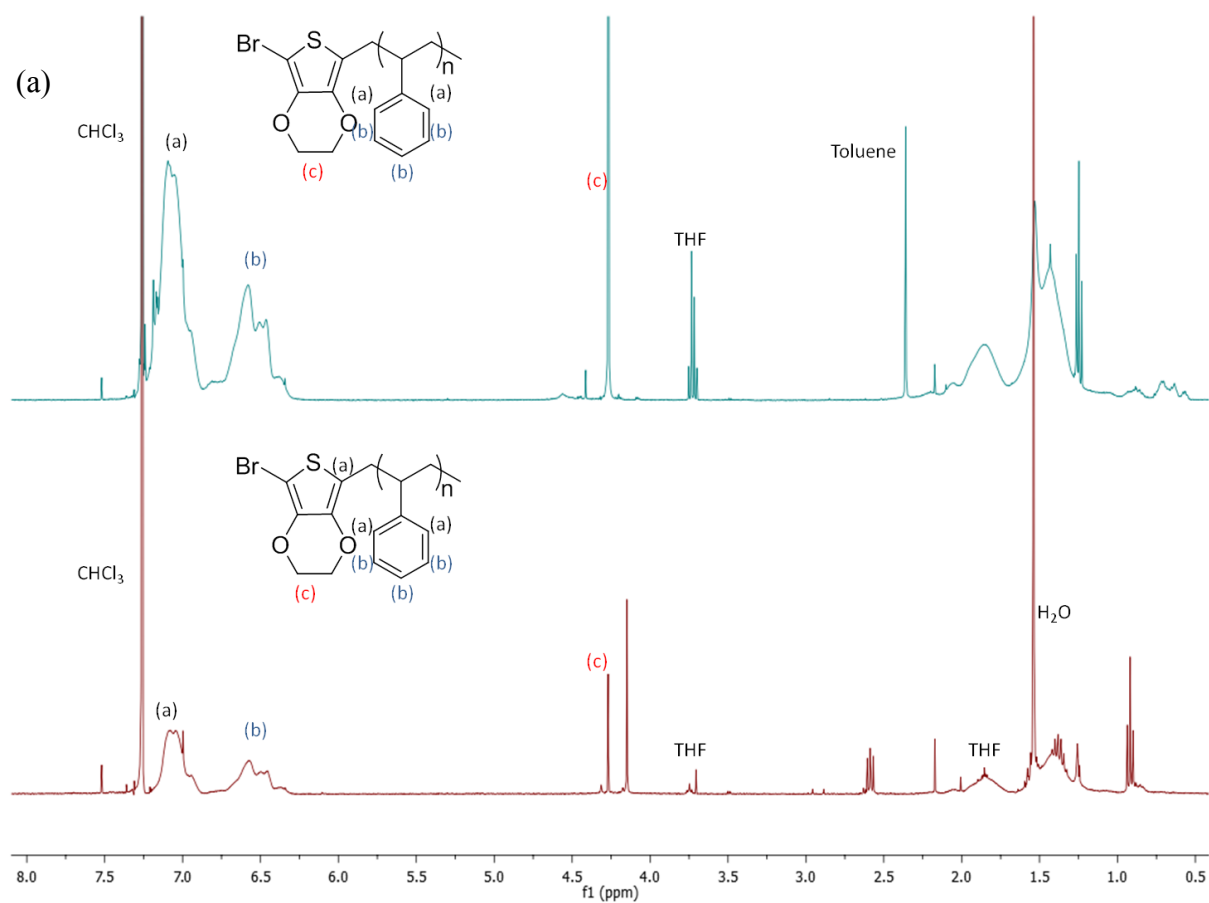
(b)
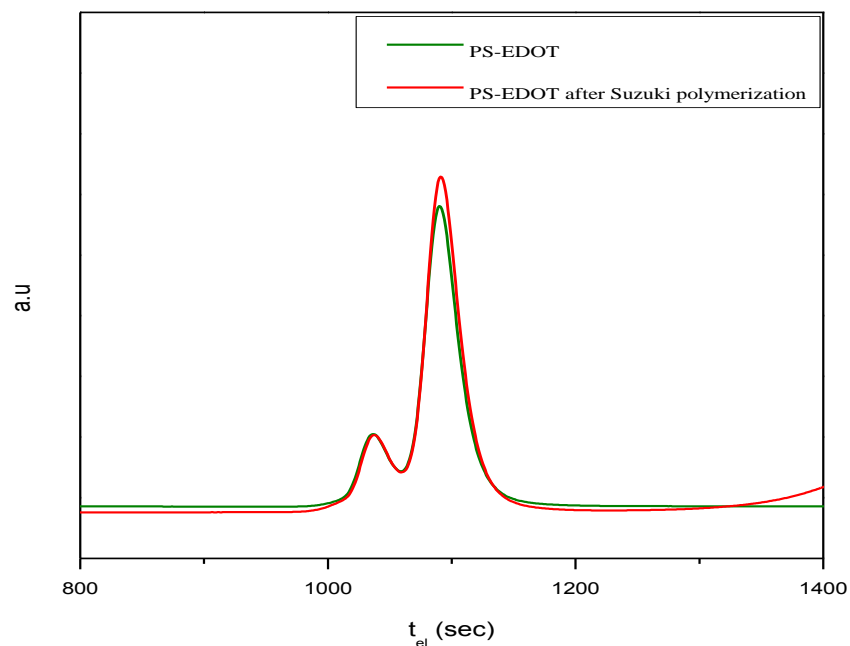
There are several reasons that may influence the Suzuki polymerization of the EDOT. First of all questions about the purity of our products can be raised, since by the ^{1}H NMR spectra we have noticed small quantities of impurities that we could not be removed. In addition it is possible that the polymerization conditions that we tested were not correct for EDOT monomers. Even though the palladium catalyst has been successfully used for the synthesis of numerous π-conjugated polymers, it is possible that it can not initiate the polymerization of EDOT monomers.

II.1.3.2 Oxidative and Coupling polymerizations

Due to the limitations described above, other polymerization methods were examined following the same strategy of polymerization of EDOT units in the presence of an EDOT

terminated PS chain (scheme 4). The usual methods for the synthesis of PEDOT polymers are via oxidation and coupling polymerizations.

Even though these techniques do not lead to well-defined polymers they were chosen due to their efficiency. The oxidative polymerization is taking place between EDOT monomers in the presence of several oxidants, like FeCl$_3$. The coupling polymerization is taking place in the presence of Lewis acids and the monomers can be either Br$_2$EDOT or EDOT, depending on the acid.

Scheme 4. Oxidative and coupling polymerizations of EDOT/Br$_2$EDOT monomers with their corresponding ω-EDOT-PS chain stopper.
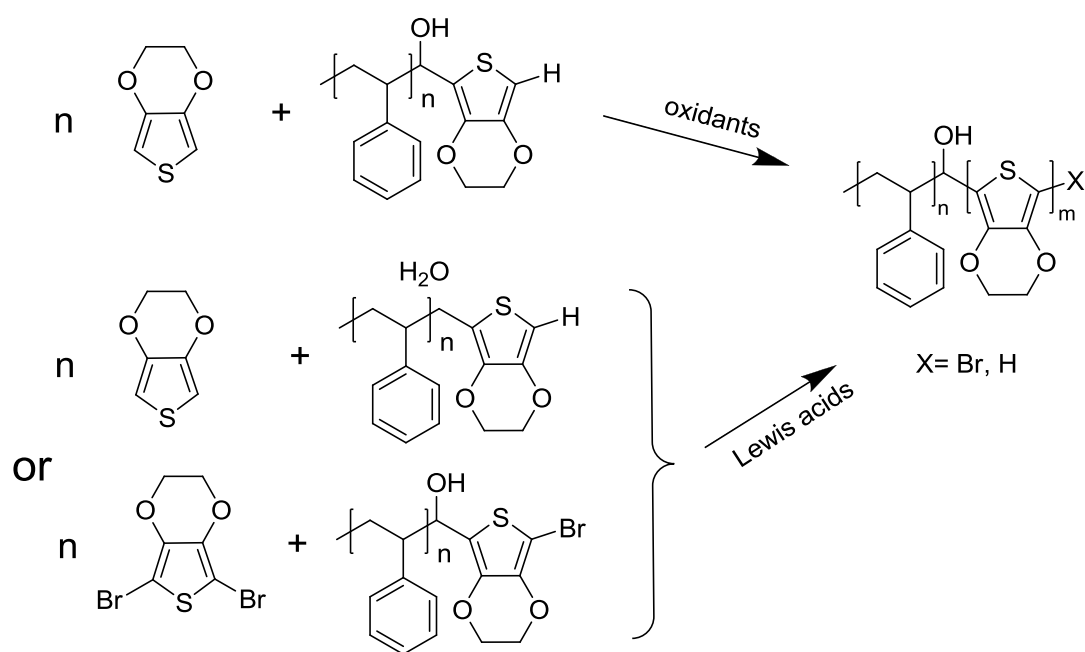
Oxidative coupling polymerization of EDOT and PS-EDOT occurred in CHCl$_3$ as solvent and in the presence of FeCl$_3$ as an oxidant. The amount of FeCl$_3$ was kept constant at 2.5 eq relative to EDOT and the reaction conditions were kept constant at 38°C for 48 hours. The amount of the EDOT monomer in relation to the PS-EDOT was varied as shown in table 2.

Table 2. The amount of ω-EDOT-PS, EDOT, FeCl₃ tested with oxidative polymerization

	PS-EDOT (Mn= 7000 g/mol)[1]	**EDOT**	**FeCl₃**	**Observations**
1	1 eq	10 eq	25 eq	No polymer
2	1 eq	30 eq	75 eq	PEDOT oligomers
3	1 eq	50 eq	125 eq	PS, PS-*b*-PEDOT oligomers

[1] Estimated by SEC calibrated on PS standards

For the polymerization with 30 eq of EDOT, the synthesis of PEDOT oligomers was observed. From the SEC analysis it seems that most of these oligomers are not attached to the PS chain. As the amount of EDOT monomer was increased at 50 eq, a small shift of the PS peak appears which could be caused by the growth of EDOT oligomers on the chain. In addition the trace which corresponds to the coupled PS chains is bigger, indicating that the end groups of the PS could react resulting in more coupled chains. The reason that PS-*b*-PEDOT block copolymers could not be achieved in high yield by this method, could be due to lower reactivity of the EDOT unit that is attached at the PS chain and in comparison to the EDOT monomers, and for that reason the PS-EDOT did not participate in the polymerization. In addition, the polymerization of the EDOT monomers was relatively slower with the presence of the PS chains in the solution which could be also a reason for the low yield in the synthesis of PEDOT block copolymers.

Figure 13. SEC of the ω-EDOT-PS and the of the mixture after oxidative polymerization with 50eq of EDOT units in THF (UV detector at 260nm, PS calibration)
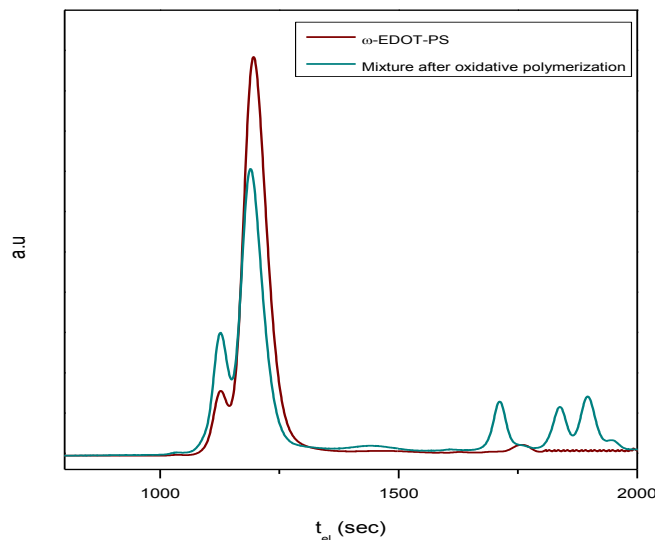
The coupling polymerization of Br_2EDOT was then tested, since it is a more reactive way for the synthesis of PEDOT. DBEDOT monomers prepared as described above, and PS-EDOT-Br were solubilized in toluene, followed by the addition of the $BF_3 \cdot O(Et)_3$ acid. The reaction was heated at 100 °C for 24 hours. Based on the SEC analysis we can make the hypothesis that the reaction yielded three different products: PS-EDOT, PS-*b*-PEDOT, and PEDOT-*b*-PS-*b*-PEDOT (scheme 5 and figure 14). In addition the elimination of the PS-EDOT from the system was not achieved, due to their solubility in common solvents. By this polymerization method we achieved our best results, but the final product was not well defined and we were not able to separate the PS-*b*-PEDOT from the reaction mixture. Similar observations with the oxidative polymerization were made about the reactivity of the EDOT unit that is attached on the PS chain.

Scheme 5 The structures of the resulted products after the coupling polymerization of PS-EDOT-Br and Br₂EDOT.

PEDOT-*b*-PS

Br-EDOT-PS

PEDOT-*b*-PS-*b*-PEDOT
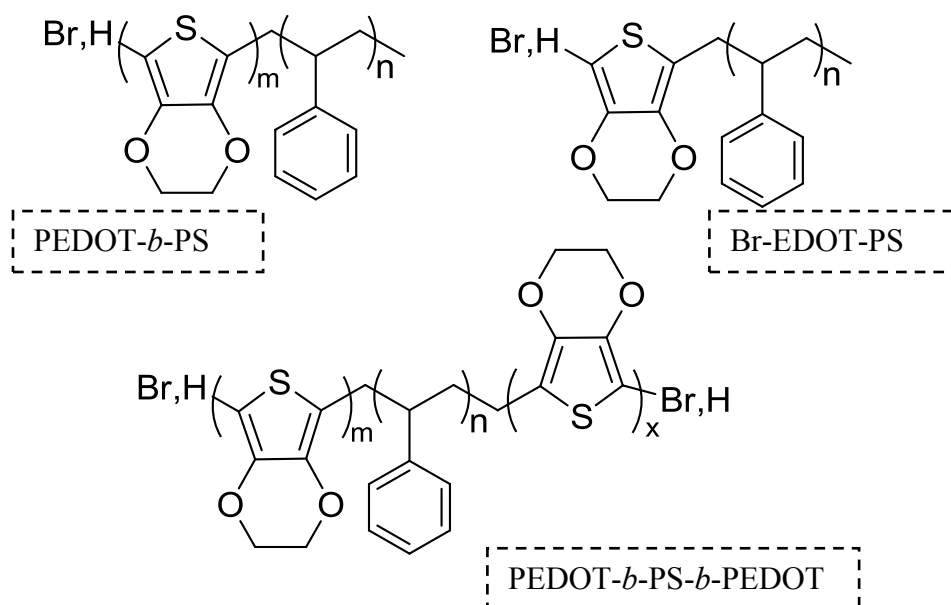
Figure 14. (a) SEC chromatography of the mixture after coupling polymerization in THF (UV detector at 260nm, PS calibration) and (b) its ¹H-NMR in CDCl₃ (400 MHz).

(a)
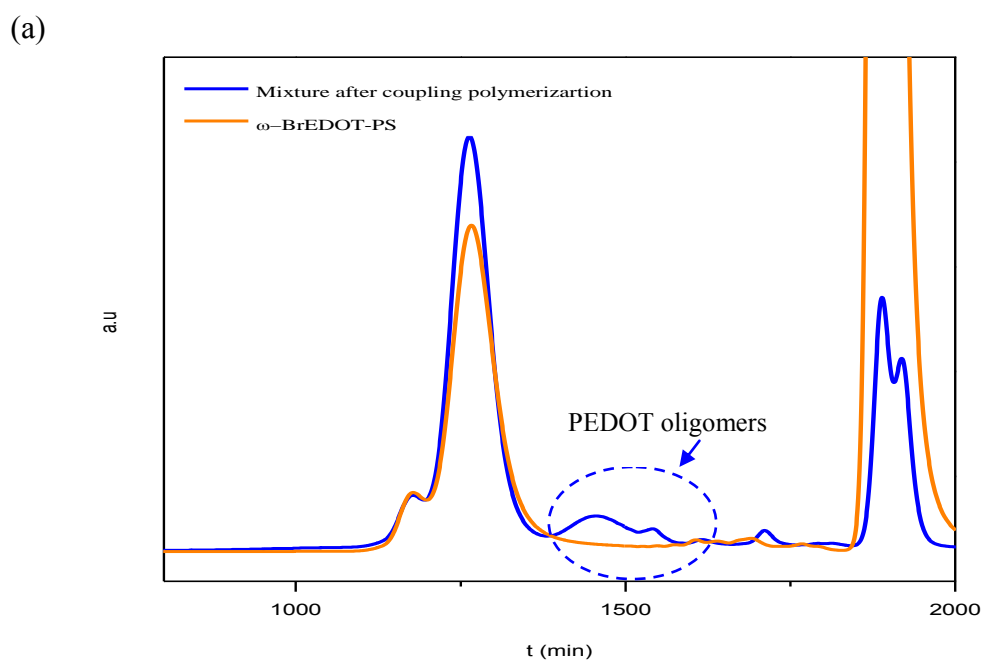
	ω-BrEDOT-PS	PS main chain after coupling polymerization	PEDOT oligomers
Mn (g/mol) (PS calibration)	3700	4700	1400-600 = 5-3 Br₂EDOT units
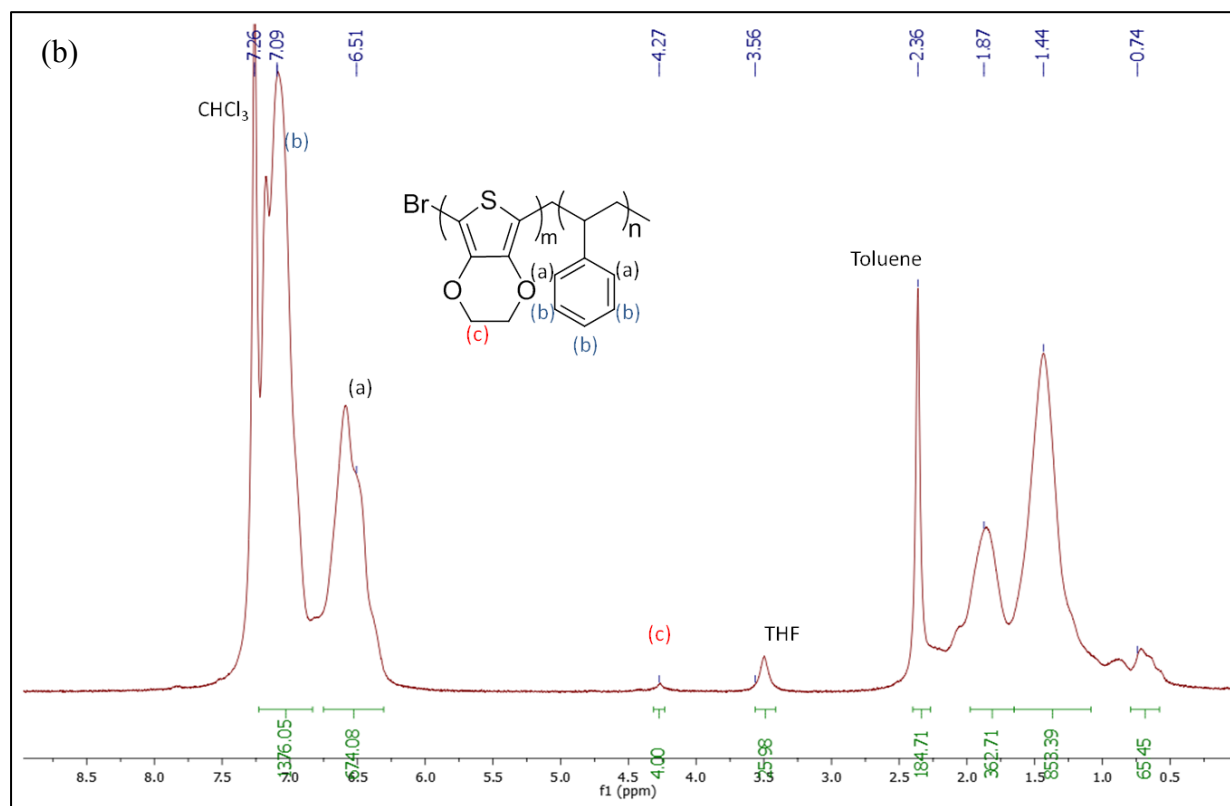
Unfortunately, the polymerization of EDOT units in the presence of PS-EDOT chains for the synthesis of PEDOT-*b*-PS was not accomplished by three different methods. For the Suzuki coupling polymerization the low purity of our products could be a reason for the failure of the reactions. In addition there has been no report of the synthesis of PEDOT by this method even though it has been widely used for several π-conjugated polymers. By oxidative and coupling polymerization, there was formation of PS-*b*-PEDOT copolymers, but the size of the PEDOT

was in the range of oligomers. In addition the polymerizations were not controlled and the purification of the copolymers from the PS-EDOT was not possible due to the solubility in common solvents. It was evident from both types of polymerizations that the reactivity of the EDOT unit that was attached on the PS chain was low, preventing the synthesis of block copolymers.

II.2   Synthesis and characterization of P3HT based block copolymers

P3HT based copolymers were synthesized following the McCullough *and coll*. method.[12] Firstly regioregular-P3HT block was synthesized by GRIM polymerization. The importance of the regioregularity of P3HT was analyzed in the introduction chapter. The mechanism of the GRIM polymerization is presented in the figure 3. By GRIM polymerization the molecular weight and the dispersity of the synthesized P3HT can be easily controlled. In addition the terminating ends of the polymer can be capped by several functional groups. These groups can be further functionalized in order to initiate the polymerization of the second block by different polymerization techniques.

The synthesis of P3HT-*b*-PS block copolymers used in this thesis was achieved by combining the GRIM polymerization (for the P3HT) and the Reversible Addition-Fragmentation chain Transfer (RAFT) polymerization (for the PS).[17] This polymerization was chosen over ATRP or "click" polymerization in order to reduce the use of transition metal catalysts which can act as poisoning agents in organic electronic devices.

The mechanism of RAFT polymerization is described in the chapter V (V.3.14) and it is based on the use of a chain transfer agent (CTA or RAFT agent) that is controlling the molecular weight and the dispersity during the free-radical polymerization. The transfer agent will be attached as an end-group in the P3HT, creating a RAFT-macroiniator.

The polyelectrolyte character of the block copolymer was added after by the controlled sulfonation of the PS block. This type of reaction has been used before for the synthesis of poly (styrene sulfuric acid) (PSSA) homo-polymers but also for the sulfonation of PS block copolymers.[13,18] By this method the sulfonation level can be easily controlled and characterized. In addition the reaction conditions are not harmful for the other polymers that are participating.

Following the same strategy of combining the GRIM and RAFT polymerization, the synthesis of P3HT-*b*-PVA block copolymers was investigated. In addition different architectures of the P3HT/PVA system were investigated.

The synthesis of well-defined copolymers with different architecture will be described in this chapter. The reaction procedures and methodologies will be analyzed and the complete characterization of the P3HT based copolymers will be presented.

II.2.1   Synthesis of P3HT-b-PS block copolymers

As shown in scheme 6 our strategy requires the synthesis of well defined ω-functionalized P3HT, i.e allyl terminated P3HT. The general synthesis of regioregular allyl terminated P3HT polymers via GRIM metathesis polymerization is presented in the figure 3. The 2,5 (dibromo-3-hexylthiophene) is reacting with the Grignard reagent tert-butylmagnesium chloride for the synthesis of an active group on the thiophene group. After the end of the polymerization another Grignard reagent, which is carrying the functional group, is added. The resulting polymer is purified by Soxhlet extraction and then characterized by ^{1}H-NMR as shown in figure 15 and SEC. The appearance of characteristic peaks at 6 ppm, 5.2 ppm and 3.5 ppm which correspond to the allyl functional group, proves the successful addition of the end group to the polymer. Based on these peaks we can also calculate the molecular weight of the P3HT. The molecular weights calculated by NMR and by SEC are not the same, since the molecular weight by SEC is calculated based on PS calibration. As real molecular weight we accept the one calculated by ^{1}H-NMR.

Figure 15. ^{1}H-NMR spectrum of allyl-terminated P3HT (CDCl₃, 400MHz).
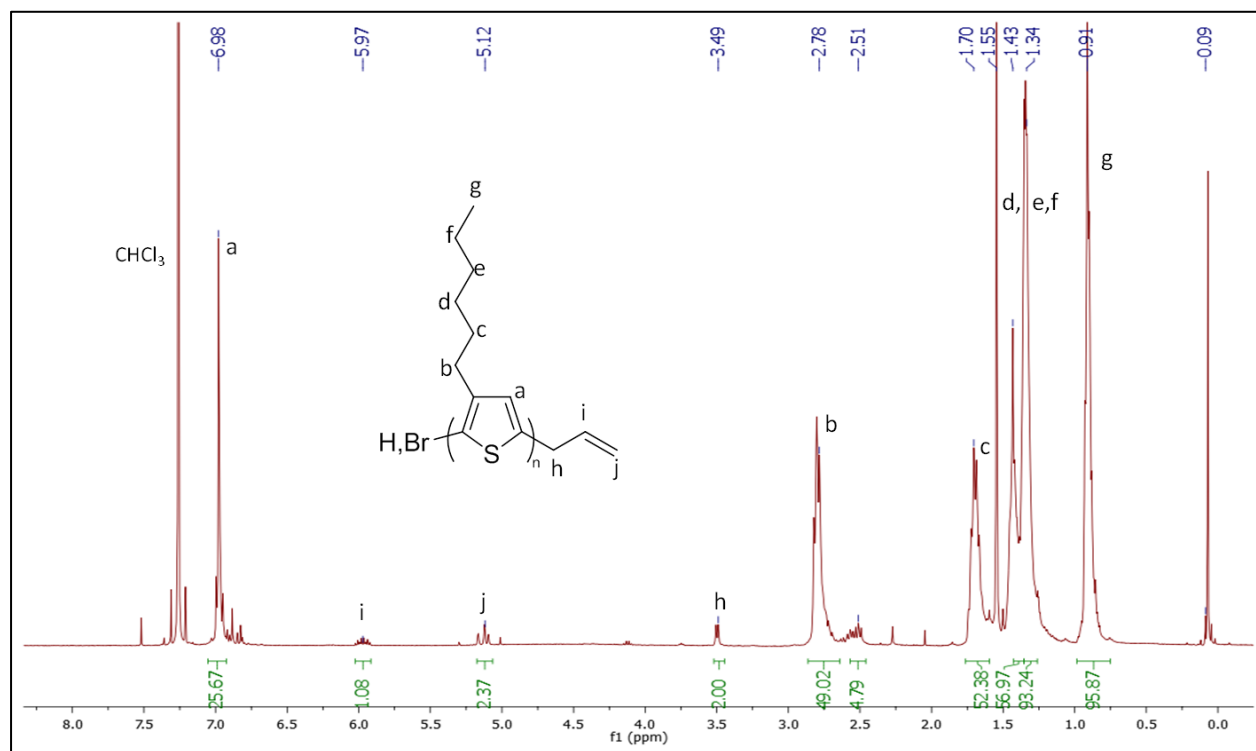
The peak at 2.51 ppm corresponds to the protons of a carbon that is connected in the α position of the thiophene ring, like the protons of the peak at 2.78 ppm (b in the P3HT structure). The difference between them is that the peak of 2.78 ppm corresponds to protons in a regioregular environment while the peak at 0.51 in a non regioregular one. For the ratio of these two peaks we can calculate that the P3HT is 90% regioregular. In the table 3 the characteristics of all the P3HT polymers synthesized by that way are presented.

Table 3. Characteristics of the P3HT synthesized by GRIM polymerization. The SEC analysis were made in THF with UV detector at 260nm and PS calibration. [1] H NMR spectra were obtained in CDCl₃ (400 MHz). The regularity was calculates as described above.

Mn SEC (g/mol)	Dispersity (by SEC)	Mn ^{1}H NMR (g/mol)	% regularity
12000	1.1	10500	93%
9700	1.2	9000	89%
6000	1.2	5200	90%

The 3-benzylsulfanylthiocarbonylsulfanylpropionic acid RAFT agent is a typical RAFT agent for the polymerization of the styrene and it was synthesized according to the literature.[19] Since the RAFT agent bears a carboxyl acid group, we have to introduce a hydroxyl end group to the P3HT in order to be attached through esterification reaction. The reactions for the functionalization of the P3HT and the RAFT polymerization of the PS are shown in scheme 6.

Scheme 6. Synthesis of P3HT-b-PS by RAFT process.
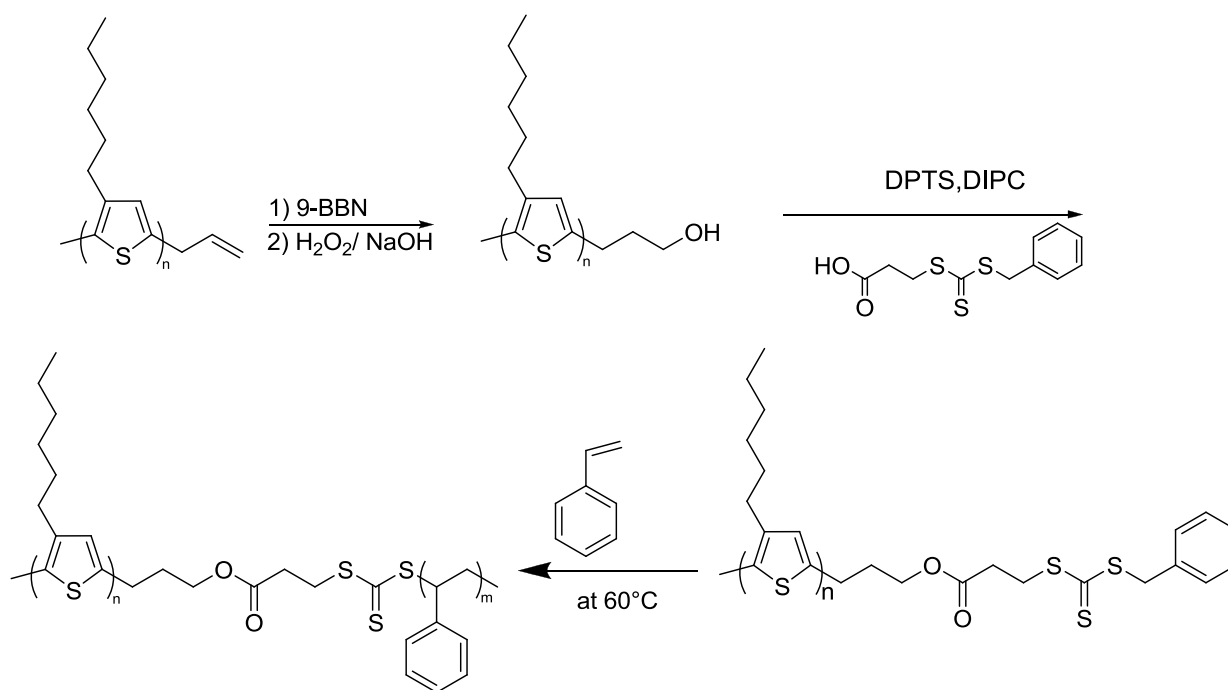
For the synthesis of hydroxyl propyl terminated P3HT, the allyl end group of the polymer was further treated with 9-borabicyclo[3.3.1]nonane followed by the addition of hydrogen peroxide and aqueous NaOH solutions in order to obtain a hydroxypropyl end group. The successful reaction was verified by ^{1}H-NMR and IR spectroscopy. In the ^{1}H-NMR spectra the disappearance on the peaks of the allyl group and also the presence of the new peaks at 3.7 ppm and 3.9 ppm verify the complete functionalization of the P3HT (figure 16). In addition the IR spectra of the hydroxylpropyl terminated P3HT exhibits a broad absorption peak at 3000-3400 cm^{-1}, which is characteristic of the O-H stretch for alcohols and phenols.

Figure 16. ^{1}H-NMR spectrum of hydroxylpropyl terminated P3HT (CDCl$_3$, 400MHz).
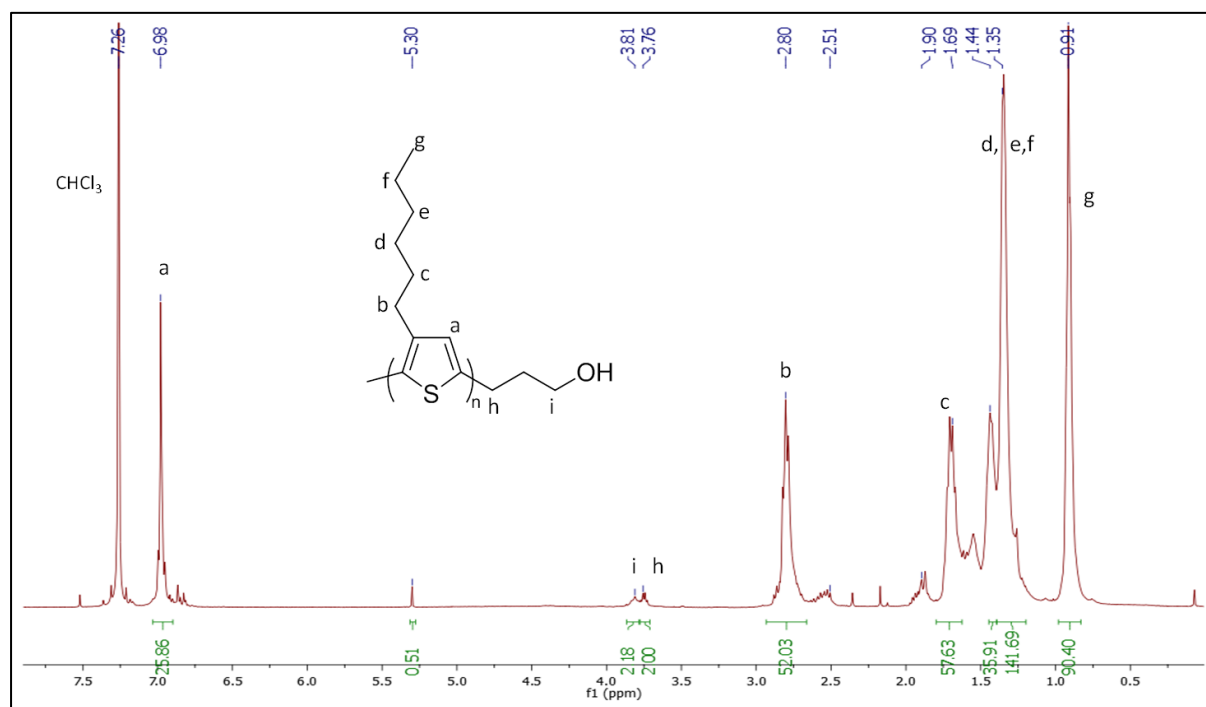
The successful esterification reaction of the 3-benzylsulfanylthiocarbonylsulfanylpropionic acid RAFT agent and the hydroxylpropyl terminated P3HT resulting the macro-RAFT initiator. The macro-initiator was characterized by ^{1}H-NMR, where the new end group appears. The P3HT-macro initiator was used for the RAFT polymerization of styrene in bulk. The molecular weight of the styrene can be controlled by the time of the reaction. The resulting block copolymers were precipitated in MeOH and then characterized by ^{1}H-NMR and SEC. The molecular weights of both blocks were calculated based on the ^{1}H-NMR spectra and the dispersity calculated based on the SEC.

Figure 17 (a) ^{1}H-NMR spectra of P3HT-*b*-PS block copolymer (CDCl₃, 400MHz) and (b) SEC of the P3HT and P3HT-*b*-PS in THF with PS calibration (UV detector at 260nm).

(b)
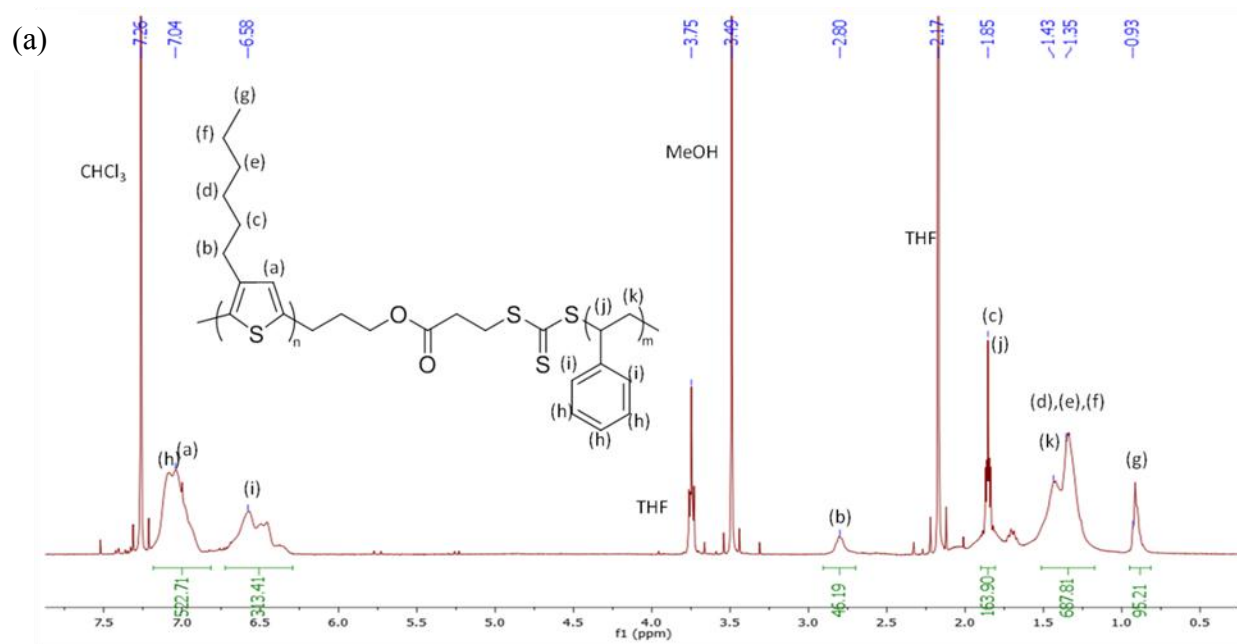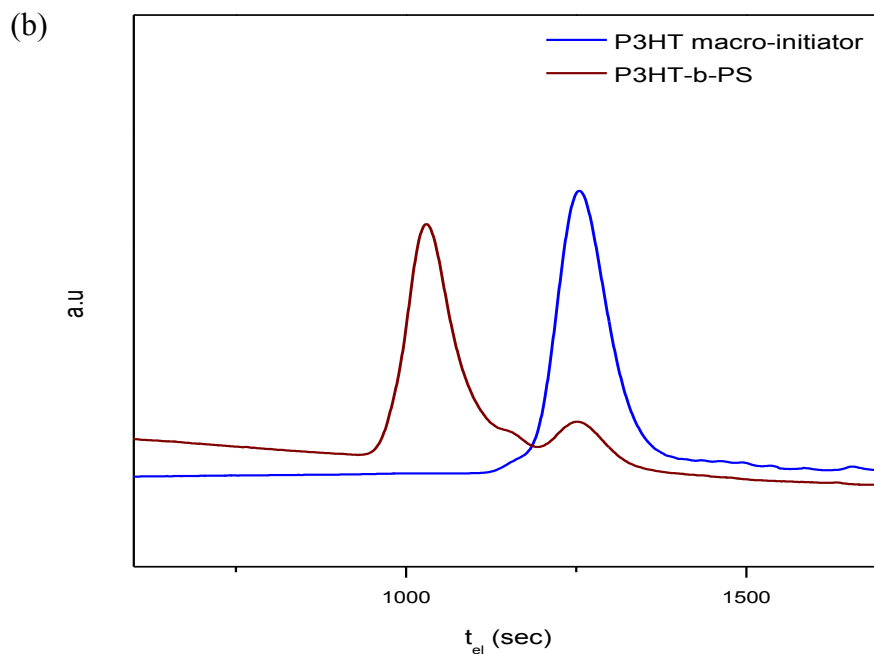
	Mn	D
P3HT-*b*-PS	49755	1.2
P3HT	5063	1.1

In the SEC chromatogram of the P3HT-*b*-PS we observe a small peak in exactly the same position as the peak of the P3HT homopolymer. The presence of this peak signifies that there is a small amount of P3HT that did not participate in the RAFT polymerization, due to its functionalization with the RAFT agent. From this observation we conclude that the functionalization of the P3HT is not 100% successful, a phenomenon that was observed in all the polymerizations through this method.

A library of four block copolymers P3HT-*b*-PS were synthesized according to this methodology and their macromolecular characteristics are presented in the table 4.

II.2.2   Synthesis of P3HT-*b*-PSSA block copolymers

The synthesis of the P3HT-*b*-PSSA was achieved by the controlled sulfonation of the PS block of the P3HT-*b*-PS copolymers previously synthesized. The sulfonation reaction is achieved through the addition of acetic anhydride to a solution of P3HT-*b*-PS in degassed dichloroethane (scheme 7).

Scheme 7. The sulfonation reaction of the P3HT-*b*-PS copolymers.
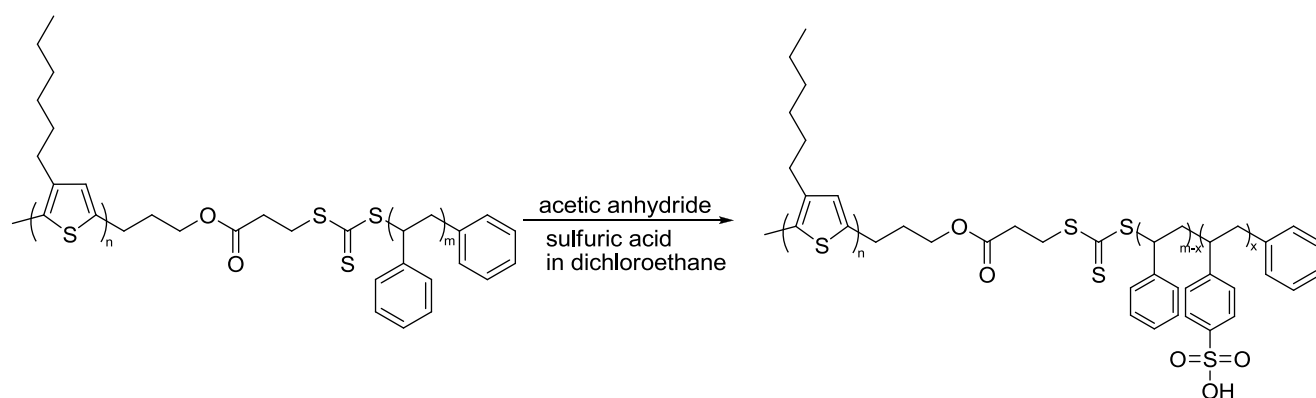
The sulfonation levels (SL) were determined by ^{1}H-NMR by following the characteristic peak at 7.5 ppm corresponding to the sulfonic acid styrene units (figure 18). The equation that is used for the calculation of the sulfonation level of the PS is given in the figure 18.

Figure 18. A zoom of a ¹H-NMR of PS-*co*-PSSA (CDCl₃, 400 MHz) and the equation for calculating the sulfonation level.
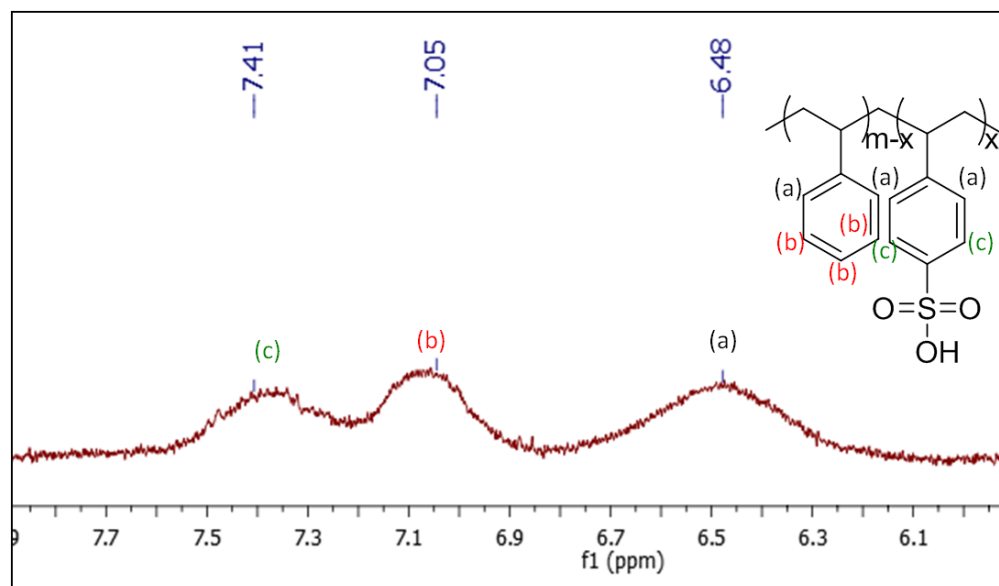
$$\%SL = \frac{integrals \; of \; peak \; \frac{c}{2}}{integrals \; of \; (peak \; \frac{b}{3} + peak \frac{c}{2})}$$

There are two parameters that influence the sulfonation level of the PS chain: the amount of the added reactant and the temperature of the reaction. In order to obtain the desired sulfonation level, a small excess as regards to the stoichiometry of sulfonation agent should be added. In fact, for 30% sulfonation level we added the amount for 50% sulfonation in order to achieve the desired percentage. Furthermore the reaction takes longer (at least three days) for a sulfonation level around 50% while it takes only one day for <30% sulfonation level. All the data are gathered in table 4.

Regarding higher sulfonation levels (% SL) some difficulties were encountered. Even though the amount of the sulfonation agent was high and the duration of the reaction was more than three days, we could not realize %SL higher than 50%. This difficulty was overcome by heating the reaction at 60°C. The results of this reaction are in the table 3 and correspond to the copolymer 3 and 4. It is noteworthy that there is a limitation on the sulfonation level we can obtain, which is due to the change in the nature of the copolymer. Indeed, as the sulfonation level increases, the copolymer starts to behave like an amphiphilic copolymer and when a certain degree of sulfonation is reached the copolymer has a strong hydrophilic character and consequently is no more soluble in organic solvents. The result of this solubility change, leads to the precipitation of the copolymer during the sulfonation reaction in the reaction medium (*i.e* dichloroethane).

For comparison, we evaluated the solubility and the physico-chemical behavior of these copolymers as a function of the volume fraction (f) of each block. The copolymers 1 and 2 have the same P3HT volume fraction (f_{P3HT} = 0.34) but the PSSA volume fraction is varying from 0.23 to 0.33. The copolymer with the lower PSSA volume fraction (f_{PSSA1}= 0.23) was soluble in common organic solvents, such as dichloroethane and DCM. By a small increase of the PSSA volume fraction to 0.33, the copolymer was soluble only in highly polar solvents, such as DMSO. These preliminary results confirm that the highly polar character of the PSSA block directly affects the solubility of the copolymers in organic solvents and polar media.

Table 4. Characteristics of P3HT-*b*-(PS-*co*-PSSA) copolymers.

Copolymer	$Mn_{,P3HT}^a$(g/mol)	$Mn_{,PS}^a$ (g/mol)	SL^b (%)	Volume fraction^c $f_{P3HT}/f_{PS}/f_{PSSA}$
1	10500	20000	30	0.34/0.33/0.23
2	10500	20000	50	0.34/0.43/0.33
3	9000	10000	66	0.43/0.17/0.40
4	5200	14000	60	0.25/0.27/0.48

^{a}Molecular weight of the P3HT and PS blocks determined by ^{1}H-NMR in CDCl$_3$. ^{b}sulfonation level of the PS block calculated by 1H-NMR. ^{c}calculated by using ρ_{P3HT} = 1.1 g/cm^3, ρ_{PS} = 1.056 g/cm^3 and ρ_{PSSA} =0.801 g/cm^3.

As mentioned before, the increase of the PSSA volume fraction leads to copolymers only soluble in very polar solvents. Yet, the copolymer 3 with PSSA volume fraction of 0.40 (higher than copolymers 1 and 2) was soluble only in organic solvents. This behavior was probably due to the higher volume fraction of the P3HT (f_{P3HT} = 0.43), which also affects the solubility of the copolymer. Finally the preparation of the only P3HT-*b*-(PS-*co*-PSSA) copolymer that was found soluble in polar solvents (DMSO and water) was achieved by increasing the volume fraction of the PSSA (f_{PSSA}= 0.48), as well as keeping the volume fraction of the P3HT at a low level (f_{P3HT} = 0.25). In parallel the molecular weight of the P3HT was decreased so as to facilitate the self assembly of the copolymer. The ^{1}H NMR of this copolymer is presented in figure 19. The characteristic peaks of the PS-co-PSSA copolymer allows us to calculate the sulfonation level. In addition some peaks that correspond to the P3HT protons are also present. Their identification is not straightforward since DMSO is not a good solvent for P3HT which is probably surrounded by the PS-*co*-PSSA part, thus hiding the P3HT protons signals.

Figure 19 ^{1}H-NMR spectra of P3HT-*b*-(PS-co-PSSA) (DMSO d$_6$, 400 MHz).
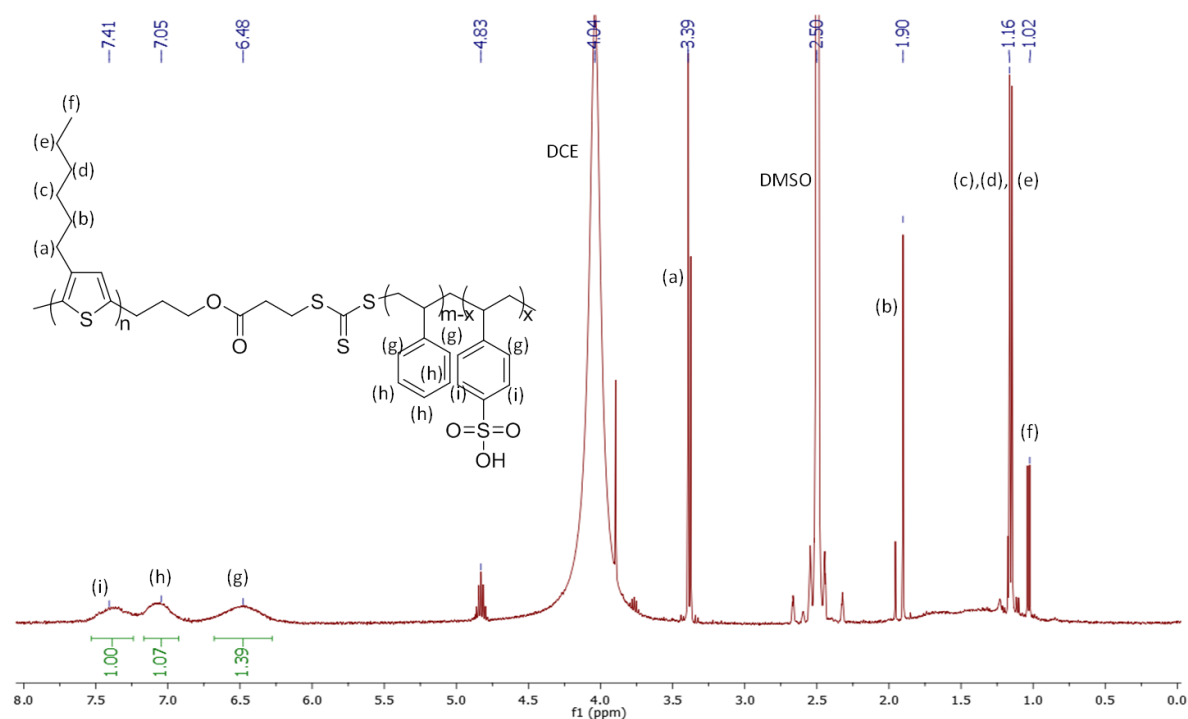
It is noteworthy, that even though there are examples in the literature of P3HT block copolymers with polyelectrolytes, none of them were directly soluble in aqueous media. [20,21] Consequently, to our knowledge, the first water soluble P3HT- polyelectrolyte block copolymers for CNTs dispersion in water as synthesized following the developed methodology.

In summary, well-defined π-conjugated-*b*-polyelectrolyte block copolymers P3HT-*b*-(PS-*co*-PSSA), were obtained through a simple synthetic route. Such block copolymers can be either soluble in organic solvents or in aqueous media, depending on the volume fraction of the PSSA. The self-assembly and the physical-chemical properties of the aqueous soluble copolymer 3 were further investigated in the chapter III due to its water solubility which is crucial. All the copolymers will be examined as dispersants of CNTs for applications in organic electronics in chapter IV.

II.2.3 Synthesis of P3HT-*co*-PVA copolymers

One of the most common ways to synthesize PVA type polymers consists in the synthesis of poly(vinyl acetate) (PVAc) followed by hydrolysis of the acetate moieties into alcohols. PVAc can be obtained by a controlled polymerization technique, the Cobalt-mediated radical polymerization (CMRP).[22] The monomers are activated by Co catalyst, creating cobalt(II) complexes creating an equilibrium between active and dormant species. Consequently, poly(vinyl acetate) chains end capped by a cobalt complex can be synthesized with a predictable molecular weight and low dispersity.[23] Block copolymers of PVAc with poly(*N*-vinylpyrrolidone) have been synthesized by CMRP, since both monomers can be polymerized by this method.[22] In order to synthesize block copolymers comprising a PVAc block, the later should be converted into a macroiniator for the controlled polymerization of the second chain. An alternative route for the controlled synthesis of the PVAc is by RAFT polymerization.[24] Starting from PVAc homopolymers, block copolymers have been synthesized either by RAFT or "click" chemistry.[25,26]

In the literature, there are no references for the synthesis of P3HT-*co*-PVA copolymers. We tried two different architectures for these copolymers, *i.e* grafted and block copolymers. PVA polymers made by CMRP were used for the synthesis of PVA-*g*-P3HT graft copolymers. The

graft copolymers were made via an esterification reaction of the carboxylic end groups of the P3HT and the hydroxyl group of the PVA. In comparison P3HT-*b*-PVA copolymers were synthesized for the first time by RAFT polymerization. The physico-chemical properties of the two different structures were also investigated.

Figure 20. Targeted P3HT-*co*-PVA copolymers with different architectures.
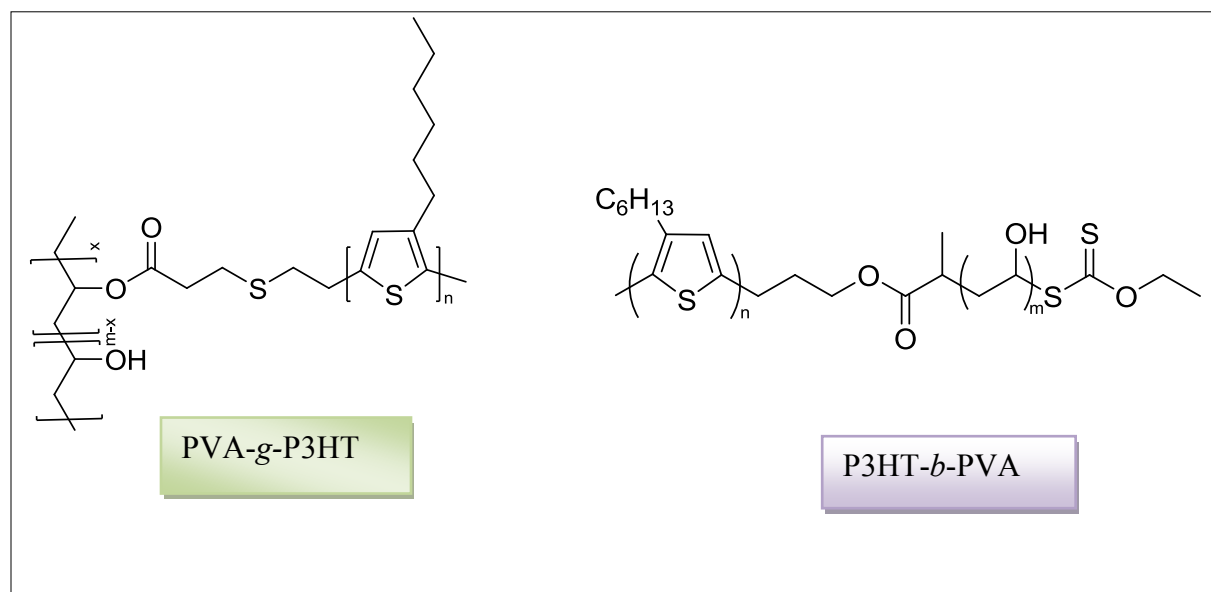
II.2.3.1   Synthesis of PVA-g-P3HT copolymers

As described before PVAc was synthesized by CMRP polymerization starting from the vinyl acetate monomer. The polymerization took place under pure condition where Co(acac)$_3$ was used as the catalyst and V70 as the initiator (scheme 8). The polymer was characterized by ^{1}H NMR and SEC and then was fully hydrolyzed in PVA polymer, which was also characterized by FTIR, ^{1}H NMR and SEC.

Scheme 8. The synthesis of PVAc by CMRP.
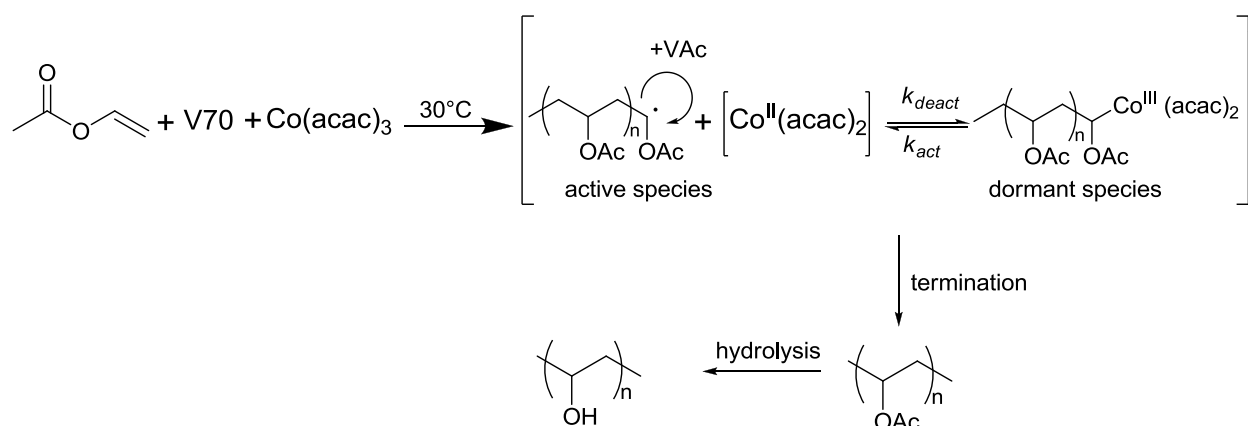
Figure 21. (a) SEC of PVAc in THF (IR detector, PS calibration (b) FTIR spectroscopy of PVAc (green) and PVA (red).

(a)

(b)
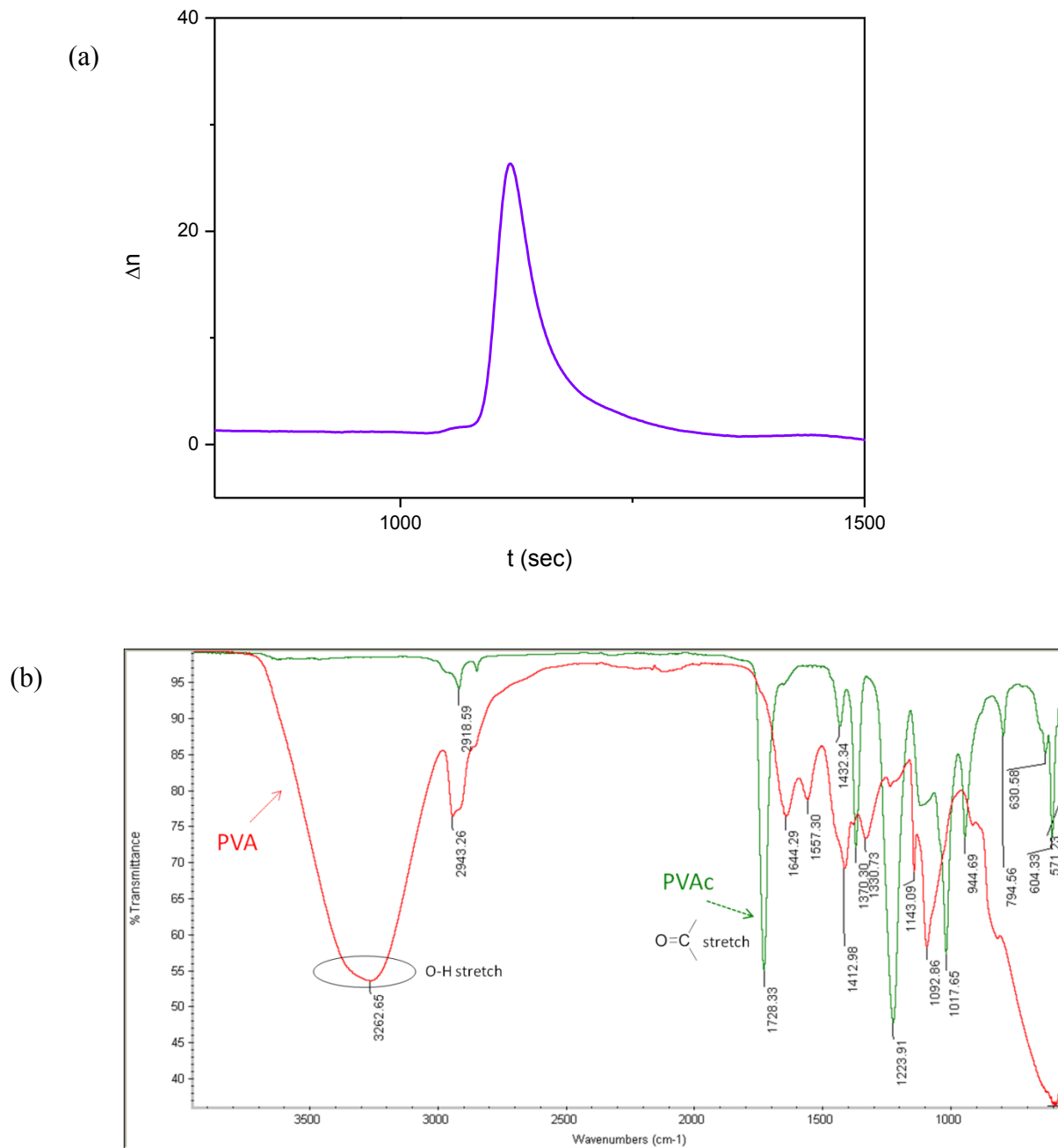
In figure 21 the SEC chromatogram of the PVAc in THF is presented. From the SEC chromatogram we verified the synthesis of the PVAc polymer whose molecular weight was determined to be 13000 g/mol. The dispersity was found to be 1.2 which is a good value for radical polymerization method. In order to verify the ful hydrolysis of the PVAc into PVA FTIR spectroscopy was performed (figure 21). After hydrolysis the characteristic peak of the PVAc at 1730 cm^{-1} disappeared and at the same time a large peak at 3200 cm^{-1} appeared, which corresponds to the OH groups of the PVA.

Prior to the esterification reaction onto the hydroxyl moieties along the PVA backbone, the P3HT chains were end capped with a carboxyl acid group.[27] Thus allyl terminated P3HT was treated with 3-mercaptopropanoic acid and TEA in an one step reaction in order to obtain carboxylic acid-terminated P3HT (ω-COOH-P3HT) as shown in the scheme 9. The successful functionalization of the P3HT was verified by ^{1}H NMR spectroscopy (figure 22).

Scheme 9. (a) Synthesis of ω-COOH-P3HT polymer.
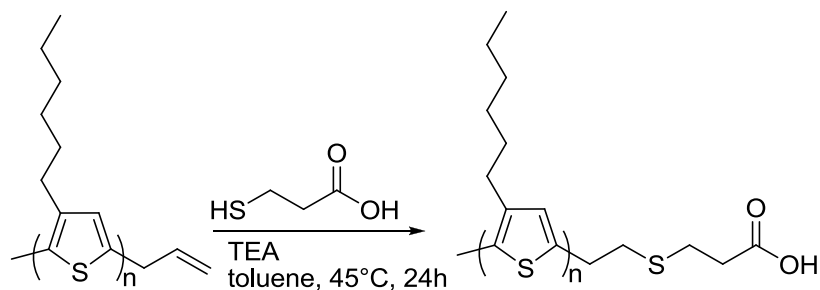
Figure 22. ^{1}H-NMR spectrum of ω-COOH-P3HT in CDCl$_3$ (400 MHz).
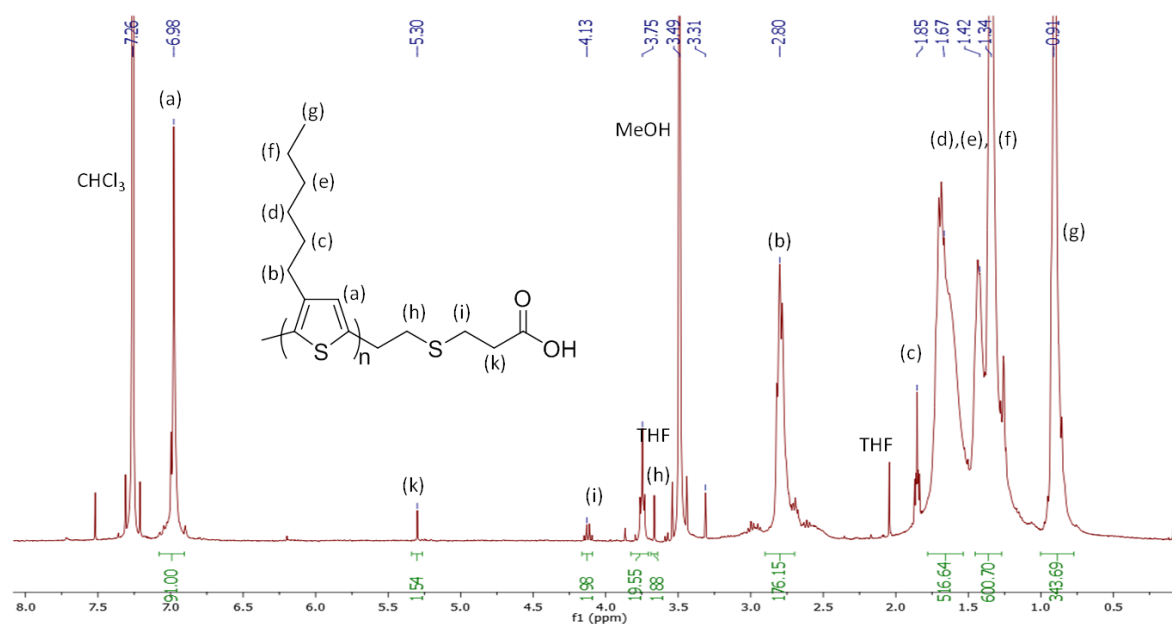
In order to perform the esterification reaction between ω-COOH-P3HT and a PVA backbone we first investigated the appropriate solvent or mixture of solvents. Indeed, both P3HT and PVA do show almost orthogonal solubility (in terms of polarity). While PVA is soluble in DMSO and water, P3HT is soluble in THF, CHCl$_3$ and DCM. Finally a mixture of DMSO/DCM (1/1) was found to be suitable for the esterification reaction (scheme 10).

Scheme 10. The esterification reaction for grafting P3HT on the PVA backbone chain.

(a)
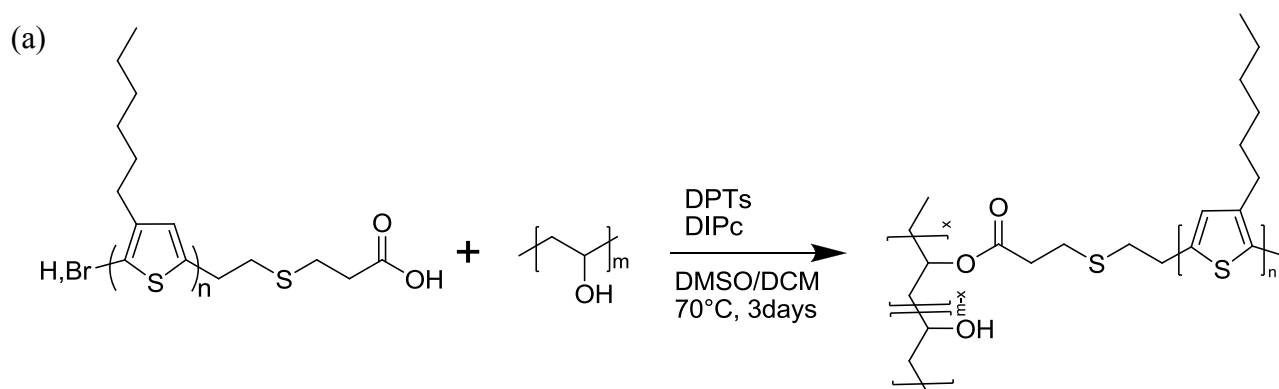
The ratio of P3HT/PVA was calculated in order to obtain 2 grafted P3HT chains per PVA chain. The final copolymer was soluble in aqueous media limiting the characterization methods that could be used. In the ^{1}H NMR of the copolymer in D_2O solvent the signal of P3HT was not strong enough to allow us to calculate the ratio between PVA and P3HT. By FTIR analysis we could only verify the existence of the esterification bond at ~1600 cm^{-1}, but still it is not a method that permits us to calculate the exact amount of grafted P3HT (figure 23). Finally from the TGA analysis, showing in the figure 23, the weight percentage of P3HT per PVA chain was calculated to be 30%.

Figure 23. (a) FTIR characterization of the ω-COOH-P3HT (red), PVA (pink) and PVA-*g*-P3HT (blue) and (b) TGA of the PVA-*g*-P3HT (under nitrogen atmosphere).

(a)

(b)

Decomposition temperature
of PVA ~250°C

70%

Decomposition temperature
of P3HT ~380°C

30%
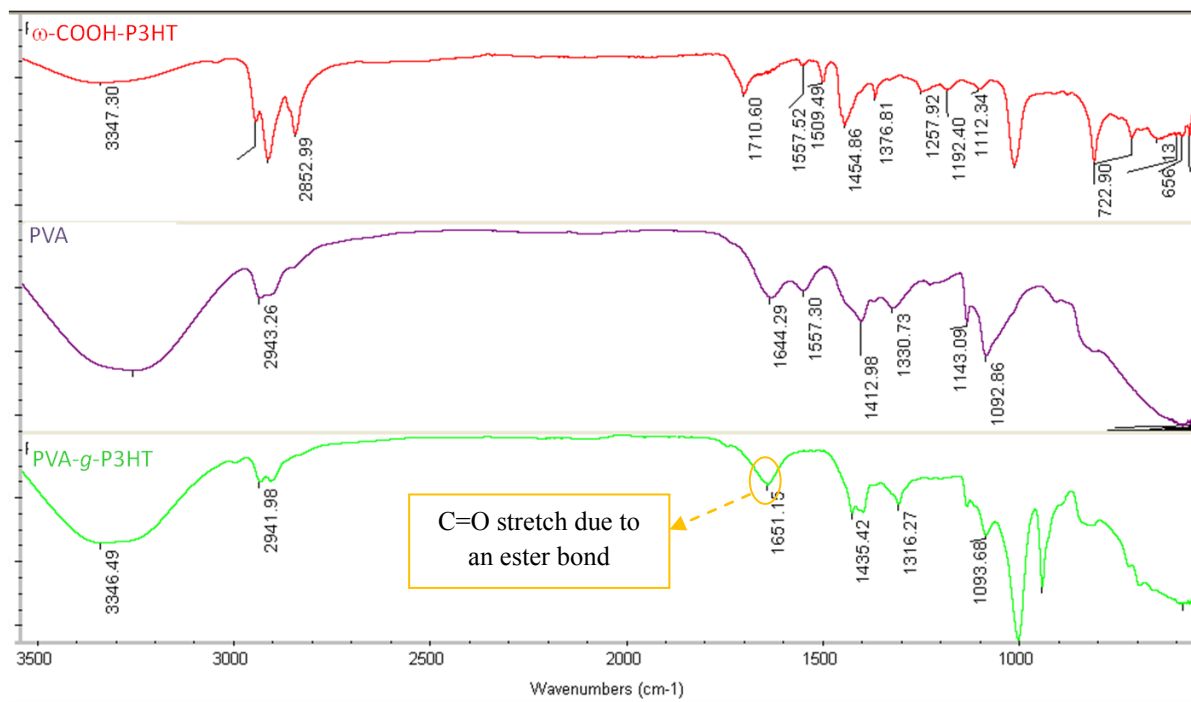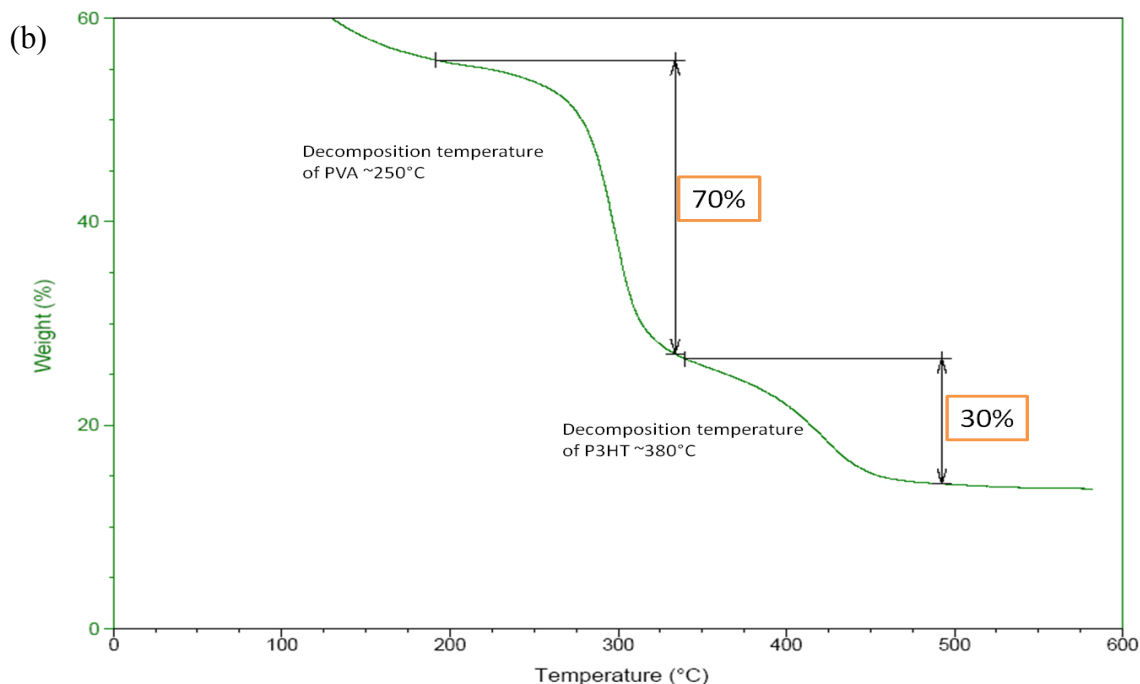
In conclusion PVA-*g*-P3HT copolymers were synthesized by an esterification reaction of the ω-COOH-P3HT and the PVA. The lack of common solvents, between the two copolymers does not allow us to obtain well defined copolymers. For that reason we changed our strategy in the synthesis of PVA-*b*-P3HT copolymers by RAFT polymerization.

II.2.3.2   *Synthesis of P3HT-b-PVA copolymers*

P3HT-*b*-PVA was synthesized to compare to P3HT-*b*-(PS-co-PSSA) block copolymer, knowing that both bring water solubility. Indeed, we were interested by the effect of the flexible chain in a π-conjugated block copolymer when it contains charges (PSSA) and when it is neutral (PVA). This electrostatic difference will influence the electrical properties of the P3HT but also the self-

assembly of the copolymer in aqueous media. In addition, we want to investigate the effect of the presence of the polyelectrolyte segment in the stability of the CNTs dispersions.

The followed strategy was similar to the synthesis of P3HT-*b*-PS copolymers, beginning from the synthesis of a P3HT macroinitiator suitable for the RAFT polymerization of the PVA. Two different P3HT-macroinitiators were synthesized and were used for the RAFT polymerization of PVAc as showed in the scheme 11.

Scheme 11. Design of two P3HT macro-initiators for RAFT polymerization process.
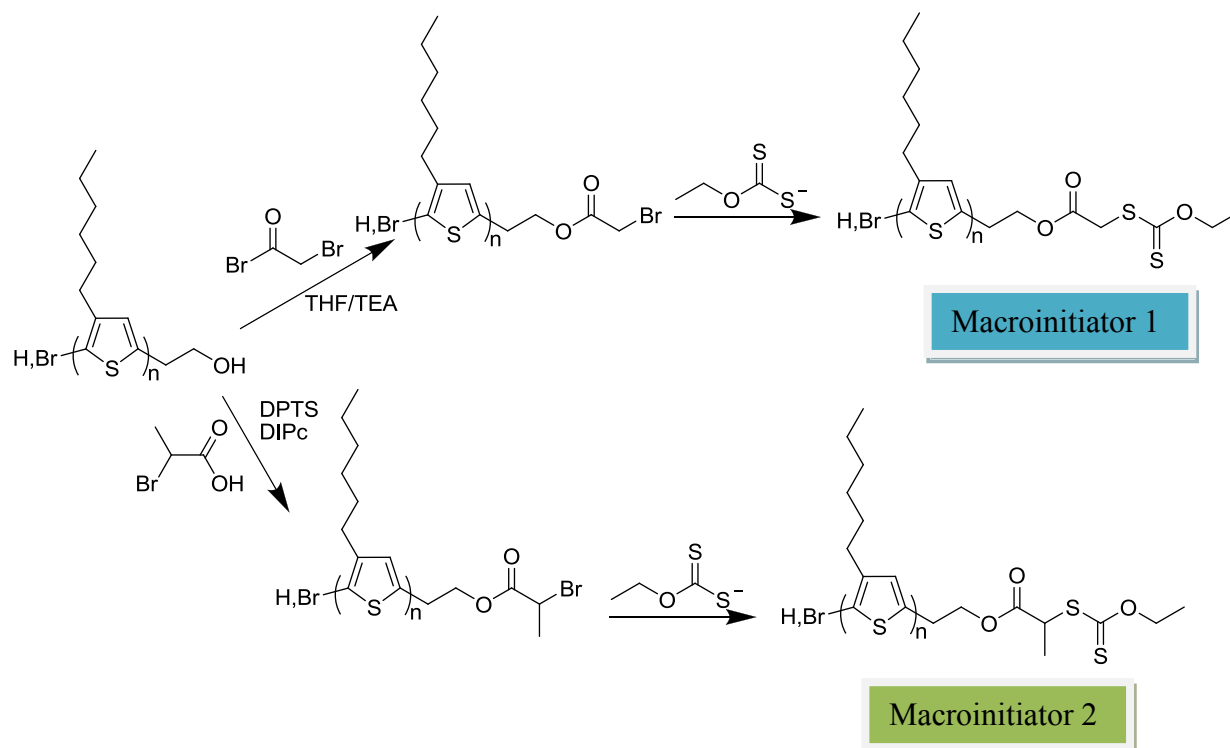
The first try for RAFT polymerization of the vinyl acetate monomer with the use of the macroinitiator 1 (T = 60°C for 48 hours) did not lead to the formation of block copolymers. The reaction (scheme 12) was repeated at the same temperature but the reaction time was increased to 5 days. Only some traces of small molecular weight PVAc homopolymers were identified by ^{1}H NMR and SEC characterizations (figure 24).

Scheme 12. (a) The RAFT polymerization of vinyl acetate from the macroinitiator 1.

Macroinitiator 1
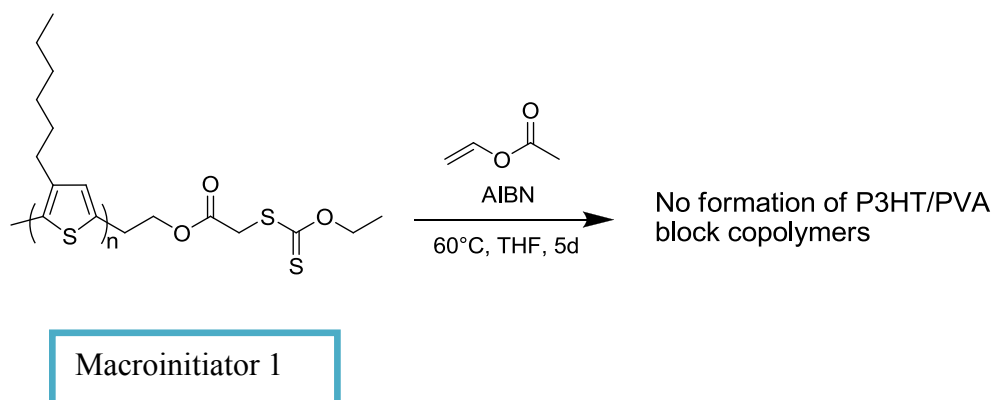
Figure 24. SEC chromatogram (UV detector) of the P3HT before and after the RAFT polymerization in THF where no shift is observed (PS calibration).
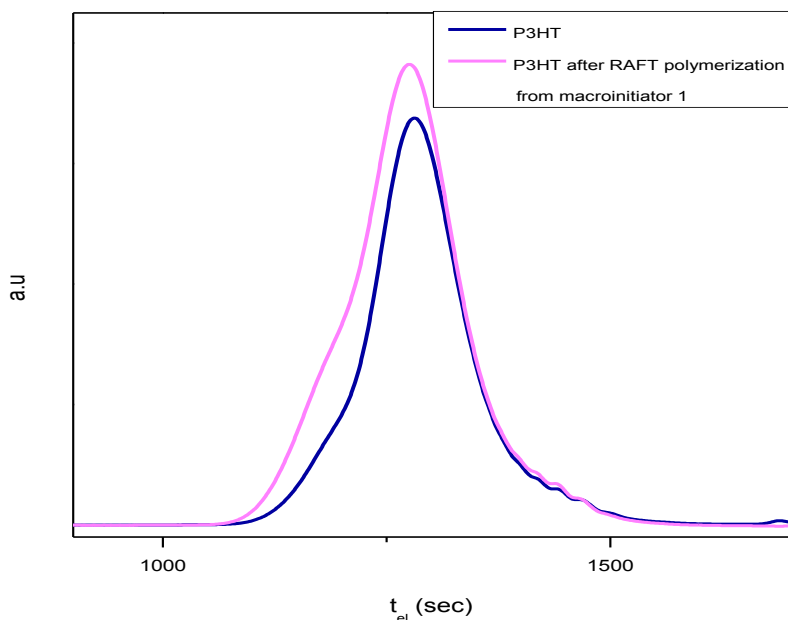
A possible explanation for the lack of formation of block copolymers could be the structure of the macroinitator. Indeed, it is possible that this structure is preferable for the synthesis of homopolymers preventing the growth of the PVAc chain on the P3HT macroinitator. Alternatively, the P3HT macroinitiator 2 was synthesized carrying a methyl group used for the RAFT polymerization of the PVAc. Under the same conditions as before after three days of polymerization, the synthesis of block copolymer was achieved (scheme 13).

Scheme 13. RAFT polymerization of vinyl acetate in the presence of the macroinitiator 2.
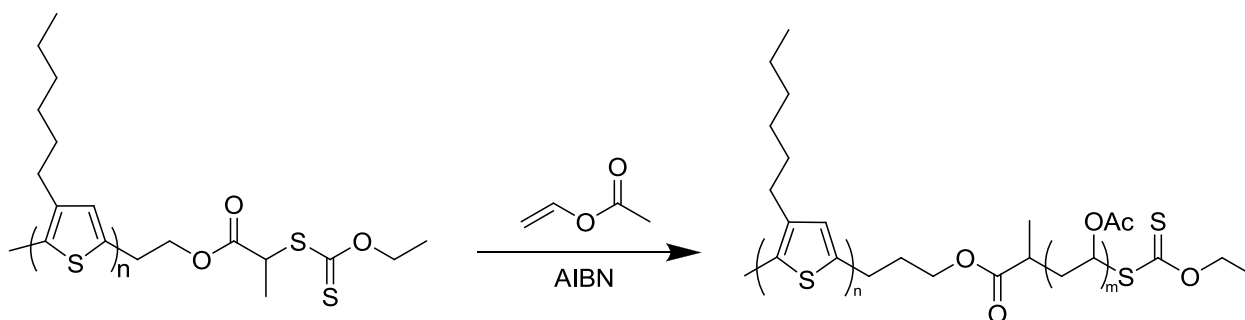
The ^{1}H-NMR and SEC characterizations exhibit the presence of a small molecular weight PVAc attached on the P3HT (figure 25). In the ^{1}H-NMR the peak that corresponds to the main back bone of the vinyl acetate appears at 5 ppm and it is broadened, signl that PVAc has been formed. In addition the methyl end of the acetate groups is also present at 2.00 ppm verifying the formation of PVAc. The molecular weight of the PVAc was calculated by the ^{1}H NMR at 2000 g/mol.

Figure 25. (a) ^{1}H-NMR of the P3HT-*b*-PVAc in CDCl$_3$ (400MHz) and (b) the SEC (UV detector) of the P3HT macroinitiator 2 and the P3HT-*b*-PVAc copolymer in THF.

(a)

(b)
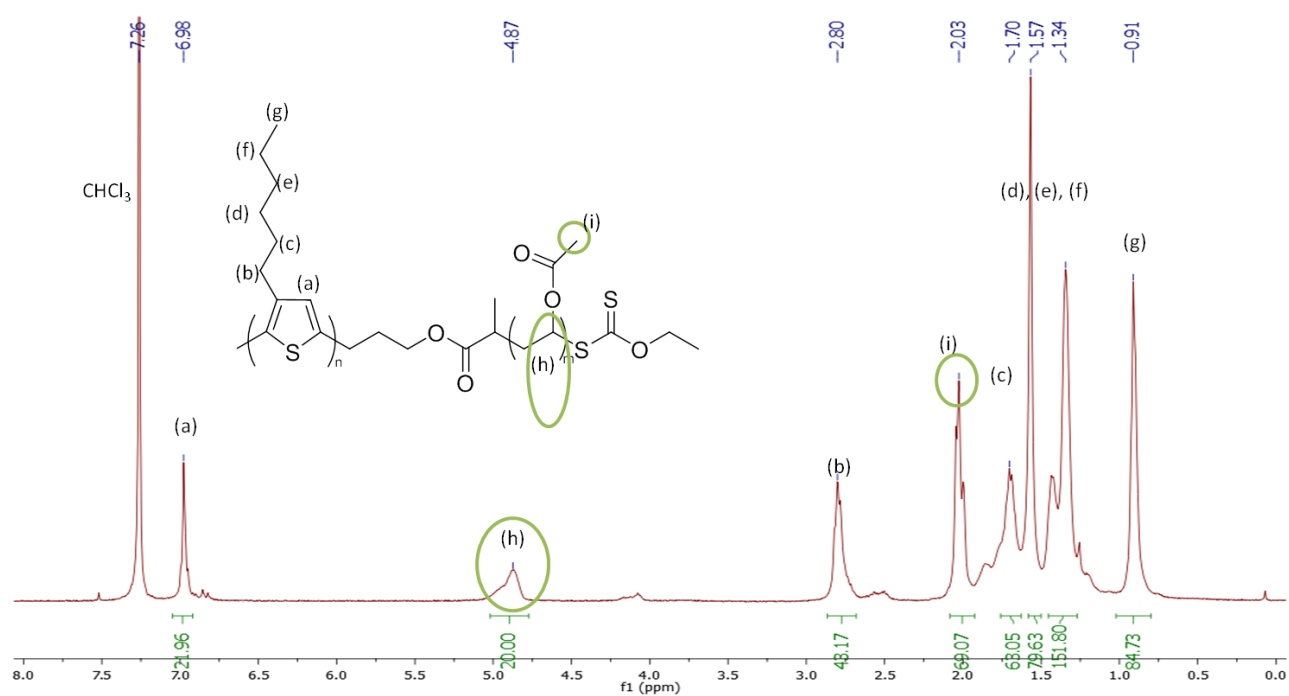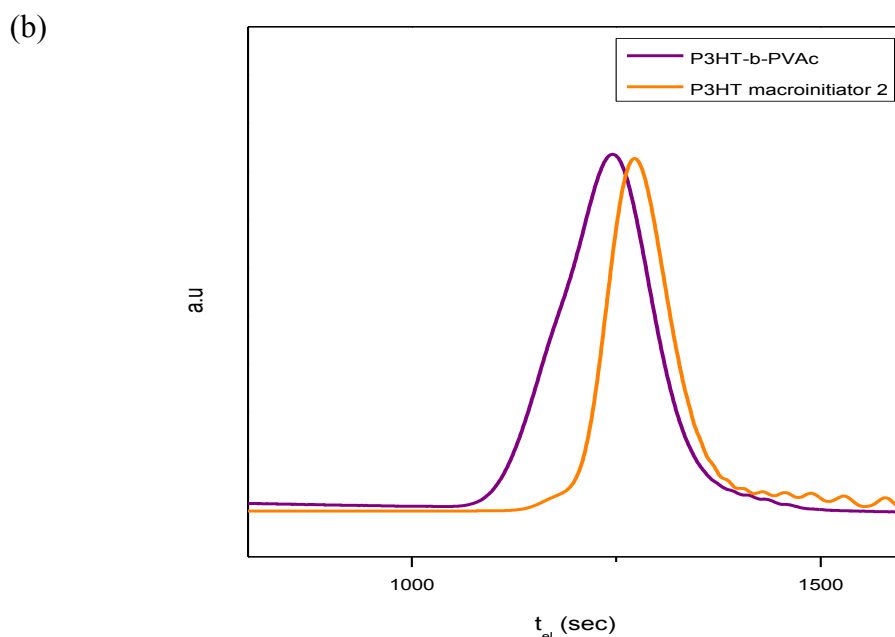
II.3   Conclusion

In this chapter, the synthesis of well-defined copolymers consisting of a π-conjugated block and a water soluble block copolymers was described. First the synthesis of PEDOT block copolymers was investigated. A strong polyelectrolyte (PSSA) was chosen as a second block which apart from increasing the water solubility, could also act as dopant of the PEDOT. Until now the synthesis of PEDOT block copolymers has not been achieved due to lack of solubility of the PEDOT. Our strategy was the polymerization of EDOT monomers in the presence of a PS chain, terminated by an EDOT functional group, which will keep the formed PEDOT polymer soluble. Three different polymerization methods were tried: Suzuki coupling, coupling polymerization and oxidation polymerization. Only the last two methods resulted in PEDOT based block copolymers. These block copolymers though were mixed with PS homopolymers and PEDOT oligomers while the purification of this system was not possible due to similar

solubilities of the products. Following this strategy the synthesis of well defined PEDOT block copolymers was not achieved, since the formed block copolymers could not be purified.

Continuing in the idea of the synthesis π-conjugated-b-polyelectrolyte copolymers, P3HT was used as the semiconductive polymer. The synthesis of P3HT-*b*-(PS-*co*-PSSA) block copolymers was achieved by the sulfonation of the styrene units of well-defined P3HT-*b*-PS copolymers. The sulfonation level was easily tuned and followed by ^{1}H NMR spectroscopy. Copolymers with different volume fractions of P3HT and PSSA were synthesized, and the resulting copolymers were soluble in organic or aqueous media depending on the volume fraction of the PSSA and the size of the P3HT block.

P3HT-*co*-PVA copolymers were synthesized in order to compare with the P3HT-*b*-(PS-*co*-PSSA) copolymer knowing that both are soluble in aqueous media. The difference of the second block is that PSSA is charged since it is a strong polyelectrolyte while PVA is neutral. Two different architectures of the P3HT-*co*-PVA were tested, graft and block copolymers. The PVA-*g*-P3HT copolymer was synthesized by esterification reaction of the two polymers, and the resultting compound was soluble in water solutions. The non-compatibility of the solvents on the two polymers does not allow us to control the number of the grafted P3HT units per PVA chain. Besides, well defined P3HT-*b*-PVA block copolymers were synthesized combining GRIM and RAFT polymerization.

The physico-chemical properties of these copolymers will be presented in the chapter III while their ability to disperse CNTs will be discussed in the chapter IV.

(1)   Groenendaal, L.; Jonas, F.; Freitag, D.; Pielartzik, H.; Reynolds, J. R. *Adv. Mater. (Weinheim, Ger.)* **2000**, *12*, 481.

(2)   Jiang, H.; Taranekar, P.; Reynolds, J. R.; Schanze, K. S. *Angewandte Chemie International Edition* **2009**, *48*, 4300.

(3)   Perepichka, I. F.; Levillain, E.; Roncali, J. *J. Mater. Chem.* **2004**, *14*, 1679.

(4)   Yamazaki, K.; Kuwabara, J.; Kanbara, T. *Macromol. Rapid Commun.* **2012**, n/a.

(5)   Reeves, B. D.; Grenier, C. R. G.; Argun, A. A.; Cirpan, A.; McCarley, T. D.; Reynolds, J. R. *Macromolecules* **2004**, *37*, 7559.

(6)   McCullough, R. D. *Adv. Mater. (Weinheim, Ger.)* **1998**, *10*, 93.

(7)   Jeffries-El, M.; Sauvé, G.; McCullough, R. D. *Macromolecules* **2005**, *38*, 10346.

(8)   Iovu, M. C.; Sheina, E. E.; Gil, R. R.; McCullough, R. D. *Macromolecules* **2005**, *38*, 8649.

(9)   Yokoyama, A.; Miyakoshi, R.; Yokozawa, T. *Macromolecules* **2004**, *37*, 1169.

(10)   Jeffries-El, M.; Sauvé, G.; McCullough, R. D. *Adv. Mater. (Weinheim, Ger.)* **2004**, *16*, 1017.

(11)   Urien, M.; Erothu, H.; Cloutet, E.; Hiorns, R. C.; Vignau, L.; Cramail, H. *Macromolecules* **2008**, *41*, 7033.

(12)   Craley, C. R.; Zhang, R.; Kowalewski, T.; McCullough, R. D.; Stefan, M. C. *Macromol. Rapid Commun.* **2009**, *30*, 11.

(13)   Carretta, N.; Tricoli, V.; Picchioni, F. *J. Membr. Sci.* **2000**, *166*, 189.

(14)   Miaudet, P.; Bartholome, C.; Derré, A.; Maugey, M.; Sigaud, G.; Zakri, C.; Poulin, P. *Polymer* **2007**, *48*, 4068.

(15)   Hou, Y.; Tang, J.; Zhang, H.; Qian, C.; Feng, Y.; Liu, J. *ACS Nano* **2009**, *3*, 1057.

(16)   Zhang, F.-m.; Chang, J.; Eberhard, B. *New Carbon Materials* **2010**, *25*, 241.

(17)   Iovu, M. C.; Jeffries-El, M.; Sheina, E. E.; Cooper, J. R.; McCullough, R. D. *Polymer* **2005**, *46*, 8582.

(18)   Park, M. J.; Balsara, N. P. *Macromolecules* **2008**, *41*, 3678.

(19)   Stenzel, M. H.; Davis, T. P.; Fane, A. G. *J. Mater. Chem.* **2003**, *13*, 2090.

(20)   Li, Z.; Ono, R. J.; Wu, Z.-Q.; Bielawski, C. W. *Chem. Commun. (Cambridge, U. K.)* **2011**, *47*, 197.

(21)   Aissou, K.; Pfaff, A.; Giacomelli, C.; Travelet, C.; Müller, A. H. E.; Borsali, R. *Macromol. Rapid Commun.* **2011**, *32*, 912.

(22)   Debuigne, A.; Poli, R.; De Winter, J.; Laurent, P.; Gerbaux, P.; Wathelet, J.-P.; Jérôme, C.; Detrembleur, C. *Macromolecules* **2010**, *43*, 2801.

(23)   Debuigne, A.; Willet, N.; Jérôme, R.; Detrembleur, C. *Macromolecules* **2007**, *40*, 7111.

(24)   Fleet, R.; McLeary, J. B.; Grumel, V.; Weber, W. G.; Matahwa, H.; Sanderson, R. D. *Macromol. Symp.* **2007**, *255*, 8.

(25)   Tong, Y.-Y.; Wang, R.; Xu, N.; Du, F.-S.; Li, Z.-C. *Journal of Polymer Science Part A: Polymer Chemistry* **2009**, *47*, 4494.

(26)   Pound, G.; Aguesse, F.; McLeary, J. B.; Lange, R. F. M.; Klumperman, B. *Macromolecules* **2007**, *40*, 8861.

(27)   Mougnier, S.-J.; Brochon, C.; Cloutet, E.; Fleury, G.; Cramail, H.; Hadziioannou, G. *Macromol. Rapid Commun.* **2012**, *33*, 703.

Chapter III

Physical-chemical characterization of the P3HT based copolymers

TABLE OF CONTENTS

Physico-chemical characterization of P3HT based copolymers

I   Introduction

In the previous chapter the synthesis of novel amphiphilic water soluble P3HT-based block copolymers was described. It was our good to study the self-assembly of these polymers both in solution and solid state, as they will be used as dispersants of CNTs in solution and then casted on various substrates. Besides the photophysical properties of the copolymers, which are correlated with the type of self-assembly, were examined

When rod-coil block copolymers are solubilized in a selective solvent of the rod or the coil blocks, the formation of self-organized mesostructures (micelles, vesicles ...) is expected depending on intrinsic macromolecular parameters. The typical parameters governing the self assembly of rod-coil block copolymers are the Flory-Huggins parameter (the thermodynamics of the polymer in solution), the Maier-Saupe parameter (describing the intermolecular potential function based on the dispersion forces), the volume fraction and molecular weight of the copolymer.

In solution, the solubility Hilldebrand parameter inherits to the interactions with the copolymers and the solvents have also to be taken into account. On one hand, rod-coil block copolymers in rod selective solvent form self-assemblies with the rod block outside the micelles or the vesicles. The structure of the assemblies is strongly depending on the size of the rod block as regards to the coil block. For relatively short rod block the copolymers tend to form bilayer vesicles while when the rod block is relatively large as regards to the coil block sheet-like of vesicle assemblies are favorable. For π-conjugated rod blocks these self-assemblies strongly affect the photophysical properties of the copolymer,[1] resulting in characteristic UV-vis and photoluminescence spectra inherent to the different structures.

On the other hand, in coil-selective solvents, the rod blocks are organized in the center of the self-assemblies. Due to various intramolecular and intermolecular interactions developing between the rod blocks, several structures such as vesicles, micelles or cylinders can be formed. Copolymers with long rod-blocks tend to form vesicles while for short rod-blocks spherical or cylindrical micelles are more favorable.[2] Several other parameters influence the type and the size of the self-assemblies, like the composition and nature of the solvents, the polymer concentration and the type of the aggregation of the rod block. The organization of the π-conjugated rod block in the center of the vesicle or the micelles is the result of the π-π interactions between the blocks. The type of these interactions (lamellar, J-aggregates, H-aggregates) can be followed by the changes in the UV-vis spectra of the conjugated block.

Figure 1. General trends in the solution structure of the rod-coil block copolymers depending on the selective solvent and the volume fractions of the copolymers.[3] Reproduced with permission from Elsevier, Copyright 2011
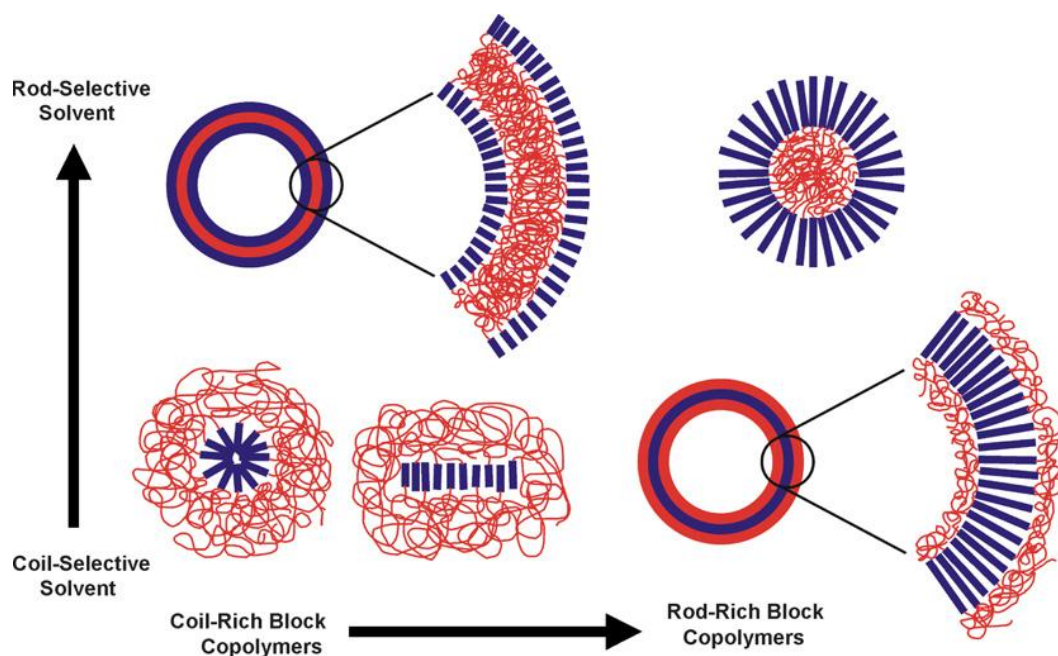
Besides, the rod-coil block copolymers can self-assemble when they are cast in thin films. In general, the films are formed from solutions where the copolymers are either very soluble or in a solvent selective for one block. Consequently, the resulting mesostructures in thin films are dependent on the solution preparation. The ratio between the rod and the coil block strongly influences the morphology of the films.[4] Copolymers with a short rod block can easily create an organized structure when they are cast in films, since the rod block can be packed in different morphologies. The organization of the chains can be varied between a simple parallel stacking to spherical or hexagonal morphologies. As the volume fraction of the rod block increases, the nature of the organization is modified and in some examples the organized structure is completely destroyed. Different types of aggregates have been observed in thin films for the π-conjugated rod block (H-type, J-type or simple parallel aggregation).[5]

In conclusion, the self-assemblies of the rod-coil block copolymers both in solution and in thin films can be tuned by controlling several macromolecular and environmental factors. The morphology of the self-assemblies depends on the selectivity of the solvent to the rod or the coil block. The size of the vesicles or the micelles is strongly influenced by volume fractions of the rod-coil block copolymers. Furthermore the strong interactions between the rod block due to π-π stacking brings one more parameter in the final mesostructures.

Following this discussion we do expect interesting self assembly behavior for copolymers consisting of a π-conjugated block and a polyelectrolyte segment with preferential solubility in water. The π-conjugated block will be exposed to a poor solvent, which will force the creation of self-assembled structures where it will be protected from the polar environment. The internal structure of this organization, created by the π-π stacking of the rod-block, will also be examined. Around of the rod-block, the polyelectrolyte block will stabilize the colloidal system, and the electrostatic interactions between these assemblies which can lead to supra-macromolecular mesostructures will be investigated.

II   *Results and discussion*

II.1   Physico-chemical characterization of the P3HT-b-(PS-co-PSS) copolymer

The synthesis and macromolecular characterization of P3HT-*b*-(PS-*co*-PSSA) block copolymers were described in **Chapter II**. We chose to study the behavior of the water soluble copolymer (f_{P3HT}= 0.25, f_{PS}= 0.2, f_{PSSA}= 0.48) $P3HT_{0.25}$-*b*-($PS_{0.27}$-*co*-$PSSA_{0.48}$). Its self-assembling ability was studied both in solution and in thin (~30 nm) films by different techniques such as UV-vis, photoluminescence and microscopy.

II.1.1   Determination of Critical Micelle Concentration

Block copolymers solubilized in a selective solvent have the tendency to organize in the form of micellar structures. At low concentrations, molecularly dissolved copolymers are present in the solution, usually as unimers. Above a critical concentration, the unimers start to form micellar organizations in the solution which are associated in equilibrium with the unimers. This particular concentration is called the Critical Micelle Concentration (CMC) and it depends on the size and the nature of each block, the temperature and the nature of the solvent. There are several methods for the determination of the CMC, such as Dynamic light scattering (DLS), conductivity measurements, fluorescence spectroscopy, and surface tension measurements etc. The most commonly used method is the DLS, which can determine not only the CMC but also the size and in some cases the shape of the micellar organization. Unfortunately it was not possible to use this method in our case, since the P3HT-*b*-(PS-*co*-PSSA) copolymer strongly absorbs at the wavelength of the laser used for the DLS measurements (632 nm) due to the P3HT block.

Consequently we performed the determination of the CMC by fluorescence spectroscopy, which is a very accurate method even for the low CMCs of the block copolymers. This technique is based on the use of a fluorescent probe which detects the formation of hydrophobic microdomains. A molecule complying with these characteristics is the pyrene; and the ratio of the first (I_1) over the third (I_3) vibronic band of the pyrene emission spectrum was used to detect the formation of the hydrophobic domains.[6] The I_1/I_3 ratio is stable for sharp concentrations below

the CMC, while a decrease is observed at concentrations where hydrophobic microdomains (the micelles) start to form. Aqueous solutions of the P3HT$_{0.25}$-*b*-(PS$_{0.27}$-*co*-PSSA$_{0.48}$) copolymer with different concentrations were prepared containing the same amount of pyrene probe. The excitation wavelength was fixed at 334 nm, and the I$_1$/I$_3$ ratios are presented in the figure 2 as a function of the copolymer concentration. The photoluminescence spectra of these solutions is presenting in the experimental section. A clear decrease of the ratio I$_1$/I$_3$ is observed for the copolymer concentration at 0.008 g/L, indicating the formation of hydrophobic areas. The ratio remains stable for higher concentrations, allowing us to conclude that the CMC is located at 0.008 g/L. Taking advantage of the strong absorption of the P3HT around 500 nm, UV-vis absorption spectra were performed for the same copolymer concentrations in order to correlate the CMC with the band changes occurring when the block copolymer self-assembles at the CMC. The P3HT absorption is stronger and shifted due to its aggregation for the concentrations higher than 0.008 g/L. This observation confirms CMC around 0.008 g/L which is in the lower range of typical CMC for amphiphilic block copolymers.

Figure 2. (a) The I$_1$/I$_3$ ratio of the pyrene probe as a function of the copolymer's concentration (b) UV-vis spectra of aqueous solutions of the copolymer at different concentrations 4 10^{-4}< c< 0.2 g/L.

174
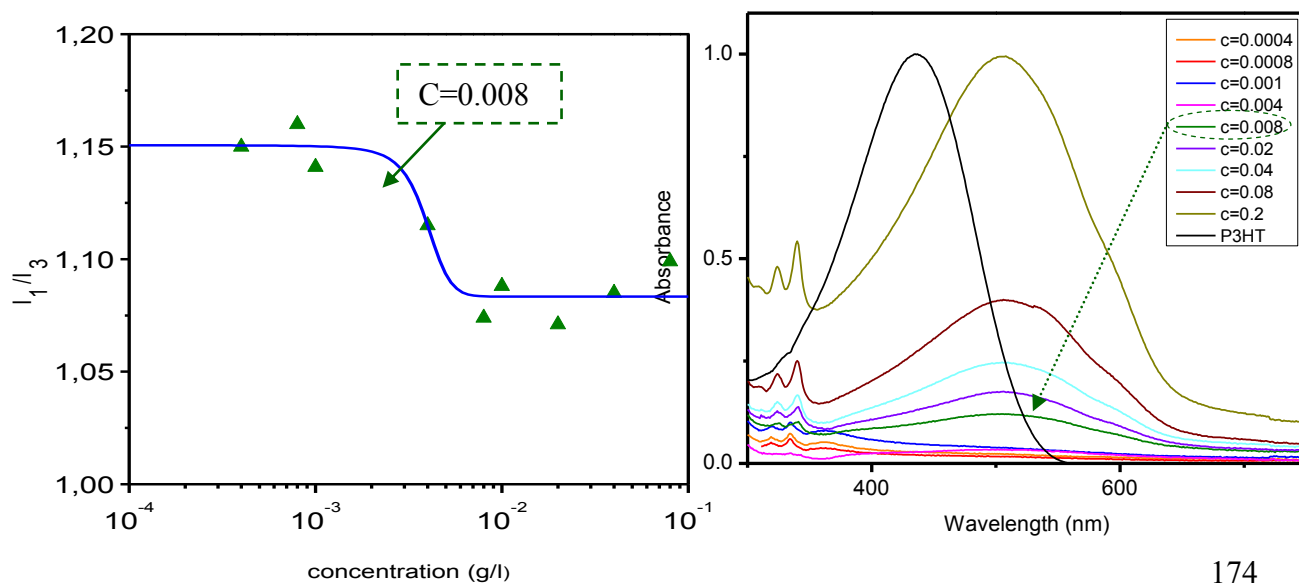
Both fluorescence and UV-Vis characterization allow us to conclude that the $P3HT_{0.25}$-*b*-($PS_{0.27}$-*co*-$PSSA_{0.48}$) copolymer self-assembles in solution. Considering the structure of the $P3HT_{0.25}$-*b*-($PS_{0.27}$-*co*-$PSSA_{0.48}$) copolymer, we expect the formation of micellar structures with a P3HT core and PSSA shell. In order to verify this structure, zeta potential measurements were performed (figure 3). The zeta potential is determined by measuring the electrophoretic mobility of the colloidal particles in the solution when a voltage is applied. Based on these measurements we can collect information about the charge of the particles and also about their stability. The zeta potential depends on the magnitude of the electrostatic interaction between the colloidal particles, thus it can be used as characterization for the colloidal stability. Particles with zeta potential lower than -25 mV or higher than 25 mV are considered as stable.

Figure 3. The zeta potential in mV as a function of the particles concentration in % in water solution of the $P3HT_{0.25}$-*b*-($PS_{0.27}$-*co*-$PSSA_{0.48}$) copolymer c=0.2 g/L.
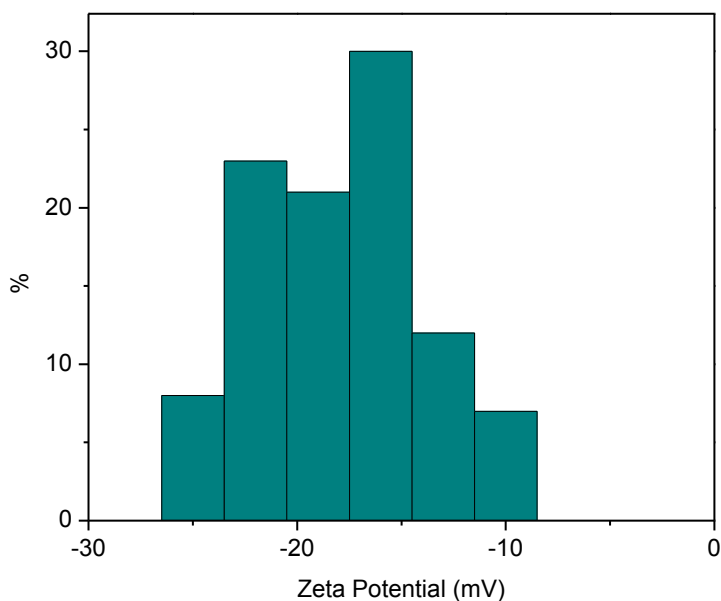
The zeta potential measurement of a $P3HT_{0.25}\text{-}b\text{-}(PS_{0.27}\text{-}co\text{-}PSSA_{0.48})$ copolymer solution with concentration higher than the CMC, indicates the presence of polydisperse particles with a zeta potential around -20 mV (figure 3). Based on the theory of colloidal particles, the self-assemblies in our solutions cannot be characterized as stable. As mentioned earlier, it was not possible to use DLS analysis in order to determine the size of these particles. Consequently an alternative method was used, the Nanoparticle Tracking Analysis (NTA). The principle of this method is similar to the DLS, but it can be operated at various laser wavelengths. In addition the measurements of the NTA are less influenced by large amorphous objects in the solutions, as it is observed in the DLS analysis. $P3HT_{0.25}\text{-}b\text{-}(PS_{0.27}\text{-}co\text{-}PSSA_{0.48})$ copolymer solution with concentration at 0.2 g/L was characterized by NTA analysis with a wavelength of the laser fixed at 640 nm (figure 4). The size distribution graph shows polydisperse particles with sizes from 60 nm to 300 nm.

Figure 4. The Nanoparticle Tracking Analysis graph of the particle size (nm) as a function of the particle concentration.

Particle Size (nm)
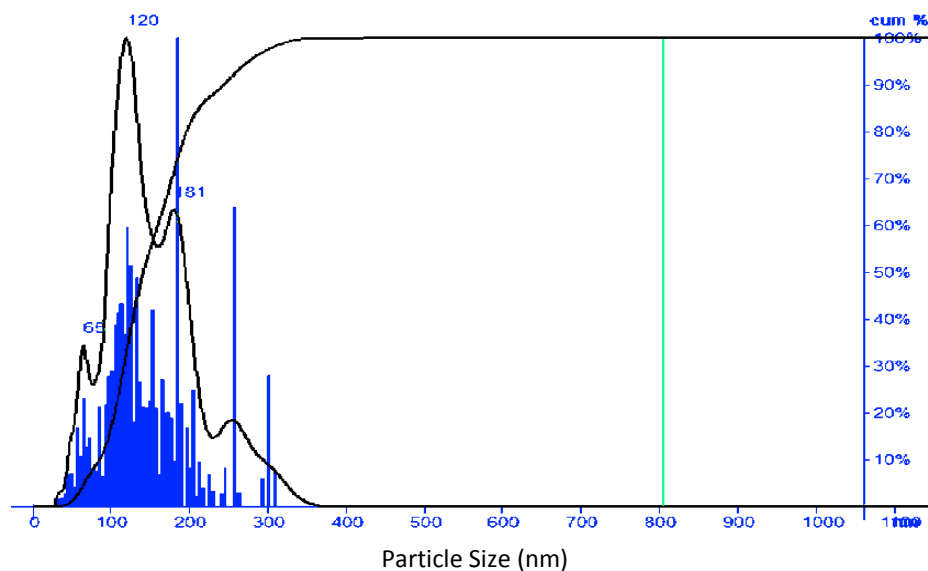
In conclusion the P3HT$_{0.25}$-*b*-(PS$_{0.27}$-*co*-PSSA$_{0.48}$)) copolymer self-assembles in micelles in water solutions. The CMC was determined at 0.008 g/L by pyrene probe technique as well as by UV-vis spectra; a typical concentration for amphiphilic copolymers. The nature of these particles was further determined by zeta potential measurements. Polydispersed negatively charged particles were observed and their size was determined by NTA analysis from 60-300 nm. Thus we can conclude that the structures obtained from the self-assembly of the copolymers in aqueous media exhibit a negatively charged corona formed by the hydrophilic PS-*co*-PSSA blocks. However the large distribution of the particles size is typical of the formation of aggregates. The aggregation behavior of the block copolymer was consequently further investigated along with self assembly.

II.1.2 Direct imaging analysis

Three different microscopy techniques, *i.e* TEM, Cryo-TEM and AFM, were used in order to visualize the type of self-assembled structures formed by the P3HT$_{0.25}$-*b*-(PS$_{0.27}$-*co*-PSSA$_{0.48}$) copolymer in aqueous solutions. First Transmission Electron Microscopy (TEM) was performed using copolymer solutions casted on a carbon grid thin substrate. The concentration of the initial solutions was larger than the CMC, and they were prepared by stirring at 90°C for three days. In figure 4(a) TEM images of copolymer films made from a solution with a concentration of 0.2 g/L are presented. Rice grain shaped objects are clearly observed with ∼200 nm width and 400-500 nm length. Around these objects, smaller spherical particles are also present, with size of 30-60 nm. These images with objects of different sizes and shapes are in agreement with the previous NTA analysis in which polydisperse objects were detected. Due to the large size of the rice grain objects they cannot be considered as vesicles or micelles. Their shape and the existence of smaller objects around them make us conclude that they are formed from the aggregation of the micelles.

Since the TEM analysis was performed using copolymer solutions casted on substrates, it is possible that the observed structures result from the casting method and the subsequent solvent evaporation. Analysis of the P3HT$_{0.25}$-*b*-(PS$_{0.27}$-*co*-PSSA$_{0.48}$) water solutions were thus

performed by Cryogenic Transmission Electron Microscopy (Cryo-TEM). By this method the observed structures are truly representative of the morphology in solution.

Figure 5. (a) TEM images of P3HT$_{0.25}$-*b*-(PS$_{0.27}$-*co*-PSSA$_{0.48}$) copolymers solutions of c = 0.2 g/l, scale 1 μm (left) and 100 nm (right) (b) Cryo-TEM images of the same solution, scale 0.5 μm (left) and 100 nm (right).

(a)

(b)
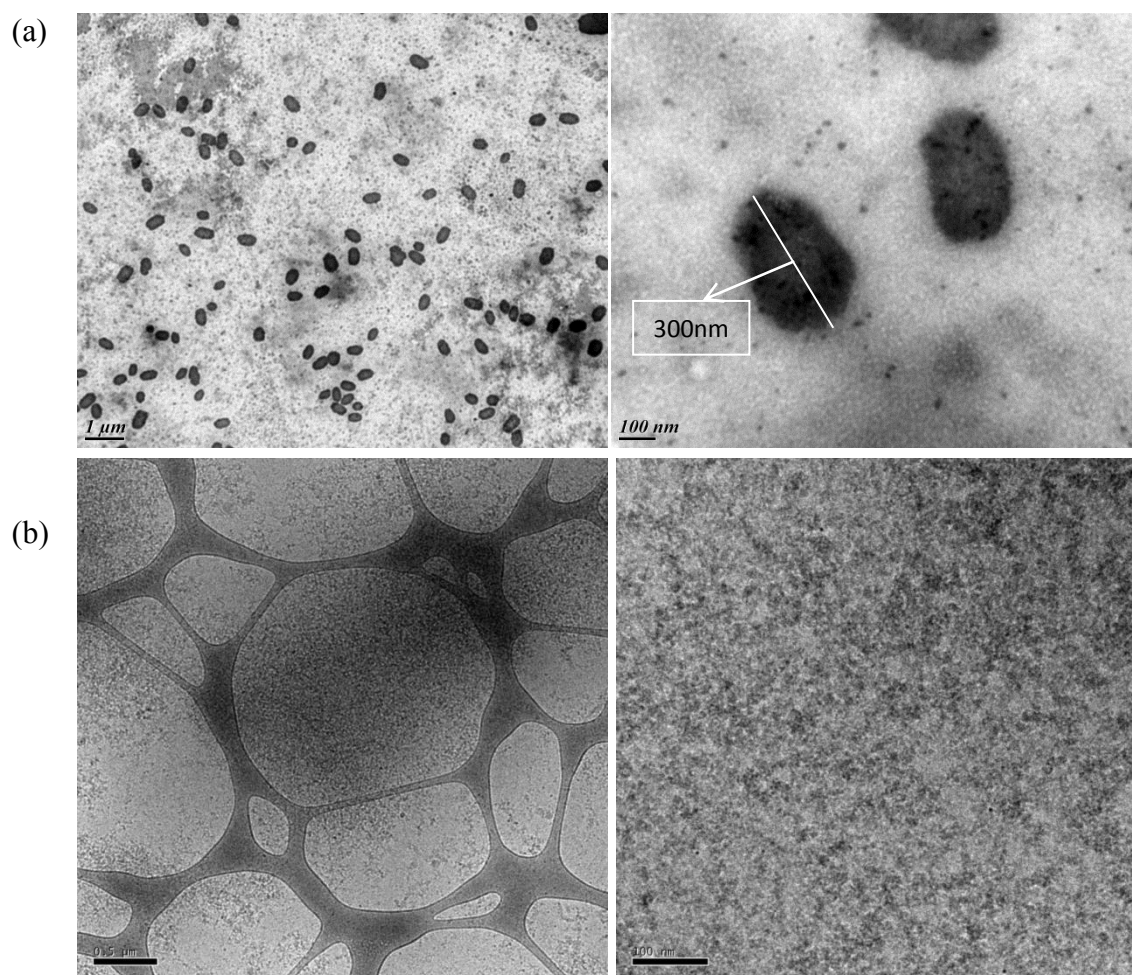
The cryo-TEM images of copolymer solutions with a concentration of 0.2 g/L are presented in figure 4(b). In these images the organization of small particles into big aggregates is clearly observed. The size of the aggregates observed by cryo-TEM is larger than the one derived for the rice grain objects in TEM analysis. This difference is related to a larger swelling of these

structures in solution and to the shrinking when they are casted in films due to the solvent evaporation. It is clear that these aggregates consist of many smaller spherical objects. The Cryo-TEM images allow us to conclude that the self-assembly behavior of the rod-coil block copolymer is not resulting from the casting method from the solvent evaporation.

In order to study the stability of these structures, copolymer solutions were submitted to sonication using a sonicator probe. It has been reported before,[7] polymeric micelles with poor solubility are not obtained by normal solution preparation methods because of their organization in aggregates. Sonication has been used to split the aggregates into individual micelles. In addition, the use and study of sonication is of particular importance as further investigation in this work need the use of sonication for the formulation with carbon nanotubes (CNTs). All the studied solutions that were examined were sonicated for 20 minutes with a probe sonicator and the concentration was kept constant at 0.2 g/L in order to be able to compare our results with the previous studies. It is noteworthy that the structure and the size of the copolymer are not affected by the sonication as it can be seen from IR and ^{1}H-NMR characterizations (annexes V.6).

TEM images of the sonicated solutions casted as films are presented in the figure 5(a). It is clear from these images that the big rice grain structures observed for the non-sonicated solutions have disappeared. Instead, small particles of 30 nm are present, similar to the one observed around the aggregates in the TEM images of the non-sonicated solutions. Some long fibers are also present, probably due to the sonication of the solution and the brake of the aggregates.

Figure 6. (a) TEM images of P3HT$_{0.25}$-*b*-(PS$_{0.27}$-*co*-PSSA$_{0.48}$) copolymer sonicated solutions of c=0.2 g/l, scale 200nm (left) and 100 nm (right) (b) Cryo-TEM images of the same sonicated solution, scale 50 nm (left) and 0.5 µm (right).
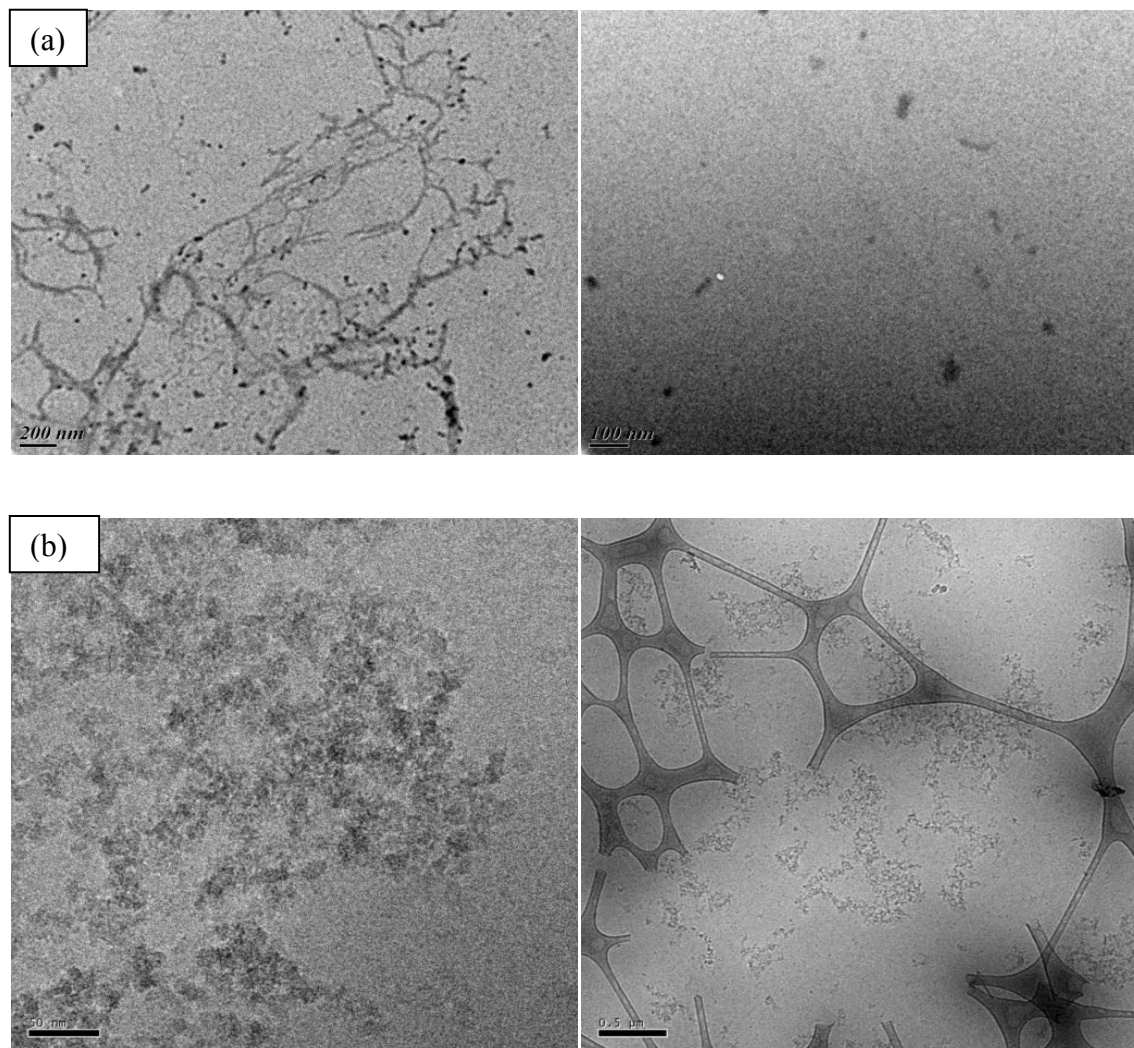
Similarly, in the Cryo-TEM images of the sonicated solutions (figure 5 (b)) the big aggregates have disappeared and have been replaced by a network of micellar structures with a particle size between 30 nm and 50 nm. These new structures observed for the sonicated solutions indicate that the sonication breaks the inter-micellar associations and only the micelles organization with size of 30-60 nm remains.

The self-assembling behavior of the block copolymer in aqueous media was further investigated by Atomic Force microscopy (AFM) on films. AFM images of sonicated solution caste on mica substrate are shown in figure 7. Once again rather homogeneous micelles with diameter of 40-60nm were observed in accordance with the TEM images shown in figure 6.

Figure 7. (a) AFM images of P3HT$_{0.25}$-*b*-(PS$_{0.27}$-*co*-PSSA$_{0.48}$) copolymer sonicated solution deposited on mica surface.
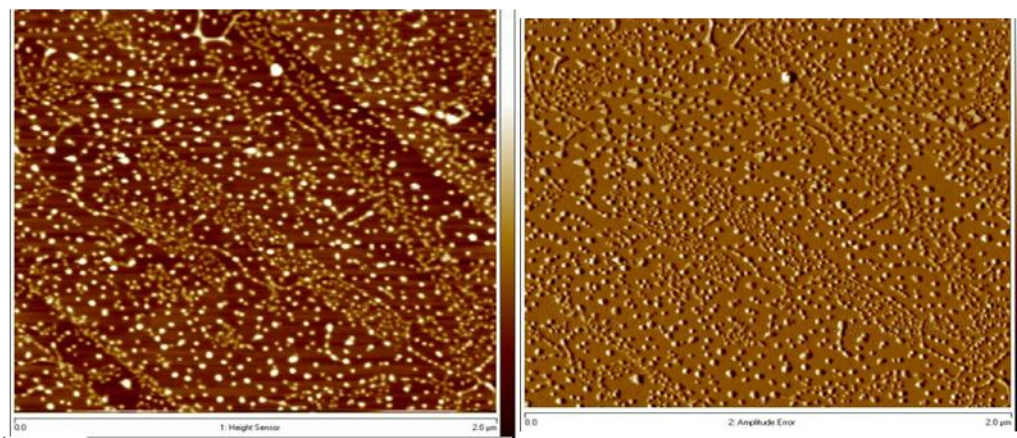
In summary, the rod-coil P3HT$_{0.25}$-*b*-(PS$_{0.27}$-*co*-PSSA$_{0.48}$) block copolymer self-assembles in metastable aggregates of micelles when it is dispersed in water solutions. The shape and the size of these aggregates were visualized by TEM and Cryo-TEM analysis. Both techniques showed rice grain shape while the size was bigger for the Cryo-TEM analysis due to the swelled structures in the solutions. These metastable structures can be disrupted by the sonication of the solutions. Indeed after sonication (20 min with 225 Watt) new micellar structures were visualized by TEM, Cryo-TEM, AFM and environmental AFM, all showing images of spherical micelles with size ranging between 30 nm and 60nm.

II.1.3 Photophysical properties

The self-assembly structures of the π-conjugated rod-coil block copolymers have a direct impact on the physical properties[8]. Indeed the latter are mainly governed by the packing type of the π-conjugated rod blocks (*i.e* π-π stacking). Two different types of organization of the rod chains have been widely studied: the J- and H-aggregates.[9] These types of aggregation are usually associated with a shift of the maximum of absorption of the π-conjugated blocks. The J-aggregates are associated with a bathochromic spectral shift, toward longer wavelengths, while the H- aggregates exhibit a hypsochromic spectral shift toward shorter wavelengths.

Figure 8. Schematic illustration of the proposed H-and J-aggregates structures and their corresponding energy levels. [3] **Reproduced with permission from Elsevier, Copyright 2011**
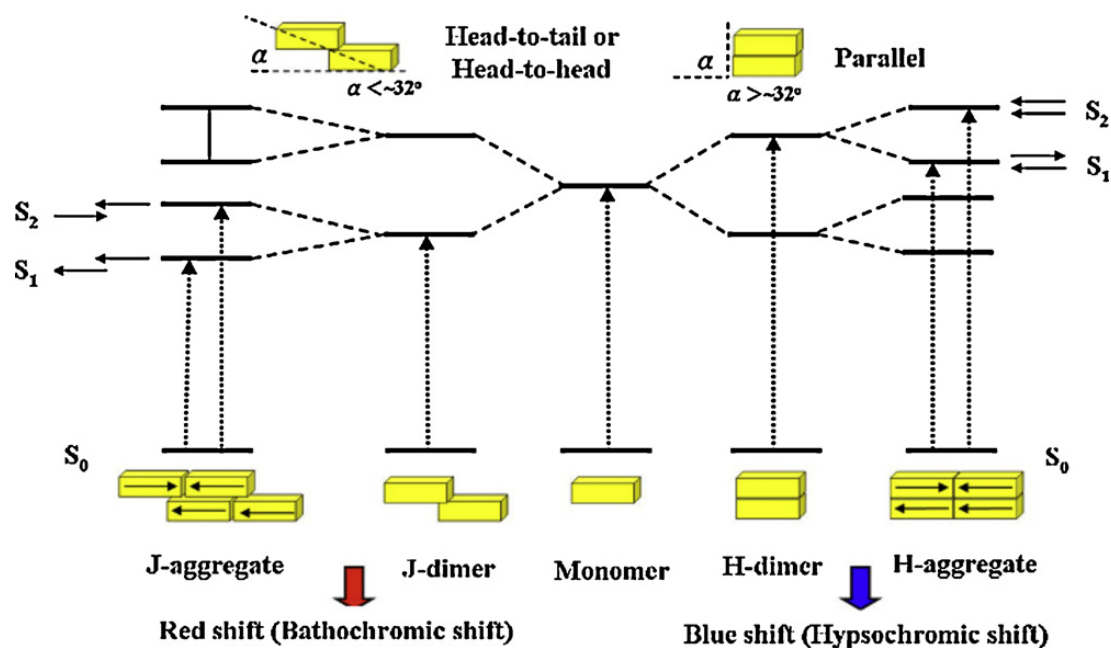
These two effects of aggregation have been explained in terms of molecular exciton coupling (figure 8). The formation of J- or H- aggregates strongly depends on the angle (slippage angle) between the line-of-centers of a column of molecules and the long axis of any one of the

parallel molecules, as explained by Tsao *and coll*. (figure 9)[10] When planes are oriented with a slippage angle larger than a certain value there is a bathochromic shift (J-aggregates) while for slippage angle less than that value result in hypsochromic shifts (H-aggregates). These aggregates have been reported for π-conjugated block copolymers both in solutions and films. [11] Regarding the organization of the π-conjugated blocks when they participate in these type of aggregates, the blocks are oriented in a parallel "sandwich" way for the H-aggregates and in parallel but shifted one to the other way for the J-aggregates, as shown in the figure 8.

Figure 9. Schematic representation of the included angle (θ) and the slippage angle (α) in rod-coil systems.
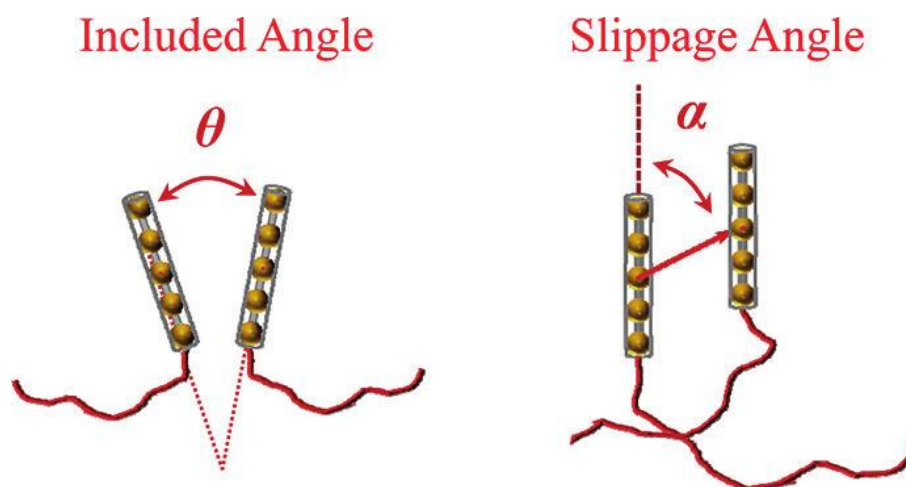
Based on these theoretical studies and previous reports about the organization of the π-conjugated rod-coil block copolymers in J- and H- aggregates, the photophysical properties of the P3HT$_{0.25}$-*b*-(PS$_{0.27}$-*co*-PSSA$_{0.48}$) were studied in solution and solid states.

***II.1.3.1.   Photophysical   characterization   of   P3HT$_{0.25}$-b-(PS$_{0.27}$-co-PSSA$_{0.48}$)
copolymer sonicated solutions and films***

First the photophysical behavior of the sonicated P3HT$_{0.25}$-*b*-(PS$_{0.27}$-*co*-PSSA$_{0.48}$) solution
and its corresponding films was studied. UV-vis spectroscopy was performed for a sonicated
copolymer solution with c = 0.2 g/L and for its drop-casted film (figure 10). The UV-vis spectra
of the probe sonicated solution, where micelles and unimers are present, exhibit an maximum of
absorption at 497 nm, which corresponds to the P3HT absorption. The maximum of absorption in
the solid state (thin film) is shifted to shorter wavelength as compared to the solution. This blue
shift of 23nm (from 497nm to 474nm) suggests that the rod coil copolymer micelles are further
organized in the drop casted film. This hypsochromic shift indicates the organization of the
solutions micelles in H- type aggregates when they are casted in thin film.

**Figure 10. UV-vis spectra of the P3HT$_{0.25}$-*b*-(PS$_{0.27}$-*co*-PSSA$_{0.48}$) copolymer water solution
(c= 0.2 g/L) after probe sonication (green) and its corresponding film (red).**
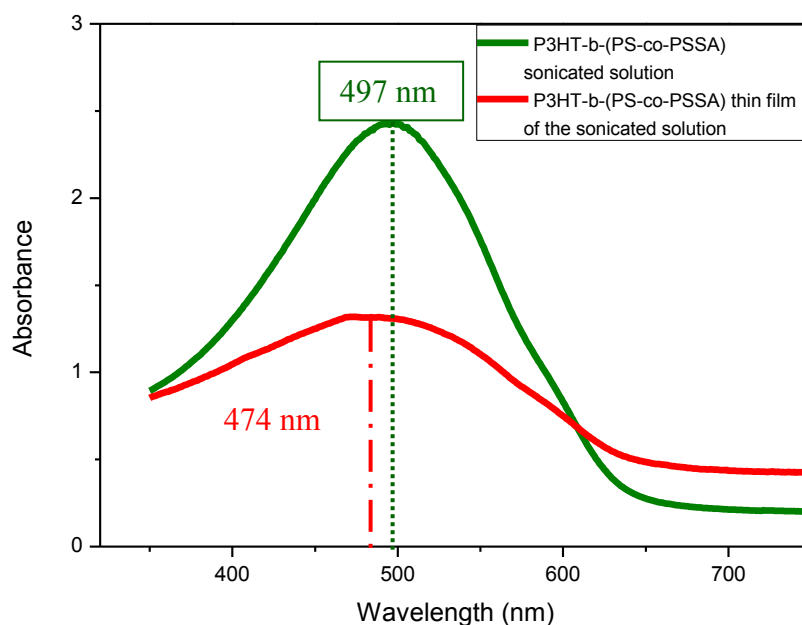
An illustration of these H-aggregates formed from the sonicated water solution of the copolymer when it is caste in thin film (30 nm) is presented in figure 11. A micelle is consisting of many unimers in which the P3HT blocks are located in the center creating π-π interactions and the PS-*co*-PSSA part surrounds this hydrophobic core. When a film is formed out of a sonicated solution, which contains these micelles, H-type aggregates are formed from the organization of these micelles on the film surface.

Figure 11. An illustration of the H-aggregates formed in the thin films of the P3HT$_{0.25}$-*b*-(PS$_{0.27}$-*co*-PSSA$_{0.48}$) copolymer
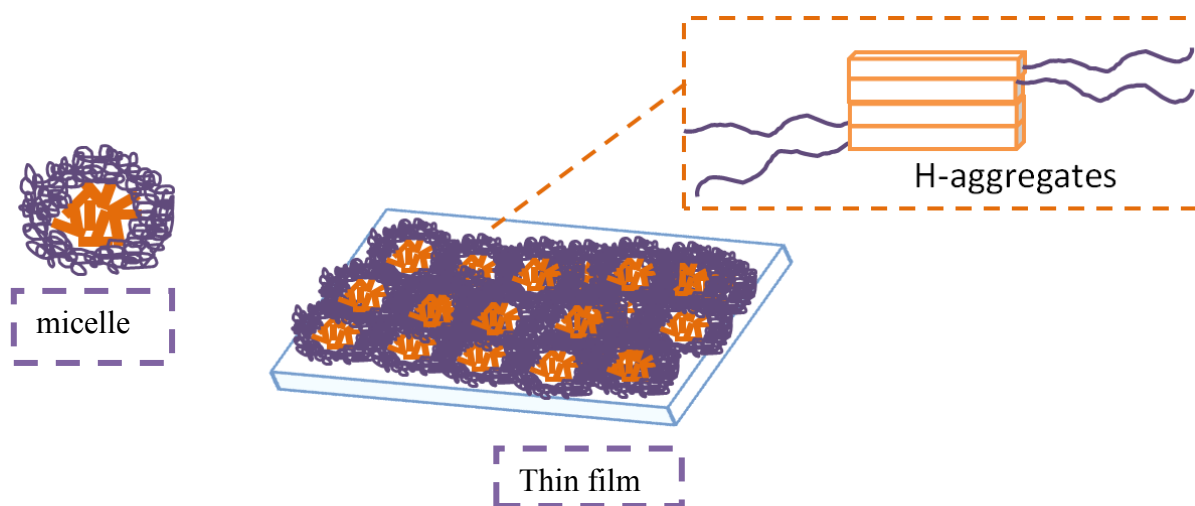
The absorption difference between the solution and the solid states is typical for regioregular P3HT and it is a result of a different π-π packing of the π-conjugated chains in the film. Moreover, the hypsochromic shift of the absorption maximum indicates the formation of H-type aggregates. Several studies have been made considering the type of aggregations that P3HT polymers are forming in solutions and in thin films. It is known that parameters like the regioregularity, the molecular weight and the solvent strongly influence the type of aggregation of the P3HT. Unfortunately, no experimental studies on the structure of P3HT-based block

copolymers aggregates have been made. Nevertheless F. Spano has made a systematic theoretical study on the H- and J- aggregations of the P3HT, developing a new theoretical model.[12] Based on this theory, P3HT aggregated chains can act as H-aggregates with face-to-face oriented chains exhibiting weak excitonic coupling. The excitonic coupling is related to the blue or the red shift that we observe in the absorption spectra and it is positive for the H-aggregates and negative for the J-aggregates. As the polymer chains are oriented more planar the polymer becomes more conjugated and the intermolecular coupling between polymer chains decreases.

Combining the theory about the different organizations of P3HT and our results from the UV-vis spectra, we can conclude that the P3HT blocks are further organized when they are casted in films. Indeed, due to the blue shift of the absorption between the sonicated solution and the casted film, we can assume that the P3HT blocks are organized in a plane to plane fashion resulting in H-aggregates.

II.1.3.2. *Photo-physical characterization of P3HT$_{0.25}$-b-(PS$_{0.27}$-co-PSSA$_{0.48}$) copolymer solutions before and after sonication*

As presented in paragraph I.1.2, the P3HT$_{0.25}$-*b*-(PS$_{0.27}$-*co*-PSSA$_{0.48}$) copolymer forms aggregates when it is dispersed in water solutions. The nature of these aggregates was examined by UV-vis spectroscopy (figure 12). Two copolymer solutions at 0.2 g/L were prepared: the first one, which contained aggregates, was obtained after stirring at 90 °C for 48 hours and the second which was submitted to the same stirring at 90 °C followed by a probe sonication treatment for 20 min with 225 Watt power. The absorption peak of the non-sonicated solution, in which the polymer micelles are organized in aggregates, exhibits a maximum at 504 nm and a small shoulder at 600 nm. This spectrum is in good agreement with reported P3HT aggregates spectra, indicating the existence of strong π-π interactions between the P3HT chains.[13]

The spectra of the probe sonicated solution exhibits an absorption band centered at 497 nm, indicating a small red shift of 7 nm between the sonicated and the aggregated solution. This observation signifies that the P3HT$_{0.25}$-*b*-(PS$_{0.27}$-*co*-PSSA$_{0.48}$) is self-assembled when it is

dispersed in a poor solvent (water) for the P3HT block. This organization results of strong π-π interactions between the P3HT blocks, and the particular slippage angle of the packing leading to the red shift confirms the formation of J-aggregates.

Figure 12. UV-vis spectra of the P3HT$_{0.25}$-*b*-(PS$_{0.27}$-*co*-PSSA$_{0.48}$) copolymer water solution after probe sonication for 20 min with 225 Watt power (red) and non-sonicated (green).
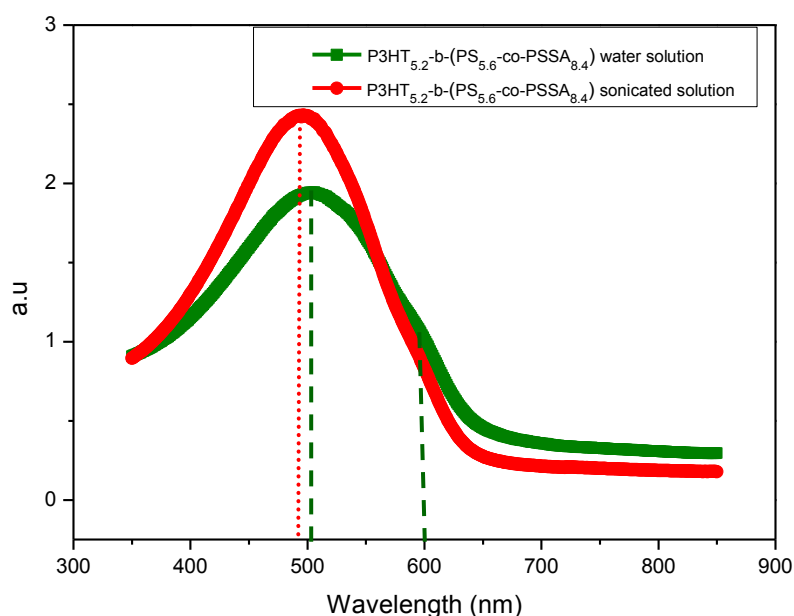
In the figure 13 an illustration of the organization of the P3HT$_{0.25}$-*b*-(PS$_{0.27}$-*co*-PSSA$_{0.48}$)) in water solution is presented. The aggregates, that are initially formed when the P3HT$_{0.25}$-*b*-(PS$_{0.27}$-*co*-PSSA$_{0.48}$) copolymer is dissolved in aqueous media, contain micelles organized in J-aggregates.

Figure 13. An illustration of the possible organization of the P3HT$_{0.25}$-*b*-(PS$_{0.27}$-*co*-PSSA$_{0.48}$) copolymer in water solution.
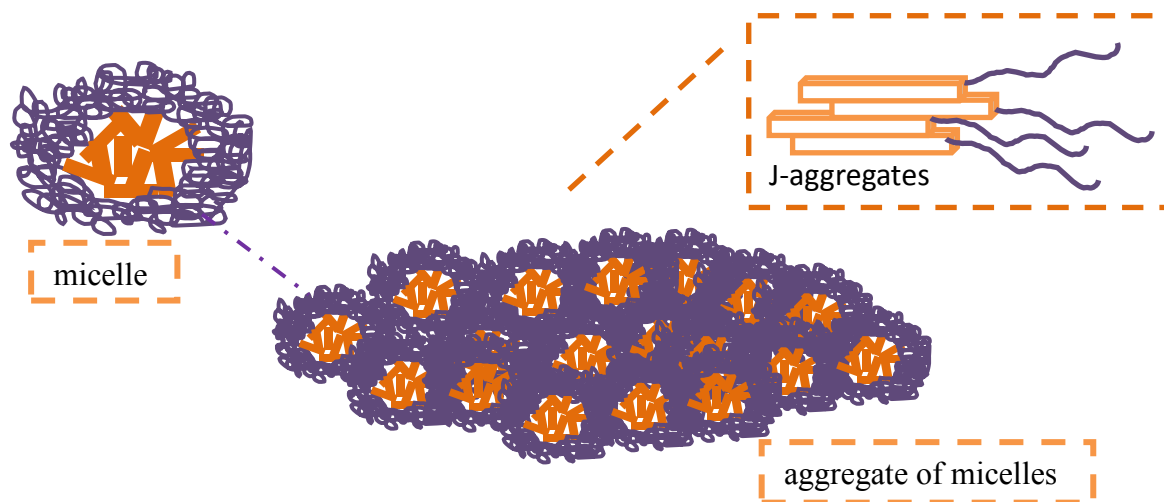
From the UV-analysis of the solutions and the films of the P3HT$_{0.25}$-*b*-(PS$_{0.27}$-*co*-PSSA$_{0.48}$) copolymer, we can conclude that the P3HT is organized in either J- or H- aggregates depending on the conditions. By comparing the absorption peaks of the sonicated solution and the corresponding film, the P3HT micelles are forming H- aggregates under the film formation conditions. In contrast, when the micelles are dispersed in aqueous media they are organized in J-type aggregates, forced by the hydrophobicity of the environment. These observations are in accordance with the theory developed by F. Spano who is demonstrating that the P3HT can be associated in both H- and J- aggregates depending on the type of the organization.

Figure 14. Photoluminescence spectra of P3HT$_{0.25}$-*b*-(PS$_{0.27}$-*co*-PSSA$_{0.48}$) copolymer water solution (c= 0.2 g/L) without sonication (blue) and after probe sonication for 20 min with power of 225 Watt (purple)
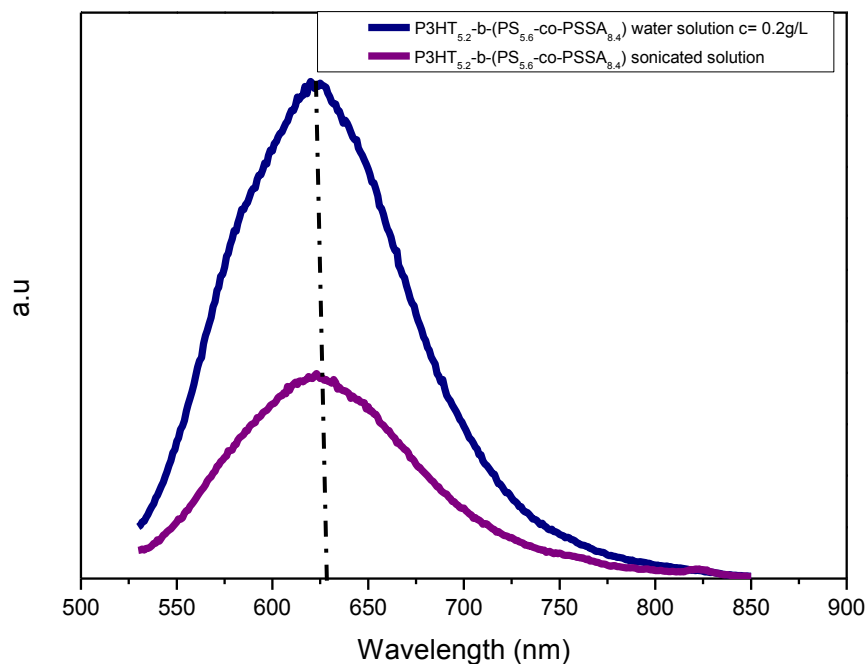
The P3HT$_{0.25}$-*b*-(PS$_{0.27}$-*co*-PSSA$_{0.48}$) copolymer solutions were also examined by photoluminescence spectroscopy. In figure 14, the fluorescence spectrum is presented for both the non-sonicated and sonicated copolymer solutions with concentration at 0.2 g/L. The two solutions exhibit a fluorescence emission maximum at 620 nm, but the emission of the sonicated solution is much smaller. The high concentration (in comparison with the CMC of the copolymer)of these solutions is not allowing us to make safe conclusions for the photoluminescence behavior. Indeed we could have expected a higher fluorescence yield from the sonicated solution signifying a stronger signal from the P3HT block that is less quenched. By quenching we refer to the π-π interactions that a π-conjugated polymer develops. In our case is

the π-π stacking of the P3HT blocks during their self assembly. Since the concentration is much higher than the CMC the formation of small aggregates is possible, influencing the photoluminescence signal.

The damage of the chemical structure of the P3HT under the force of the sonication could explain this change in the luminescence spectra, but as mentioned before we have verified that there is no influence. A simple explanation can be given by the change of the organization before and after sonication. In both cases the copolymer unimers are organized in micelles (sonicated solution) or aggregates (non-sonicated solution), so the P3HT blocks are quenched. The packing of P3HT in micelles could be characterized as more compact, due to the small size of the micelles. In comparison the organization of the copolymer in big aggregates result in a more dense packing for the P3HT chains, explaining the more intense photoluminescence.

II.2   Physicochemical characterization of the P3HT-co-PVA copolymer

In order to investigate the effect of the charged versus neutral water soluble block the physico-chemical properties of the compare the P3HT-*b*-PVA was examined and compared with $P3HT_{5.2}$-*b*-$(PS_{5.6}$-*co*-$PSSA_{8.4})$ properties. The good was to compare the shape and the size of the self-assemblies in the two systems, considering the different hydrophilic parts (charged and non-charged). In addition, the possible formation of J- and H-type aggregates will be investigated for the P3HT-*b*-PVA copolymer. Another comparison study will take place, considering the different architectures of the P3HT/PVA system. The self-assemblies in water solution of $P3HT_{4.6}$-g-$PVA_{12.5}$ (3 P3HT per PVA chain) copolymers will also be investigated.

II.2.1   Physicalchemical characterization of $PVA_{12.5}$-*g*-$P3HT_{4.6}$ copolymers

Similar study, as for the $P3HT_{5.2}$-*b*-$(PS_{5.6}$-*co*-$PSSA_{8.4})$ copolymer, was made for the $PVA_{12.5}$-g-$P3HT_{4.6}$ (3 P3HT per PVA chain) copolymer with P3HT molecular weight at 4.6

kg/mol and PVAc at 12.5 kg/mol. Water solutions of the grafted copolymer with concentrations from 0.0002 g/L to 0.2 g/L were prepared for the determination of the CMC by a pyrene probe, as described before. The photoluminescence spectra of the pyrene showed no change for the different concentrations of the polymer, starting from very low until quite high for CMC concentrations (figure 15). In order to verify the absence of micelles in solutions we additionally performed UV-vis analysis for detecting possible P3HT self-assemblies by the vibronic changes that were not strong enough to be detected by the pyrene probe. No change on the P3HT signal was also observed in the UV-vis spectra (figure 14), indicating that there are no π-interactions between the P3HT chains. After these first investigations we assume that the $PVA_{12.5}$-g-$P3HT_{4.6}$copolymers do not create self-assemblies in the water solutions. The graft architecture of the copolymer in combination with the volume fraction of the P3HT, are preventing the self-assembly in the solution.

Figure 15. (a) UV-vis spectra of the $PVA_{12.5}$-g-$P3HT_{4.6}$ (3 P3HT per PVA chain) copolymer water solutions at different concentrations ($2·10^{-4}$<c< $2 ·0^{-2}$ g/L) (b) the I_1/I_3 ratio of the pyrene probe as a function of the copolymer in the same concentrations.

(a)

(b)

191
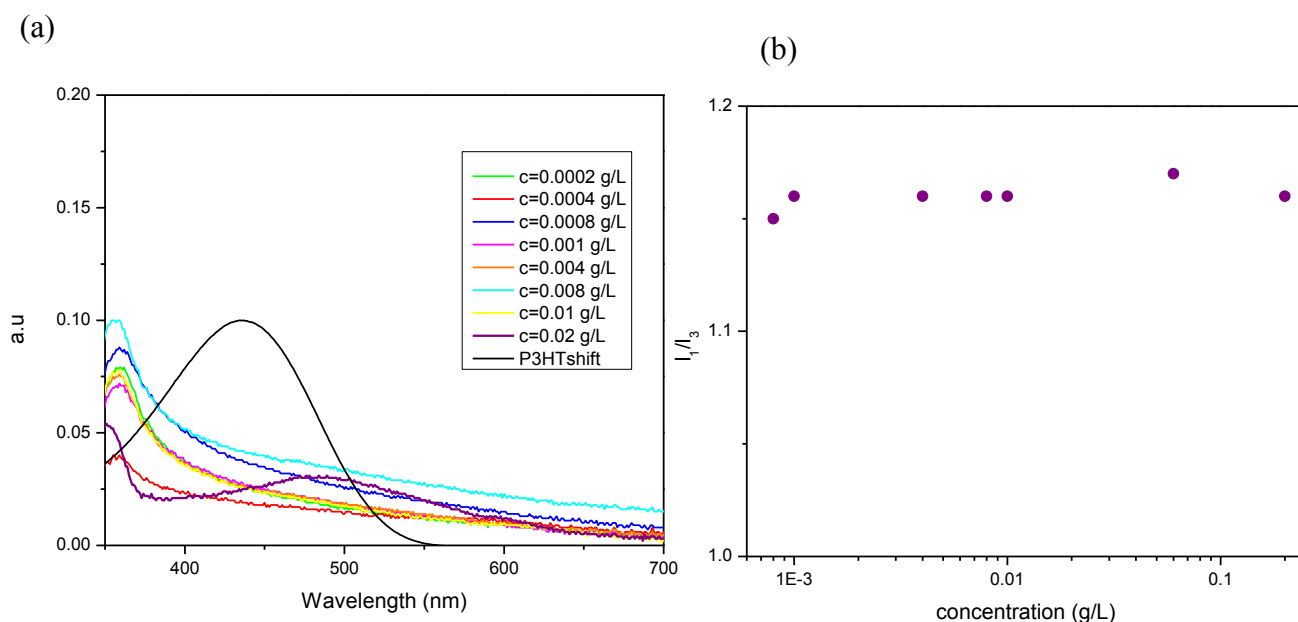
III *Conclusion*

In this chapter the physico-chemical properties of the P3HT-based copolymers in aqueous media were examined. In addition two comparison studies were made, one between the P3HT block copolymers with charged (PSSA) and neutral (PVA) side chains and the other between P3HT/PVA copolymers with different architectures (graft and block copolymers).

The self assembly of the P3HT$_{0.25}$-*b*-(PS$_{0.27}$-*co*-PSSA$_{0.48}$) copolymer was examined in both aqueous solution and in solid state. CMC was determined by fluorescence spectra with the use of pyrene probe and by UV-vis at 0.008 g/L. In addition zeta potential measurements showed negatively charged objects indicating a morphology where the P3HT block is located in the center creating a core surrounded by the PS-*co*-PSSA chains. From the microscopic studies the formation of rice grain shaped objects was visualized (size of 300 nm) when the P3HT$_{5.2}$-*b*-(PS$_{5.6}$-*co*-PSSA$_{8.4}$) copolymer is solubilized in water solutions at concentrations higher than CMC (c=0.2g/L). The size and the nature of these assemblies were closer to aggregate morphologies. Indeed these assemblies disappeared under the sonication treatment giving rise to small particles of 30 nm. After these studies we conclude that negatively charged micelles of 30nm are initially formed when the P3HT$_{0.25}$-*b*-(PS$_{0.27}$-*co*-PSSA$_{0.48}$) is in aqueous media, which are further assembled in rice shape aggregates of 300 nm.

The photophysical properties of the P3HT$_{0.25}$-*b*-(PS$_{0.27}$-*co*-PSSA$_{0.48}$) copolymers solutions and thin films were studied by UV-vis spectroscopy. The maximum of absorption on the copolymers solution after sonication is located at 497 nm while that of the corresponding thin film is found at 474 nm. This blue shift of 23 nm suggests that the micelles are organized in J-aggregates. In contrast, a red shift of 7 nm is observed between the sonicated water solution of the copolymer and the original one. This observation signifies the formation of H-type aggregates of the micelles when the P3HT$_{5.2}$-*b*-(PS$_{5.6}$-*co*-PSSA$_{8.4}$) is solubilized in aqueous solutions.

1.   Jenekhe, S. A.; Chen, X. L., Self-Assembled Aggregates of Rod-Coil Block Copolymers and Their Solubilization and Encapsulation of Fullerenes. *Science* **1998,** *279* (5358), 1903-1907.
2.   Tung, Y.-C.; Wu, W.-C.; Chen, W.-C., Morphological Transformation and Photophysical Properties of Rod-Coil Poly[2,7-(9,9-dihexylfluorene)]-block-poly(acrylic acid) in Solution. *Macromol. Rapid Commun.* **2006,** *27* (21), 1838-1844.
3.   Liu, C.-L.; Lin, C.-H.; Kuo, C.-C.; Lin, S.-T.; Chen, W.-C., Conjugated rod-coil block copolymers: Synthesis, morphology, photophysical properties, and stimuli-responsive applications. *Prog. Polym. Sci.* **2011,** *36* (5), 603-637.
4.   Sary, N.; Rubatat, L.; Brochon, C.; Hadziioannou, G.; Ruokolainen, J.; Mezzenga, R., Self-Assembly of Poly(diethylhexyloxy-p-phenylenevinylene)-b- poly(4-vinylpyridine) Rod−Coil Block Copolymer Systems. *Macromolecules* **2007,** *40* (19), 6990-6997.
5.   Bu, L.; Qu, Y.; Yan, D.; Geng, Y.; Wang, F., Synthesis and Characterization of Coil−Rod−Coil Triblock Copolymers Comprising Fluorene-Based Mesogenic Monodisperse Conjugated Rod and Poly(ethylene oxide) Coil. *Macromolecules* **2009,** *42* (5), 1580-1588.
6.   Oikonomou, E. K.; Bethani, A.; Bokias, G.; Kallitsis, J. K., Poly(sodium styrene sulfonate)-b-poly(methyl methacrylate) diblock copolymers through direct atom transfer radical polymerization: Influence of hydrophilic–hydrophobic balance on self-organization in aqueous solution. *Eur. Polym. J.* **2011,** *47* (4), 752-761.
7.   Zhao, J.; Pispas, S.; Zhang, G., Effect of Sonication on Polymeric Aggregates Formed by Poly(ethylene oxide)-Based Amphiphilic Block Copolymers. *Macromol. Chem. Phys.* **2009,** *210* (12), 1026-1032.
8.   Olsen, B. D.; Segalman, R. A., Self-assembly of rod–coil block copolymers. *Materials Science and Engineering: R: Reports* **2008,** *62* (2), 37-66.
9.   Dautel, O. J.; Wantz, G.; Almairac, R.; Flot, D.; Hirsch, L.; Lere-Porte, J.-P.; Parneix, J.-P.; Serein-Spirau, F.; Vignau, L.; Moreau, J. J. E., Nanostructuration of Phenylenevinylenediimide-Bridged Silsesquioxane: From Electroluminescent Molecular J-Aggregates to Photoresponsive Polymeric H-Aggregates. *J. Am. Chem. Soc.* **2006,** *128* (14), 4892-4901.
10.   Hung, J.-H.; Lin, Y.-L.; Sheng, Y.-J.; Tsao, H.-K., Structure–Photophysical Property Relationship of Conjugated Rod–Coil Block Copolymers in Solutions. *Macromolecules* **2012,** *45* (4), 2166-2170.
11.   de Cuendias, A.; Ibarboure, E.; Lecommandoux, S.; Cloutet, E.; Cramail, H., Synthesis and self-assembly in water of coil-rod-coil amphiphilic block copolymers with central π-conjugated sequence. *Journal of Polymer Science Part A: Polymer Chemistry* **2008,** *46* (13), 4602-4616.
12.   Spano, F. C., Absorption in regio-regular poly(3-hexyl)thiophene thin films: Fermi resonances, interband coupling and disorder. *Chem. Phys.* **2006,** *325* (1), 22-35.
13.   Scharsich, C.; Lohwasser, R. H.; Sommer, M.; Asawapirom, U.; Scherf, U.; Thelakkat, M.; Neher, D.; Köhler, A., Control of aggregate formation in poly(3-hexylthiophene) by solvent, molecular weight, and synthetic method. *Journal of Polymer Science Part B: Polymer Physics* **2012,** *50* (6), 442-453.

Chapter IV

Composites of P3HT-based copolymers with carbon nanotubes and their use as transparent conductive electrodes

TABLE OF CONTENTS

Composites of P3HT-based copolymers with carbon nanotubes and their use as transparent conductive electrodes.

I   *Introduction*

In this chapter the possibility of the P3HT-based copolymers to be used as dispersion agent for CNTs and their further application in formation of conductive transparent films is investigated. As described in the first chapter (paragraph II.2.2.5.3) CNTs can be dispersed in both aqueous and organic media by π-conjugated polymers.[1] The dispersion process is based on the strong π-π interactions developed between the sp^2-carbons of the nanotubes and the π-conjugated polymer (figure 1). Under mechanical shearing the bundles of the CNTs, made by Van der Waals interactions, are forced to relax and then the π-conjugated polymer interacts with the surface of the CNTs preventing the reformation of the bundles. Even though this method of dispersion is favorable due to the strong affinity between the dispersion aid and the nanotubes, it suffers solubility problems.

Indeed, the π-conjugated polymers have the tendency to aggregate by developing π-π interactions which can impact the stability of the CNTs dispersions. In order to overcome this difficulty block copolymers consisting of a π-conjugated segment and a coil block have been designed. In fact, the π-conjugated block has affinity for CNTs while the coil block is aimed to interact with the dispersing phase. The nature of the coil block can be tuned in order to play with the dispersing phase from aqueous to organic media.

Figure 1. A schematic representation of the dispersion of CNTs by the use of π-conjugated block copolymers
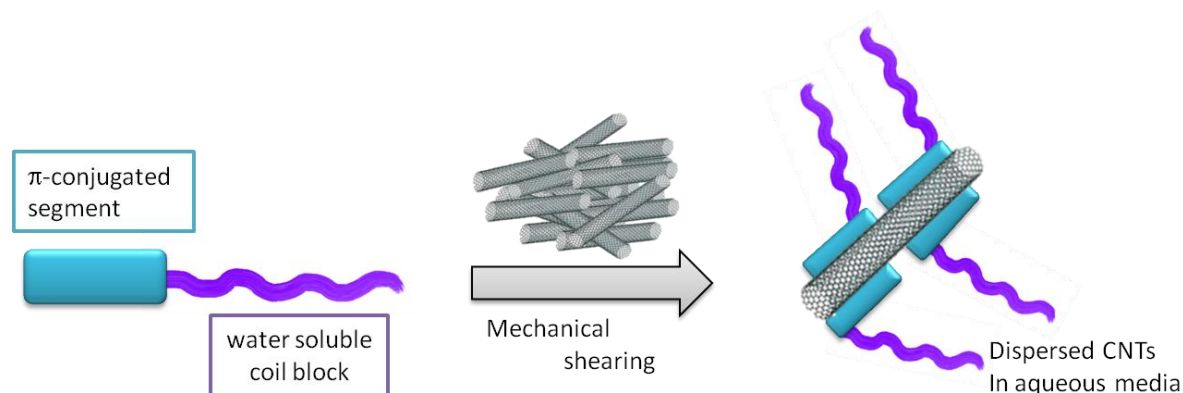
I.1. Deposition techniques

Inks constituted of CNTs and P3HT-based copolymers are formed after the dispersion procedure. These formulations will be further casted in thin films in order to investigate their optical and electrical properties. There are several film deposition techniques that have been developed targeting homogenous films with controlled thickness. Several parameters affect the quality of the deposited films concerning both the ink characteristics (*e.g* viscosity, concentration) and the deposition surface properties (*e.g* flexibility, functionality). In the following section, the different characteristics of several techniques that have been reported in the literature for the preparation of CNTs films are presented.

I.1.1   *Vacuum filtration technique*

One of the simplest methods of formation of CNT thin films is by the vacuum-filtration method.[2] The process is simple and involves the vacuum filtering of a dilute dispersion of CNTs onto a filtration membrane followed by rinsing through with solvent to remove the dispersion aid. The resulted films are transparent, homogenous and can be transferred to other substrates. This deposition method has several advantages. It is low cost, easy to apply and the dispersion aids can be removed at the end of the process. In addition, under vacuum the CNTs tend to lie straight increasing the electrical conductivity of the film while the film thickness can be controlled by the concentration and the volume of the filtered suspension. However this technique has an obvious limitation on the size of the film and it is relatively slow since the films have to be transferred to other substrates. Therefore, up to now this procedure is limited to academic research level and can not be industrialized.

Figure 2. Diagram of: carbon based dispersion (a) deposited by vacuum filtration in a thin film on a membrane substrate (b,c). The membrane is removed (d) when the composite is introduced in DI water while the carbon film is floating (e). The film is then deposited on a flexible PET surface (f,g) [3] Reproduced with permission from Elsevier, Copyright 2012
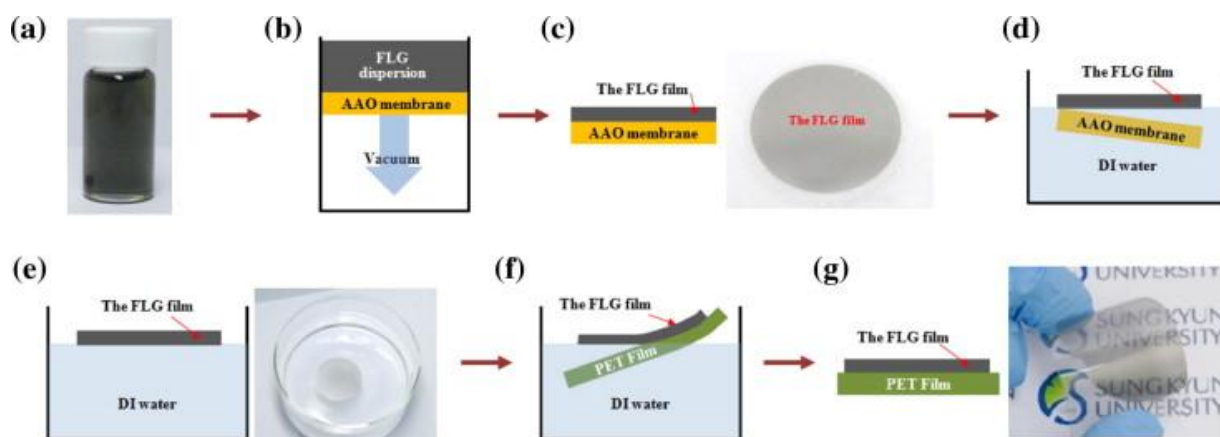
I.1.2   Convective self-assembly technique for film deposition

Self-assembly is another fast and low cost method for the formation of films, which is based on chemical interactions between the CNTs and the surface. Silane or polymer treatment of the substrates helps the interactions between the CNTs and the substrate.[4] When the substrate is placed in the CNTs dispersion, the nanotubes will randomly cover the surface. The formation of films depends on the chemical functionalization of the CNTs and the surface. The main disadvantage of this method is the requirement of covalently functionalized CNTs. In addition the resulting films have very low thickness.

I.1.3   Dip coating, spin coating and spray coating techniques

Transparent and conductive films have been fabricated by dip coating.[5] This type of coating is a quite simple process that can be extended to large scale production. Indeed, the procedure only requires the dipping of the substrate in the CNTs dispersion while the film is formed during its raising. The viscosity of the solution (from 20 to 2000 mPa.s)[6], the interactions with the substrate along with the coating rate influences the quality and the thickness of the films. The substrates can be treated in order to help in the film formation. The lifting process of the substrate from the dispersion can be horizontal or vertical thus affecting the orientation of the nanotubes on the film. The dip coating method has a limitation on the type of the dispersions that can be used, since high viscosities are required. In addition by that method both sides of the substrates are coated, which may not be preferable for many applications.

Another type of deposition method called spin coating needs small volumes of solution and film are formed after high-speed spinning. This procedure is widely used because solutions with viscosities from 2 to 30 mPa.s can be deposited offering an advantage over dip coating methods.[7] The thickness of the films can be controlled by the rotation speed of coating and multilayer films can be made by this method increasing the percolation of the CNTs. The main

disadvantage of the spin-coating method is that the formed thin films have not homogenous thickness due to the spin procedure.

Lastly, the spray coating technique has been used for the formation of transparent films of CNTs dispersions. Spray coating is an easily applied and fast method where the dispersion is sprayed onto a heated surface to facilitate the evaporation of the dispersing phase. Dilute CNTs dispersions with viscosities from 0.05 to 1 mPa.s can be sprayed and the thickness of the films can be tuned by multiple spray steps. Spray coating can be used for all the types of dispersions and it can be applied on all surfaces even if they are rough. The only disadvantage of the thin films made by spray coating is the appearance of the "coffee stain" effect as the droplets are drying on the surface. This problem can be solved by making the evaporation of the solvent faster and also by post treatment of the films. Besides, spray coating remains a popular method that could be used in industry.

Figure 3. Schematic of different deposition techniques (a) Spin-coating (b) Dip-coating (c) spray-coating.
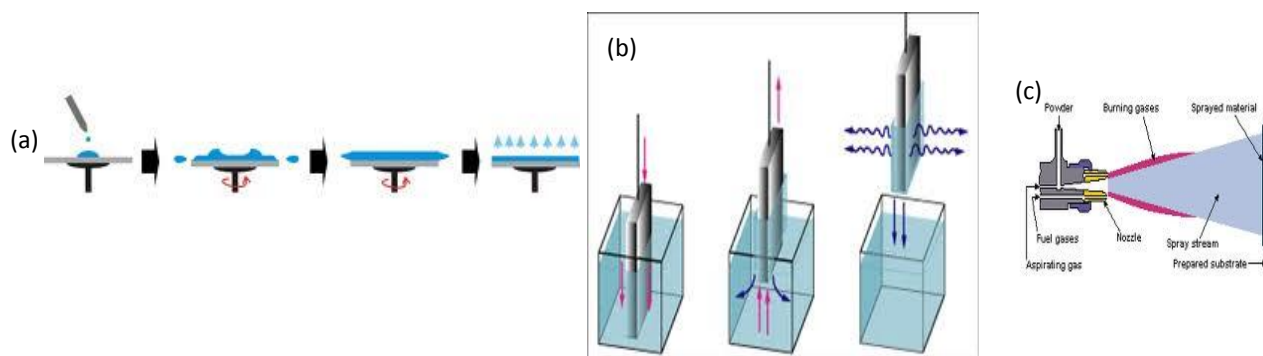
I.1.4 Roll-to-roll deposition techniques

Roll-to-roll deposition techniques are among the most used in industry nowadays. The principle of these techniques is the transfer of the inks to the printed substrates by the physical contact of two rollers. By these techniques flexible substrates can be printed while the size of the substrate can vary from laboratory scale (from 5 to 10 cm) to industrial scale (30 to 180 cm). Among the advantages of the roll-to-roll process we could site the high speed of film deposition and facility in use. Besides the roll-to-roll technique is already common in industry making it cheap, easily accessible and an efficient deposition method for the organic electronics. Examples of roll-to-roll procedures used in industry today are presented in the figure 4.

Figure 4. Illustrations of roll-to-roll coating techniques used in industry (a) gravure printing (b) flexographic printing (c) screen printing (d) rotary screen printing.[8] Reproduced with permission from Elsevier, Copyright 2012
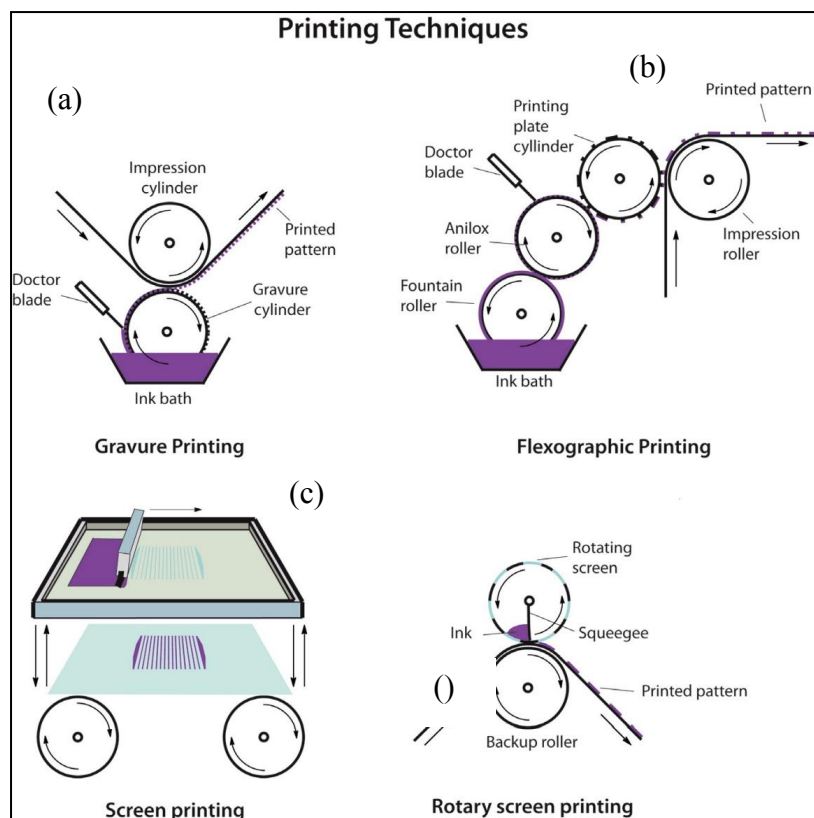
I.1.5 Doctor blade deposition technique

Another method that is widely used is the doctor blade. This technique can be used for the formation of films on small and with some modifications on large scale. In the doctor blade process, the solution is deposited on one end of the surface beyond the blade. After setting the blade at a certain height, it starts moving with a fixed speed, thus forming the film. The viscosity of the inks that can be deposited by this method is from 20 to 2000 mPa.s. The height of the blade and the speed of coating are responsible for the thickness of the films. The substrates can be heated, achieving a direct drying of the films. In industry the doctor blade method is combined with the roll-to-roll techniques.

Figure 5. (a) Representation of the doctor blade principal using a frame that is moving over the liquid (b) an image of a common doctor blade apparatus.
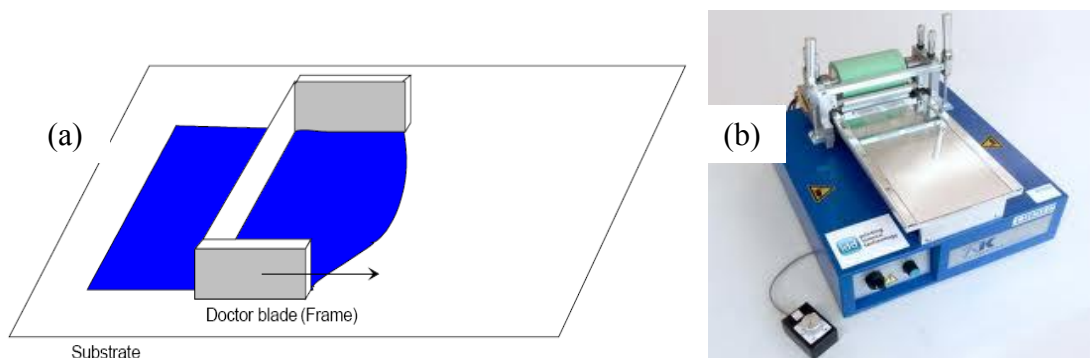
I.1.6 Conclusion

In summary, several techniques have been developed for the casting of inks into films. The viscosity of the inks is a crucial factor in order to choose the suitable method. In the table 1 the viscosity values of the solutions that can be casted by each technique are presented. Some of

these techniques, after some modifications, can be applied at the industrial scale. For example, doctor blade and spray coating methods can be used both at the laboratory and industry scales. They can both cast films with different thickness and on different substrates (glass,PET).

Table 1. Summary of the characteristics of all the techniques used for the deposition of inks into films.

Technique	Viscosity	Scale
Vacuum filtration		Laboratory use
Convective self-assembly	20-2000 mPa.s	Laboratory use
Dip coating	20-2000 mPa.s	Laboratory use/ Applied in industry
Spin coating	2-30 mPa.s	Laboratory use
Spray coating	0.05-1 mPa.s	Laboratory use/ Applied in industry
Doctor Blade	20-2000 mPa.s	Laboratory use/ Applied in industry

II   Results and discussion

II.1   Dispersion of CNTs by P3HT-b-(PS-co-PSSA) block copolymers and film formation

As described in chapter II.2, copolymers with a π-conjugated part (P3HT) and a polyelectrolyte block (PSSA) were synthesized. The volume fraction of the PSSA part as well as the molecular weight of the P3HT block influence directly the solubility of the copolymers.

Solutions of copolymers soluble in a mixture of polar solvents (DMSO/H$_2$O), in organic solvents (toluene) and in aqueous media were prepared. In table 2, the library of the P3HT-*b*-(PS-*co*-PSSA) copolymers that were synthesized and examined as dispersants of CNTs are presented.

Table 2. Characteristics of the P3HT-*b*-(PS-*co*-PSSA) rod coil copolymers used for the dispersion of CNTs.

No	Mn,P3HT[a] (g/mol)	Mn,PS[a] (g/mol)	SL[b] (%)	Volume fraction[c] f$_{P3HT}$/f$_{PS}$/f$_{PSSA}$
1	10500	20000	30	0.34/0.33/0.23
2	10500	20000	50	0.34/0.43/0.33
3	9000	10000	66	0.43/0.17/0.40
4	5200	14000	60	0.25/0.27/0.48

[a]Molecular weight of the P3HT and PS blocks determined by ^{1}H-NMR in CDCl$_3$. [b]sulfonation level of the PS block calculated by ^{1}H-NMR. [c]calculated by using ρ_{P3HT} = 1.1 g/cm^3, ρ_{PS} = 1.056 g/cm^3 and ρ_{PSSA} =0.801 g/cm^3.

The procedure of the dispersion of CNTs involves the mechanical sonication and the use of a dispersion aid; in our case the P3HT-*b*-(PS-*co*-PSSA) copolymer. Under the force of sonication, the CNTs bundles are loosened and the P3HT block starts developing π-π interactions with the sp^2 carbons of the nanotubes. Under the creation of these new forces the nanotubes bundles are destroyed and individual nanotubes are created. The charged polyelectrolyte block of the copolymer is used to enhance the solubility of the dispersion and prevents the re-aggregation of the individual CNTs. Equally, it can act as dopant for P3HT part. Both multi and single wall carbon nanotubes were used for the dispersions.

The resulting inks were further characterized for application as transparent conductive electrodes. Films were made by different techniques depending on the solvent and the viscosity of the solution. For the dispersions of MWCNTs in a mixture of DMSO/H_2O (viscosity ~ 1 mPa.s), the doctor blade technique was used for film formation. Dispersions viscosity lower than 1 mPa.s were deposited by spray coating. The optical properties (transmittance) of the films were investigated by UV-vis measurements at 550 nm, comparing the absorption of a transparent substrate (transmission 100 %) with the absorption of the casted sample. The transmittance spectra of the whole UV-vis range (200 nm-1400 nm) of the dispersions CNTs/copolymer are presented in the experimental part. The electrical properties were determined with the four-point probe method leading to resistance values in Ω/sq. The principle of this method is further developed in the experimental part. Finally the thicknesses of the films were calculated with a profilometer, which is commonly used for thin films (up to 4 μm).

All the dispersions that will be further presented were characterized by optical microscopy in order to verify the absence of the CNTs bundles. In addition, microscopy techniques, AFM, TEM and Cryo TEM, were used in order to visualize the dispersed CNTs as well as the assembly of the copolymer around them. Photophysical characterization of the CNTs/P3HT-*b*-(PS-*co*-PSSA) allowed us to follow the π-π interactions between the nanotubes and the π-conjugated block.

II.1.1   Dispersion of CNTs by P3HT$_{0.34}$-b-(PS-co-PSSA) copolymer with sulfonation level of 30% and 50%

The **copolymer 1** P3HT$_{0.34}$-*b*-(PS$_{0.33}$-*co*-PSSA$_{0.23}$) with fraction volume of P3HT $f_{P3HT} = 0.34$ and $f_{PSSA} = 0.23$ was tested as dispersant of MWCNTs in a mixture of solvents DMSO/H_2O 3/1. The **copolymer 2** with the same volume fraction of P3HT but higher for the PSSA, $f_{PSSA} = 0.33$, was also examined in a mixture of DMSO and water but with a ratio 1/1. This difference in solubility is directly related to the size of the polyelectrolyte block. The amount of the copolymers was kept constant at 0.5% per weight in 5 g of dispersion while the percentage of the MWCNTs was varied from 0.1 to 0.75 % w/w. The highest percentage of dispersed MWCNTs was 0.5% w/w,

and the quality of the dispersion was verified by optical microscopy (figure 6), where the absence of CNTs bundles can be observed. The optical microscopy images were taken at two different moments, 30 minutes after the centrifugation and 24 hours after the dispersion procedure in order to verify the stability of the dispersion. In continuation, the dispersions were casted in thin films for measuring the optical and electrical properties. The first method of casting that was chosen was spin coating but due to the low viscosity of the solutions no films were formed by that method.

Figure 6. Optical microscopy images of MWCNTs dispersions 24 hours after the sonication procedure (a) 0.5% of MWCNTs with 0.5% copolymer 1 in DMSO/H$_2$O 3/1 (scale 100 µm) and (b) 0.5% MWCNTs with 0.5% copolymer 2 in DMSO/H$_2$O 1/1 (scale 100 µm).
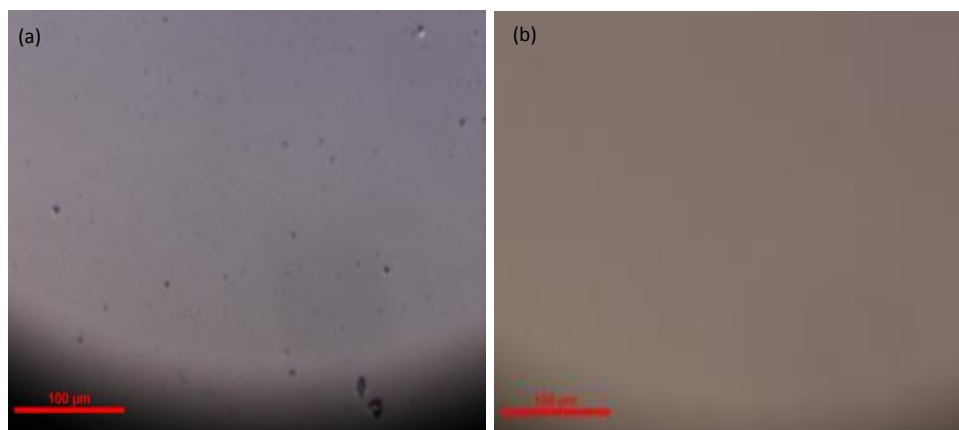
Alternatively, the doctor blade method was used for the formation of films from the CNTs/**copolymer 1** system in DMSO 3/1 but the resulting films were not homogenous and did not give rise to any useful result. The reason of the inhomogeneity of these films is the mixture of solvents with different evaporation rates. Similarly, solutions obtained with the system CNTs/**copolymer 2** in DMSO/H$_2$O 1/1 could be deposited. Films of different thicknesses were thus obtained with 0.5 wt% og MWCNTs as illustrated in figure 7. The two basic characteristics of the films, the transmittance and the resistivity, are plotted so as to be easily comparable. As it

was expected, as the transmittance of the films is decreasing, the films are becoming more conductive underlining the challenge of obtaining conductive high transparent thin films.

Figure 7. Resistivity versus transmittance for films with different thicknesses casted from MWCNT (0.5%) dispersion in the presence of the 0.5% copolymer 2 in DMSO/H$_2$O (1/1) as solvent.
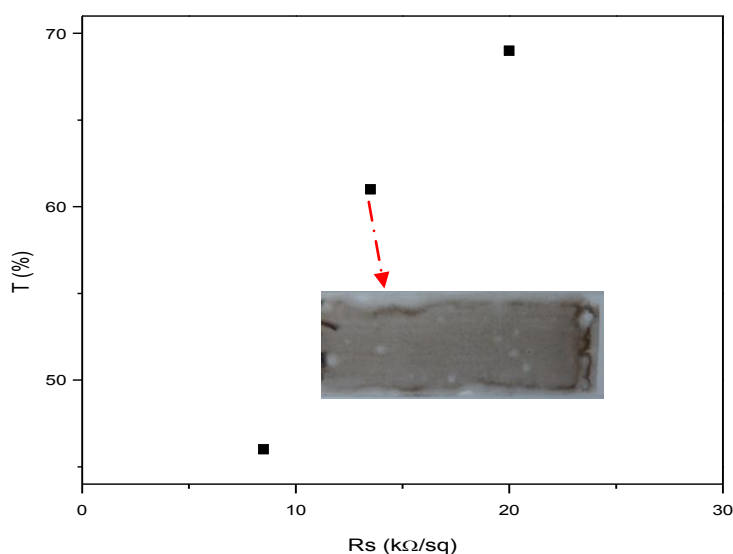
The resistivity of these films ($13.5 \cdot 10^3$ Ω/sq for T = 61%) is quite high for being used as transparent electrodes which require transmittance of >80% and resistivity of >10 Ω/sq. The use of MWCNTs, that are less conductive than the SWCNTs, is a reason for these values. In addition the bad morphology of the films also influences negatively the conductivity. Nevertheless, from this first attempt of using the P3HT-*b*-(PS-co-PSSA) copolymer as dispersant of CNTs, we can conclude that these copolymers can successfully disperse the CNTs. In order to improve these results we decided to tune two key parameters:

- The nature of the CNTs changing to SWCNTs instead of MWCNTs. Indeed the conductivity of the SWCNTs is at least ten orders of magnitudes higher than the MWCNTs.

209

- The morphology and the homogeneity of the films. The use of only one solvent for the dispersions was decided as well as the investigation of different deposition techniques like spray coating.

II.1.2 Dispersion of CNTs by P3HT$_{0.43}$-b-(PS$_{0.17}$-co-PSSA$_{0.4}$) copolymer with sulfonation level of 66%

The copolymer P3HT$_{0.43}$-*b*-(PS$_{0.17}$-*co*-PSSA$_{0.4}$) with equal volume fraction of P3HT and PSSA (f_{P3HT} = 0.43 and f_{PSSA} = 0.40) was soluble in organic solvents. In order to be able to compare its dispersion properties with **copolymers 1** and **2**, we continued to work with the MWCNTs. The dispersion of MWCNTs by this copolymer was examined in two solvents that are commonly used for CNTs dispersions, toluene and THF. The dispersion procedure was similar to the one described above, with the concentration of the copolymer stable at 0.5% w/w and the amount of MWCNTs gradually increased. Unfortunately, the results of the dispersions were not satisfying in both solvents, even at low amount of MWCNTs (0.1% and 0.3%) in the copolymer solution.

Figure 8. Optical microscopy images of MWCNTs dispersions with 0.5% copolymer 3 in toluene (a) 0.1 % CNTs (scale 100 µm) (b) 0.3% CNTs (scale 500 nm).
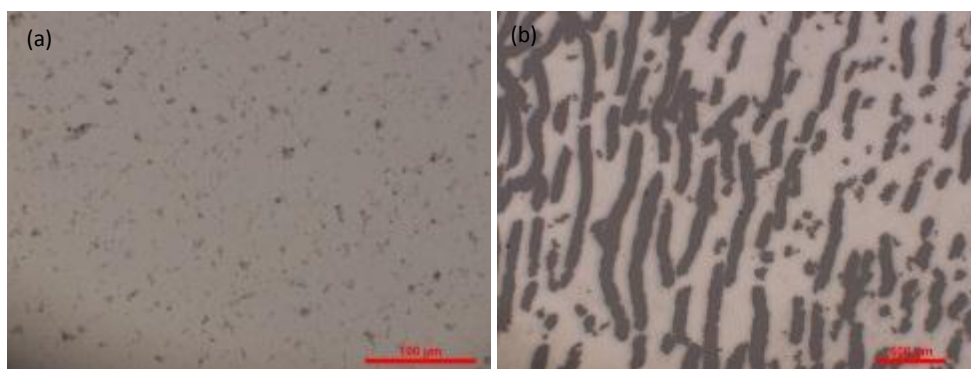
The poor dispersion was evident by simple observation of the solutions and was further verified by optical microscopy images (figure 8). In figure 8(a) aggregates of MWCNTs (0.1%) with diameter of 100 nm are observed meaning that the nanotubes are not individually dispersed in the solution and that the copolymer is not participating in the dispersion process. By increasing the amount of MWCNTs (0.3%) the aggregates of nanotubes are not destroyed and they can be clearly seen in optical microscopy image (figure 8(b)).

Different ratios of MWCNTs and copolymer 3 were tested in both toluene and THF as solvent but the resulting solutions were not containing dispersed CNTs. The different behaviors of the **copolymers 1** and **2** versus the **copolymer 3** in the dispersion of the CNTs can be explained by the different assembly of the copolymers in the solution. For the copolymers that are soluble in DMSO or/and water, the P3HT block is self-assembled creating a hydrophobic area. The CNTs due to their hydrophobic nature have the tendency to self-organize in hydrophobic micro-domains formed by the P3HT block. Under such conditions the development of π-π interactions is favorable and the dispersion of the CNTs by the copolymer more efficient. On the contrary, the P3HT-*b*-(PS-*co*-PSSA) copolymer that is soluble in good solvent for the P3HT (THF and toluene) does not form self-assemblies in the solution (no hydrophobic microdomain) and the interactions of the CNTs with the copolymer are not easily developed.

II.1.3 Dispersion of CNTs by $P3HT_{0.25}$-b-($PS_{0.27}$-co-$PSSA_{0.48}$) copolymer with sulfonation level of 60%

Based on the results obtained with the dispersion of MWCNTs in the presence of the various P3HT-*b*-(PS-*co*-PSSA) copolymers as described above, it appears that the copolymer which is soluble in water can be a good dispersant. The first try was made for the dispersion of MWCNTs with **copolymer 4** in aqueous solution. The amount of the copolymer was kept stable at 0.5% w/w for comparison reasons with the other copolymers of the table 1. The amount of MWCNTs was varied from 0.1% to 0.8% per weight and stable dispersions were obtained when up to 0.5% w/w of MWCNTs was charged. The dispersions were characterized by optical microscopy (figure 9(a)) and films with different thicknesses were casted by doctor blade

technique. Similar to the previous results, the lower resistance is obtained for the dispersion containing the bigger amount of MWCNTs (figure 9(b)). The electrical and optical properties of these films are much better than those previously tested, with higher transmittance (76%) and lower resistivity (7 kΩ/sq). The amelioration of the results is related to the homogeneity of the films and the better percolation of the nanotubes, casted from dispersions in aqueous media.

Subsequently, dispersions of SWCNTs with the use of the $P3HT_{0.25}$-*b*-($PS_{0.27}$-*co*-$PSSA_{0.48}$) as dispersion aid were made in aqueous solution. By using single wall nanotubes we hoped to decrease the resistance of the films since they are more conductive than the MWCNTs. Two different types of SWCNTs were used, purified and non-purified. The main difference between these types is that the purified nanotubes contain functional groups (f-SWCNTs), mostly carboxylic, due to the purification procedure. These functional groups aid the solubility of the nanotubes but they negatively affect the electronic properties of the SWCNTs.

Figure 9. (a) Optical microscopy image of 0.5% MWCNTs dispersion with 0.5% copolymer 4 in water solution (scale 100µm) (b) photo of the film made out of this dispersion with 30 nm thickness T = 76% and resistivity = 7 kΩ/sq.

(a)

(b)

The dispersion properties of the SWCNTs are different from the MWCNTs due to their smaller size. For that reason, several concentrations of the $P3HT_{0.25}$-*b*-($PS_{0.27}$-*co*-$PSSA_{0.48}$) copolymer and the SWCNTs were tried in aqueous solutions with different ratios. We conclude that a lower amount of copolymer was needed to efficiently disperse the SWNCTs. Consequently, the concentration of the copolymer in the dispersions of SWCNTs was lower than in the MWCNT dispersions, avoiding the presence of big aggregates of the copolymer which could prevent the dispersion of the single walled CNTs. The different concentrations and ratios of the copolymer and the SWCNTs are presented in the table 3.

These dispersions were then casted in thin films in order to determine under which conditions we obtain the best optical and electrical results. For the film formation a new method was used, spray coating, since it is an ideal method for low viscosity solutions. In figure 10 the transmittance (at 550nm) versus the resistivity of these films is presented and their performances are compared with the dispersion of SWCNTs by SDS surfactant as reference.

Figure 10. Transmittance at 550nm versus the film resistance of the SWCNTs dispersions with the P3HT$_{0.25}$-*b*-(PS$_{0.27}$-*co*-PSSA$_{0.48}$) in several concentrations and ratios.
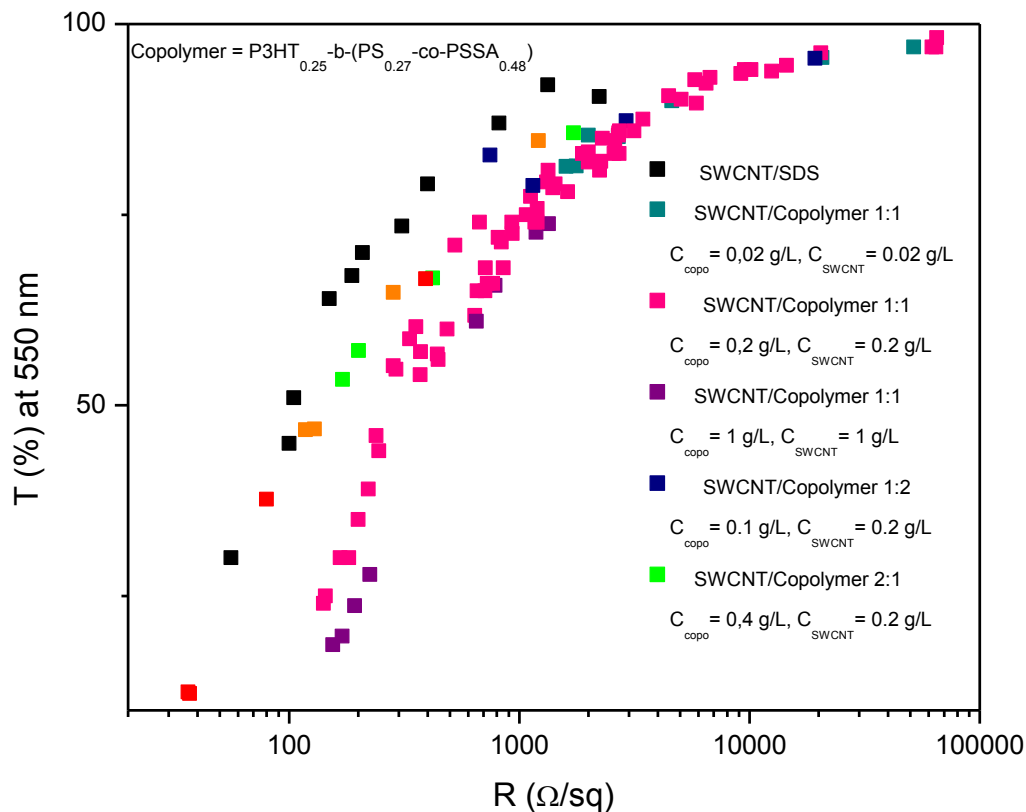
Table 3. Concentrations and ratio details for making dispersions out of SWCNTs/P3HT$_{0.25}$-*b*-(PS$_{0.27}$-*co*-PSSA$_{0.48}$) systems.

SWCNTs concentration (g/l)	P3HT$_{0.25}$-*b*-(PS$_{0.27}$-*co*-PSSA$_{0.48}$) concentration (g/l)	Ratio SWCNTS/copolymer	Dispersion
0.02	0.02	1/1	OK
0.1	0.2	1/2	OK
0.2	0.2	1/1	OK
0.4	0.2	2/1	OK
0.8	0.2	4/1	NO
1	1	1/1	OK

Figure 10 clearly shows that the most promising dispersion is the one with 0.2 g/L concentration for both SWCNT and $P3HT_{0.25}$-*b*-$(PS_{0.27}$-*co*-$PSSA_{0.48})$ copolymer in 1:1 ratio. Nevertheless, as can be observed from figure 11, there is a "coffee stain" phenomenon on the film formed by spray coating. Thus a washing procedure (dipping in water for 3 minutes) was followed in order to circumvent this problem and resulted in an increase of the conductivity.

Figure 11. (a) Optical microscopy images of the spray casted film dispersions before (left) and after (right) washing treatment and (b) the graph of the transmittance versus sheet resistance under the same conditions.
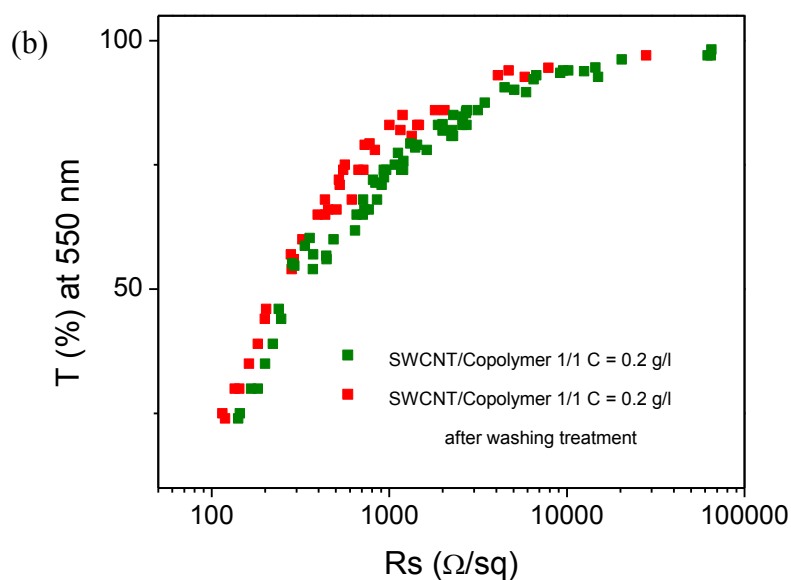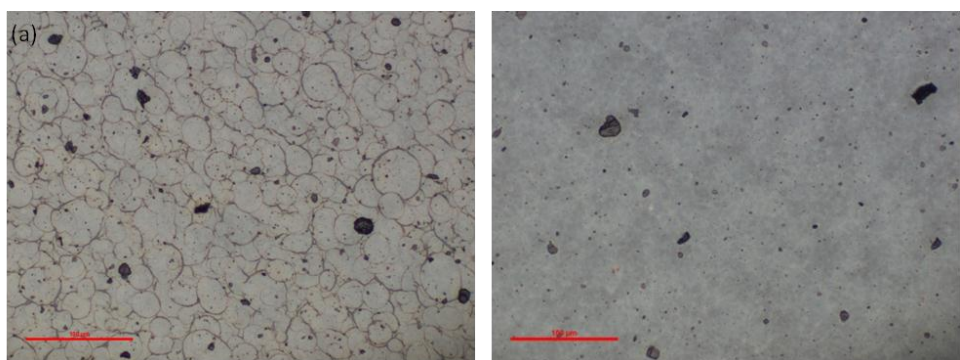
Following these results, the procedure and quantity of compounds were kept constant. The study was completed with the comparison of the functionalized and non-functionalized SWCNTs. As shown in figure 12, the films made out of the dispersions with $P3HT_{5.2}$-b-(PS_{14}-co-PSSA) and functionalized SWCNTs have lower resistance in comparison to the dispersions with non-functionalized nanotubes.

Figure 12. The transmittance versus the resistivity for films deposited from $P3HT_{5.2}$-b-(PS_{14}-co-PSSA) dispersions with functionalized (green) and non-functionalized (orange) SWCNTs.
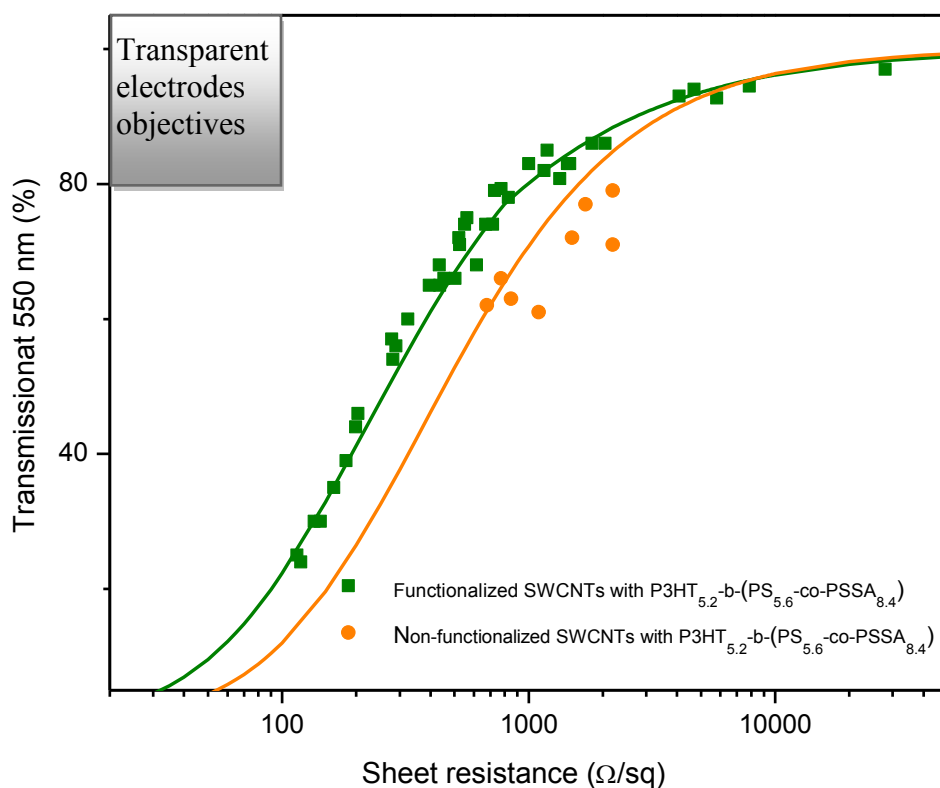
This difference is based on the fact that in the dispersions of the f-SWCNTs there are nanotubes that are individually dispersed due to the functional groups and not due to the presence of the copolymer. In our dispersion procedure there is a step of centrifugation in order to remove possible aggregates. Since in the f-SWCNTs dispersions the amount of nanotubes aggregates is lower, in comparison to the nf-CNTs dispersions, the amount of SWCNTs that are removed by centrifugation is lower. Consequently, the copolymer/f-CNTs dispersions contain more individual nanotubes resulting in a lower resistivity. Dispersions of both types of SWCNTs were further visualized by microscopy techniques and the interactions of the CNTs with the copolymer were investigated by spectroscopic methods. The results of these studies are presented in the following chapter (chapter IV paragraph II.2)

Summarizing, the P3HT-*b*-(PS-*co*-PSSA) block copolymers (table 2) were used for the dispersion of both multi and single wall carbon nanotubes. The dispersion ability of each block copolymer is directly related with its composition. More specifically, the copolymers with PSSA and P3HT volume fractions leading to a solubility in polar solvents (DMSO and/or water) successfully disperse CNTs. In contrast, the P3HT-*b*-(PS-*co*-PSSA) copolymer that was soluble in organic solvents was not able to disperse CNTs. The reason for this behavior is the self-assembling of each copolymer in solution. The formation of hydrophobic microdomains, as demonstrated for the P3HT-*b*-(PS-*co*-PSSA) copolymers in polar solvents, is crucial for the dispersion of nanotubes. As the CNTs are also hydrophobic, they tend to interact with hydrophobic domains when they are surrounded by a polar environment. Due to the hydrophobic forces, the P3HT part and the CNTs are starting to associate whichresulted in the development of π-π interactions and the formation of stable dispersions.

II.2. Photophysical characterization and imaging of SWCNT aqueous dispersions by the P3HT$_{0.25}$-*b*-(PS$_{0.27}$-*co*-PSSA$_{0.48}$) copolymer

First of all we studied the stability of the dispersions of the SWCNTs with the P3HT$_{0.25}$-*b*-(PS$_{0.27}$-*co*-PSSA$_{0.48}$) copolymer in aqueous media. As mentioned above, the zeta potential is a value that indicates the stability of colloidal particles in a solvent. When the particles are well dispersed a high zeta potential is measured meaning that the system is stable (the dispersion resists to the aggregation). Inversely, when the potential is low there are attractions between the colloidal particles meaning that dispersion will collapse shortly. A value of 25 mV (positive or negative) is taken as the arbitrary value that distinguishes a stable from a non-stable colloidal system. This concept has been applied to evaluate the stability of the CNTs dispersions from several surfactants.[9]

Zeta potential measurements were made only for the dispersions of the nf-SWCNTs since the charges of the f-SWCNTs would influence the measurements. A value of zeta potential of -50 mV was measured for the dispersion of nf-SWCNTs by the P3HT$_{0.25}$-*b*-(PS$_{0.27}$-*co*-PSSA$_{0.48}$) copolymer in aqueous solution (figure 13). This value is much higher than the ζ-potential of the copolymer alone at the same concentration (chapter 3 figure 3), implying that the SWCNT-P3HT$_{0.25}$-*b*-(PS$_{0.27}$-*co*-PSSA$_{0.48}$) complex is much more stable and have no tendency to aggregation like the copolymer micelles. In addition this zeta potential value is close to that measured for SWCNTs dispersions by surfactants in the literature. We can conclude that the P3HT$_{5.2}$-*b*-(PS$_{14}$-*co*-PSSA) copolymer can efficiently disperse SWCNTs in water solution resulting in small colloidal particles that are stable over time.

Figure 13. Zeta potential of the nf-SWCNT dispersion in water with the P3HT$_{0.25}$-*b*-(PS$_{0.27}$-*co*-PSSA$_{0.48}$) copolymer.
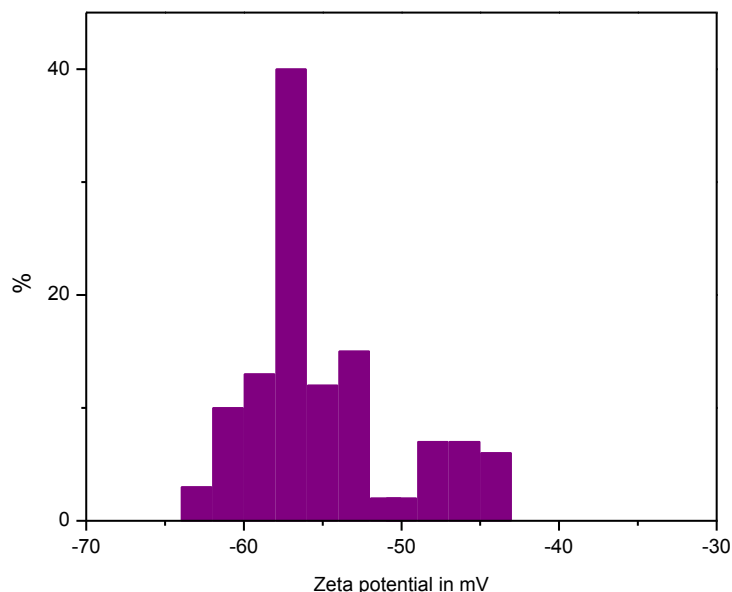
II.2.1 Imaging of the system CNTs/P3HT$_{0.25}$-b-(PS$_{0.27}$-co-PSSA$_{0.48}$) copolymer

In order to visualize these dispersions, microscopy techniques like AFM, TEM and Cryo-TEM analysis were used for both types of SWCNTs. The concentrations of the SWCNTs and the copolymer were at 0.2 g/L and the ratio between them 1/1 for all the analysis. AFM images of the f-SWCNTs dispersions are presented in the figure 14. A network of CNTs is shown made of individual SWCNTs and of small bundles. The white objects are impurities coming from the synthesis of the nanotubes. Even though the dispersion of the nanotubes is evident, the assembly of the copolymer around them cannot be easily observed in these pictures.

Figure 14. AFM phase image of the system f-SWCNTs/P3HT$_{0.25}$-*b*-(PS$_{0.27}$-*co*-PSSA$_{0.48}$) copolymer 0.2 (g/l)/0.2 (g/l) casted as films followed by washing treatment (scale 2 μm).
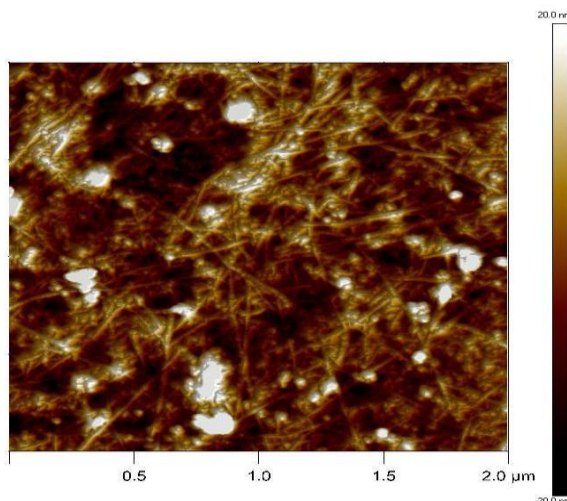
TEM images of both functionalized and non-functionalized SWCNTs dispersions were taken and the solutions were drop casted on carbon grid thin substrates (figure 15). The black big objects appearing in the images correspond to the remaining catalyst and to other impurities from the synthesis of the SWCNTs. In addition, the length of the SWCNTs is on average in the scale of μm proving that our sonication conditions are "soft" and at least does not harm the shape of the tubes. The TEM image of the f-SWCNT dispersion shows mostly well dispersed individual carbon nanotubes along with some small bundles (8-20 nm).

Similar results were obtained for the dispersions of the nf-SWCNTs but the presence of bigger bundles of SWCNTs (20-25 nm) is observed. It is noteworthy that the fabrication analysis reports that the SWCNTs bundles are from 20 nm to 40 nm. The difference between the two types of nanotubes is clear: with the use of f-SWCNTs there is better dispersion in individual nanotubes due to the functional groups on their surface in contrast to the nf-SWCNTs were the dispersion is only due to the interactions with the copolymer. In both cases we do not observe micelles on the

surface of the CNTs. That makes us conclude that the copolymer micelles "open" when they interact with the nanotubes, resulted in CNTs covered from copolymers chains.

Figure 15. TEM images of f-SWCNTs (left, scale 100 nm) and nf-SWCNTs (right, scale 200 nm) dispersion using P3HT$_{0.25}$-*b*-(PS$_{0.27}$-*co*-PSSA$_{0.48}$) copolymer.
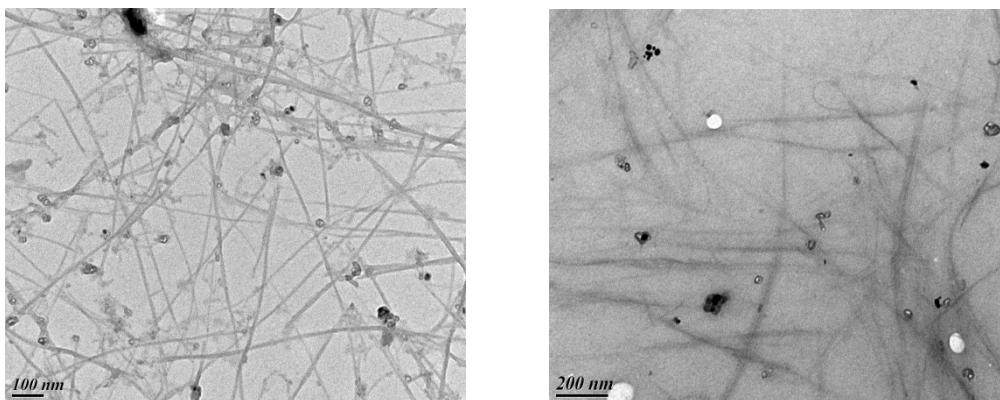
The copolymer chains that are wrapping the SWCNTs have a size of 2-8 nm. High resolution TEM (HRTEM) was carried out in order to visualize the presence of copolymer on the surface of the CNTs. In the figure 16, HRTEM images are presented, where nanotubes with a diameter of 4-6 nm are observed, 2-4 nm bigger than the individual nanotubes (according to the manufacturer data). Considering that the size of the copolymer is about 2 nm, it is possible that the nanotubes with diameters 4-6 nm are individual SWCNTs wrapped by the copolymer. Next to the individual SWCNT there is a bundle of nanotubes with a 20 nm thickness that has not been dispersed. In the high magnification image (scale100 nm) we can clearly remark the presence of both individual and SWCNTs bundle concluding that not all of the nanotubes are dispersed.

Figure 16. HRTEM images of the dispersed nf-SWCNTs by the P3HT$_{0.25}$-*b*-(PS$_{0.27}$-*co*-PSSA$_{0.48}$) copolymer (right scale 100 nm, left scale 20 nm).
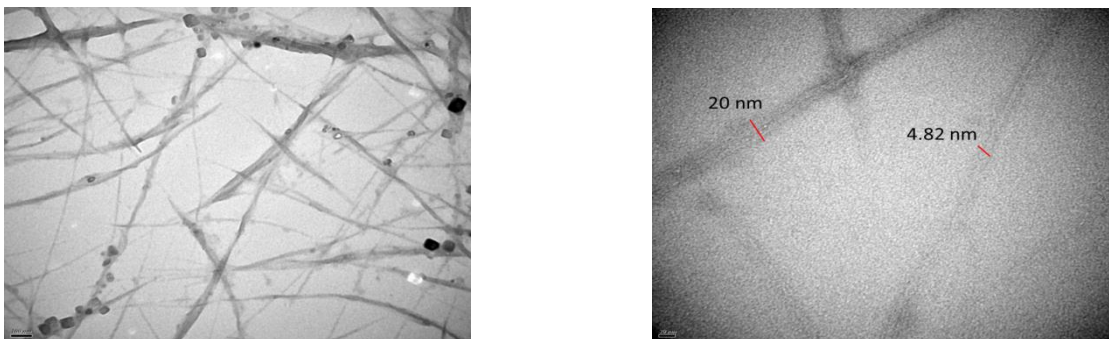
Since the dispersions of the SWCNTs are in water solution, Cryo-TEM was performed, in order to observe the nature of the dispersions in solution form (figure 15). Well dispersed f-SWCNTs are observed in the images, consisting of a small bundle of 2-5 nanotubes as well as individual tubes. As in the TEM images the surface of the nanotubes looks modified by the presence of the copolymer around them.

Figure 17. Cryo-TEM images of the f-SWCNT dispersions using P3HT$_{0.25}$-*b*-(PS$_{0.27}$-*co*-PSSA$_{0.48}$)copolymer (right scale 200 nm, left scale 50 nm).
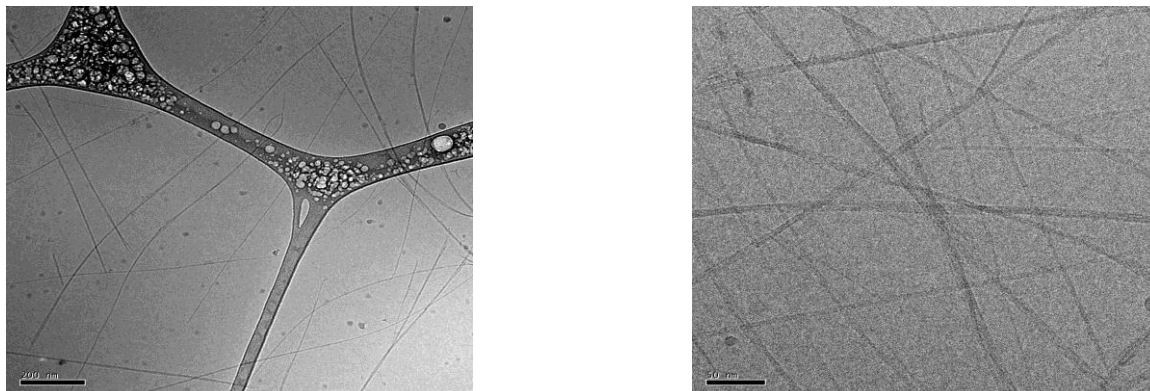
In summary, images of the SWCNTs dispersions by the P3HT$_{0.25}$-*b*-(PS$_{0.27}$-*co*-PSSA$_{0.48}$) copolymer were made by AFM, TEM and Cryo-TEM analysis. By all techniques, well-dispersed CNTs were observed in the form of individual tubes or in small bundles of 2-5 nanotubes. The presence of the copolymer on the surface of the nanotubes was noted in the TEM and Cryo-TEM images and in higher magnitude in the HRTEM images. We believe that the copolymer is interacting with the SWCNTs through π-π interactions of the P3HT and the carbons of the nanotubes, while the (PS-co-PSSA) block is stabilizing the dispersion in the aqueous media. The existence of these interactions was further investigated by spectroscopic techniques (*i.e* Raman, UV-vis, photoluminescence)

II.2.2 *Photophysical characterization of the system CNTs/P3HT$_{5.2}$-b-(PS$_{5.6}$-co-PSSA$_{8.4}$) copolymer*

II.2.2.1 *Photoluminescence and UV-vis characterization*

Photoluminescence (PL) and UV-vis analysis of the system SWCNTs/P3HT$_{0.25}$-*b*-(PS$_{0.27}$-*co*-PSSA$_{0.48}$) were performed and presented in figure 18. In the photoluminescence spectra (excited at 495 nm), the sonicated copolymer solution shows a maximum peak at 600 nm characteristic for the P3HT block. The PL intensity was decreased (quenched) when SWCNTs were added in the copolymer solution, indicating electron or/and energy transfer of the P3HT. The quenching of the P3HT photoluminescence due to the presence of CNTs has been widely studied in the literature.[10] The quenching of the photoluminescence intensity of the P3HT is observed due to the electron/energy transfer that is related to the π-π interactions of the P3HT and CNTs. The change in the absorption spectra of the copolymer after the addition of SWCNTs

is also presented in figure 18. In addition to the absorption peak of the copolymer, a peak at 1000 nm, appears corresponding to the presence of the SWCNTs in the solution.

Figure 18. Photoluminescence spectra (left) and UV-vis spectra (right) of the P3HT$_{0.25}$-*b*-(PS$_{0.27}$-*co*-PSSA$_{0.48}$) (0.2 g/L) copolymer and the SWCNT (0.2 g/L) dispersion in water.
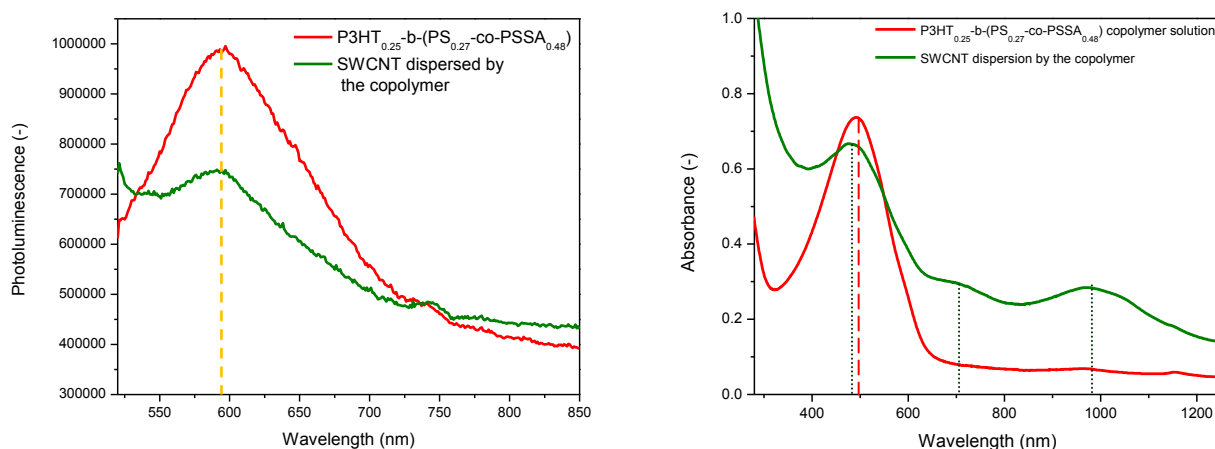
On figure 18, we can observe that the maximum absorption of the copolymer in aqueous solution is at 490 nm and that it is blue shifted (together with a decrease of the intensity) to 474 nm for the composite solution. The shift of the absorption maximum of the P3HT copolymer indicates that there are interactions between the P3HT block and the SWCNTs, following the well known π-π interactions. These observations are in good agreement with reports from the literature concerning the interactions between the P3HT and the CNTs.[11]

II.2.2.2   *Raman spectroscopy characterizations*

Raman spectroscopy is a very useful characterization tool to evaluate specific issues occurring with the carbon nanotubes. In typical SWCNT Raman spectra there are three characteristic peaks that can be observed. The radial breathing mode (RBM) appears between 120 $cm^{-1} < \omega_{RBM} < 250$ cm^{-1} and corresponds to the atomic vibration of the C atoms in the radial direction, as if the tube is breathing. This value depends on the diameter and the (n,m) values of the nanotubes and it is characteristic of each SWCNT. The disorder-induced D band appears at around 1300 cm^{-1} and represents the "disorder" of the sp^2-hydrized carbon system. This peak is used for identification of the covalent modification of the surface of the CNTs. Finally the G-band peak features around 1500 cm^{-1} is common to all sp^2 carbon systems and it is sensitive to strain effects of the carbon bonds. This value is used for the detection of energy transfer to and from the CNTs and so it can be used for the verification of the non-covalent functionalization of the nanotubes. It is noteworthy, that the metallic and the semi-conducting SWCNTs have a different G-band peak.

The Raman spectra of the pristine nf-SWCNTs and their dispersion with the copolymer in solution and film are presented in the figure 19. We mainly investigated the G-band as it gives important information on the non-covalent interactions between the nanotubes and the copolymer. In solution, the characteristic G-band of the SWCNT appears at 1594 cm^{-1} and it is shifted to higher frequencies by 3 cm^{-1} when the SWCNT are dispersed with the copolymer. This G-band shift at higher frequency indicates that the nanotubes are interacting with the copolymer and that they lose electrons through this interaction.[12] The peak at 1456 cm^{-1} corresponds to the P3HT block of the copolymer. More specifically this peak is a result of the vibration of the carbon-carbon double bond of the thiophene ring.[13] The Raman spectrum of the films of the pristine nf-SWCNT and their dispersion with the copolymer was also examined. Unfortunately, the thickness of the films made by spray coating was two low and the intensity of the spectroscopy signal was not that strong. Though, we clearly observe the peak of the P3HT

copolymer at 1457 cm^{-1}, at the same value as in the solution. Similarly, as in solution the G-band is shifted between the pristine nf-SWCNT (1595 cm^{-1}) and the dispersed nanotubes (1593 cm^{-1}). However one can note that this shift is toward shorter wavelength.

Figure 19. The Raman spectra of the pristine nf-SWCNT and their dispersion with P3HT$_{0.25}$-*b*-(PS$_{0.27}$-*co*-PSSA$_{0.48}$) copolymer in solution (left) and in glass film (right).
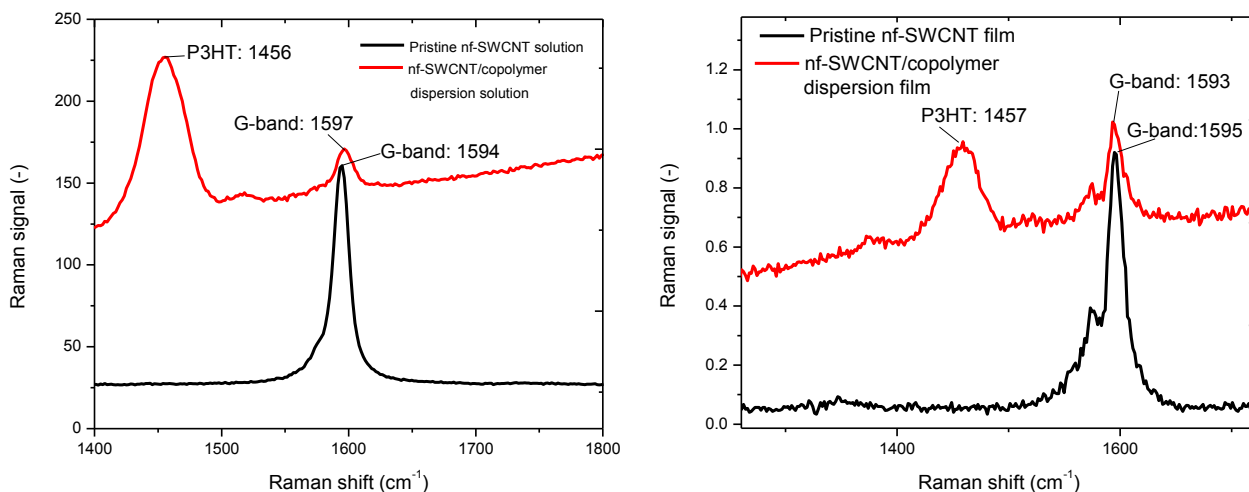
The existence of the shift indicates that the SWCNTs interact with the copolymer by exchanging electrons with the P3HT. From the solution spectra, where the signal is stronger, we observe a blue shift indicating that the CNTs withdraw electrons form the P3HT in an donor-acceptor system. Taking into consideration all the parameters of the Raman spectroscopy, we can conclude that the P3HT block of the P3HT$_{0.25}$-*b*-(PS$_{0.27}$-*co*-PSSA$_{0.48}$) copolymer is creating π-π interactions with the surface of the nanotubes.

From the spectroscopic studies we verified that the SWCNTs are dispersed due to their interaction with the copolymer. In addition, it was verified by both photoluminescence and UV-vis that the P3HT is creating π-type interactions with the carbons of the nanotubes. The Raman

spectroscopy helps us to understand that there is an exchange of the electrons between the CNTs and polymer, with the polymer acting as a donor and the CNTs as an acceptor.

II.3. Amelioration of the electrical properties of the SWCNTs dispersions by the P3HT$_{0.25}$-b-(PS$_{0.27}$-co-PSSA$_{0.48}$) copolymer with sulfonation level of 60%

As described above the P3HT$_{0.25}$-*b*-(PS$_{0.27}$-*co*-PSSA$_{0.48}$) copolymer was used for the dispersion of SWCNTs in water solutions. These dispersions were characterized considering their stability, the capability of the copolymer to separate the nanotubes from their bundle configuration and the type of interactions between the P3HT block and the SWCNTs. In the continuity the dispersion inks were casted by spray coating on glass surfaces and the electrical and optical properties were measured (figure 8 and 9). The best values measured for a film after the washing treatment is sheet resistance of 521 Ω/sq for transmittance at 71% (at 550nm). In order to ameliorate the electrical properties of the SWCNTs dispersions it was chosen to study the doping level of the block copolymer.

In chapter 1 the capacity of the π-conjugated polymers to be doped and how it affects their conductivity was discussed. The improvement of the electrical properties of the dispersion aid has a direct influence to the properties of the nanotube dispersions. Studies have been already performed for dispersions of SWCNT by a doped and non-doped π-conjugated moiety. The electrical properties of the dispersion were enhanced with the use of the doped π-conjugated moiety without any change in the optical properties.[14] As shown in the figure 11 of chapter 1, there are several ways that the π-conjugated polymers can be doped. As discussed below, we chose the chemical doping of the copolymer in solution and the electrochemical doping of the film of the dispersion.

II.3.1   Chemical doping of P3HT$_{0.25}$-b-(PS$_{0.27}$-co-PSSA$_{0.48}$) copolymer

The chemical doping of the P3HT can be achieved through several oxidants like, FeCl$_3$, BF$_3$, NOPF$_6$ acids, HAuCl4·3H2O etc. From all the candidates we chose the hydrogen tetrachloro aurate-(III) trihydrate (HAuCl$_4$·3H$_2$O) because it is a strong dopant and it has already been successfully used for doping the P3HT.[15] The reaction of the doping of the P3HT by the HAuCl$_4$·3H$_2$O is as below:
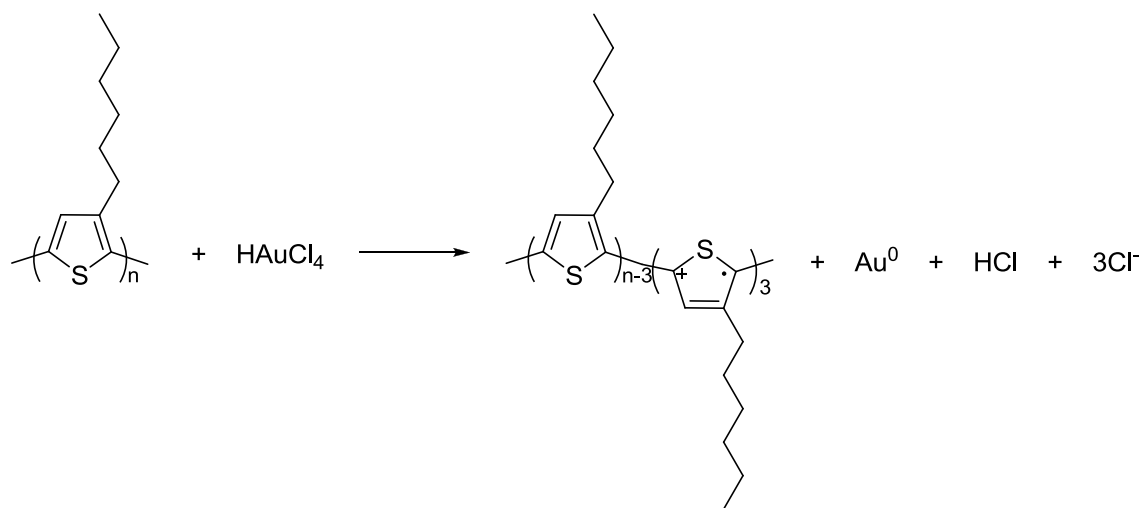
From the stoichiometry of the reaction we can calculate the amount of dopant in order to have 100% doping of the copolymer but not over-doping which destroys the chemical structure of the polymer. In addition the doping level can be observed by UV-vis spectroscopy since the P3HT maximum is shifted at higher wavelength and it is broader. A water solution of P3HT$_{0.25}$-*b*-(PS$_{0.27}$-*co*-PSSA$_{0.48}$) copolymer was prepared with concentration of 0.2 g/L and the equivalent of fully doping HAuCl$_4$ was added. The color of the solution was immediately changed from red to brown and the UV-vis spectra of the solution before and after doping is presented in the figure 20.

Figure 20. UV-vis spectra of the P3HT$_{0.25}$-*b*-(PS$_{0.27}$-*co*-PSSA$_{0.48}$) copolymer before and after doping by HAuCl$_4$ in water solution.
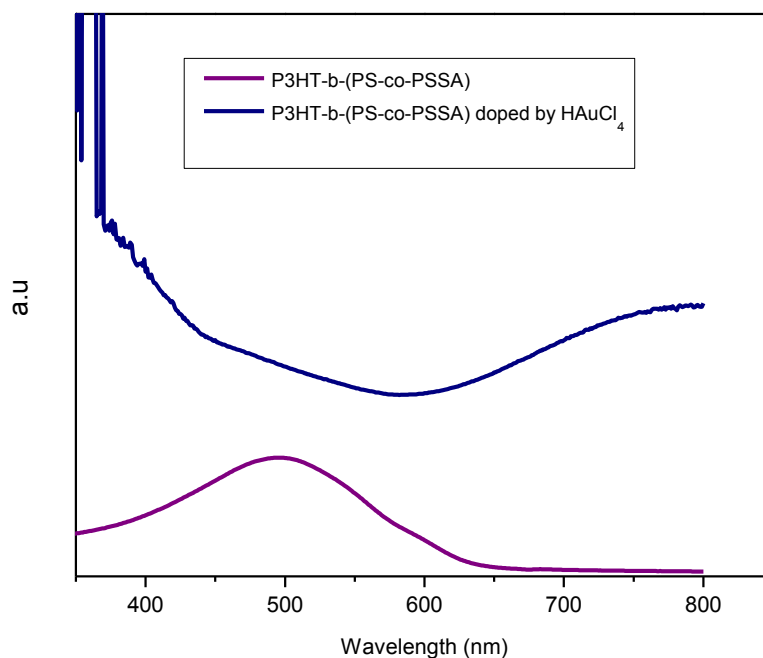
In the UV-vis spectra we verify the doping of the P3HT since the characteristic maximum of the P3HT at 500 nm has been shifted at 800nm, where the maximum of the doped P3HT appears.

The doped copolymer solution was then used for the dispersion of SWCNTs in the same way as described before. The dispersion was characterized by optical microscopy and then casted by spray coating on a glass surface and the electrical and optical properties are shown in the figure 21.

Figure 21. The transmittance versus the resistance of SWCNT dispersions with the help of P3HT$_{0.25}$-*b*-(PS$_{0.27}$-*co*-PSSA$_{0.48}$) copolymer before and after doping.
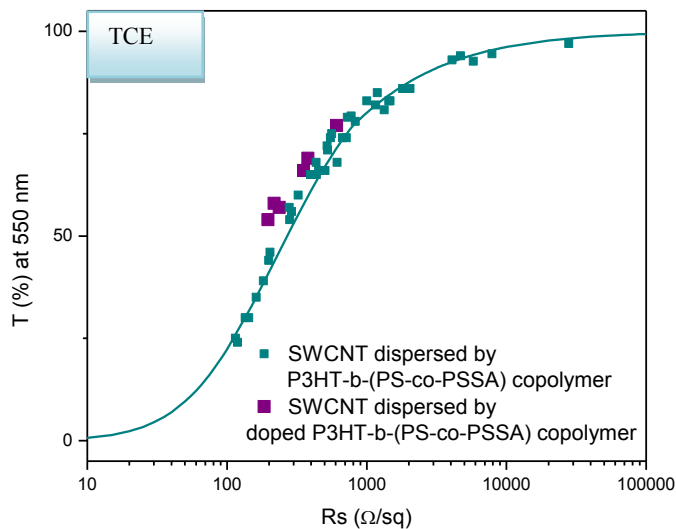
The sheet resistance of the films has been clearly decreased while the transmittance remains high. For comparison with the dispersions containing non-doped copolymer the resistance was at 521 Ω/sq for 70% transmittance (at 550nm). For the same optical values the resistance has dropped at 379 Ω/sq by just doping the P3HT block of the copolymer. In order to characterize the stability of this doping process over time, we observed the doped copolymer by UV-vis spectroscopy and the doping level remained stable for at least 10 days. Similarly resistance of the films was measured over a period of 2 weeks and the values remained stable.

In conclusion, by taking advantage of the different doping levels of the π-conjugated polymer (P3HT) we improved the electrical properties of the dispersion films by 30 %. It is evident that the use of π-conjugated copolymers for the dispersion of the CNTs can serve not only in the π-π interactions between the copolymer and the nanotubes but also to the increase of the conductivity of the dipsersions.

II.3.2 Electrochemical doping of P3HT$_{0.25}$-b-(PS$_{0.27}$-co-PSSA$_{0.48}$) copolymer

An alternative method for doping the P3HT based copolymer is to use electrochemistry. In the electrochemical doping, the electrode supplies the charges to the π-conjugated copolymer, while ions diffuse into or out of the polymer structure from the nearby electrolyte to compensate the electronic charges. This electrochemical doping was first tested on commercial P3HT homo-polymers of Mw = 54 000 g/mol. Films of P3HT were casted by spin coating and then dipped in an acetonitrile solution containing the electrolyte. Cyclic-voltammetry was performed on these films in order to identify the voltage where the oxidation reaction is taking place (figure 22).

Figure 22. Cyclic-voltammetry of the P3HT film with oxidation at 0.8 V upon 4 oxidation cycles.
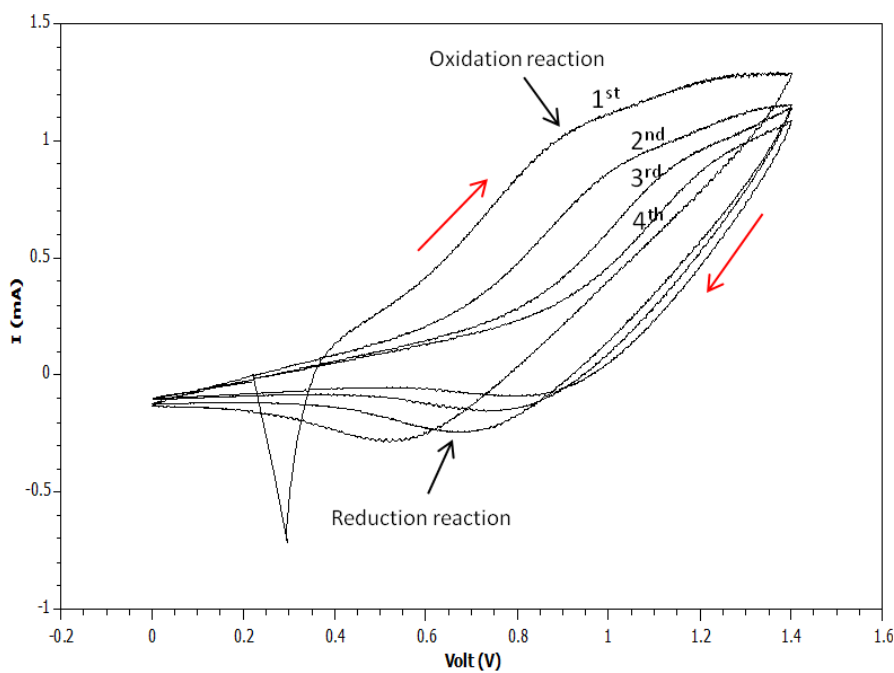
This voltage value was then applied on the P3HT films for 1 minute. The first observation was the change of the color of these films, from purple to black, after the oxidation doping procedure. This was the first sign that the P3HT was doped and it was further verified by the UV-vis spectra (figure 23) since a maximum absorption at 800 nm appears, which corresponds to the signal of the doped P3HT.

Figure 23. The UV-vis spectra and photos of P3HT film before (pristine) and after the electrochemical doping
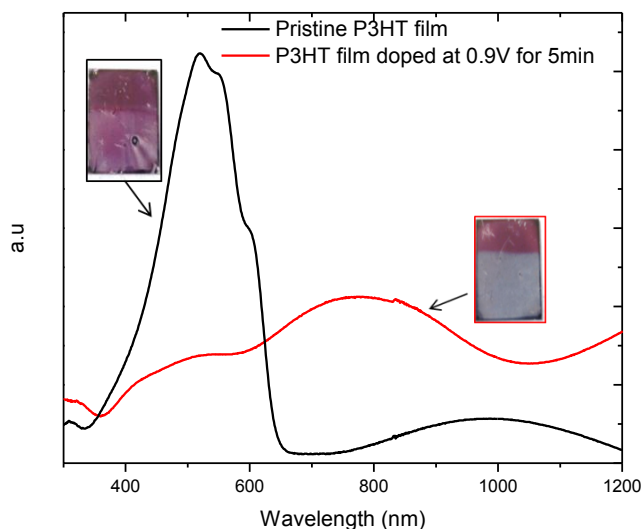
The same procedure was followed for the P3HT$_{0.25}$-*b*-(PS$_{0.27}$-*co*-PSSA$_{0.48}$) copolymer films but in DCM as a solvent. Unfortunately, during the cyclic voltammetry of these films there was no clear signal of an oxidation reaction. When they were exposed at the same voltage as the P3HT films (0.8 V) no color change was observed and we could not observe any signal of doped P3HT in the UV-vis spectra. The reason for this difference between the P3HT films and the copolymer films could be due to the low concentration of the copolymer and due to low thickness of the films. Further investigation will be performed with copolymer solutions avoidthese problems.

To summarize, the P3HT$_{0.25}$-*b*-(PS$_{0.27}$-*co*-PSSA$_{0.48}$) copolymer was successfully doped by the oxidant HAuCl$_4$. The doped copolymer was used for the dispersion of SWCNTs and a diminution of 30% in the resistivity of the films was measured without an influence of the transmittance. The doping of the copolymer by electrochemistry was not successful even though it was previously tested on P3HT films. The possible reasons for these results are the low concentration of the copolymer within the film and the low thickness of the spray coated films. Efforts of doping the copolymer, and further the CNT dispersion, are still in progress.

II.4   *Dispersion of CNTs by PVA-g-P3HT copolymer*

The PVA-*g*-P3HT copolymer was also tested as dispersion aids for both single and multi wall carbon nanotubes. Representative concentrations of nanotubes and PVA-*g*-P3HT copolymer were chosen so as to be able to compare with the P3HT-*b*-(PS-*co*-PSSA) copolymer system. Films were made out of these dispersions and the electrical and optical properties were examined.

First MWCNTs were used in order to test the dispersion properties of the copolymer. Only one concentration was tested with 0.5% of copolymer and 0.1% MWCNTs in aqueous solution. The good dispersion was verified by optical microscopy (figure 22) and it was stable for at least one month. Films were made out of these dispersions on glass surfaces by doctor blade and their electrical properties were measured. High resistivity was measured (more than 100 kΩ/sq) while their transmittance remained high (> 80%).

Figure 24. Optical microscopy image of the MWCNTs dispersion by the PVA-*g*-P3HT copolymer in water (scale 100 μm).

Following the same strategy like for the P3HT-*b*-(PS-*co*-PSSA) copolymer, dispersions with SWCNTs were made for increasing the conductivity. The same concentrations of 0.2g/L of SWCNT and copolymer were used for comparison reasons. The quality of the dispersions was quite good even though some small aggregates are present (figure 25). The films were made by spray coating and the resistivity was measured. Even though the electrical properties were improved, the resistivity remains high (10 kΩ/sq) and far from the values observed by the P3HT-*b*-(PS-*co*-PSSA) copolymer.

Figure 25. SWCNT dispersion by the PVA-*g*-P3HT copolymer in aqueous solution: left optical microscopy image (scale 100 μm) and right the sheet resistance of the films versus the transmittance.
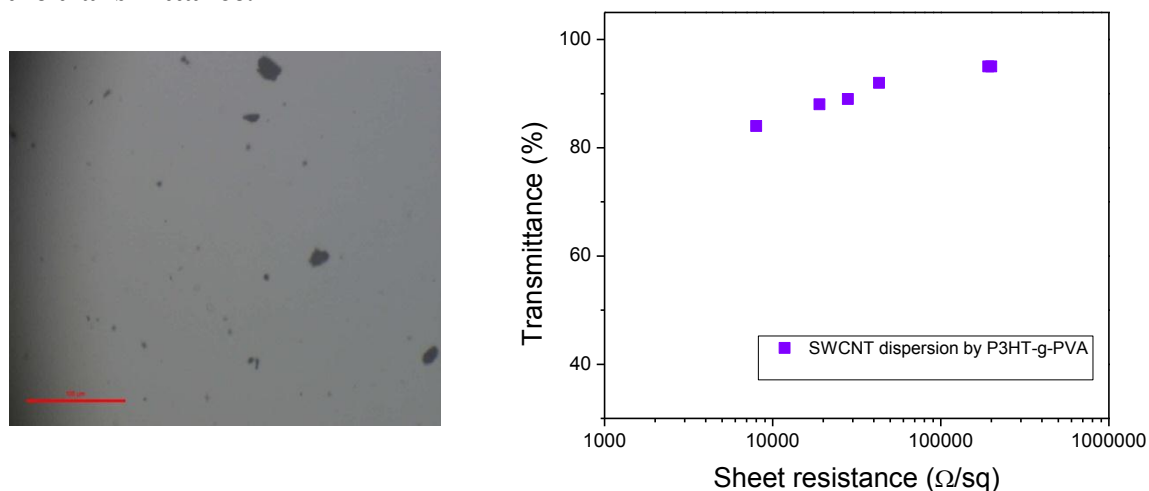
There are several factors that may influence the conductivity of these dispersions. The large size of the PVA backbone, which is not conductive, could affect negatively the electrical properties of the copolymer. Unfortunately, the size of the PVA chain has to be large in order to provide the water solubility of the copolymer.

III   Conclusion

In this chapter the copolymers that were synthesized in chapter 2 were tested as dispersion aids for CNTs. Films were cast these dispersions and the electrical and optical properties were measured. Out of this investigation we observed that the P3HT-*b*-(PS-*co*-PSSA) copolymers that were soluble in a mixture of solvents (DMSO/H$_2$O) were good dispersants for the MWCNTs but their films were not homogenous, due to the different evaporation rates of the two solvents. Further, the copolymer that was soluble in organic solvents, good for the P3HT block, was not able to disperse CNTs. We believe that this phenomenon is related to the absence of self-assemblies of the copolymer in the solution. By the formation of micelles in water a hydrophobic micro-domain is created and it is compatible with the hydrophobic nature of the nanotubes, assisting to the interactions between them.

The P3HT-*b*-(PS-*co*-PSSA) copolymer that was soluble in water was found to be a good dispersant for both types of CNTs. The stability of the dispersion was characterized by the zeta potential measurement. The quality of the dispersed CNTs was visualized by AFM, TEM and Cryo-TEM images while the interactions of the copolymer with the nanotubes were observed by HRTEM images. In order to verify that the P3HT block develops π-interactions with the SWCNT UV-vis and photoluminescence spectroscopy were used. The quenching of the copolymer photoluminescence, due to electron exchange, was observed. In addition the non-covalent interaction of the copolymer with the SWCNTs was verified by Raman spectroscopy. Films of these dispersions were made by spray-coating, and resistivity as low as 521 Ω/sq for transmittance 71% (at 550nm) was obtained. In order to increase to conductivity of these films the chemical doping of the P3HT block of the copolymer was found efficient with an increase of electrical properties of 30%.

Further a PVA-g-P3HT copolymer was used as dispersant of the CNTs. The copolymer was a good dispersant for both SW- and MW- CNTs, but more studies need to be done for the characterization of these dispersions. The electrical properties were not satisfying and they were inferior to the ones observed for the P3HT-*b*-(PS-*co*-PSSA).

In conclusion, from aqueous dispersions of the SWCNTs/P3HT$_{0.25}$-*b*-(PS$_{0.27}$-*co*-PSSA$_{0.48}$) we were able to fabricated film (on glass substrate) with 379 Ω/sq resistance and 71 % transmittance (at 550 nm). These results are far from the properties of the ITO films but they represent a promising system for the transparent conductive electrode development.

1.   Ma, P.-C.; Siddiqui, N. A.; Marom, G.; Kim, J.-K., Dispersion and functionalization of carbon nanotubes for polymer-based nanocomposites: A review. *Composites Part A: Applied Science and Manufacturing* **2010,** *41* (10), 1345-1367.

2.   Wu, Z.; Chen, Z.; Du, X.; Logan, J. M.; Sippel, J.; Nikolou, M.; Kamaras, K.; Reynolds, J. R.; Tanner, D. B.; Hebard, A. F.; Rinzler, A. G., Transparent, Conductive Carbon Nanotube Films. *Science* **2004,** *305* (5688), 1273-1276.

3.   Hwang, T.; Oh, J. S.; Hong, J.-P.; Nam, G.-Y.; Bae, A.-H.; Son, S.-I.; Lee, G.-H.; Sung, H.-K.; Lee, Y.; Nam, J.-D., One-step metal electroplating and patterning on a plastic substrate using an electrically-conductive layer of few-layer graphene. *Carbon* **2012,** *50* (2), 612-621.

4.   Liu, K.; Roth, S.; Duesberg, G.; Wagenhals, M.; Journet, C.; Dernier, P., Transport properties of single-walled carbon nanotubes. *Synth. Met.* **1999,** *103* (1–3), 2513-2514.

5.   Saran, N.; Parikh, K.; Suh, D.-S.; Muñoz, E.; Kolla, H.; Manohar, S. K., Fabrication and Characterization of Thin Films of Single-Walled Carbon Nanotube Bundles on Flexible Plastic Substrates. *J. Am. Chem. Soc.* **2004,** *126* (14), 4462-4463.

6.   Wagner, J. J. R., Multilayer Flexible Packaging *SPIE Ditigal Library* Elsevier: 2009; p 258.

7.   Li, X.; Lehmann, T.; Greene, W., Evaluation of photo resist coating performance of small dispense nozzle size in photolithographic spin coating process. **2005**, 1094-1101.

8.   Søndergaard, R.; Hösel, M.; Angmo, D.; Larsen-Olsen, T. T.; Krebs, F. C., Roll-to-roll fabrication of polymer solar cells. *Materials Today* **2012,** *15* (1–2), 36-49.

9.   White, B.; Banerjee, S.; O'Brien, S.; Turro, N. J.; Herman, I. P., Zeta-Potential Measurements of Surfactant-Wrapped Individual Single-Walled Carbon Nanotubes. *The Journal of Physical Chemistry C* **2007,** *111* (37), 13684-13690.

10.   Goutam, P. J.; Singh, D. K.; Giri, P. K.; Iyer, P. K., Enhancing the Photostability of Poly(3-hexylthiophene) by Preparing Composites with Multiwalled Carbon Nanotubes. *The Journal of Physical Chemistry B* **2011,** *115* (5), 919-924.

11.   Goutam, P. J.; Singh, D. K.; Iyer, P. K., Photoluminescence Quenching of Poly(3-hexylthiophene) by Carbon Nanotubes. *The Journal of Physical Chemistry C* **2012,** *116* (14), 8196-8201.

12.   Zou, J.; Liu, L.; Chen, H.; Khondaker, S. I.; McCullough, R. D.; Huo, Q.; Zhai, L., Dispersion of Pristine Carbon Nanotubes Using Conjugated Block Copolymers. *Adv. Mater.* **2008,** *20* (11), 2055-2060.

13.   Baibarac, M.; Lapkowski, M.; Pron, A.; Lefrant, S.; Baltog, I., SERS spectra of poly(3-hexylthiophene) in oxidized and unoxidized states. *J. Raman Spectrosc.* **1998,** *29* (9), 825-832.

14.   Sung, J.; Jo, P. S.; Shin, H.; Huh, J.; Min, B. G.; Kim, D. H.; Park, C., Transparent, Low-Electric-Resistance Nanocomposites of Self-Assembled Block Copolymers and SWNTs. *Adv. Mater.* **2008,** *20* (8), 1505-1510.

15.   Park, Y. D.; Kim, D. H.; Lim, J. A.; Cho, J. H.; Jang, Y.; Lee, W. H.; Park, J. H.; Cho, K., Enhancement of Field-Effect Mobility and Stability of Poly(3-hexylthiophene) Field-Effect Transistors by Conformational Change. *The Journal of Physical Chemistry C* **2008,** *112* (5), 1705-1710.

General Conclusions

The synthesis of new organic materials designed for applications as transparent conductive electrodes is of prime importance for the development of organic electronics. Thus, the main objective of this study was the elaboration of conductive inks based on a formulation of CNTs and semiconducting polymers. The synthesis of new well-defined copolymers for the dispersion of the CNTs was first targeted. Subsequently, formulations of CNTs/copolymers were investigated as transparent conductive electrodes. The overall strategy was to combine the electrical functionalities of the CNTs with the processing functionalities of block copolymers.

The targeted block copolymers were designed with a π-conjugated part (for the enhancement of the electrical properties of the CNTs through their individualization) and a hydrophilic part (for processing and solubility purposes in aqueous media). The poly(3-hexylthiophene) (P3HT) and the poly(3,4-ethylenedioxythiophene) (PEDOT) were used as π-conjugated polymers, the first due to its processability and the second due to its high intrisic conductivity. As a hydrophilic moiety, a strong polyelectrolyte was chosen, the poly(styrene sulfuric acid) (PSSA). In order to investigate the role of the charged hydrophilic part, macromolecular architectures with a neutral hydrophilic part, the poly(vinylalcohol) (PVA), were also synthesized.

Since PEDOT is not soluble in any solvent, a strategy of growing the PEDOT chain on a solubilizing flexible block was followed. First PS chains were synthesized by anionic polymerization and EDOT monomers with different functionalities were used as terminating groups. The synthesis of the PS-EDOT polymers was already challenging since coupling between the chains was observed. Three different polymerization methods were used for the synthesis of the PEDOT-based block copolymers: Suzuki coupling, coupling polymerization and oxidative polymerization. The Suzuki polymerization method was not successful since no copolymers were synthesized. The purity of the monomers as well as complexity of the polymerization could explain the absence of copolymers. By oxidative polymerization, with different ratios of monomer/oxidant, the synthesis of PEDOT oligomers was observed but no presence of block copolymers was attested. Finally the coupling polymerization was investigated due to its more aggressive character. Indeed, after the coupling polymerization, PEDOT-*b*-PS, PS-*b*-PEDOT-*b*-PS, PS and PEDOT oligomers were detected. Unfortunately, the separation of the block copolymers from the homopolymers was not possible.

Consequently we shifted our attention to the synthesis of P3HT based copolymers, which is already well-described in the literature. P3HT-*b*-PS block copolymers were synthesized by RAFT polymerization, since it is a method that does not involve transition metals which are poisons for electronic devices. First ω-allyl-terminated P3HT polymers were synthesized by GRIM polymerization. The allyl end group of the P3HT was further functionalized resulting in an ω-hydropropoxyl-P3HT. The esterification reaction of the ω-hydropropoxyl-P3HT with a RAFT agent resulted in the synthesis of the P3HT macro-initiator for the subsequent polymerization of the styrene units. Once the P3HT-*b*-PS copolymers were synthesized and characterized, sulfonate groups were added on the styrene units of the PS by a controlled reaction. A library of P3HT-*b*-(PS-*co*-PSSA) copolymers was prepared by that methodology. The volume fraction of the PSSA part as well as the molecular weight of the P3HT block were subsequently tuned since they play an important role in the solubility properties of the copolymers. Water solubility was finally achieved for copolymers with PSSA volume fraction 0.48 and with a short P3HT chain (4500 g/mol).

Besides, P3HT/PVA copolymer architectures were achieved in order to investigate the role of the polyelectrolyte block. Graft PVA-*g*-P3HT copolymers were synthesized by an esterification reaction between the hydroxyl groups of the PVA backbone chain and the ω-COOH-P3HT. For a ratio of three P3HT segments per PVA chain, the copolymers were soluble in aqueous media. In addition block copolymers of P3HT-*b*-PVA copolymers were synthesized for the first time. A P3HT-macro RAFT initiator was synthesized in order to start the polymerization of the second block.

The self-assembly and the photophysical properties of the water soluble copolymers were further examined. The CMC of the $P3HT_{0.25}$-*b*-($PS_{0.27}$-*co*-$PSSA_{0.48}$) (with volume fractions $f_{P3HT} = 0.25$, $f_{PS} = 0.27$, $f_{PSA} = 0.48$) copolymer was determined at 0.008 g/L and negatively charged particle were detected through zeta potential analysis. The size and the shape of these particles were visualized by several microscopy techniques. The copolymer was found to self-assemble in large aggregates (300nm) in water solution. The stability of these assemblies was further tested by applying a sonication treatment. The big aggregates were broken and replaced by small (30nm) spherical micelles. A photophysical analysis was also performed for the $P3HT_{0.25}$-*b*-($PS_{0.27}$-*co*-$PSSA_{0.48}$) solutions (before and after sonication) and for the corresponding films. Comparing the UV-vis maximum absorbance of the

copolymer solution before and after sonication, a blue shift was detected, which is an indication of a organization in H-type aggregates. A similar study was performed for the copolymer sonicated solution and the corresponding films. The UV-vis maximum shows a red shift, signifying that the micelles reorganized in J-aggregates when they are in the form of films.

The self-assembly of the PVA-*g*-P3HT copolymers in the aqueous media was also investigated. This type of copolymer did not show self-assembly behavior in the form of micelles or aggregates, so no further physico-chemical studies were performed.
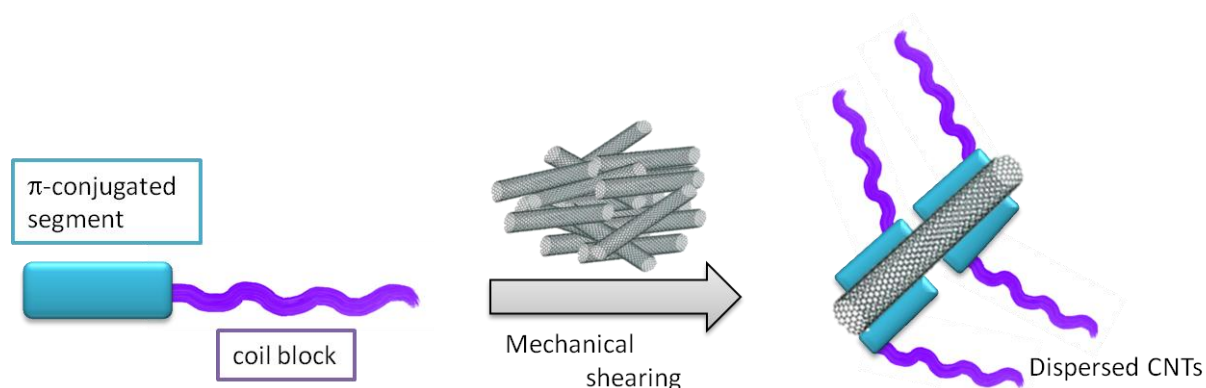
As shown in the above scheme, the π-conjugated-*b*-water soluble block copolymers of rod-coil type (*e.g.* P3HT-*b*-(PS-*co*-PSSA)) were tested as dispersants for both multi and single wall carbon nanotubes. The dispersions with the P3HT$_{0.25}$-*b*-(PS$_{0.27}$-*co*-PSSA$_{0.48}$) copolymer and the SWCNTs in aqueous media were further analyzed due to encouraging preliminary results. The stability of these dispersions was verified by zeta potential measurements. Two different types of SWCNTs were examined: functionalized and non-functionalized. The best electrical and optical properties were obtained for dispersions of functionalized SWCNTs/copolymer (0.2 g/L / 0.2 g/L) sprayed in thin films (thickness of ~30 nm), subsequently washed by water. The values for these films were 521 Ω/sq sheet resistance for 72% transmittance at 550 nm.

Moreover we investigated the interactions between the SWCNTs and the block copolymer by microscopic techniques as well as by photo-physical methods. Clear evidence of strong interactions between the copolymer and the SWCNTs were demonstrated leading to an enhanced individualization of the SWCNTs. The quenching of the absorption peak of

P3HT is another proof which indicates an energy exchange between the polymer and the CNTs. In order to ameliorate the electrical properties of the dispersions, chemical doping of the copolymer was performed. **Indeed dispersion films with sheet resistance at 379 Ω/sq and transmittance at 69% (at 550 nm) were subsequently realized**.

To sum up, in regards to the targeted features of the ANR project, IMPEC (*i.e.* T > 80-85% [300 nm< λ < 800 nm] and R_{sq} < 50-100 Ω/sq.), we have developed a promising methodology in order to find an all organic alternative to ITO combing both carbon nanotubes and semi-conducting block copolymers in formulations.

Besides there are number of parameters that can be tuned in order to improve our results:

- On a chemistry basis: by changing the nature and the architecture of the semi-conducting polymer part, by the addition of a co-solvent or conducting polymer latexes improving the electrical properties of the copolymer.
- From a physico-chemical point of view: by improving the features of the CNTs/copolymer formulations (phase diagram, rheology, viscosity etc.)
- From a process approach: by developing new deposition techniques for the films formation leading to an enhancement of the CNTs percolation.

More generally the concept that consists in the association within copolymers structures of a semi-conducting block with a water soluble designed as a polymer electrolyte, opens a large range of investigations. Indeed, to the best of our knowledge there is no report on such materials that combine in one polymer chain an electronic conducting segment with an ionic conducting one. The range of applications thus concerns many domains of researches apart only organic electronics, such as batteries or biological sensors.

Chapter V

Experimental section

TABLE OF CONTENTS

Experimental Section

I.1   *Materials*

I.1.1   *Purification of solvents*

All the solvents used in synthesis reactions and polymerizations were purified before use. Common methods were used for the purification of the solvents. Flasks containing the solvent and an appropriate drying agent were made and the solutions were kept in vacuum conditions. The pure solvent was received after cryogenic distillation under vacuum.

- ➤ **Dichloromethane (DCM)** (*X*ilab, 99%) was dried over calcium hydride (CaH_2) and refluxed for 3 hours before we collect the pure solvent.

- ➤ **Tetrahydrofuran (THF)** (Sigma Aldrich, 99%) was dried first over CaH_2 and was collected after 3 hours of reflux in a flask containing benzophenone and sodium. The color of this solution was purple and the pure solvent was collected by cryogenic distillation under vacuum.

- ➤ **Dimethylformamide (DMF)** (JT Baker) was dried over CaH_2 and cryodistilled under vacuum conditions.

- ➤ **Toluene** (*X*ilab) was dried first over CaH_2 and was collected after 3 hours of reflux in a flask containing polystyryl lithium. The pure solvent was collected by cryo-distillation.

- ➤ **Dioxane** (Alfa Aesar) was dried over CaH_2 and cryo-distilled under vacuum conditions.

- ➤ **Dichloroethane (DCE)** (99% Alfa Aesar) was degassed three times before use.

- ➤ **Diethyl ether** (JT Baker) was dried over CaH_2 and cryodistilled under vacuum conditions in a flask containing polystyryl lithium. The pure solvent was collected by cryo-distillation.

➢ Water used in reactions was ultra pure through an PURLAB Option apparatus with water conductivity at 5 MΩ/cm.

Chloroform (CHCl₃) (Sigma Aldrich), methanol (MeOH) (Sigma Aldrich), heptane (JT Baker), ethyl acetate (Scharlau) were used as received. *Milli-Q* water was purified Hydrochloric acid (HCl) (97%) and acetic acid (AcOH) were provided from *X*lab and the sulfuric acid (H₂SO₄) (95-98%) from Fisher Scientific.

I.1.2   *Purification of monomers*

The 3,4-ethylenedioxythiophene (EDOT) (97% Sigma-Aldrich) was used as received and stocked in the fridge. The 2,5 (dibromo-3-hexylthiophene) (99,4 %) monomer was synthesized from us following a procedure that will be further described

➢ **Styrene** (> 99% Sigma-Aldrich) was dried over calcium hydride and cryo-distilled under vacuum before use.

➢ **Vinyl acetate** (VAc) (99% Acros Organics) was dried over calcium hydride and cryo-distilled under vacuum before use.

I.1.3   *Materials used for the synthesis of PEDOT-based copolymers*

The N-bromosuccinimide (NBS) (99%), 2-isopropoxy-4,4,5,5-tetramethyl-1,3,2-dioxaborolane (98%), triisopropyl borate (98%), sodium bicarbonate (99%), iron (III) chloride (45%) and boron trifluoride diethyl etherate (46%) were purchased from Sigma-Aldrich and were used without further purification. From the same producer the n-butyllithium(n-But-Li) 1.6 M and 2.5M in hexane and sec-butyllithium (sec-ButLi) 1.4 M in cyclohexane were received and their concentration was not recalculated. Anhydrous magnesium sulfate was used for the purification

of the monomer and it was provide from Fisher Scientific. Pinacol (99%) was purchased from Alfa Aesar Tetrakis(triphenylphosphine)palladium(0) (99%) from Strem Chemicals and was stored in a glove-box.

I.1.4   Materials used for the synthesis of P3HT-based copolymers

- For the synthesis of the 2,5 (dibromo-3-hexylthiophene) monomer we used: Magnesium powder (99.8% Interchim) dried in oven at 110°C for 48 hours, 1-bromohexane (99%, Sigma-Aldrich), 3-Bromothiophene(97%, TCI), N-bromosuccinimide (NBS) (99%. Sigma-Aldrich)

- For the synthesis of P3HT polymers: tert-butyl-magnesium chloride 1M in THF, [1,3-Bis(diphenylphosphino)propane]dichloronickel(II) (Ni(dppp)Cl$_2$) stored in glove-box, allylmagnesium-bromide 1M in diethyl ether were purchased from Sigma-Aldrich and were used without further purification.

- For the functionalization of the ω-end group of P3HT: Sodium hydroxide and hydrogen peroxide (H$_2$O$_2$) 30% in water solution were purchased from Sigma-Aldrich. The 9-borabicyclo-3.3.1)nonane (9-BBN) 0.5M in THF was purchased from Acros Organics.

- For the synthesis of RAFT agent: 3-Mercaptopropionic acid (99%) and potassium hydroxide were purchased from Fisher Scientific. The carbon disulfide (99%) was provided from Sigma-Aldrich and the benzyl bromide (99%) from Alfa Aesar.

- For the synthesis of the block copolymers: *p*-Toluenesulfonic acid monohydrate (*p*-Tos) (99%), 4-Dimethylaminopyridine (99%) were provide from TCI, N,N′-Diisopropylcarbodiimide (DIPc) (98%), acetic anhydride (99%) were purchased from Sigma-Aldrich.

- For the synthesis of P3HT-*co*-PVA copolymers: Cobalt(III) acetylacetonate (99%), V70 (), potassium hydroxide, triethylamine, 3-Mercaptopropionic acid, 2-bromopropanoic acid (Sigma-Aldrich), Bromoacetyl bromide (Sigma-Aldrich), potassium (carbodithioatooxy)ethane (Sigma-Aldrich), Azobisisobutyronitrile (Across) recrystallized in ethanol.

251

I.1.5   Carbon nanotubes

- ➢ Multi Wall Carbon nanotubes purified with H_2SO_4 were provided by Arkema Group of researched Lacq.
- ➢ Single Wall Carbon nanotubes purified (P3) were purchased from Carbon solution and the non-purified SWCNTs (ASP-100F) form Hanwa/Iljin.

I.2   Synthesis of PEDOT-based copolymers

I.2.1   Synthesis of 2,5–dibromo-3,4-ethylenedioxythiophene (DBEDOT)
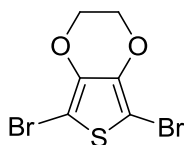
The synthesis of the 2,5–dibromo-3,4-ethylenedioxythiophene was a one step reaction. In a flame dried flask, 50 mL of $CHCl_3$ and equal amount of AcOH were added followed by the addition of 3,4-ethylenedioxythiophene (2.25 mL, 21 mmol). The solution was cooled to ~4°C with the use of an ice-water bath and the N-bromosuccinimide (9.35g, 52.5 mmol) was added in small portions. The reaction mixture was stirred for 1 hour in ~4°C and for other 3 hours at room temperature. The color of the solution was yellow and 50 mL of $NaHCO_3$ water solution were added. The product was purified by phase separation with water and DCM. The organic phase dried over magnesium sulfate and it was collected after vacuum filtration. The solvent was evaporated by rotary evaporator and the product was further solubilized in EtOH and heated at 80°C. The solution was then placed in the freezer at -20°C for 3 days. The 2,5–dibromo-3,4-

ethylenedioxythiophene was collected in the form of white crystals and it was stored at -20°C. The change in color (grey-black) is a sign of homo-polymerization of the monomer.

^{1}H-NMR (CDCl$_3$, 400 MHz): δ (ppm) = 4.27 (s, 4H, (O-CH$_2$)$_2$)

I.2.2 Synthesis of 2,5-di(-1,3,2-dioxaborolane)-3,4-ethylenedioxythiophene (DBoEDOT)
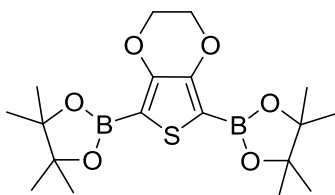
<u>1st way</u>

In dry-flamed three necked flask containing dry THF 40 mL, DBEDOT (3g, 10.2 mmol) was added under argon. The solution was cooled at -80°C with an ethanol/liquid nitrogen bath. The n-butyl lithium 1.6 M (16.9 mL, 20.4 mmol) was added dropwise and the mixture was stirred for one hour at room temperature. The addition of the 2-isopropoxy-4,4,5,5-tetramethyl-1,3,2-dioxaborolane (4.15 mL, 20.4 mmol) was made at -80 °C and the reaction was left for 48 hours at room temperature. A mixture of 100 mL ice and water was added at the solution and the product was collected by phase separation with water and diethyl ether as eluents. The organic phase was dried over magnesium sulfate, filtered and the solvent was evaporated yielding a yellow viscous liquid. Further purification of the product was achieved by passing through a silica gel column (eluent: heptane/ ethyl acetate 3/1).

<u>2nd way</u>

In a flamed dried three necked flask 50 mL of dried THF were added. Under argon atmosphere EDOT monomer (0.75 ml, 7.14 mmol) was added and the solution was cooled at -40°C. Keeping

the low temperature n-butyllithium (11.16 mL, 17.85 mmol) was added followed by the addition of triisopropyl borate (4.11 mL, 17.85mmol) after 30 minutes. The reaction continued for two hours at -40°C and for one hour at room temperature. In a flamed dried flask anhydrous THF solution containing pinacol (1.69g, 14.28 mmol) was prepared and added in the previous solution in acidic conditions (~1 ml of acetic acid). The reaction was left under stirring for two hours. The solvent was evaporated and the product was purified by passing through a silica gel column (eluent: cycloHexane/ ethyl acetate 7/1 v/v).

^{1}H-NMR (CDCl$_3$, 400 MHz): δ (ppm) = 4.27 (s, 4H, OCH$_2$CH$_2$O), 1.20 (s, 3H, CH$_3$), 1.17 (s, 1H, CHO)

^{13}C-NMR (CDCl$_3$, 100 MHz) : δ (ppm) = 137 (s, 1C, OC), 133 (s, 1C, BCS), 82 (s, 1C, CH), 64.82 (s, 1C, CH$_2$), 25 (m, 1C, CH$_3$)

I.2.3   Synthesis of 2-bromo-5-formaldehyde-3,4-ethylenedioxythiophene

X= H, Br
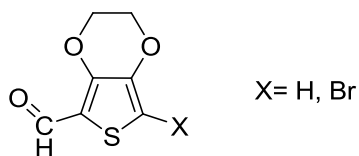
The synthesis of the 2-bromo-5-formaldehyde-3,4-ethylenedioxythiophene is an one step reaction: in a dry-flamed flask containing 50 ml dried diethyl ether, DBEDOT (3 g, 10.2 mmol) was added under argon atmosphere. The solution was cooled at -80°C followed by the addition dropwise of the n-butyllithium 2.5M (4.89 mL, 12.24 mmol) and kept under stirring for 1 hour. A solution of dry DMF (1 mL, 12.24 mmol) in dry diethyl ether was prepared in another flask and kept at 0 °C. At that temperature the addition of the first solution took place and the reaction was stirred for 20 hours. The final product was collected after phase separation with diethyl ether and purified by passing through a silica gel column (eluent: heptane/ DCM 1/1 v/v).

^{1}H-NMR (CDCl$_3$, 400 MHz): δ (ppm) = 9.83 (s, 1H, CHO), 4.27 (s, 4H, (O-CH$_2$)$_2$),

I.2.4 Synthesis of 2-formaldehyde-3,4-ethylenedioxythiophene

The synthesis of the 2-formaldehyde-3,4-ethylenedioxythiophene was the same as for the 2-bromo-5-formaldehyde-3,4-ethylenedioxythiophene.

^{1}H-NMR (CDCl$_3$, 400 MHz): δ (ppm) = 9.83 (s, 1H, CHO), 6.78 (s,1H, HCS), 4.27 (m, 4H, OCH$_2$CH$_2$O)

I.2.5 Synthesis of functionalized PS macro-monomers
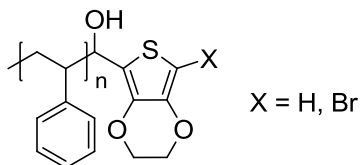
The PS chains were synthesized by anionic polymerization as followed: In a flamed dried flask three cycles of vacuum/argon were applied. Dry toluene 50 mL was added, followed by the addition of distilled styrene monomer (11.03 mL). Under argon atmosphere a few drops of sec-butyllithium were added in order to neutralize possible impurities. When the color of the solution starts to turn red we add the calculated amount of the sec-butyllithium 1.6 M (0.476 mL, 0.667 mmol). The reaction mixture was left under vigorous stirring for hours. All the terminated groups were degassed before the addition to the living PS chains. In order to increase the number of terminated PS chains two different procedures for the addition of the terminating groups were

performed. In all the cases our target was the amount of the terminating groups to be in excess of the living polystyrene chains.

<u>1st way</u>

In a dry flamed flask a concentrated solution of degassed terminating ageant (2-10 eq) was prepared in dry toluene. The solution was kept in argon atmosphere while the polystyrene solution was in vacuum conditions. The two flasks were connected and the addition was very fast due to the difference of the atmosphere in the two solutions. The polymer was precipitated in MeOH and it was collected after filtration. The white powder was dried in vacuum oven for 24 hours before characterizations.

<u>2nd way</u>

The polymerization reaction is taking place in the flask part of a burette. This solution was then added dropwise from the burette part in a concentrated solution of the terminated agent (prepared as before). The resulted polymer was treated as described before.

^{1}H-NMR (CDCl$_3$, 400 MHz): δ (ppm) = 7.09 (m, 3H, (CH)$_3$), 6.58 (m, 2H, C(CH)$_2$), 4.27 (m, 4H, (O-CH$_2$)$_2$)

I.2.6   *Suzuki coupling polymerization*
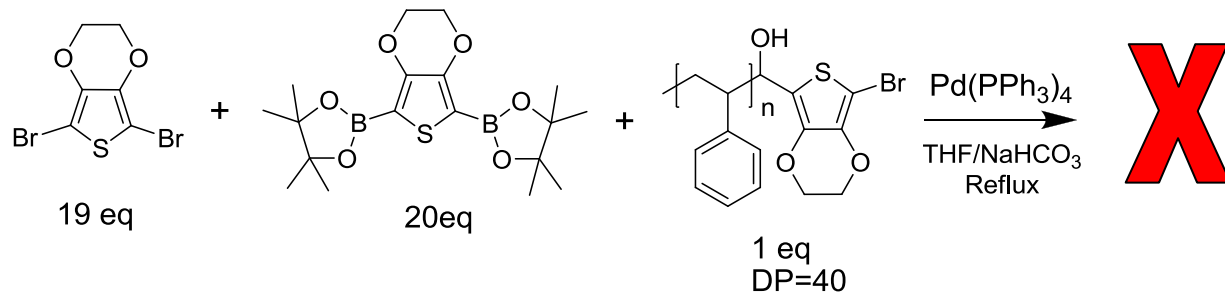
To a one necked flamed-dried flask the following reactants were added: PS-EDOT-Br(1g, 0.25 mmol), DBEDOT (1.05g, 3.5 mmol) and DBoEDOT (1g, 3.75 mmol) followed by conducting three cycles of vacuum/argon. A degassed water solution 1M of $NaHCO_3$ (5.03g in 40 mL) and degassed THF (50 mL) were refluxed under argon atmosphere at 90 °C for 3 hours. 10 mL of the solvent solution were added under argon atmosphere in the reactants flask followed by the addition of the $Pd(PPh_3)_4$ (1.2%, 0.05 g). The reaction was left stirring for one day at 90°C. After the addition of 15mL of the solvents the reaction was let at the same temperature for 3 more days. The product was isolated by precipitation in MeOH and filtration.

^{1}H-NMR ($CDCl_3$, 400 MHz): δ (ppm) = 7.09 (m, 3H, $(CH)_3$), 6.58 (m, 2H, $C(CH)_2$), 4.27 (m, 4H, $O(CH_2)_2O$)

I.2.7 *Oxidative polymerization*
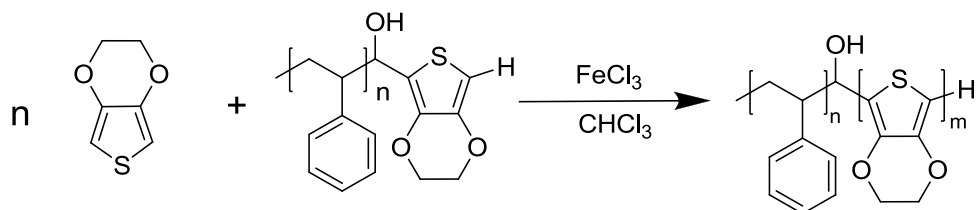
In a dried flask we add 20 mL of CHCl$_3$, PS-COH-EDOT (1g, 0.135 mmol), EDOT (0.15 mL, 1.35 mmol) and FeCl$_3$ (0.48g, 3.46 mmol). The reaction was stirred for 2 days at 38 °C and then the solution was diluted with MeOH and centrifugated in order to collect the final product.

I.2.8 Coupling polymerization
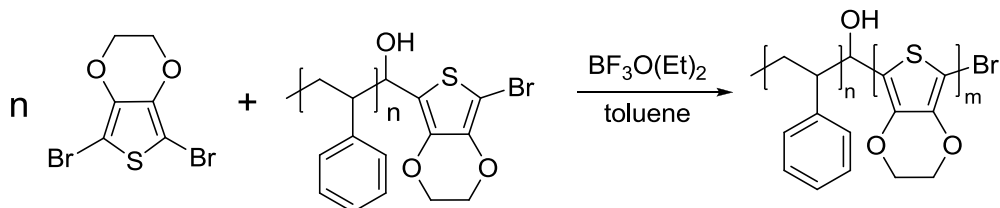
In a dried flask 20 mL of toluene were introduced, followed by the addition of PS-EDOT-Br (1g, 0.25 mmol), DBEDOT (3.7g, 12.5 mmol) and BF$_3$·O(Et)$_2$ acid (4.5g, 31.25 mmol). The reaction was heated at 100 °C for one day. The solution was then diluted with MeOH and centrifugated 2 times.

^{1}H-NMR (CDCl$_3$, 400 MHz): δ (ppm) = 7.09 (m, 3H, (CH)$_3$), 6.58 (m, 2H, CHCCH), 4.27 (m, 4H, (OCH$_2$)$_2$)

I.3 Synthesis of P3HT-based copolymers

I.3.1 RAFT polymerization

The mechanism of RAFT polymerization is described in the figure 1 and it is based on the use of a chain transfer agent (CAT or RAFT agent) that is controlling the molecular weight and the dispersity during the free-radical polymerization. In the early stages of the polymerization the propagating radical ($P_n^{\cdot}$) is added to the thiocarbonylthio compound [RSC(Z)=S] followed by fragmentation of the intermediate radical resulting in a polymeric thiocarbonylthio compound [PnS(Z)C=S] and a new radical ($R^{\cdot}$) (Pre-equilibrium state). This new radical reacts with a monomer and forms a new propagating radical ($P_m^{\cdot}$) (Reinitiation state). The equilibrium between the active propagating radicals ($P_n^{\cdot}$), ($P_m^{\cdot}$) and the polymeric thiocarbonylthio compounds provides equal probability for all chains to grow and allows for the production of narrow dispersity polymers.

Figure 1. Raft polymerization

Initiation

Pre-equilibrium
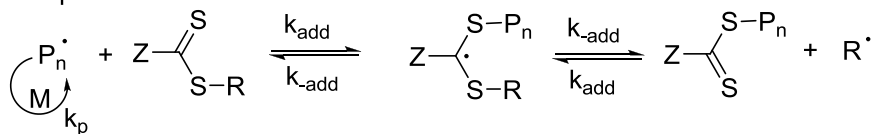
Reinitiation
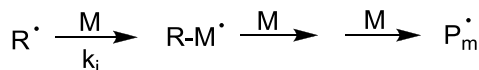
Main equilibrium

Termination

259
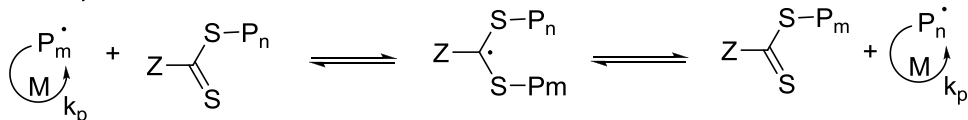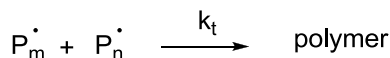
I.3.2 Synthesis of 3-hexylthiophene
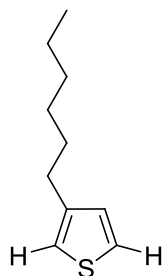
We flame-dry a two necked flask of 500 mL equipped with a condenser. We add 230 mL of distilled diethyl ether and under argon atmosphere magnesium (19.22g, 0.79mol). The addition of the 1-Bromohexane (86 mL, 0.633 mol) was added gradually: 5 mL of the reactant were added and immediately intense bubbling was observed. The next portion (5 mL) of the 1-Bromohexane was added when the bubbling had finished. The solution (1) was then put in an ice-bath and the addition of the reactant was continued in small portions. After the addition of the 1-Bromohexane was completed the reaction was stirred for 3 hours in room temperature. In another flamed and dry flask of 1000 mL, equipped with condenser and transfer funnel, we add 120 ml of distilled diethyl ether. In continuation the 3-Bromothiophene (28.7 mL, 0.306 mol) and the [1,3-Bis(diphenylphosphino)propane]dichloronickel(II) (0.95g, 1.38 mol) were introduced under argon atmosphere. The solution (1) was then transfer in the poured funnel and was added dropwise in the new mixture. After the addition the color of the solution becomes brown and the reaction was left stirring for 4 days.

Water (100 mL) slightly acidified with HCl was added slowly in the reaction mixture. The product was recuperated by phase separation with chloroform and water and the organic phase was dried over $MgSO_4$. The 3-hexylthiophene was purified by distillation with oil bath temperature at 95°C and solution temperature 45°C in a transparent liquid.

^{1}H-NMR (CDCl$_3$, 400 MHz): δ (ppm) = 7.25 (m, 2H, S-CH thiophene ring), 6.95 (m, 1H, S-CH-C, thiophene ring), 6.94 (m, 1H, CH, thiophene ring), 2.63 (m, 2H, CH$_2$, alkyl chain), 1.63 (m, 2H, CH$_2$, alkyl chain), 1.28 (m, 6H, (CH$_2$)$_3$, alkyl chain) 0.88 (m, 3H, CH$_3$, alkyl chain)

I.3.3   *Synthesis of 2,5-Dibromo-3-hexylthiophene*
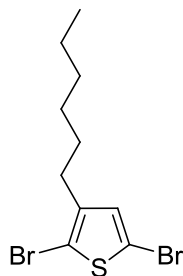
We flame-dry a flask of 1000 mL. Under argon atmosphere we add distilled 3-hexylthiophene (36.91 g, 0.219 mol) and we perform three cycles of argon-vacuum. Distilled DCM (200 mL) and 200ml of acetic acid were then introduced followed by the addition of the N-bromosuccinimide (70.19 g, 0.394 mol). The reaction mixture was left under stirring for 24 hour and when the reaction was completed the solution had orange color. 200 mL of saturated water solution of NaHCO$_3$ were added in the reaction and then the product was recuperated by phase separation with chloroform. The organic phase was dried over MgSO$_4$ for 12 hours. The solution was filtered, the solvent was evaporated and the yellow liquid was purified through distillation. The distillation took place in high vacuum conditions, where at oil bath temperature 120°C we collect 2-bromo-3-hexylthiophene. At temperature of 130°C we collected our pure product. In order to achieve higher purity (99.98%) we repeated the distillation procedure two times.

^{1}H-NMR (CDCl$_3$, 400 MHz): δ (ppm) = 6.98 (m, 1H, CH, thiophene ring), 2.63 (m, 2H, CCH$_2$, thiophene ring), 1.63 (m, 2H, CH$_2$, alkyl chain), 1.28 (m, 6H, (CH$_2$)$_3$, alkyl chain) 0.88 (m, 3H, CH$_3$, alkyl chain)

I.3.4 Synthesis of allyl terminated poly(3-hexylthiophene)
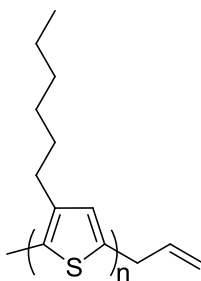
50 mL of distilled THF were added into a 500 mL two neck round bottom flask, previously flamed under vacuum and it was also subjected to some freeze thaw cycles. Under stirring the 2,5-dibromo-3-hexylthiophene(7 g, 21.46 mmol) was added followed by a 1M solution of tert-butyl-magnesium chloride (10.7 mL, 21.46 mmol) in THF. The reaction was left for 3 hours at room temperature. After the addition of 150mL distilled THF and the catalyst Ni(dppp)Cl$_2$ (2.3%, 0.3628 g) the reaction was stirred for 30min. Then 10eq of a 1M solution of allylmagnesium-bromide (8.64 mL, 8.64 mmol) in diethyl ether were added. After the evaporation of the solvent under vacuum, the polymer was precipitated in excess of MeOH. The purification was made by Soxhlet, 3 days with MeOH and 2 days with CHCl$_3$ in order to collect the polymer.

^{1}H-NMR (CDCl$_3$, 400 MHz): δ (ppm) = 6.98 (m, 1H, CH, thiophene ring), 5.97 (m, 1H, CHC, end-group), 5.12 (m, 2H, CH$_2$, end group), 3.49 (m, 2H, CCH$_2$, alkyl chain), 2.78 (m, 2H, CCH$_2$, alkyl chain), 1.70 (m, 2H, CH$_2$, alkyl chain), 1.43-1.34 (m, 6H, (CH$_2$)$_3$, alkyl chain) 0.91 (m, 3H, CH$_3$, alkyl chain)

I.3.5 Synthesis of hydroxypropyl terminated poly(3-hexylthiophene)
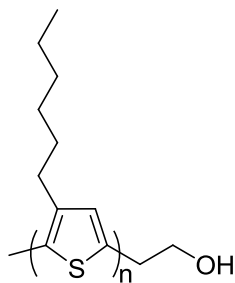
In a dry flask of 500 mL were added 120 mL of distilled THF. Under argon 1.4g of P3HT (0.32 mmol, DPn(NMR)= 31.6) functionalized with allyl-group and a 0.5M solution of 9-BBN (11.662 mL, 16 mmol) in anhydrous THF were added . The solution was heated at 45°C for 24hours. NaOH water solution(1.75 mL, 32 mmol) of 6M was prepared and added in the reaction. Then the solution was cooled at room temperature and then the H_2O_2 30 wt.% in water (1.21mL, 35.2 mmol) were added. The mixture was heated again at 45°C for 24 hours. The polymer was precipitated in MeOH and filtered.

^{1}H-NMR (CDCl$_3$, 400 MHz): δ (ppm) = 6.98 (m, 1H, CH, thiophene ring), 3.81 (m, 2H, CCH$_2$O end group), 3.76(m, 2H, CCH$_2$, end group), 2.78 (m, 2H, CCH$_2$, alkyl chain), 1.70 (m, 2H, CH$_2$, alkyl chain), 1.43-1.34 (m, 6H, (CH$_2$)$_3$, alkyl chain) 0.91 (m, 3H, CH$_3$, alkyl chain)

I.3.6   Synthesis of 3-benzylsulfanylthiocarbonylsulfanylpropionic acid (RAFT agent)
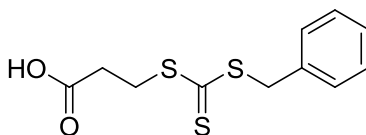
A water solution (120 mL) of potassium hydroxide (13 g, 0.23 mol) was added in a 250 mL flask containing 3-mercaptopropionic acid (10 mL, 0.115 mol,). Carbon disulfide (15 mL, 0.23 mol) was added dropwise and the solution was left under stirring for 5 hours. Benzyl bromide (13.7 mL, 0.115 mol) was added and the reaction was heated at 80°C for 12 hours. The reaction was then cooled down at room temperature and 200 mL of chloroform were added. The organic phase, which has orange color, was acidified with hydroxyl acid until the color changes to yellow. The aqueous phase was washed 4 times with chloroform and the organic phase was then dried with magnesium sulfate. The product was further purified by flash chromatography (eluent= hexane/ethyl acetate 3/1 v/v) to yield a yellow powder.

^{1}H-NMR (CDCl$_3$, 400 MHz): δ (ppm) = 7.32 (m, 5H, phenyl group), 4.62 (s, PhCH$_2$S), 3.77 (m, 2H, CH$_2$S), 2.80 (m, 2H, C-O-CH$_2$)

I.3.7 Synthesis of P3HT-macro RAFT agent
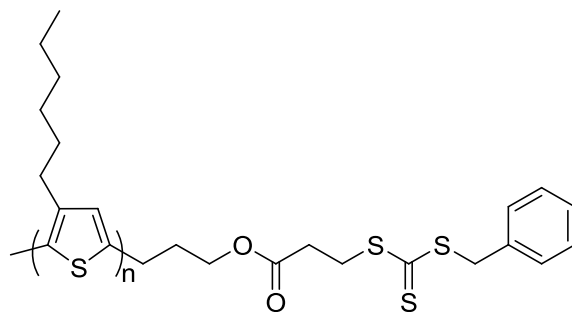
In a flamed-dry flask of 100ml, hydroxylpropyl terminated P3HT (1.2g, 0.28 mmol) was dissolved in 30ml of distilled dichloromethane at 40°C. When the polymer is completely dissolved, the RAFT agent (0.38g, 1.4mmol), DPTS[1](0.09g, 0.28mmol,) and N,N'-diisopropylcarbodiimide (0.3mL, 1.82 mmol,) were added in the solution under nitrogen

atmosphere. The reaction was heated at 30°C for 3 days. The RAFT macro-initiator was precipitated in MeOH and filtered.

^{1}H-NMR (CDCl$_3$, 400 MHz): δ (ppm) = 6.98 (m, 1H, CH, thiophene ring), 4.61 (s, 2H, CH$_2$Ph), 3.75 (m, 2H, CH$_2$S), 3.65 (m, 2H, COCH$_2$), 3.20 (m, 2H, COCH$_2$C, alkyl chain), 2.78 (m, 2H, CCH$_2$, alkyl chain), 1.70 (m, 2H, CH$_2$, alkyl chain), 1.43-1.34 (m, 6H, (CH$_2$)$_3$, alkyl chain) 0.91 (m, 3H, CH$_3$, alkyl chain)

[1]DPTS: In 15 mL of toluene we dissolve p-Toluenesulfonic acid (4.6g, 26.8mmol) and 4-Dimethylaminopyridine (3.29g, 26.8mmol). When the salt is formed it immediately precipitates and it recuperated by filtration.

I.3.8   Synthesis of P3HT-b-PS copolymer by RAFT
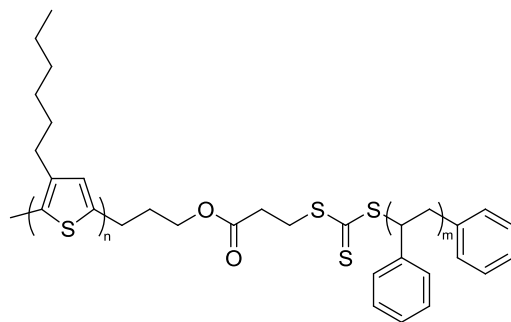
In a flamed-dry flask of 100 mL, P3HT-macro RAFT agent (1.1 g) was added under argon atmosphere. Then freshly distilled styrene (6 mL) was added and the solution was heated at 45 °C until the P3HT macro-iniator is completely dissolved in the styrene. Then three freeze-pump-thaw cycles were done, at the end of each the solution was always heated at 45 °C for the solubilization of the P3HT macro-iniator. Finally the reaction mixture was heated at 120 °C and the time of the reaction was varied with the molecular weight of the polystyrene. The reaction

was terminated by freezing the solution over liquid nitrogen. The block copolymer was precipitated in MeOH, filtered and dried in vacuum oven.

^{1}H NMR (CDCl$_3$, 400 MHz): δ (ppm) = 7.0-7.1 (m, 1H, CH, thiophene ring, m, 3H, (CH)$_3$, phenyl ring), 6.58 (m, 2H, (CH)$_2$C, phenyl ring), 2.78 (m, 2H, CCH$_2$), 1.70 (m, 2H, CH$_2$, alkyl chain), 1.43-1.34 (m, 6H, CH$_2$)$_3$, alkyl chain) 0.93 (m, 3H, CH$_3$, alkyl chain)

I.3.9   *Sulfonation reaction of the P3HT-b-PS copolymer*
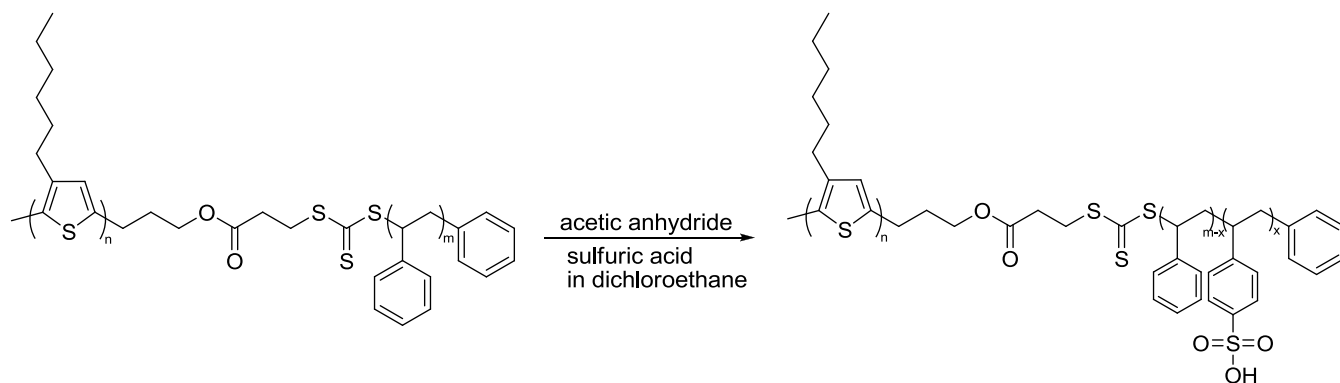
In a flamed dried flask of 100 mL we add 10 mL of degassed DCE and the P3HT-*b*-PS copolymer (1.2g, mol(styrene) = 8.64mmol). In a flamed-dry flask of 50 mL we prepare the acetyl sulfate solution: under argon atmosphere acetic anhydride (1.6 mL, 17.28 mmol) and DCE twice the volume of acetic anhydride (4 mL) were introduced. The solution was cooled to 0°C and the sulfuric acid (0.7 mL, 13 mmol) was added. The acetyl sulfate was then added in the copolymers solution under argon atmosphere and the reaction was heated at 60°C for 3 days.

^{1}H NMR (DMSO-d$_6$, 400MHz)): δ (ppm) = 7.41 (m, 2H, (CH)$_2$-SO$_3$), 7.05 (m, 3H, (CH)$_3$, phenyl ring), 6.48 (m, 2H, (CH)$_2$C ,phenyl ring)

The sulfonation level can be tuned by calculating the percentage on the styrene unit that will be sulfonated. For example the description given above is for 100% theoretical sulfonation. If we wanted 50% of the styrene units to be sulfonated then the mol of styrene will be 4.32 mmol and on this base is the amount of the acetyl sulfate solution will be calculated. For sulfonation levels lower than 50% the reaction could be performed at room temperature for 4 days.

I.3.10 Synthesis of PVA polymer
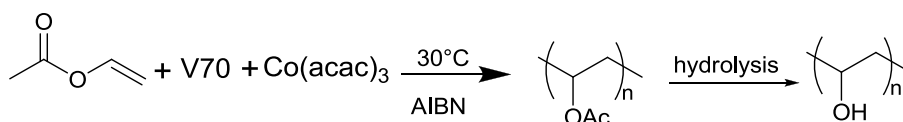
In a flamed-dry flask under argon atmosphere we introduced the initiator Cobalt (III) acetylacetonate (Co (acac)$_3$) (0.05g, 0.214 mmol) and the V70 (0.2 g, 0.64 mmol). After passing three cycles of argon-vacuum, we added distilled vinyl acetate (9.6ml, 0.104mol) and we heated the reaction at 60 °C for 56 hours. The reaction was stopped by putting the flask in liquid nitrogen. We dissolve the PVAc in small amount of MeOH and mix it with a KOH/MeOH solution. We let the solution under stirring for 24 hours. We evaporate 2/3 of the solvent and we introduce the rest of the mixture in a dialysis membrane. The membrane was then deposited in a water solution and stirred for 2 days. The PVA polymer was recuperated by lyophilization.

I.3.11 Synthesis of ω-COOH-P3HT polymer
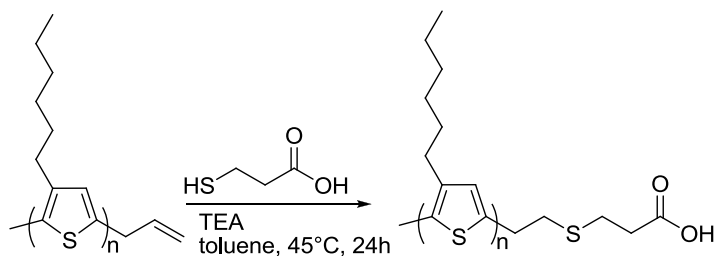
P3HT (1g, 0.2 mmol) terminated by an allyl chain was introduced in a flamed-dry flask containing distilled toluene. The solution was then heated at 45 °C in order to solubilize the P3HT. After the addition of the triethylamine (3mL, 21 mmol) the solution was cooled down at 0°C. At that temperature the 3-mercaptopropionic acid (1.6mL, 18.36 mmol) was added slowly and the reaction was left under stirring for 24 hours. The functionalized polymer was then precipitated in MeOH.

^{1}H NMR (CDCl$_3$, 400 MHz): δ (ppm) = 6.98 (m, 1H, CH, thiophene ring), 5.30 (s, 2H, CH$_2$-COOH, end group), 4.13 (m, 2H, S-CH$_2$, end group) 3.76(m, 2H, C-CH$_2$, end group), 2.78 (m, 2H, C-CH$_2$, alkyl chain), 1.70 (m, 2H, CH$_2$, alkyl chain), 1.43-1.34 (m, 6H, (CH$_2$)$_2$, alkyl chain) 0.91 (m, 3H, CH$_3$, alkyl chain)

I.3.12 Synthesis of PVA-g-P3HT copolymers[2]
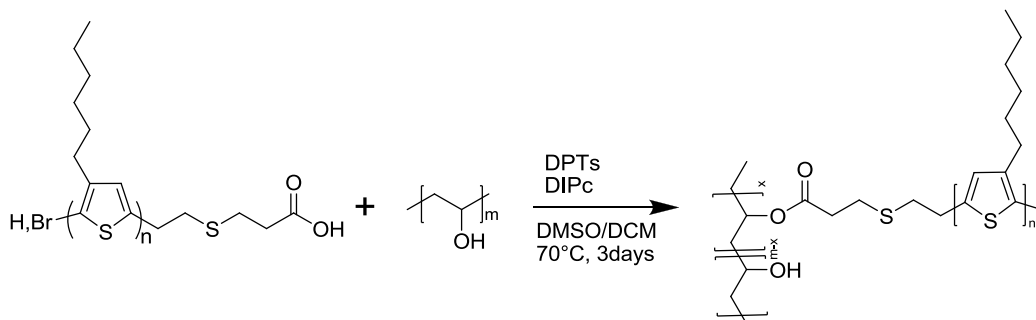
In a flamed and dry flask we added distilled DMSO (10 mL) and the PVA polymer (0.5g, 0.036 mmol). In another 250ml flamed-dry flask we added distilled DCM and the ω-COOH-P3HT polymer (0.36 g, 0.071 mmol). When the P3HT is completely soluble DPTS (0.005 g, 0.0143 mmol) and DIPC (0.1 mL, 0.0856 mmol) were added. In continuation, the DMSO solution was added too and the reaction was heated at 70°C for 3 days. The copolymer was precipitated in MeOH.

I.3.13 Synthesis of P3HT-macroinitiators for RAFT polymerization of PVA
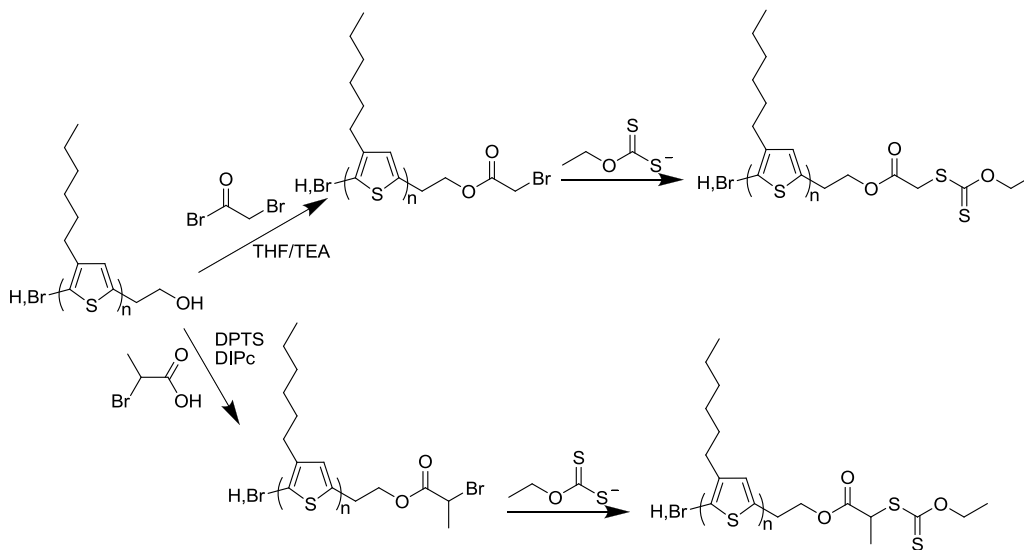
The synthetic route was the same for all the RAFT macroinitiators we tried for the synthesis of the P3HT-*b*-PVA copolymers. An example is following:

In a flamed dry flask 20 mL of distilled DCM were introduced followed by the addition of the hydroxypropyl terminated P3HT (1g, 0.25 mmol). After the addition of the DPTS (0.02g, 0.05 mmol), DIPC (1.2mL, 0.065 mmol) and the 2-bromopropanoic acid (0.2g, 1.25 mmol) the reaction was heated at 35 °C for 3 days. The product was precipitated in MeOH. In continuation the bromoethanoate-P3HT (1g, 0.25 mmol) was solubilized in chloroform and the potassium

(carbodithioatooxy)ethane (2g, 12.5 mmol) was added and the reaction was kept stirring for 3 days. The P3HT-macroinitiator was precipitated in MeOH.

^{1}H NMR (CDCl$_3$, 400 MHz): δ (ppm) = 6.98 (m, 1H, CH, thiophene ring), 4.64 (M, 2H, CH$_2$-C-O, end group), 4.43 (m, 1H, C-CH-S, end group) 4.23 (m, 2H, O-CH$_2$, end group), 2.78 (m, 2H, C-CH$_2$, alkyl chain), 1.70 (m, 2H, CH$_2$, alkyl chain), 1.43-1.34 (m, 6H, (CH$_2$)$_3$, alkyl chain) 0.91 (m, 3H, CH$_3$, alkyl chain)

I.3.14 Synthesis of P3HT-b-PVA copolymers by RAFT polymerization
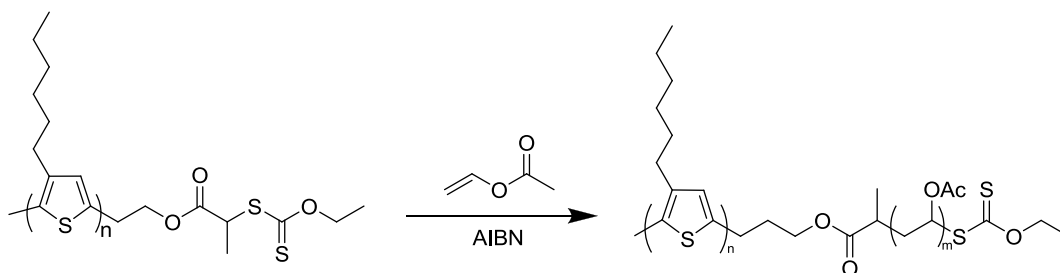
In a flamed dry flask of 100 mL we add the P3HT-macro initiator (0.8g, 0.2 mmol) and we pass three cycles of argon-vacuum. 20 mL of distilled THF were added followed by the vinyl acetate monomer (6.45 mL, 70 mmol). The solution was then freeze-dried and under argon atmosphere recrystallized AIBN (0.006g, 0.04mmol) was added. The reaction was heated at 65 °C for 5 days. The copolymer was precipitated in MeOH (or pentane for big molecular weights of PVAc) and filtered.

^{1}H NMR (CDCl$_3$, 400 MHz): δ (ppm) = 6.98 (m, 1H, CH, thiophene ring), 4.64 (M, 2H, CH$_2$-C-O, VAc), 4.43 (m, 1H, CH-S, end group) 4.23 (m, 2H, O-CH$_2$, end group), 2.78 (m, 2H, C-CH$_2$,

alkyl chain), 1.70 (m, 2H, CH_2, alkyl chain), 1.43-1.34 (m, 6H, $(CH_2)_3$, alkyl chain) 0.91 (m, 3H, CH_3, alkyl chain)

I.4   Procedure for dispersion of CNTs and film formation

I.4.1   Dispersion of CNTs

The procedure for the dispersion of both single wall and multi wall carbon nanotubes was the same:

The copolymer solution was prepared by stirring in the solvent for 2-3 days. For the copolymer soluble in aqueous media the solutions were additionally heated at 90°C. Before using the copolymer solutions in the CNTs dispersions, they were sonicated in sonication bath for 10 minutes. The desired amount of CNTs and copolymer solution was added followed by the addition of solvent. The dispersion was sonicated by probe sonicator (Bioblock scientific) with a tip of 3mm diameter for 10 min with power of 225 Watt. The CNTs/copolymer dispersion was then centrifugated (Thermo scientific) for 300min with 700 rpm.

I.4.2   Film formation

- Films made by doctor blade technique were casted at room temperature in an Erichsen apparatus. The glass surfaces were first cleaned with methanol and isopropanol and then were treated with UV-vis light. The distance of the blade from the surface was varied so as to control the thickness of the films.

- The spray coating was based on the Harder and Steenbeck Colani airbrush. A glass substrate (cleaned with isopropanol and ethanol) is placed on a heating plate with the temperature fixed around 100 °C. The spray is deposited around 20 cm above the substrate and the pressure of the spraying is 40psi. The films were than deposited for 10 minutes in a water solution in order to eliminate the coffee stain effect.

I.4.3   Characterization of thin films

The optical microscopy of the films was measured by a UV-vis spectrometer.

The sheet resistance of the films was measured by a four point probe. The principal of the four-point probe measurements is presented in the figure 2.

Figure 2. Schematic of measuring the sheet resistance by four point probe.
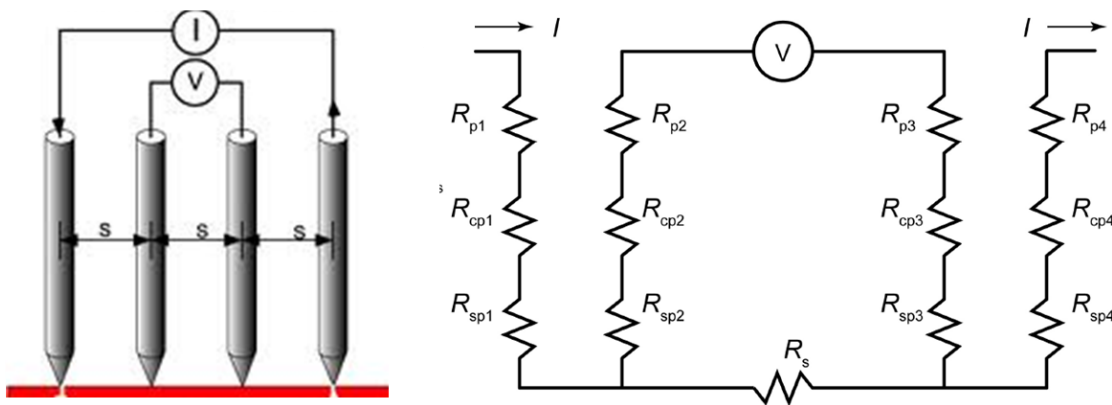
Two probes carry the current and the other two probes sense the voltage. Each probe has a probe resistance Rp, a probe contact resistance Rcp and a spreading resistance Rsp associated with it. However, these parasitic resistances can be neglected for the two voltage probes because the voltage is measured with a high impedance voltmeter, which draws very little current. The voltage reading from the voltmeter is approximately equal to the voltage drop across the semiconductor sheet resistance. By this method the sheet resistance can be calculated from the formula:

$$R_s = F \frac{V}{I}$$

where V is the voltage reading from the voltmeter, I is the current carried by the two current carrying probes, and F is a correction factor.

I.5. Characterization techniques

I.5.1 Spectroscopic analysis

- ^{1}H-NMR and ^{13}C-NMR spectra were recorded using a Bruker AC-400 NMR spectrometer at room temperature. The resonance frequency was at 400 MHz for ^{1}H-NMR and at 100 MHz for ^{13}C-NMR and the tetramethylsilance (TMS) was used as reference. For the analysis performed in deuterium chloroform $CDCl_3$, the reference that was used for the calibration was the residual peak of chloroform δ_H= 7.26 ppm at 298K.

- The UV-vis spectra for both films and solutions were obtained by a SHIMADZU 3600 UV-Vis-NIR spectrometer. The measurement wavelength range was from 200 nm to 3300 nm. The spectrometer is equipped with three different detectors, one for the ultraviolet and visible regions, one for the near infrared region and one to bridge the gap between the different regions. All the measurements were normalized by taking as a reference a background spectrum.

- Photoluminescence (PL) spectroscopy measurements were performed on a Horiba scientific Fluoromax-4 fluorometer. For the measurements of the P3HT-*b*-(PS-*co*-PSSA) copolymers and its dispersions with CNTs the excitation wavelength was around 500nm (±5nm), the slit at 10 nm and the integration time at 0.1 sec. All the measurements were normalized by a background spectrum taking as a reference.

- Raman spectroscopy measurements were performed on a Horiba Jobin-Yvon HR800-UV spectrometer, in the Institut des Sciences Moléculaires (ISM) - Groupe Spectroscopie Moléculaire under the supervision of Dr. Thierry Tassaing and David Talaga. Different conditions (laser wavelength, laser power, and excitation time) were examined for both solution and film samples. The optimal conditions for our systems were with the use of laser 513 nm and power of 0.5 or 4 µW and excitation time for 30 sec. We observed that for higher laser power and longer excitation time the Raman signal was decreased.

- Fourier Transformed Infrared Spectroscopy (FTIR) measurements were performed on a Bruker Tensor 27 spectrometer using a 0.6 mm-diameter beam, a 4 cm^{-1} resolution and spectral range from 4000 cm-1 to 400 cm-1. Samples are analyzed with the attenuated total reflectance (ATR) method.

I.5.2   *Microscopy analysis*

- Transmission Electron Microscopy (TEM) images were taken using a Hitachi H-7650 (at Bordeaux Imaging center) transmission electron microscope. The measurements were performed by A.Charbonnier (LCPO) with S162 formvar/carbon 200mesh Cu grids. The HRTEM were performed with high resolution analysis.

274

- Atomic Force Microscopy (AFM) measurements were obtained with a Dimension Icon Atomic Force Microscope (Bruker) system operated in tapping mode in air at room temperature. Commercial silicon cantilevers with typical force constants between 32.0 and 54.4 N.m^{-1} were used. The measurements were carried out at specific positions of the sample with different scan sizes (typically 0.5, 1 and 2 μm). Each scanned micrograph consists of 512 lines. Images were taken continuously with a scan rate of 1.0 Hz. The preparation of the AFM samples of the copolymers was performed by introducing substrates covered by graphene sheets in the copolymers solution for 24 hours. The samples were dried for 24 hours in room temperature. The AFM samples of the CNTs dispersions were casted by spray coating on glass substrates. All the measurements were performed by G. Pecastaings.

- Cryo-TEM images were taken with an Cryo-Electronic microscope Philips Technai F20 (FEG), and the measurements were made at CBMN by Prof. Alain Brisson.

- Optical microscopy images were taken with a Nikon OPTIPHOT-88 apparatus equipped with a Nikon Digital sight camera. Three different objective lenses were used for x2.5, x10 and x20 objectives.

I.5.3   *General characterization techniques for polymers*

- Size Exclusion Chromatography (SEC) was performed at room temperature and the samples were prepared with THF/trichlorobenzene (1L/2mL) as solvent. THF with trichlorobenzene as flow marker at 40 °C at a flow rate of 1 mL.min^{-1} using a differential refractometer RI (Varian) and a UV-visible spectrophotometer (Varian) operating at 260 nm and using 3 TSK gel Tosoh columns (G4000HXL, G3000HXL and G2000HXL, with pore sizes of 20, 75 and 200 Å respectively, connected in series). The elution times were converted into molecular weights using a calibration curve based on low dispersity polystyrene standards.

- Thermogravimetric analysis (TGA) measurements were performed using a Q-500 TA instrument. The samples were heated to 580°C with a ramp of 10 °C per minute.

- DSC thermograms were measured using a DSC Q100 apparatus from TA instruments. Samples were first heated from 0 to 300 °C, cooled from 300 to 0 °C, heated again from 0 to 300 °C for a second heating run analysis. All experiments were performed at a rate of 10 °C/min.

I.5.4   Nanoparticles analysis

- Zeta potential measurements were carried out with a Zetaphore meter IV Z4000 from ZetaCompact. This type of instrument can measure zeta from -150 mV to 150 mV. The cell voltage was from 0 V to 225 V and the cell current from 0mA to 9.99 mA. The zeta potential was measured based on the Smoluchowski equation.

- Nanoparticle Tracking Analysis (NTA) measurement was carried out on an LM20 apparatus at room temperature with laser at 640 nm with power of 40 mW.

I.5.5   Electrochemistry experiments

The electrochemistry experiments were performed in acetonitrile as a solvent for the P3HT films and in DCM for the P3HT-*b*-(PS-*co*-PSSA). The tetrabutylammonium hexafluorophosphate was used as polyelectrolyte in both solvents. The films of P3HT were prepared by spin coating on glass substrates covered with ITO. The films of the P3HT-*b*-(PS-*co*-PSSA) were prepared by spray coating on glass substrates covered with ITO. Silver was used as a reference electrode, platinum as a counter electrode and our films were the working electrodes. A schematic of the setup is presented in the figure 1.

Figure1. Schematic of the setup used for the electrochemistry experiments
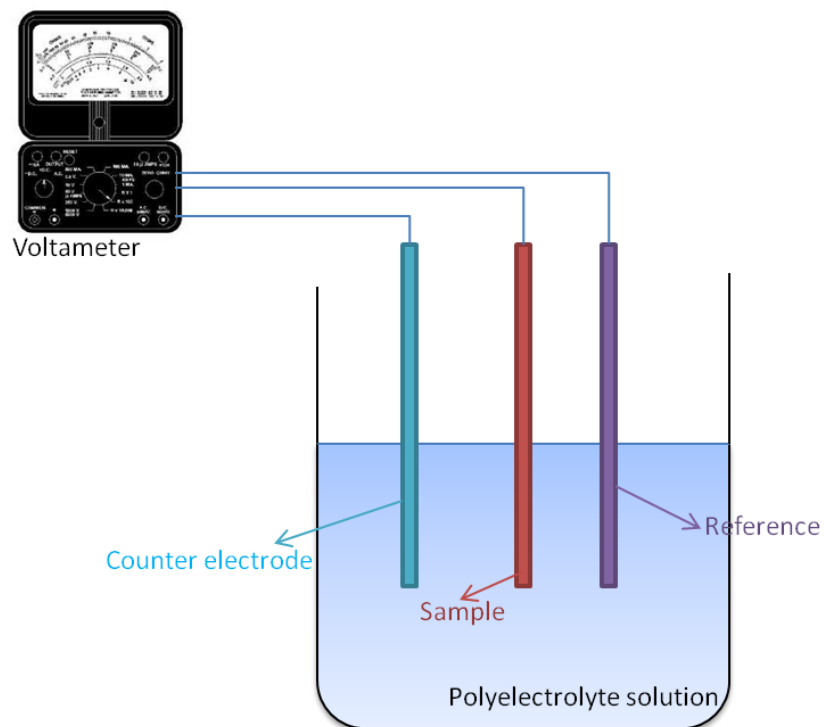
I.6.   *Additional characterizations (^{1}H-NMR, FTIR, TGA, DSC)*

I.6.1   *^{1}H-NMR spectra*

Figure 1. ^{1}H-NMR (CDCl3, 400 MHz) of the 2,5-dibromo-3-hexylthiophene
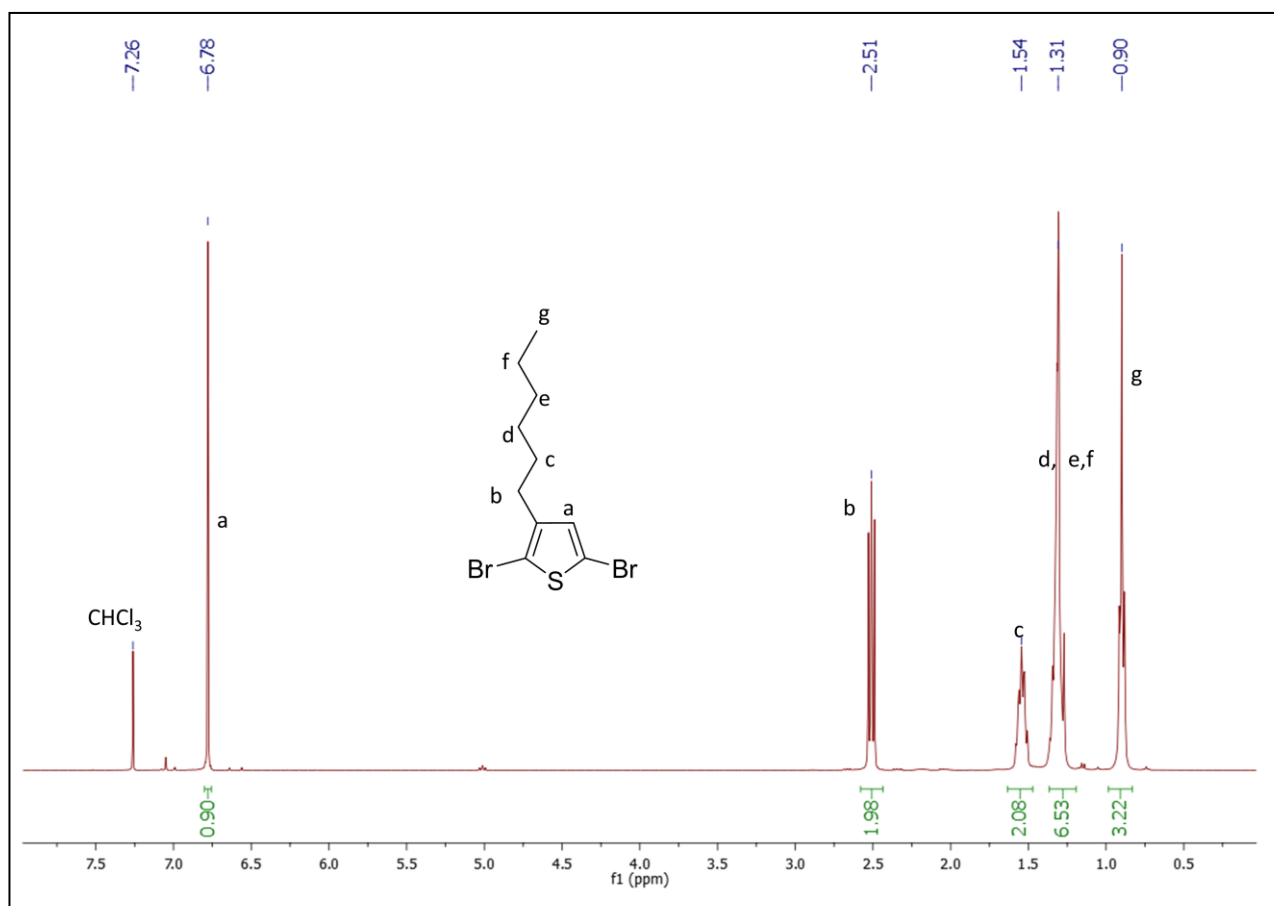
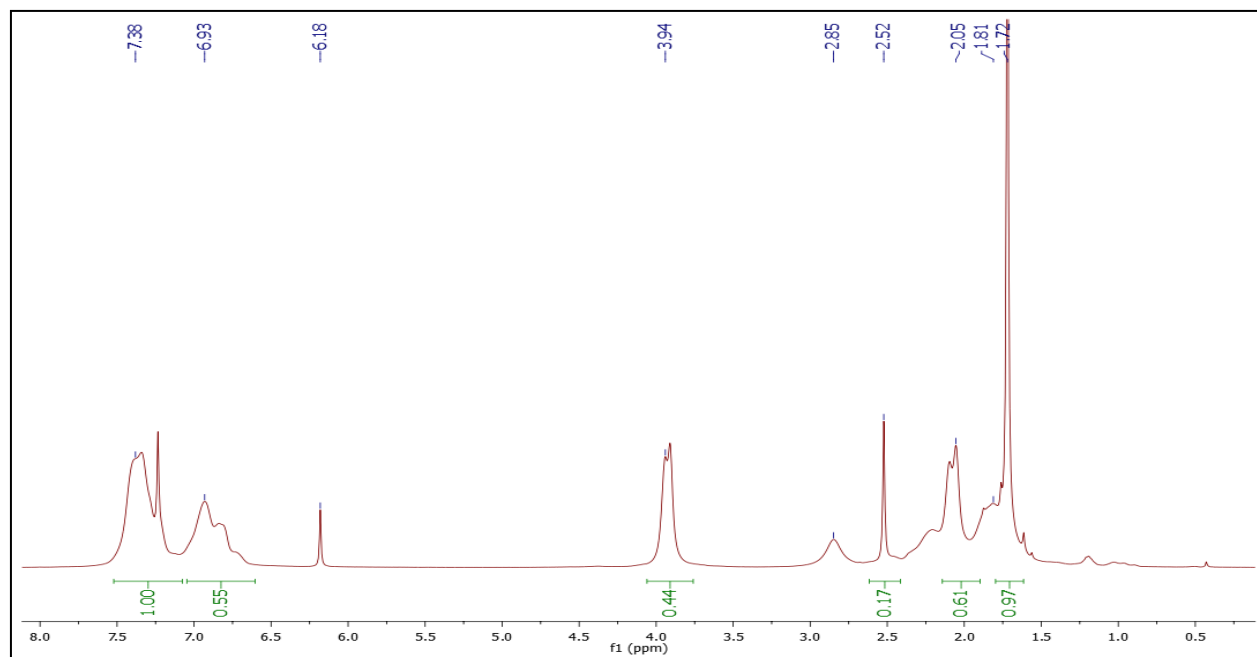**Figure 2. ^{1}H-NMR (CDCl3, 400 MHz) of the PS-EDOT/EDOT after oxidative polymerization (only PS is present)**

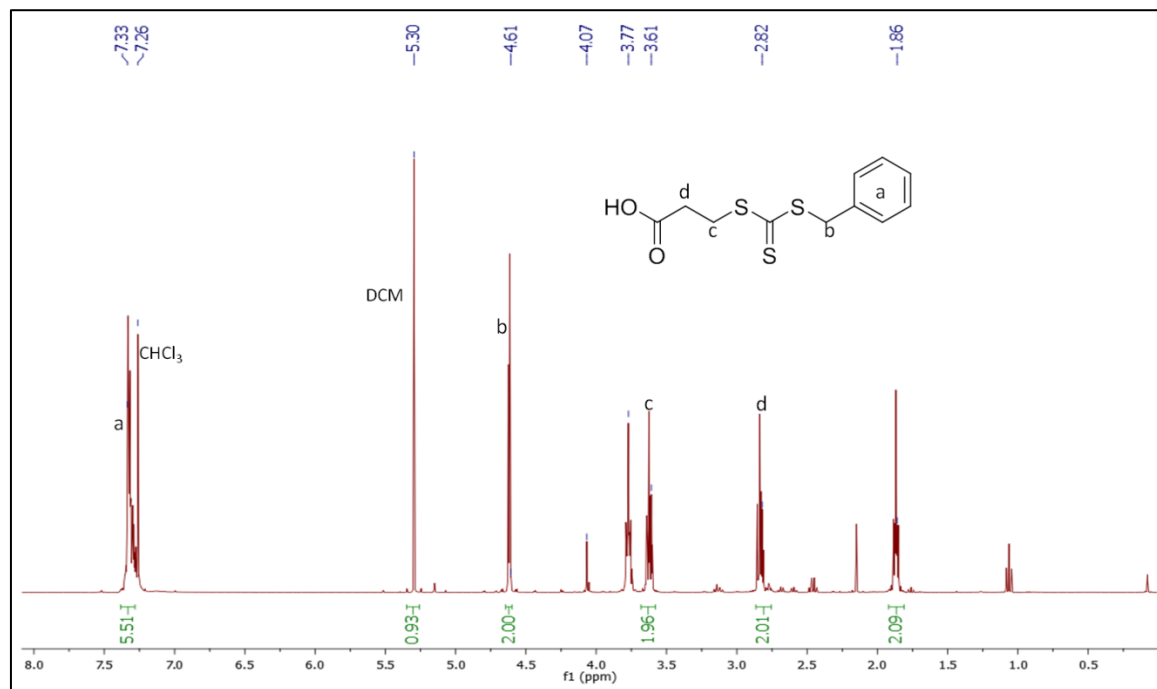**Figure 3.** ^{1}H-NMR (CDCl$_3$, 400 MHz) of the 3-benzylsulfanylthiocarbonylsulfanylpropionic acid

Figure 4. ^{1}H-NMR (CDCl$_3$, 400 MHz) of the P3HT-macro RAFT agent
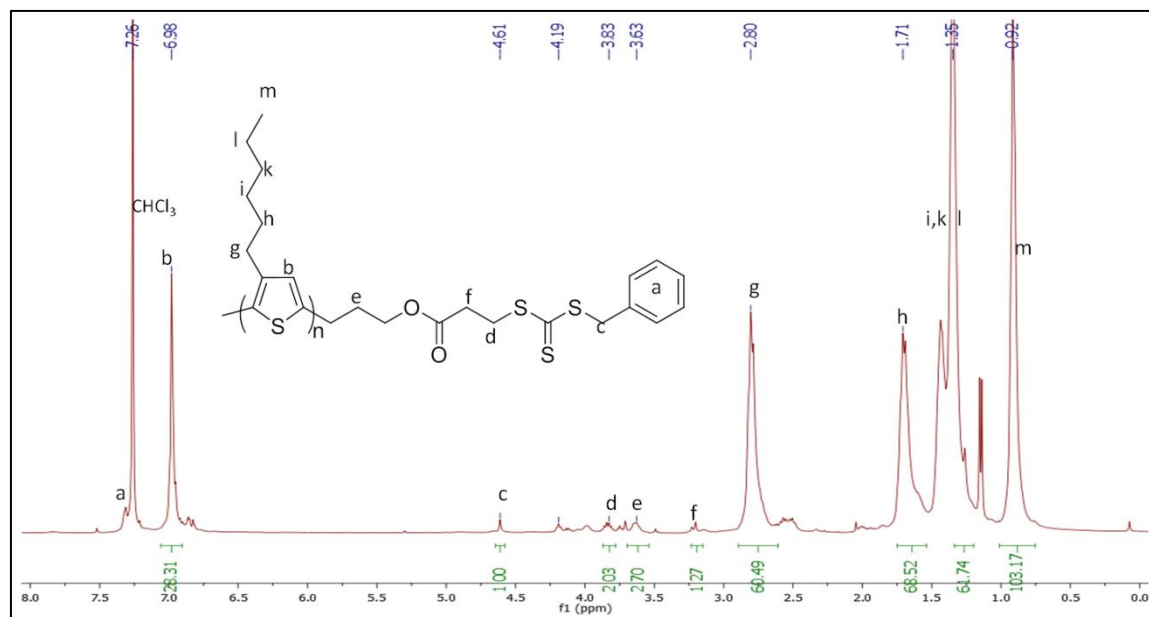
Figure 5. ¹H-NMR (CDCl₃, 400 MHz) of the P3HT-macro RAFT agent for polymerization of the vinyl acetate
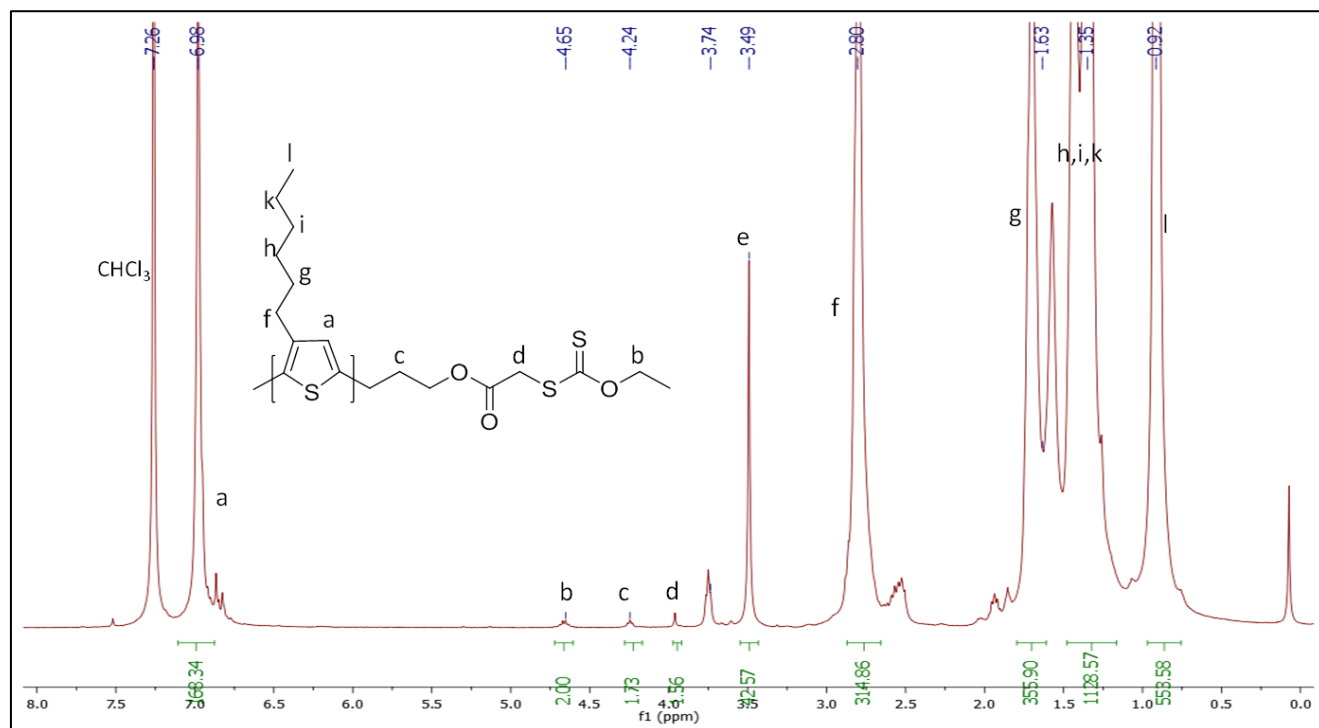
Figure 6. ^{1}**H-NMR (CDCl$_3$, 400 MHz) of the P3HT homo-polymer after 20 min of probe sonication**
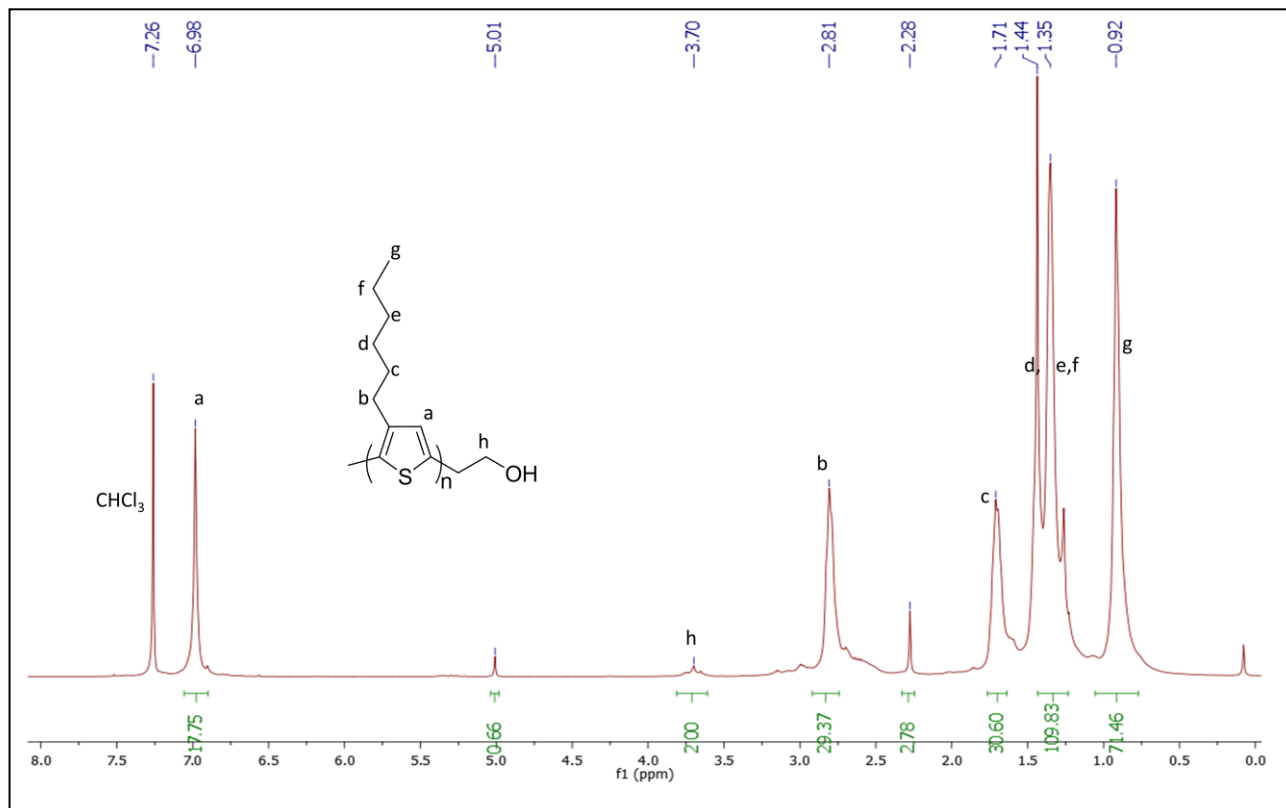
I.6.2 SEC spectum

Figure1. SEC spectra (UV-vis) of PS-EDOT/EDOT after oxidation polymerization (30eq of EDOT). Traces of PEDOT oligomers are present
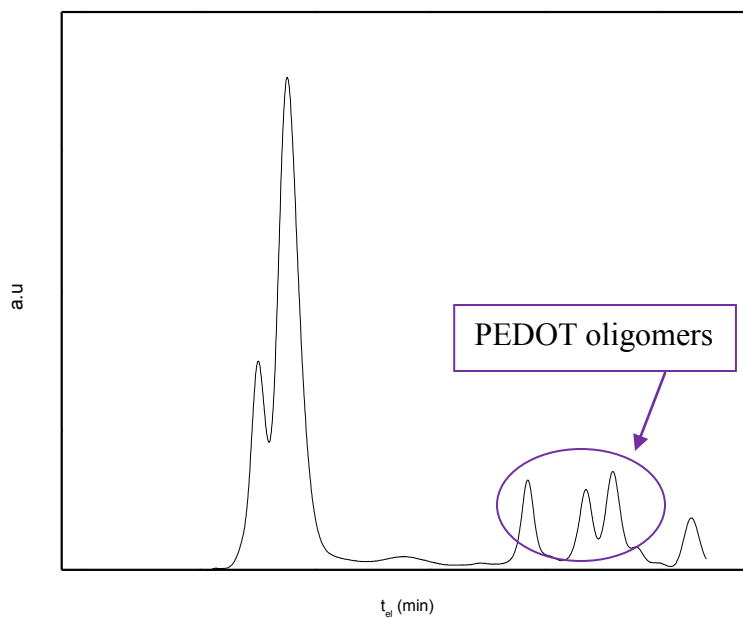
I.6.3 *Thermogravimetric analysis and Differential scanning analysis*

Figure1. TGA of the PS-*co*-PSSA, P3HT and P3HT-*b*-(PS-*co*-PSSA) in nitrogen atmosphere
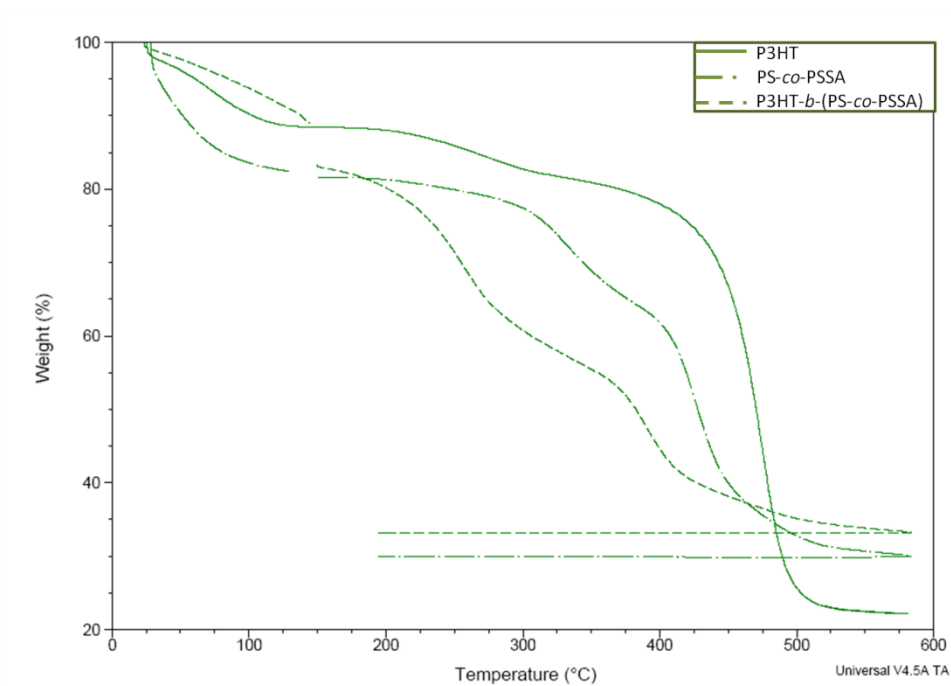
Figure2. DSC of the P3HT-*b*-(PS-co-PSSA) copolymer after three cycles of heating from -40 °C to 200 °C with a rate of 10 °C/ min
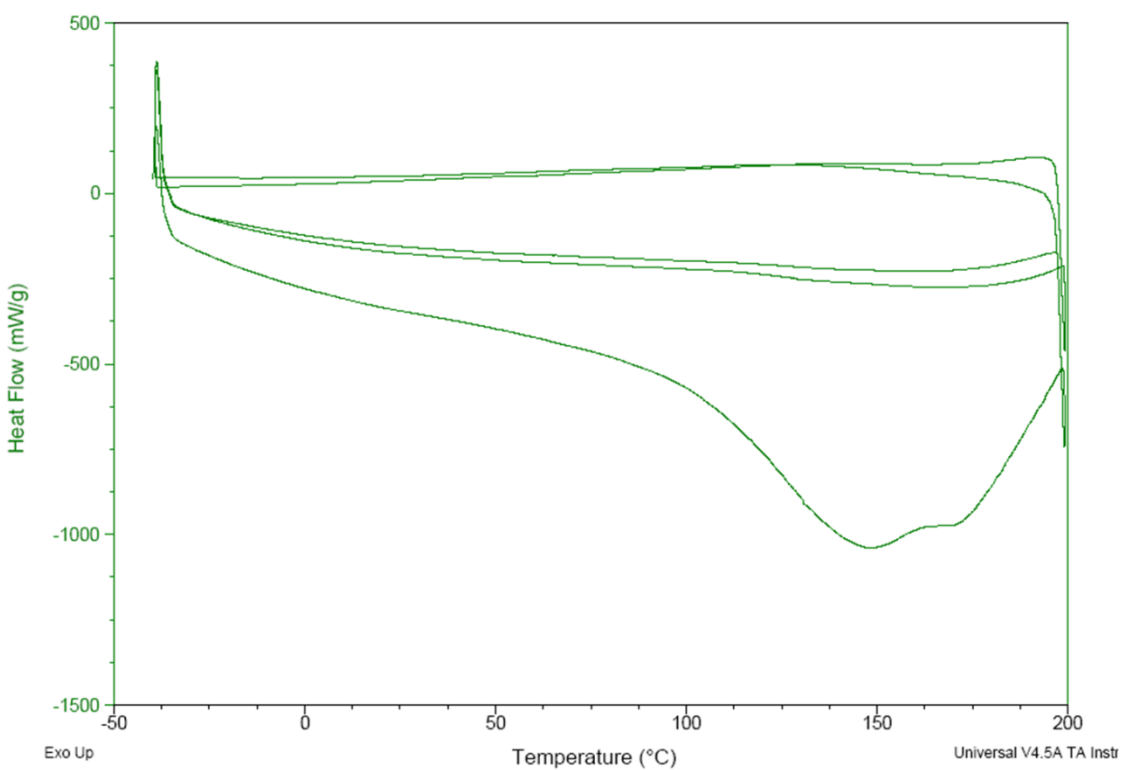
I.6.4 Fourier Transformed InfraRed (ATR), Phtoluminesence, UV-vis spectroscopy
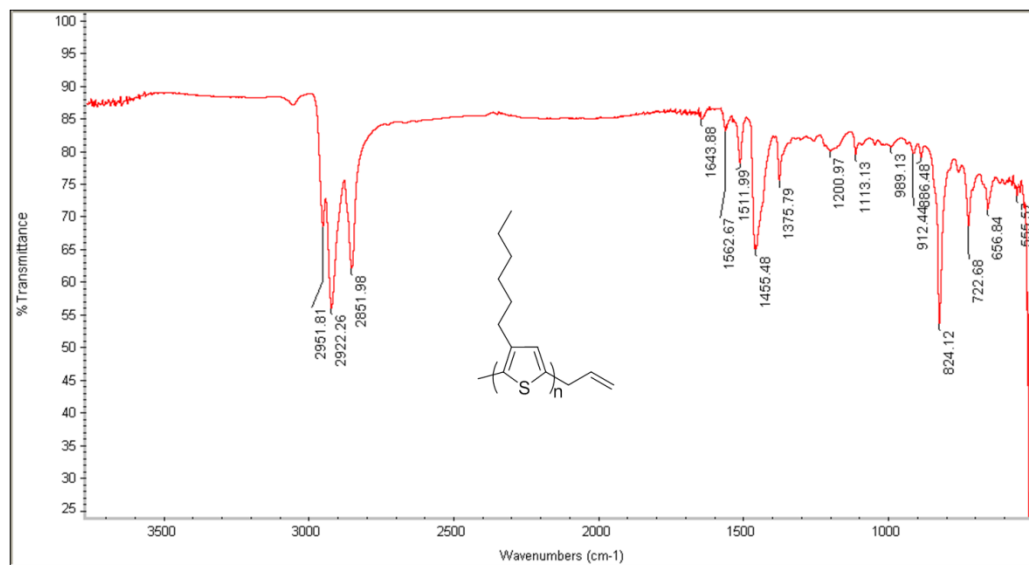
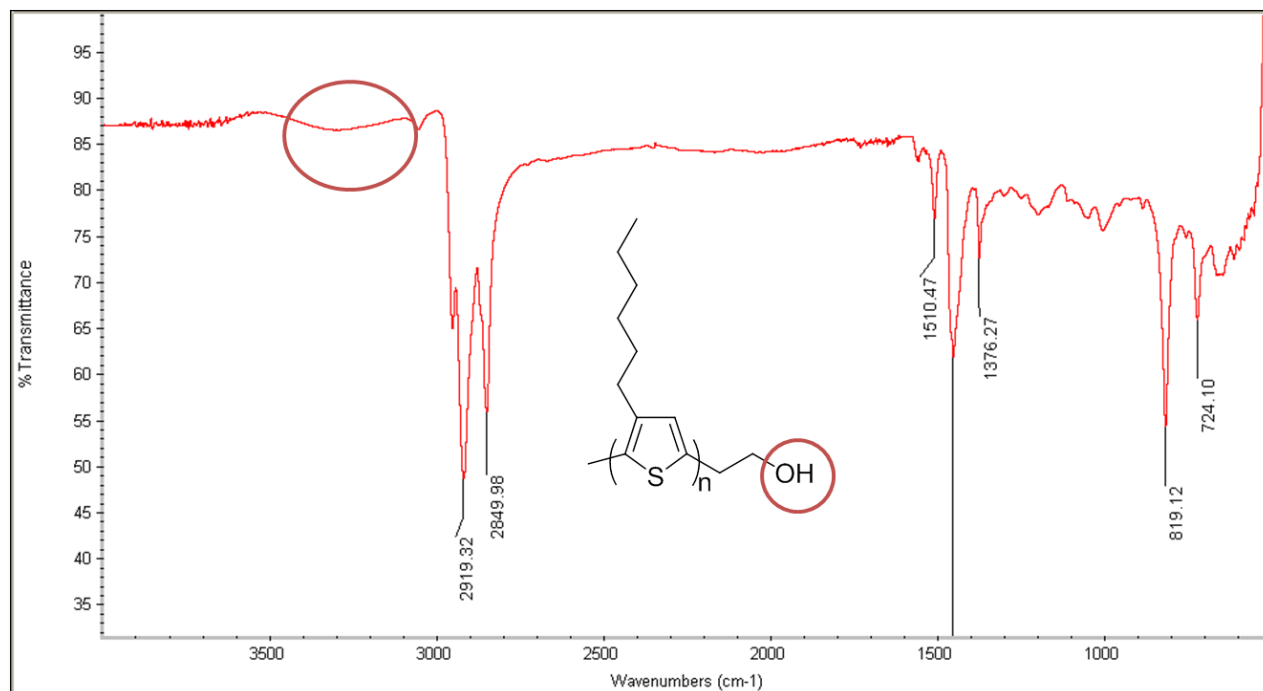**Figure1. FTIR-ATR of Allyl-terminated P3HT**

Figure2. FTIR-ATR hydroxypropyl terminated P3HT

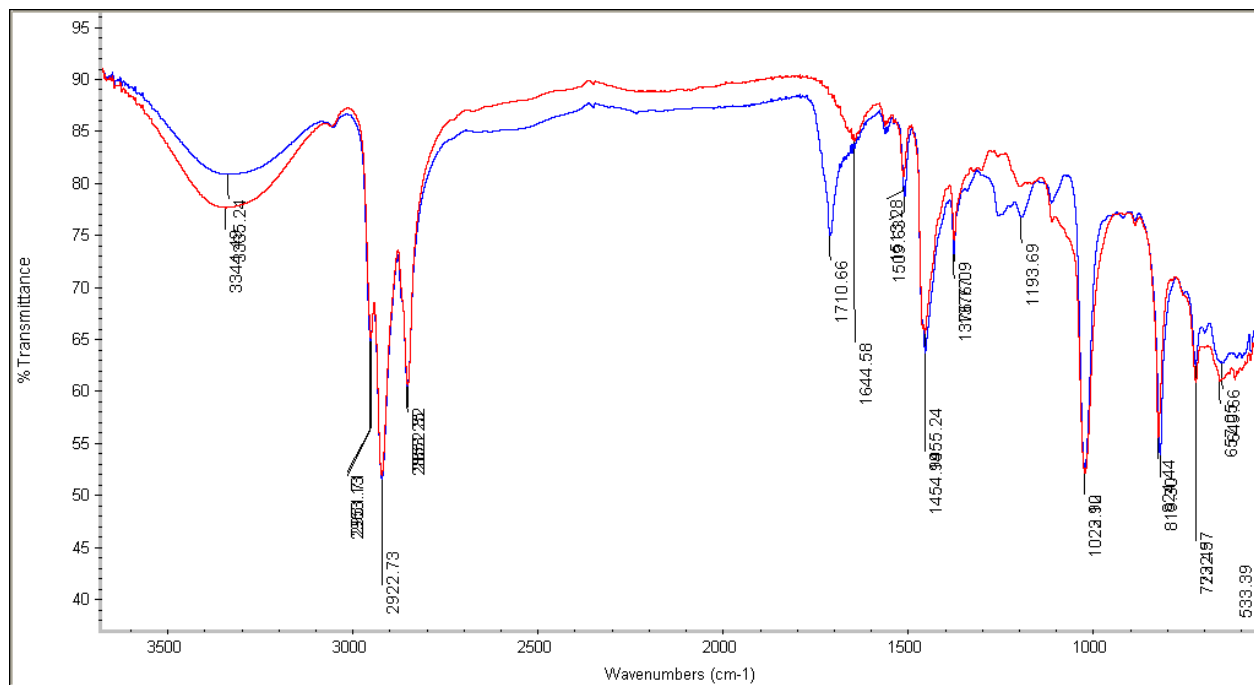**Figure3. FTIR-ATR of P3HT before (red) and after (blue) probe sonication for 20 min**
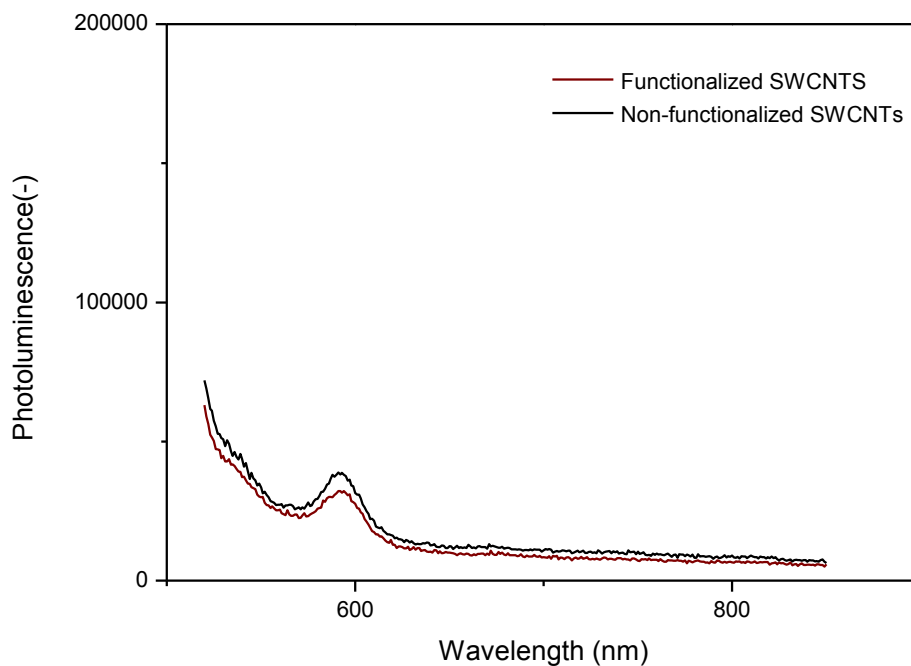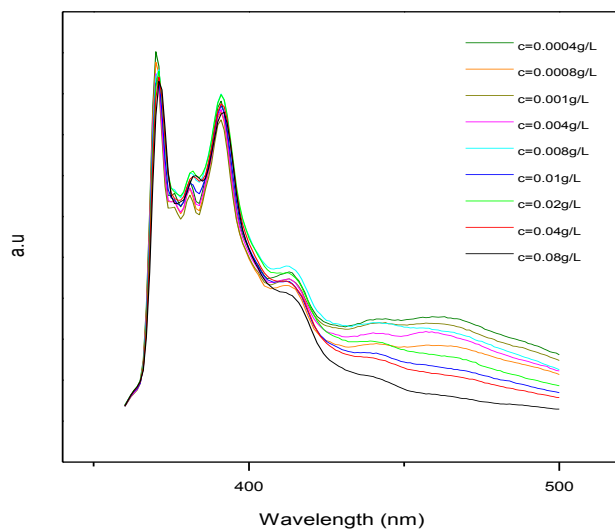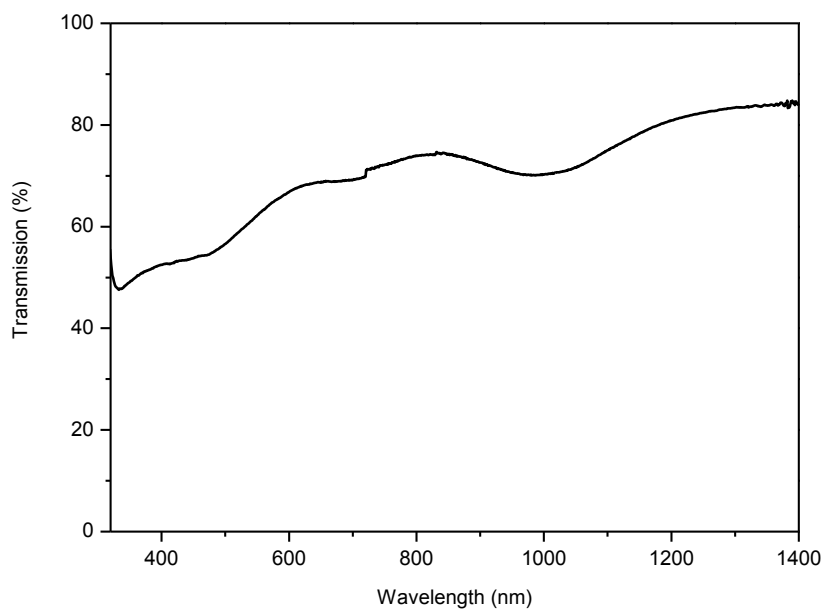

Figure4. Photoluminescence of the SWCNTs (excitation at 500 nm, slit at 10 nm and 0.1sec integration time.

Figure5. Photoluminescence of the pyrene containing in the P3HT-*b*-(PS-co-PSSA) solutions in different concentrations.

Figure6. UV-vis spectra of the nf-SWCNTs- P3HT-*b*-(PS-co-PSSA) films

(1)   Moore, J. S.; Stupp, S. I. *Macromolecules* **1990**, *23*, 65.

(2)   Mougnier, S.-J.; Brochon, C.; Cloutet, E.; Fleury, G.; Cramail, H.; Hadziioannou, G. *Macromol. Rapid Commun.* **2012**, *33*, 703.

Summary

Our work focused on the synthesis of well-defined copolymers constituted with at least a conductive polymer segment along with hydrophilic moieties in order to disperse CNTs in aqueous media. Using metal free polymerizations, copolymers with different molecular weights were synthesized in order to study the influence of the hydrophilic part on these materials. Besides the self-assembly behavior of these copolymers, both in bulk and in solution, were addressed. This type of copolymers were successfully used to disperse both single and multi wall carbon nanotubes. Electrical and optical characteristics of the dispersions together with their films will also be discussed.

Key words:

Polyelectrolyte, Carbon nanotubes, semi-conducting, transparent electrodes.

Sommaire

Cette thèse porte pour l'essentiel sur la synthèse de copolymères à blocs bien définis composés au moins d'un bloc polymère semi-conducteur et d'un segment hydrosoluble pour être utilisés comme agents dispersants de nanotubes de carbone (NTCs) dans des milieux aqueux. Des copolymères de différentes masses molaires ont été synthétisés en suivant des procédés de polymérisation sans métaux et l'influence de la fraction volumique de la partie hydrosoluble a été étudiée au regard de leur solubilité en milieux aqueux. La capacité de ces copolymères à s'organiser ou s'auto-assembler tant en solution qu'en film a été examinée. Enfin, des dispersions de NTCs avec ces copolymères ainsi que leurs films obtenus par différents types de dépôts ont été réalisés et caractérisés pour déterminer notamment leurs caractéristiques électro-optiques.

Mots clés

Polyélectrolyte, nanotube de carbone, semi-conducteur, électrodes transparents.